

**DESIGN, RATING AND EXERGY ANALYSIS OF
EVAPORATIVE HEAT EXCHANGERS**

BY

BILAL AHMED QURESHI

A Thesis Presented to the
DEANSHIP OF GRADUATE STUDIES

KING FAHD UNIVERSITY OF PETROLEUM&MINERALS

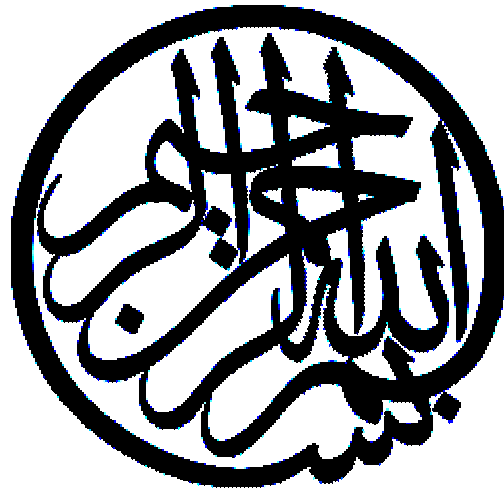
DHAHRAN, SAUDI ARABIA

In Partial Fulfillment of the
Requirements for the Degree of

MASTER OF SCIENCE

In
Mechanical Engineering

April, 2004



In the Name of Allah, Most Gracious, Most Merciful.

KING FAHD UNIVERSITY OF PETROLEUM AND MINERALS
DHAHRAN 31261, SAUDI ARABIA

DEANSHIP OF GRADUATE STUDIES

This thesis, written by **BILAL AHMED QURESHI** under the direction of his Thesis Advisor and approved by his Thesis Committee, has been presented to and accepted by the Dean of Graduate Studies, in partial fulfillment of the requirements for the degree of **MASTER OF SCIENCE IN MECHANICAL ENGINEERING.**

Thesis Committee

Dr. Syed M. Zubair (Advisor)

Dr. Mohamed A. Antar (Member)

Dr. Shahzada Z. Shuja (Member)

Dr. Faleh Al-Sulaiman
Department Chairman

Prof. Osama A. Jannadi
Dean of Graduate Studies

Date

*Dedicated to My Beloved Parents and Family Members
whose constant prayers, sacrifice and inspiration led to this
wonderful accomplishment*

ACKNOWLEDGEMENTS

All praises and thanks are due to Allah (subhana wa taala) for bestowing me with health, knowledge and patience to complete this work. Thereafter, acknowledgement is due to KFUPM for the support given to this research project through its funding as well as the tremendous facilities and for granting me the opportunity to pursue graduate studies with financial support.

I acknowledge, with deep gratitude and appreciation, the inspiration, encouragement, valuable time and continuous guidance given to me by my Committee Chairman, Dr. Syed M. Zubair. Secondly, I am grateful to my Committee members, Dr. Mohammed A. Antar and Dr. S. Z. Shuja for their constructive guidance and technical support. Thanks are also due to the Department secretaries, Mr. Jameel and Mr. Lateef for their help and assistance.

Special thanks are due to my senior colleagues at the university, Hassan, Munib, Naeem, Iqtedar, Shiraz, Itrat, Salman, Junaid, Saad, Moin Bhai, Saad bin Mansoor, Ahmed Jamal, Ghulam Arshed, Ovaisaullah and Zahid Sahib, who were always there to help me in my work. I would also like to thank my friends Iftikhar, Abdul Qayum, Abbas, Sami, Khalil, Furrukh, Hafeez, Mujahid, Khaliq, Samer and all others who provided wonderful company and good memories that will last a life time.

Finally, thanks are due to my dearest mother and father, and all my family members for their emotional and moral support throughout my academic career and also for their love, patience, encouragement and prayers.

TABLE OF CONTENTS

LIST OF TABLES	IX
LIST OF FIGURES	X
THESIS ABSTRACT.....	XV
THESIS ABSTRACT(ARABIC).....	XVI
CHAPTER 1	
INTRODUCTION.....	1
CHAPTER 2	
LITERATURE REVIEW.....	9
2.1 EVAPORATIVE FLUID COOLERS AND CONDENSERS	9
2.2 WET COOLING TOWERS.....	12
CHAPTER 3	
MATHEMATICAL FORMULATION	18
3.1 EVAPORATIVE FLUID COOLERS AND CONDENSERS	19
3.1.1 Mass balance equations	19
3.1.2 Energy balance equations	23
3.1.3 Final system of equations	24
3.2 COOLING TOWERS	28
3.2.1 Mass balance equations	29
3.2.2 Energy balance equations	29
3.2.3 Final system of equations	31
CHAPTER 4	
SPRAY AND RAIN ZONE	34
4.1 SUMMARY OF WORK BY DREYER, KROGER & FISENKO.....	35
4.1.1 Work by Dreyer	36
4.1.2 Work by Kroger.....	39
4.1.3 Work by Fisenko et al.....	42
4.2 COMPARISON AND SELECTION	46
CHAPTER 5	
FOULING OF HEAT EXCHANGERS.....	50
5.1 FACTORS OF IMPORTANCE IN FOULING PROCESS	54
5.1.1 Temperature.....	54
5.1.2 Effects of Fluid Velocity	56
5.1.3 Operation of Heat Exchangers.....	58
5.1.4 Fouling in Counter Flow Wet Cooling Towers.....	58

5.1.5	Fouling in Counter Flow Coolers and Condensers.....	62
5.2	CHARACTERIZATION OF FOULING MECHANISM.....	65
5.2.1	Fouling Models with Induction Time.....	66
5.2.2	Stochastic Analysis of Fouling Models.....	66
5.2.3	Asymptotic Fouling Model.....	68
 CHAPTER 6		
	EXERGY ANALYSIS	72
6.1	ANALYTICAL FRAMEWORK	73
 CHAPTER 7		
	SENSITIVITY ANALYSIS.....	77
 CHAPTER 8		
	VALIDATION.....	81
8.1	VALIDATION OF COOLING TOWER MODEL.....	81
8.1.1	Validation of Packing Model.....	81
8.1.2	Validation of the Spray and Rain Zone Models	82
8.1.3	Validation of the Complete Model.....	85
8.2	VALIDATION OF EVAPORATIVE COOLER MODEL.....	87
8.3	VALIDATION OF EVAPORATIVE CONDENSER MODEL.....	87
8.4	CALCULATION APPROACH	91
8.4.1	Determination of Effective Drop Diameters	93
 CHAPTER 9		
	RESULTS AND DISCUSSION	96
9.1	RESULTS FOR COOLING TOWER.....	96
9.1.1	Effect of Pressure (Elevation)	96
9.1.2	Effect of Fouling.....	98
9.1.2.1	Design.....	100
9.1.2.2	Rating	100
9.1.3	Sensitivity Analysis Results	102
9.1.3.1	Design.....	102
9.1.3.2	Rating	109
9.1.4	Exergy Analysis Results.....	119
9.1.5	Evaporation and the Effect of Mass Flow Rate.....	125
9.2	RESULTS FOR EVAPORATIVE FLUID COOLER.....	128
9.2.1	Effect of Pressure (Elevation)	128
9.2.2	Effect of Fouling.....	130
9.2.2.1	Design.....	130
9.2.2.2	Rating	131
9.2.3	Sensitivity Analysis Results	134
9.2.3.1	Design.....	134
9.2.3.2	Rating	139
9.2.4	Exergy Analysis Results.....	148

9.2.5	Evaporation and Effect of Mass Flow Rate.....	150
9.3	RESULTS FOR EVAPORATIVE CONDENSER.....	153
9.3.1	Effect of Pressure (Elevation)	153
9.3.2	Effect of Fouling.....	156
9.3.2.1	Design.....	156
9.3.2.2	Rating	157
9.3.3	Sensitivity Analysis Results	160
9.3.3.1	Design.....	160
9.3.3.2	Rating	162
9.3.4	Exergy Analysis Results.....	164
9.3.5	Effect of Mass Flow Rate	168
 CHAPTER 10		
CONCLUSIONS AND RECOMMENDATIONS.....		170
10.1	CONCLUSIONS.....	170
10.2	RECOMMENDATIONS	174
APPENDIX A		175
NOMENCLATURE		177
REFERENCES.....		185
VITA.....		196

LIST OF TABLES

TABLE 8.1: Comparison of experimental and predicted values of outlet wet-bulb temperature	83
TABLE 8.2: Comparison of experimental and predicted values of the outlet wet- and dry-bulb temperatures modeled with spray zone and packing coupled	86
TABLE 8.3: Comparison of experimental and numerical values of process fluid outlet temperature with calculated values	89

LIST OF FIGURES

Figure 1.1: Some examples of packing or fills.....	3
Figure 1.2: A counter flow wet-cooling tower	4
Figure 1.3: An evaporative cooler	6
Figure 1.4: An evaporative condenser.....	7
Figure 3.1: Infinitesimal control volume of the basic model for an evaporative fluid cooler	20
Figure 3.2: Infinitesimal control volume of the basic model for an evaporative condenser	21
Figure 3.3: Schematic representation of temperature gradients on process tubes in an evaporative fluid cooler.....	22
Figure 3.4: Schematic representation of temperature gradients on process tubes in an evaporative condenser	22
Figure 3.5: Infinitesimal control volume of the basic model for cooling tower.....	30
Figure 5.1: Behavior of normal and inverse solubility salt solutions [60]	51
Figure 5.2: Decrease in percentage design capacity versus scaling thickness	64
Figure 5.3: Typical sample functions of fouling-resistance models.....	69
Figure 8.1: Verification of spray/rain zone model by comparing velocity prediction	84
Figure 8.2: Verification of evaporative cooler model from the data of Jang and Wang....	88
Figure 8.3: Verification of the evaporative condenser model	90
Figure 8.4: Comparison of the proposed fouling model with experimental data.....	92
Figure 8.5: Determination of effective drop radius for the spray zone	95
Figure 9.1: Variation in the inlet wet-bulb temperature versus pressure change	97

Figure 9.2: Variation in required volume versus pressure change	99
Figure 9.3: Percent decrease in required volume versus pressure ratio	99
Figure 9.4: Volume fraction as a function of constant C_I	101
Figure 9.5: Normalized tower effectiveness versus reduced weight	101
Figure 9.6: Reduced water outlet temperature versus reduced weight.....	103
Figure 9.7: Variation of volume NSC w.r.t. air inlet wet-bulb temperature versus R_{ct}	103
Figure 9.8: Variation of volume NSC w.r.t. water outlet temperature versus R_{ct}	104
Figure 9.9: Variation of volume NSC w.r.t. water inlet temperature versus R_{ct}	104
Figure 9.10: Variation of all NSCs versus R_{ct} with mass flow ratio of 1	106
Figure 9.11: Variation of all NSCs versus R_{ct} with mass flow ratio of 0.5.....	106
Figure 9.12: Variation of volume NSC w.r.t. air inlet wet-bulb temperature versus R_{ct} ..	107
Figure 9.13: Variation of volume NSC w.r.t. water outlet temperature versus R_{ct}	107
Figure 9.14: Variation of volume NSC w.r.t. water inlet temperature versus R_{ct}	108
Figure 9.15: Variation of all NSCs versus R_{ct} with mass flow ratio of 1	110
Figure 9.16: Variation of all NSCs versus R_{ct} with mass flow ratio of 0.5.....	110
Figure 9.17: Variation of effectiveness NSC w.r.t. inlet water temperature versus R_{ct} ...	111
Figure 9.18: Variation of effectiveness NSC w.r.t. water flow rate versus R_{ct}	111
Figure 9.19: Variation of all NSCs versus R_{ct} with mass flow ratio of 1	113
Figure 9.20: Variation of all NSCs versus R_{ct} with mass flow ratio of 0.5.....	113
Figure 9.21: Variation of effectiveness NSC w.r.t. inlet water temperature versus R_{ct} ...	114
Figure 9.22: Variation of effectiveness NSC w.r.t. water flow rate versus R_{ct}	114
Figure 9.23: Variation of all NSCs Versus R_{ct} with mass flow ratio of 1	116
Figure 9.24: Variation of all NSCs versus R_{ct} with mass flow ratio of 0.5.....	116
Figure 9.25: Variation of water outlet NSC w.r.t. inlet wet-bulb temperature versus R_{ct}	117

Figure 9.26: Variation of water outlet NSC w.r.t. water inlet temperature versus R_{ct}	117
Figure 9.27: Variation of all NSCs versus R_{ct} with mass flow ratio of 1	118
Figure 9.28: Variation of all NSCs versus R_{ct} with mass flow ratio of 0.5	118
Figure 9.29: Variation of water outlet NSC w.r.t. inlet wet-bulb temperature versus R_{ct}	120
Figure 9.30: Variation of water outlet NSC w.r.t. water inlet temperature versus R_{ct}	120
Figure 9.31: Variation of all NSCs versus R_{ct} with mass flow ratio of 1	121
Figure 9.32: Variation of all NSCs versus R_{ct} with mass flow ratio of 0.5	121
Figure 9.33: Variation of second-law efficiency versus R_{ct} (Eq. (6.15))	123
Figure 9.34: Variation of exergy destruction versus R_{ct}	123
Figure 9.35: Variation of second-law efficiency versus R_{ct} (Eq. (6.15))	124
Figure 9.36: Variation of exergy destruction versus R_{ct}	124
Figure 9.37: Variation of effectiveness with mass flow ratio	126
Figure 9.38: Variation of temperature ratio with mass flow ratio	126
Figure 9.39: Percent evaporation for various air conditions and mass flow ratios	127
Figure 9.40: Variation in required surface area versus pressure change	129
Figure 9.41: Percent decrease in required surface area versus pressure ratio	129
Figure 9.42: Area fraction as a function of fouling resistance	132
Figure 9.43: Normalized effectiveness versus reduced thickness	132
Figure 9.44: Reduced process fluid outlet temperature versus reduced thickness	133
Figure 9.45: Variation of area NSC w.r.t. outlet process fluid temperature versus R_{efc} ..	135
Figure 9.46: Variation of area NSC w.r.t. inlet process fluid temperature versus R_{efc} ...	135
Figure 9.47: Variation of all NSCs versus R_{efc} for all mass flow ratios	137
Figure 9.48: Variation of area NSC w.r.t. process fluid outlet temperature versus R_{efc} ..	137
Figure 9.49: Variation of area NSC w.r.t. process fluid inlet temperature versus R_{efc}	138

Figure 9.50: Variation of all NSCs versus R_{efc} for all mass flow ratios.....	140
Figure 9.51: Variation of effectiveness NSC w.r.t. fluid inlet temperature versus R_{efc} ...	140
Figure 9.52: Variation of effectiveness NSC w.r.t. process fluid flow rate versus R_{efc} ...	141
Figure 9.53: Variation of all NSCs versus R_{efc} with mass flow ratio of 1	143
Figure 9.54: Variation of all NSCs versus R_{efc} with mass flow ratio of 0.5	143
Figure 9.55: Variation of effectiveness NSC w.r.t. fluid inlet temperature versus R_{efc} ...	144
Figure 9.56: Variation of effectiveness NSC w.r.t. process fluid flow rate versus R_{efc} ...	144
Figure 9.57: Variation of all NSCs versus R_{efc} with mass flow ratio of 1	146
Figure 9.58: Variation of all NSCs versus R_{efc} with mass flow ratio of 0.5	146
Figure 9.59: Variation of fluid outlet NSC w.r.t. fluid inlet temperature versus R_{efc}	147
Figure 9.60: Variation of fluid outlet NSC w.r.t. fluid inlet temperature versus R_{efc}	147
Figure 9.61: Variation of second-law efficiency versus R_{efc} (Eq. (6.15)).....	149
Figure 9.62: Variation of exergy destruction versus R_{efc}	149
Figure 9.63: Variation of second-law efficiency versus R_{efc} (Eq. (6.15)).....	151
Figure 9.64: Variation of exergy destruction versus R_{efc}	151
Figure 9.65: Variation of effectiveness with mass flow ratio	152
Figure 9.66: Variation of temperature ratio with mass flow ratio.....	152
Figure 9.67: Percent evaporation for various air conditions and mass flow ratios	154
Figure 9.68: Variation in required surface area versus pressure change.....	154
Figure 9.69: Percent decrease in required surface area versus pressure ratio	155
Figure 9.70: Area fraction as a function of fouling resistance	158
Figure 9.71: Normalized effectiveness versus reduced thickness.....	158
Figure 9.72: Normalized load versus reduced thickness.....	159
Figure 9.73: Variation of area NSC w.r.t. condensing temperature versus R_{ec}	161

Figure 9.74: Variation of area NSC w.r.t. condensing temperature versus R_{ec}	161
Figure 9.75: Variation of effectiveness NSC w.r.t. condensing temperature versus R_{ec} ..	163
Figure 9.76: Variation of effectiveness NSC w.r.t. condensing temperature versus R_{ec} ..	163
Figure 9.77: Variation of second-law efficiency versus R_{ec} (Eq. (6.15)).....	165
Figure 9.78: Variation of exergy destruction versus R_{ec}	165
Figure 9.79: Variation of second-law efficiency versus R_{ec} (Eq. (6.15)).....	167
Figure 9.80: Variation of exergy destruction versus R_{ec}	167
Figure 9.81: Variation of effectiveness with mass flow ratio	169
Figure 9.82: Variation of temperature ratio with mass flow ratio.....	169

THESIS ABSTRACT

NAME: BILAL AHMED QURESHI
TITLE: DESIGN, RATING AND EXERGY ANALYSIS OF
EVAPORATIVE HEAT EXCHANGERS
DEPARTMENT: MECHANICAL ENGINEERING
DATE: 21 APRIL, 2004

The most efficient equipment in which heat rejection processes may be realized is the cooling towers, evaporative fluid coolers and evaporative condensers. This class of heat rejection devices is defined as evaporative heat exchangers. The mathematical models of these heat exchangers are developed and validated against the experimental data available in the literature, using Engineering Equation Solver (EES) software, where the maximum error encountered is 6.5%. These devices basically consist of three zones; namely, spray zone, packing/tube-bundle and rain zone. The spray and rain zones are often neglected even though in large cooling towers, a significant portion of the total heat that is rejected may occur in these zones. Therefore, the heat and mass transfer contribution of the spray and rain zones in cooling towers is discussed as well. A parametric study is performed to evaluate the effect of fouling (which is the deposition of unwanted material on heat transfer equipment), atmospheric pressure and mass flow rate ratio on typical performance parameters such as effectiveness for rating calculations while volume/surface area for design calculations. Also, a sensitivity analysis is carried out to evaluate the response of the above parameters to various input variables such as inlet wet-bulb temperature, inlet process fluid temperature and outlet water temperature. Second-law analyses based on exergy analyses are studied as well to investigate the variation in second-law efficiency of these heat exchangers under different operating conditions. Furthermore, the rate of water evaporation under a wide range of operating conditions is also presented.

MASTER OF SCIENCE DEGREE
KING FAHD UNIVERSITY OF PETROLEUM AND MINERALS
Dhahran, Saudi Arabia

ان أكفا أدوات التخلص من الحرارة هي أبراج التبريد، المبردات التبخرية، و المكثفات التبخرية. ويعرف هذا النوع من أجهزة التخلص من الحرارة بالمبادلات الحرارية التبخرية. و قد تم في هذا البحث تطوير نموذج رياضي لمحاكاة أداء هذه المبادلات كما تم حل هذا النموذج باستخدام برنامج حل المعادلات الهندسية (EES) كما تمت مقارنة نتائج الحل مع النتائج المماثلة و المنشورة في أبحاث سابقة ووجد أن الفرق لا يزيد عن 6.5 % . و تتكون هذه الأجهزة من ثلاث مناطق أساسية وهي: منطقة التذير، منطقة الحشو الأنبوبي، و منطقة التساقط. وقد وجد أنه في الأبحاث السابق نشرها عادة ما يتم اهمال منطقتي التذير و التساقط عند تحليل أداء هذه المبادلات رغم أن جزء كبير من الحرارة يتم فقده في هاتين المنطقتين في أبراج التبريد ولتلافي أي خطأ قد ينتج من هذا الأهمال تمت دراسة انتقال الحرارة و المادة في هاتين المنطقتين و أخذ في الاعتبار عند دراسة أبراج التبريد في البحث الحالي. كما تم اجراء دراسة تحليلية لتأثير بعض عوامل التشغيل مثل الترسيب علي أسطح انتقال الحرارة، الضغط الجوي، و معدل السريان علي معاملات الأداء الرئيسية مثل الكفاءة عند تقييم الأداء و نسبة الحجم الي مساحة السطح عند التصميم. كما أجريت دراسة تحليلية لتقييم التغير في معاملات الأداء كنتيجة لتغير بعض عوامل وظروف التشغيل مثل درجة الحرارة و الرطوبة في المدخل و كذلك درجة حرارة خروج المياه. كما تم حساب الكفاءة بناء علي القانون الثاني للديناميكا الحرارية باستخدام تحليل الأكسرجي. و بالإضافة لما سبق تم حساب و عرض معدلات تبخير المياه في مثل هذه الأجهزة تحت ظروف تشغيل واسعة النطاق.

هذه الدراسة اعدت لنيل درجة الماجستير في العلوم
في جامعة الملك فهد للبترول والمعادن
الظهران
المملكة العربية السعودية

CHAPTER 1

INTRODUCTION

Most air-conditioning systems and many industrial processes generate heat, which must be removed and dissipated. In industry, water is commonly used as a heat-transfer medium to remove heat from refrigerant condensers or other process heat exchangers. However, water purchased from utilities for use in this manner has now become prohibitively expensive because of increased water supply and disposal cost. Similarly, cooling water drawn from natural sources is relatively unavailable and has become unattractive because of environmental restrictions. In many processes, the ambient air is used as a heat sink for low-quality waste heat. In this regard, air-cooled heat exchangers may be used to cool the water by rejecting heat directly to the atmosphere, but the first cost and fan energy consumption of these devices is normally very high. They are economically capable of cooling the water to within about $10^{\circ}C$ of the ambient dry-bulb temperature. Such temperature levels are often too high for cooling water requirements of most industrial processes.

The most efficient equipment in which these cooling processes may be realized is the cooling towers, evaporative fluid coolers and evaporative condensers. These are all members of a basic heat exchanger family. Heat is rejected by evaporation, from a gravity drained water film, into air flowing through a cooling tower “packing”, or a tube bundle

for fluid coolers and condensers. Some examples of different types of packing are shown in Figure 1.1. Hence, the airside heat and mass transfer process is governed by the same basic process. The key difference in the theory for each type relates to the thermal resistance of the process fluid. The resistance is quite small for cooling towers, but must be accounted for in the fluid cooler and condenser. Figure 1.2 shows a schematic diagram of a counter flow-cooling tower. The cooling towers generally consist of large chambers loosely filled with trays or decks of wooden boards as slats. The water to be cooled is pumped to the top of the tower, where it is distributed over the top deck by sprays or wooden distributor troughs. It then falls and splashes from deck to deck down through the tower. Air is permitted to pass through the tower horizontally due to wind currents or is drawn vertically upward countercurrent to the falling water. In the case of countercurrent towers, the air motion may be due to the natural chimney effect of the warm moist air in the tower or may be caused by fans at the bottom (forced draft) or at the top (induced draft) of the tower. Cooling towers are among the largest heat and mass transfer devices that are in common use. They are widely used in most industrial power generation units, space conditioning, and chemical, petrochemical and petroleum industries to reject the excess heat to the environment. In particular, steam power plants reject heat at approximately twice the rate at which electricity is generated. A wet cooling tower needs only about one-fourth the amount of contact surface for the given water-cooling effect that is needed by an exchanger (a dry tower) in which mass transfer is prevented by the use of an indirect-contact design.

The phenomenon of cooling by evaporation is well known and it has found many applications. A logical development of the cooling-tower-heat exchanger combination is the evaporative cooler and the evaporative condenser. In these equipment, the function of

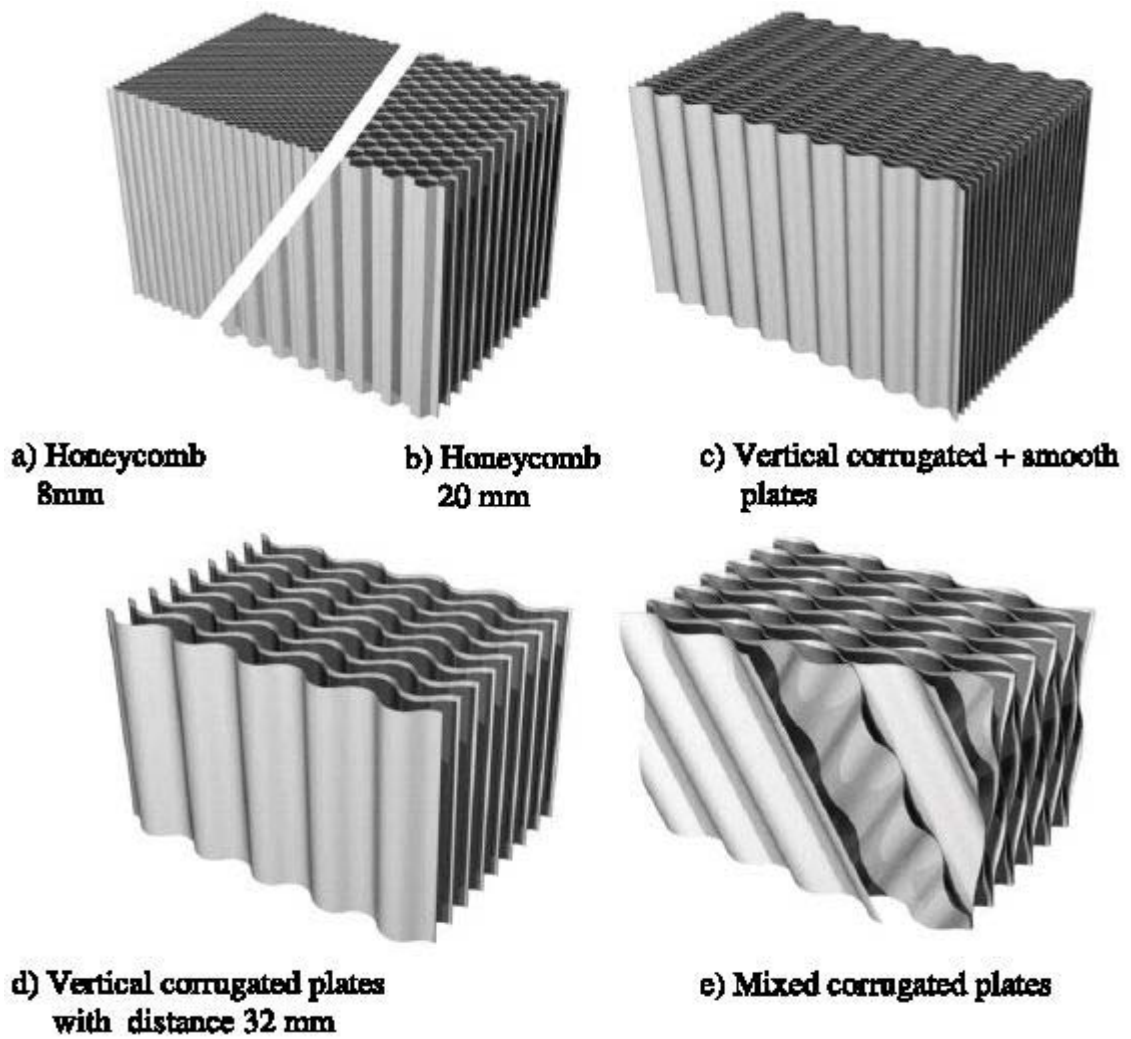


Figure 1.1: Some examples of packing or fills

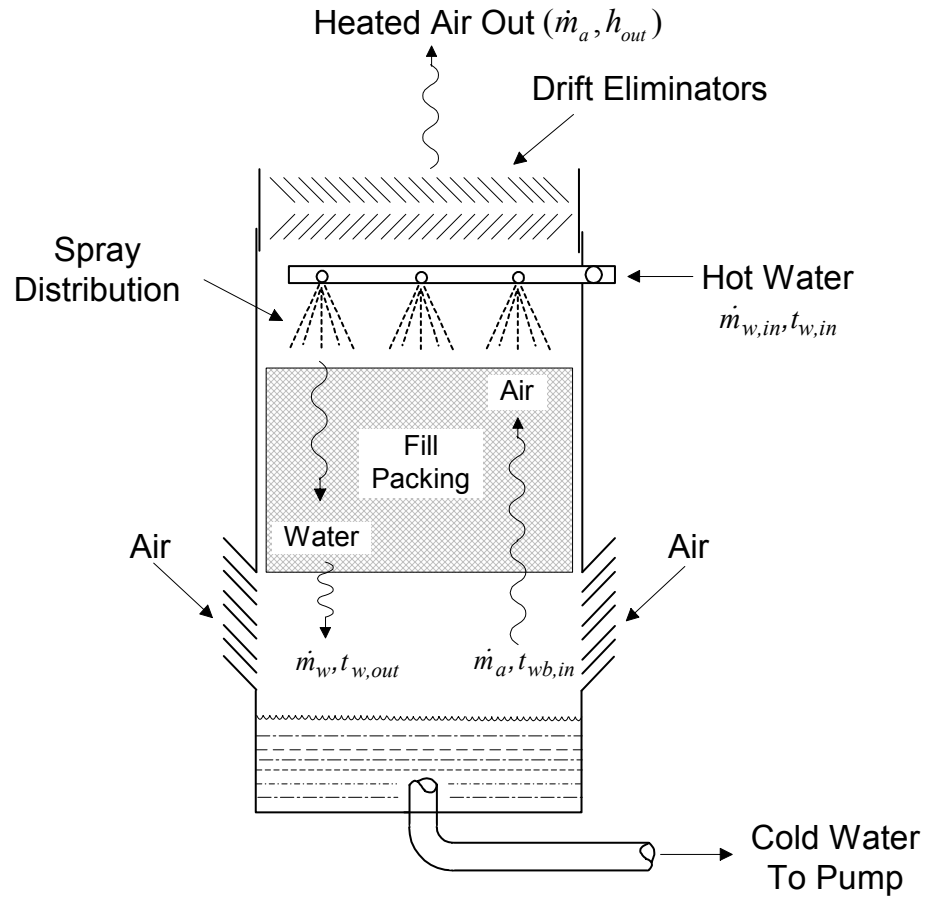


Figure 1.2: A counter flow wet-cooling tower

the cooling tower to cool water, and of the heat exchanger to cool the process fluid using the cooled water are combined. With the expansion of the refrigeration and air conditioning industry, the evaporative cooler came into wide use principally as a refrigerant condenser. Figures 1.3 and 1.4 shows schematic diagrams of the evaporative cooler and evaporative condenser, respectively. Air is drawn up through a bank of tubes while spray water falls over the tubes, part of the spray water is evaporated, and the remainder falls to the sump where it is re-circulated by the spray-water pump. The fluid to be cooled is circulated inside the tubes, while air is drawn in a counter-current direction.

The same basic theory applies to the heat and mass transfer between the evaporating water film and the air. In evaporative cooling, the medium being cooled can, theoretically, reach the air wet bulb temperature, which leads to major cost savings and improvements in thermal efficiency because of the lower temperatures that can be reached as compared to dry cooling. However, the different geometries of the cooling tower and the tube bundles used in condensers and coolers yield different equations for the heat and mass transfer coefficients between the water film and air. The primary difference between the condenser and the fluid cooler is that the refrigerant temperature is constant in the condenser, whereas the fluid temperature may change in the fluid cooler.

The air flow through the evaporative cooler or condenser may be horizontal, in which case the unit is referred to as a cross-flow evaporative cooler or condenser or vertically upwards through tube bundle where it is known as a counterflow evaporative cooler or condenser. Various other configurations for these devices have been proposed in the literature but they are not commonly used. Chapter 2 summarizes the literature survey carried out during the current work. The mathematical modeling of cooling towers, evaporative fluid coolers and evaporative condensers is outlined in chapter 3.

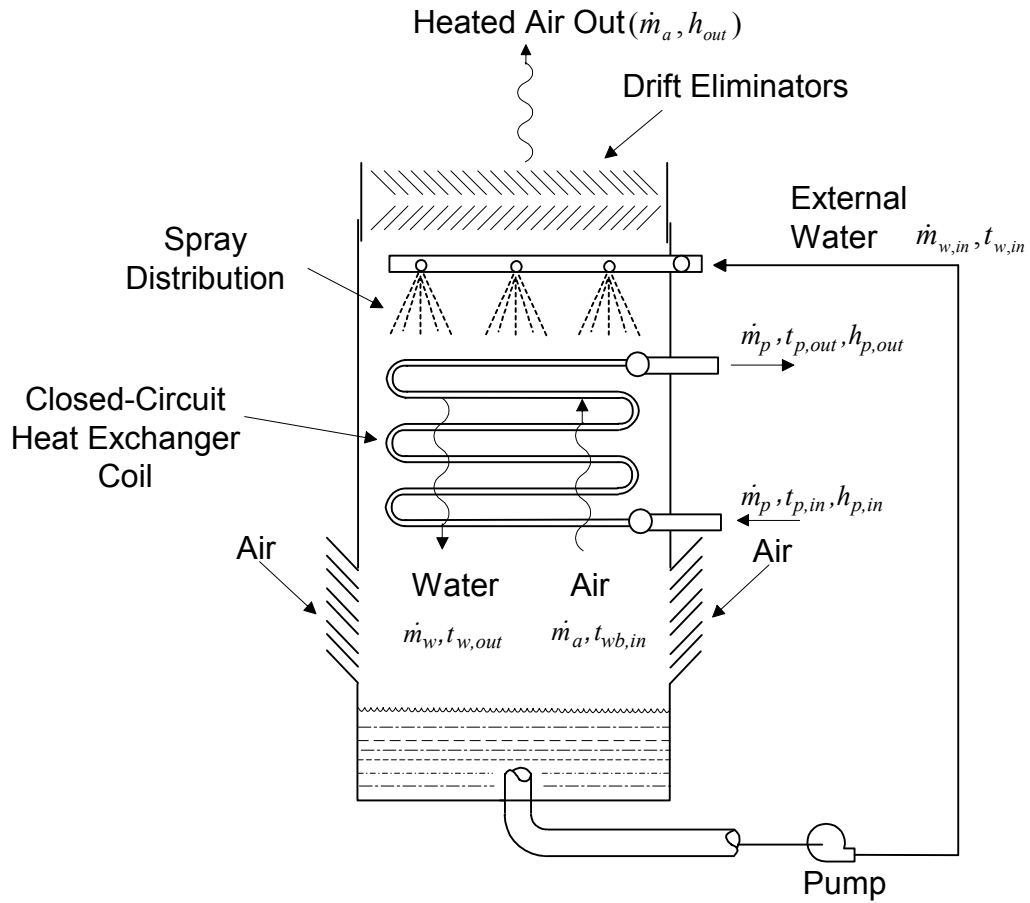


Figure 1.3: An evaporative cooler

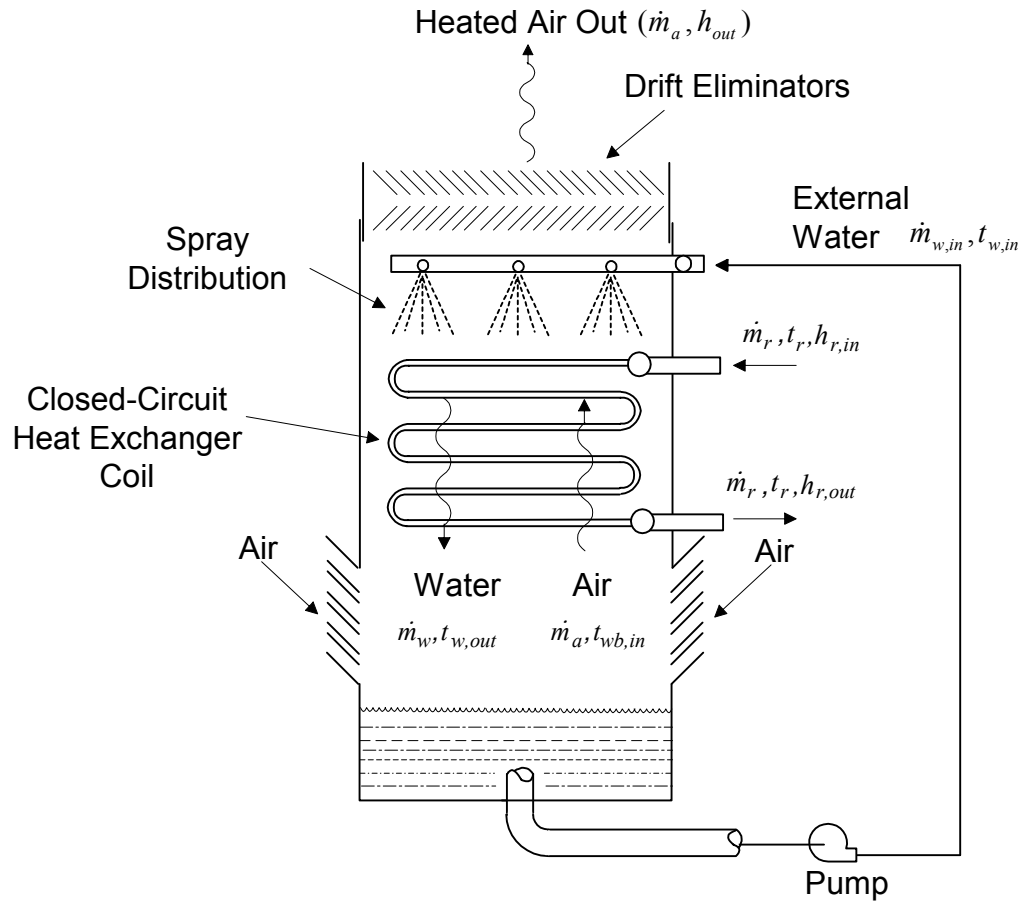


Figure 1.4: An evaporative condenser

Details regarding the spray and rain zones as well as work of some authors are presented in chapter 4. The aspect of fouling in evaporative heat exchangers is explained in chapter 5. The essentials of second-law based exergy analysis are outlined in chapter 6. Chapter 7 explains the procedure used to perform a sensitivity analysis on the above-mentioned heat exchangers as well as its significance in analysis. Chapter 8 shows the comparison of experimental and numerical data, to results obtained from the mathematical models used, in order to validate them. Chapter 9 includes the results and discussion of the current work. Finally, conclusions and recommendations are presented in chapter 10.

CHAPTER 2

LITERATURE REVIEW

This literature review focuses on the impact of fouling on the design and rating of cooling towers, evaporative condensers and evaporative fluid coolers. Furthermore, literature regarding investigation into the efficiency of these heat exchangers using the concept of exergy analysis is detailed.

2.1 EVAPORATIVE FLUID COOLERS AND CONDENSERS

The mathematical modeling of an evaporative cooler or condenser is complicated by the fact that three fluids, sometimes flowing in different directions, interact with heat and mass transfer processes taking place. Many modeling procedures, each with a varying degree of approximation, can be found in the literature. Early theoretical treatments of evaporative condensers are given by Goodman [1], Thomsen [2] and Wile [3]. The models developed in these papers assumed a constant spray water temperature. Parker and Treybal [4] realized that the assumption of constant water temperature caused the mathematical equations of the model to become inconsistent, thus, giving a meaningless answer. They reported a detailed experimental study to define the heat and mass transfer coefficients in the fluid cooler. The main assumptions made in the derivation of the model are:

1. The Lewis relation applies. This relation cannot be analytically proved but has been experimentally verified for air-water systems.
2. The enthalpy of the saturated moist air is a linear function of temperature over the whole range of bulk water and air-water interface temperatures in the unit.
3. The recirculation water flow rate is so large that changes in it due to evaporation can be neglected.

The final equations of this model are consistent and can be solved to give a simple analytical solution. Leidenfrost and Korenic [5] followed a development in their model similar to that of Parker and Treybal but stopped short of making the above three assumptions used by the latter. They also showed that the simultaneous heat and mass transfer processes in any type of evaporative condenser are very complex and solutions for proper design of a heat exchanger can only be obtained by iterative numerical methods. It was also predicted and shown by experiments that the amount of water sprayed onto a coil to produce complete wetting is sufficient for maximum performance of the condenser. Increasing this amount to even deluging rates will not increase the performance.

Mizushina et al. [6] determined various transfer coefficients in an evaporative cooler. The coefficients were not well defined and were determined by fitting the test data to empirical log-mean temperature differences that used average water and tube-wall temperatures. The coefficients determined in this manner differ from those determined by Parker and Treybal and this is not surprising as the transfer coefficients were defined differently in the two cases. Mizushina et al. [7] developed two different rating methods for evaporative coolers, one a numerical technique and the other a simpler analytical model based on the assumption of constant water temperature. Finlay and Grant [8]

showed that this assumption might lead to errors in excess of 30 percent under certain conditions, for example in large tube banks. A rating method based on cooling tower procedures was proposed by Tezuka et al. [9]. The assumptions made in this model are not as accurate as those used in the model of Parker and Treybal nor is the model simple. Kays [10] determined the heat transfer coefficient during laminar flow ($Re_f < 2300$) inside a duct with a constant wall temperature whereas Gnielinski [11] determined the same for turbulent regime. For the latter case, the friction factor for smooth tubes was defined by Fliouenko [12]. Chato [13] proposed an equation to determine the condensation heat transfer coefficient in essentially horizontal tubes but this was only valid for relatively low vapor velocities ($Re_v < 35000$) at the tube inlet. Shah [14], however, predicted the same for higher vapor velocities.

Finlay and Grant [15] simplified the equations describing the mass transfer in an evaporative cooler by assuming that the vapor pressure of saturated moist air is a linear function of temperature. The model can be expected to be very accurate, as this is the only major assumption made in the derivation. The final design equations are very complicated, however, and require a numerical solution. Peterson et al. [16] developed a simple analytical method to predict the performance of evaporative condensers, based on the method of Parker and Treybal. The transfer coefficients of the model were predicted from standard correlation. They also conducted field tests on an evaporative condenser. The measured and predicted heat loads and recirculating water temperature were compared.

Webb [17] performed a unified theoretical treatment for thermal analysis of cooling towers, evaporative condensers and evaporative fluid coolers. In this paper,

equations and correlations are discussed for calculation of the heat and mass transfer coefficients in each type of exchanger. Specific calculation procedures are outlined for sizing and rating each type of evaporative heat exchanger. Webb and Villacres [18] describe three computer algorithms that have been developed to perform rating calculations of three evaporatively cooled heat exchangers. The algorithms are particularly useful for rating commercially available heat exchangers at off-design conditions. The heat and mass transfer “characteristic equation” of a particular heat exchanger is derived from the manufacturer’s rating data at the design point. Dreyer [19] presented various mathematical models for the thermal evaluation of evaporative coolers and condensers. These models ranged from the exact model based on Poppe [20] to the simplified models of Mizushima et. al. [6,7].

2.2 WET COOLING TOWERS

The theoretical analysis of wet cooling towers has a long history, which has led to an excessively large number of publications. A complete review of the origin and history of technical papers dealing with cooling tower is surveyed by Baker [21]. He evaluated different suggestions of coupling heat and mass transfer in a single driving force. He reported that Coffey and Horne [22] proposed and proved that cooling tower performance depends on the wet-bulb temperature of the ambient air, which is the lower limit of cooling. They obtained a single driving force based on vapor pressure at the wet-bulb temperature. Merkel [23], however, apparently first developed the practical theory of cooling tower operation. His theory has been the basis of most cooling tower analysis, e.g. Nottage [24], Lichtenstein [25], Mickley [26], Carey [27] and Webb [17], which is outlined in somewhat more detail in ASHRAE Equipment Guide [28]. It is important to

note that the formulation and implementation of Merkel's theory in cooling tower design and rating is presented and discussed in detail throughout most unit operations and process heat transfer textbooks. Extensive sets of curves for cooling tower design, based on Merkel's theory, have been prepared by the ASHRAE [29]. In Merkel's theory, the sensible heat transfer because of temperature difference and the latent heat flow due to evaporation are lumped together and a single driving force for total heat transfer and a unique transfer coefficient are used. This driving force is the difference between the enthalpy of the saturated air at the interface and the enthalpy of the humid air stream. The basic postulations and approximations that are inherent in Merkel's theory may be summarized as: the resistance for heat transfer in the liquid film is negligible, the mass flow rate of water per unit of cross sectional area of the tower is constant (there is no loss of water due to evaporation), the specific heat of the air-stream mixture at constant pressure is the same as that of the dry air, and the Lewis number for humid air is unity. Sutherland [30] performed a more rigorous analysis of a cooling tower that did not utilize the assumptions of Merkel. He found that counter-flow cooling towers could be undersized between 5 to 15% through the use of the Merkel method if "true" mass transfer coefficients are used and that the underestimation of tower volume provided by the approximate analysis increases with increasing value of mass flow rate ratio. He also studied the effect of variation of atmospheric pressure on cooling towers to a certain extent and showed that the NTU increase with increasing pressure. Nahavandi et al. [31] showed that ignoring the evaporation losses introduces an error in the Merkel's results, which is not conservative, and may reach up to 12% depending on design conditions. On the other hand, Baker (1984) cited that the effect of water evaporation is relatively small and varies with the operating conditions and gives a value for number of transfer units

(NTUs) that are 1.34 percent low. Threlkeld [32] and Webb [17] have also studied the effect of water evaporation. Though, Gosi [33] developed a simple method and chart for the determination of evaporation loss of wet cooling towers. In practice, however, the errors are not nearly as large, because the mass transfer coefficients utilized in the Merkel method are generally determined by matching results of the model to measurements from small-scale tests. Another approach for modeling cooling towers was presented by Whiller [34]. He developed a simple method for correlating performance data. However, this method is not useful for design purpose. Another source of errors that has been examined is the resistance to heat transfer in the water film and the non-unity values of the Lewis number. Jefferson [35], Stevens et al. [36] and Raghavan [37] introduced an adjustment coefficient to account for the effect of the actual value of the Lewis number. Sadasivam and Balakrishnan [38] initiated a new definition of enthalpy, thereby obviating the need to invoke the Lewis relation. Yadigaroglu and Pastor [39] proved that the approximations inherent in the Merkel equation contribute to the overall error. Fortunately, these errors tend to cancel each other. Webb [17] stated that none of the available analysis is totally satisfactory in calculating the error of the Merkel's analysis. He pointed out that a more complete, systematic analysis for a range of practical interest would be of value.

Mohiuddin and Kant [40-41] described a detailed methodology for the thermal design of wet, counter flow and cross flow types of mechanical and natural draught cooling towers. In part I of their paper, different steps of cooling tower design are discussed. The steps include selection of cooling tower; determination of tower characteristic ratio; computation of moist air properties; determination of the ratio of the

water-to-air loading; integration procedure for the tower characteristic ratio. In part II of their paper, the following design steps were discussed: the fill or packing, natural draught tower, fan design for a mechanical draught cooling tower, blowdown and make-up water rate, water distribution systems and drift eliminators. Dreyer and Erens [42] developed a mathematical model to study the performance characteristics of counter-flow cooling towers having splash pack type fill material. The one-dimensional model uses basic aerodynamic, hydrodynamic and heat/mass transfer information to predict the performance of the packing material without depending on the cooling tower test data. The predicted transfer characteristics and pressure drop data obtained with the simulation program are compared with the experimental data. It is reported that the model predicts the correct trends for both the transfer characteristics and the pressure drop across the packing material. Simpson and Sherwood [43] published experimental data for six different types of packing materials, used in counter current cooling towers. The data is used for rating and design calculations of cooling tower.

Berman [44] described how the “log-mean enthalpy method” (LMED) might be applied to cooling tower design. He also developed a correction factor to account for the curvature of the saturated air enthalpy curve. In their 1940 publication, London et al. [45] introduced definitions of NTU to use in plotting tower test data. However, these definitions are not generally consistent with the basic definitions used today in heat exchanger design literature. They developed empirical curve fits of their curves for design purpose. Moffatt [46] is apparently the first to derive the effectiveness-NTU equation for a counter flow-cooling tower. Jaber and Webb [47] presented an analysis that shows how the theory of heat exchanger design may be applied to cooling towers. The effectiveness-NTU definitions are in precise agreement with those used for the heat exchanger design,

and are applicable to a cooling tower operating conditions. Braun et al. [48] presented effectiveness models for cooling towers and cooling coils. The models utilize existing effectiveness relationships developed for sensible heat exchangers with modified definitions of number of transfer units and the fluid capacitance rate ratio. Results of the models were compared with the results of more detailed numerical solutions to the basic heat and mass transfer equations and with experimental data of Simpson and Sherwood (1946). El-Dessouky et al. [49] presented a solution for the steady-state counter-flow wet cooling tower with new definitions of tower effectiveness and number of transfer units. They have also considered the resistance of the heat transfer in the water film, non-unity of the Lewis number, and the curvature of the saturated air enthalpy versus the temperature curve. Khan and Zubair [50], however, showed that the model of El-Dessouky et al., when compared to a detailed model, showed appreciable difference when the Lewis number was not taken as unity.

The modeling of the spray and rain zones of the cooling tower is much more complex as compared to its major portion. Dreyer [51] used the concept of packets to allow drops of similar diameter; temperature and velocity to be lumped together and assumed an initial drop size distribution, so that the spray and rain zones could be included in rating and design calculations of the tower. It was noted that since dripping forms the drops in the rain zone, they could be up to 8 or 9 mm in diameter. An experiment was also performed to measure drop velocity at different heights. De Villiers and Kroger [52] developed relations for various geometries and configurations and explained that the mass transfer relation could be used to calculate an effective drop diameter i.e. a diameter that would have the same effect as the actual ensemble of drops in the tower. Fisenko [53] developed a mathematical model describing evaporative cooling

of water droplets. It was explained that an experimental measurement could be used to estimate the effective drop diameter and that the model could be used to evaluate both the spray and rain zones. Although various researchers measured and correlated experimental transfer characteristic data for different types of splash pack e.g. Lowe and Christie [54], Cale [55] and Johnson [56], the size of the spray and rain zones was not given.

This study is aimed at investigating the impact of fouling on the design and rating of cooling towers, evaporative condensers and evaporative fluid coolers using experimental data available in the literature. The efficiency of any mechanical device is invariably related to its design and thus, these heat exchangers are studied, using the concept of exergy analysis. Due to its wide range of applications and easy installation, these devices find place in various parts of the world. Thus, the effect of pressure (elevation) on different parameters is also explored in detail. A comprehensive sensitivity analysis is also performed to estimate the effect of various input parameters on the response variables such as effectiveness. The Air-water vapor interface temperature is difficult to determine and often the assumption that this temperature is the same as the bulk water temperature is employed. The effect of air-water vapor interface resistance is studied to better understand the resulting temperature profile. Furthermore, water evaporation rate under a wide range of operating conditions is investigated.

CHAPTER 3

MATHEMATICAL FORMULATION

In this chapter, the modeling procedure of the evaporative heat exchangers is discussed. The major assumptions that are used to derive the basic modeling equations may be summarized as follows:

- i) The system is in a steady state.
- ii) The apparatus and the cooling water re-circulating circuit are insulated from the surroundings.
- iii) Uniform and complete surface wetting of the tube bundle or packing.
- iv) Uniform airflow rate over the cross-sectional area.
- v) Radiation heat transfer can be ignored.
- vi) Water lost by drift is negligible.
- vii) The heat and mass transfer coefficients are constant within the tube bundle or packing.
- viii) The distribution of air and water is uniform at the inlets and this uniformity is maintained. Thus, the temperatures in the unit will only depend on the vertical position in the unit, which implies the model is one-dimensional.
- ix) The interfacial effective area per unit volume is assumed equal to the dry tubes' effective area per unit volume for the fluid cooler and condenser.
- x) No sub-cooling or superheating of the refrigerant assumed.

3.1 EVAPORATIVE FLUID COOLERS AND CONDENSERS

As mentioned earlier the design theory of evaporative condensers and evaporative fluid coolers is closely related. The primary difference between the condenser and the fluid cooler is that the refrigerant temperature is constant in the condenser, whereas the fluid temperature may change in the fluid cooler. Figures 3.1 and 3.2 show an infinitesimal control volume of the basic model for the evaporative fluid cooler and evaporative condenser, respectively. Figures 3.3 and 3.4 show the temperature gradients of the fluids for an arbitrary height of the heat exchangers. As shown by arrows, the process fluids and the cooling water flow from the top to the bottom of the column while air flows in the opposite direction. The cooling water is re-circulated for reuse. Energy is transferred from the process fluid through the tube wall and into the water. From here the energy is transferred into air due to temperature gradients and evaporation. The assumptions and basic equations employed here closely follow those of Mizushima et al. [7], Webb [17] and Dreyer [19].

3.1.1 Mass balance equations

The water mass balance, for both the evaporative cooler and condenser, yields

$$\dot{m}_a W + \dot{m}_w + \left(\frac{\partial \dot{m}_w}{\partial A} \right) dA = \dot{m}_w + \dot{m}_a \left[W + \left(\frac{\partial W}{\partial A} \right) dA \right] \quad (3.1)$$

Simplifying, we get

$$\frac{\partial W}{\partial A} = \frac{1}{\dot{m}_a} \frac{\partial \dot{m}_w}{\partial A} \quad (3.2)$$

The mass flow of recirculating water evaporating into air, in terms of the mass-transfer coefficient, h_D , for both the evaporative cooler and condenser, is given as

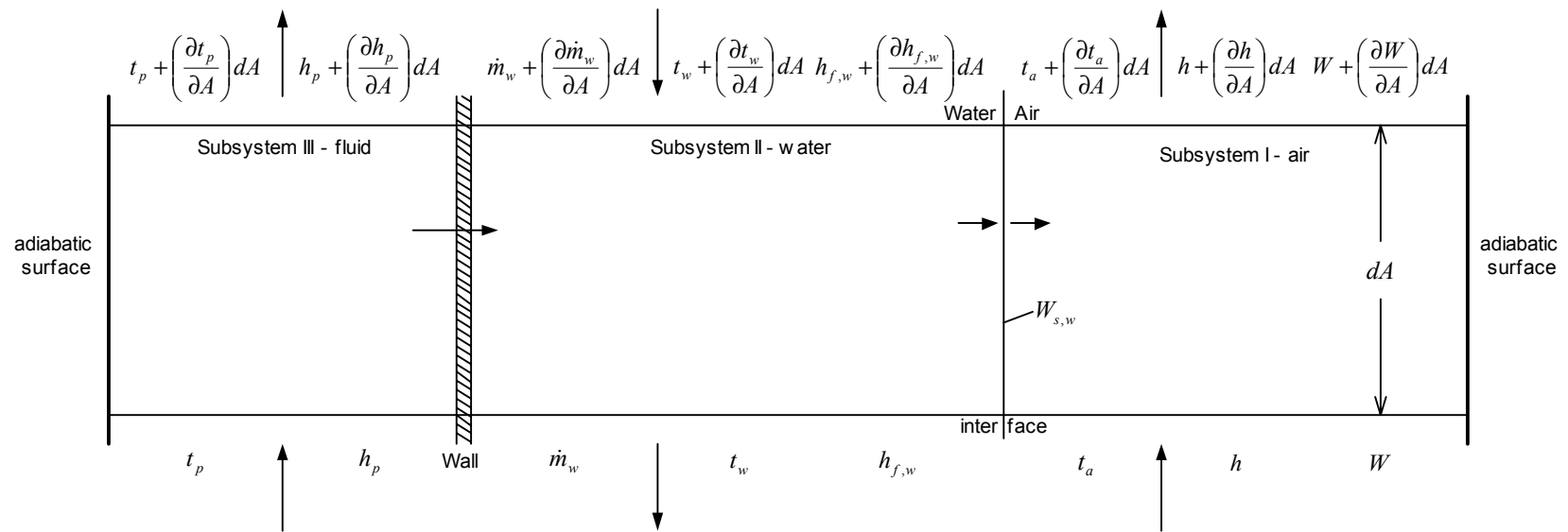


Figure 3.1: Infinitesimal control volume of the basic model for an evaporative fluid cooler

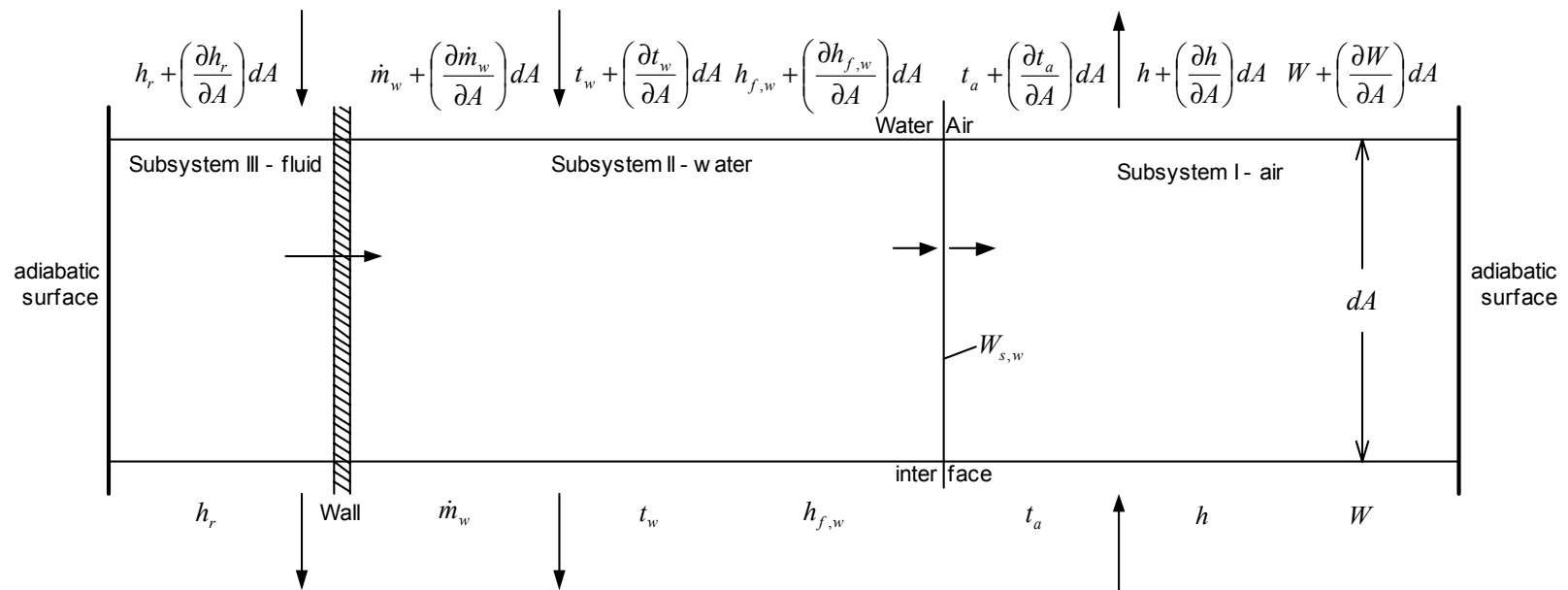


Figure 3.2: Infinitesimal control volume of the basic model for an evaporative condenser

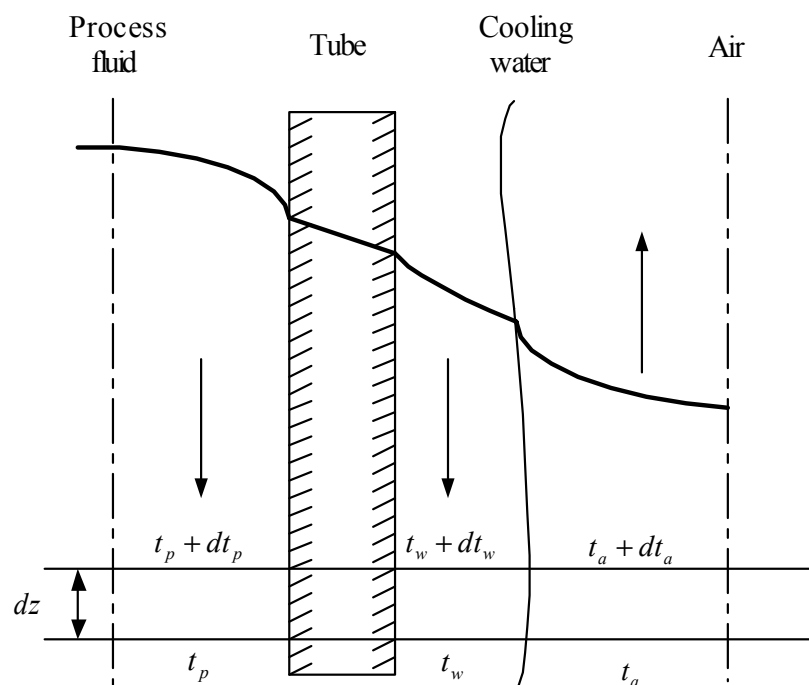


Figure 3.3: Schematic representation of temperature gradients on process tubes in an evaporative fluid cooler

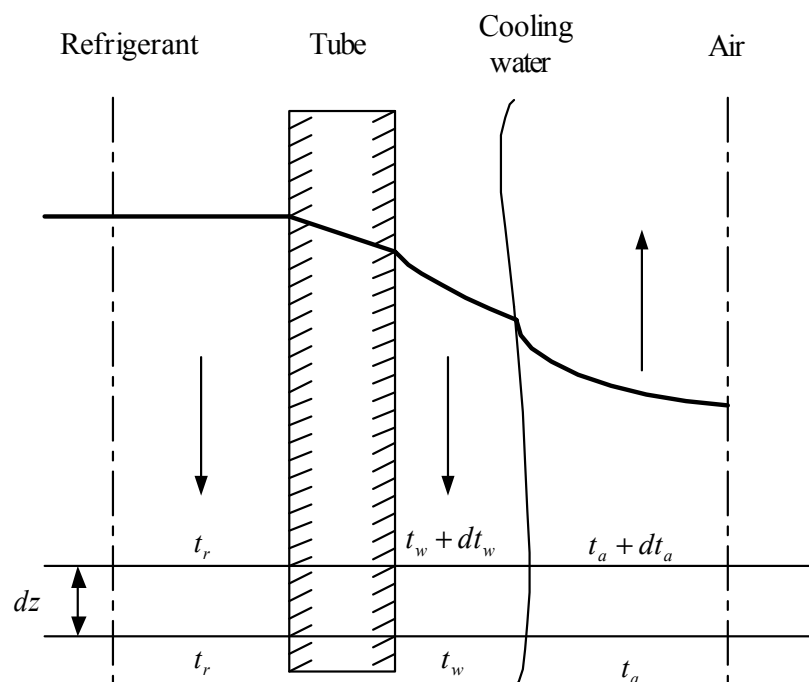


Figure 3.4: Schematic representation of temperature gradients on process tubes in an evaporative condenser

$$\dot{m}_w + \left(\frac{\partial \dot{m}_w}{\partial A} \right) dA = \dot{m}_w + h_D (W_{s,int} - W) dA \quad (3.3)$$

After simplification, we get

$$d\dot{m}_w = h_D (W_{s,int} - W) dA \quad (3.4)$$

3.1.2 Energy balance equations

In the evaporative cooler and condenser, at the air-water interface, simultaneous heat and mass transfer takes place that can be expressed as

$$\dot{m}_a \left[h + \left(\frac{\partial h}{\partial A} \right) dA \right] = \dot{m}_a h + h_c (t_{int} - t_a) dA + h_D (W_{s,int} - W) h_{fg,int} dA \quad (3.5)$$

Simplifying, we get

$$\dot{m}_a dh = h_c (t_{int} - t_a) dA + h_D (W_{s,int} - W) h_{fg,int} dA \quad (3.6)$$

For the evaporative cooler, the overall energy balance on the process fluid can be written as follows:

$$\dot{m}_p h_p = \dot{m}_p \left[h_p + \left(\frac{\partial h_p}{\partial A} \right) dA \right] + U_{os} (t_p - t_{int}) dA \quad (3.7)$$

If the enthalpies of the water and process fluid are written as

$$\frac{\partial h_{f,w}}{\partial A} = c_{p,w} \left(\frac{\partial t_w}{\partial A} \right); \quad \frac{\partial h_p}{\partial A} = c_{p,p} \left(\frac{\partial t_p}{\partial A} \right) \quad (3.8)$$

Then substituting Eq. (3.8) in Eq. (3.7) and simplifying, we get

$$dt_p = - \frac{U_{os}}{\dot{m}_p c_{p,p}} (t_p - t_{int}) dA \quad (3.9)$$

where U_{os} is the time-dependent (due to fouling) overall heat transfer coefficient.

The overall energy balance on the control volume for the evaporative cooler gives

$$\dot{m}_a h + \left[\dot{m}_w + \left(\frac{\partial \dot{m}_w}{\partial A} \right) dA \right] \left[h_{f,w} + \left(\frac{\partial h_{f,w}}{\partial A} \right) dA \right] + \dot{m}_p h_p = \dot{m}_a \left[h + \left(\frac{\partial h}{\partial A} \right) dA \right] + \dot{m}_w h_{f,w} + \dot{m}_p \left[h_p + \left(\frac{\partial h_p}{\partial A} \right) dA \right] \quad (3.10)$$

Simplifying and applying equation (3.8), we get

$$dt_w = \frac{1}{\dot{m}_w c_{p,w}} \left[\dot{m}_a dh - c_{p,w} t_w d\dot{m}_w + \dot{m}_p c_{p,p} dt_p \right] \quad (3.11)$$

Following a similar approach with regard to the overall energy balance on the control volume for the evaporative condenser gives

$$dt_w = \frac{1}{\dot{m}_w c_{p,w}} \left[\dot{m}_a dh - c_{p,w} t_w d\dot{m}_w - \dot{m}_r dh_r \right] \quad (3.12)$$

Applying a similar procedure to the evaporative condenser as was used to formulate equation (3.7), keeping in mind that the enthalpy changes but the fluid temperature remains constant and also the direction of flow of the fluid, we get

$$dh_r = \frac{U_{os}}{\dot{m}_r} (t_r - t_w) dA \quad (3.13)$$

It should be noted that, here, the fluid is a refrigerant which is not the case for an evaporative cooler. Based on outside surface area of the tubes, the overall heat transfer coefficient U_{os} , as a function of time, is given by

$$\frac{1}{U_{os}(t)} = \left[\frac{1}{h_{c,is}} \right] \frac{d_{t,os}}{d_{t,is}} + \left(\frac{d_{t,os}}{2k_t} \right) \ln \left[\frac{d_{t,os}}{d_{t,is}} \right] + \frac{1}{h_{c,w}} + R_f(t) \quad (3.14)$$

3.1.3 Final system of equations

Dreyer [19] simplified equation (3.6) into the form below (See Appendix A):

$$dh = \frac{h_D dA}{\dot{m}_a} \left[(h_{s,int} - h) + \left[\frac{h_c}{h_D c_{p,a}} - 1 \right] \left\{ (h_{s,int} - h) - (W_{s,int} - W) h_{g,int} \right\} \right] \quad (3.15)$$

where $c_{p,a}$ is the specific heat of the mixture and $h_{g,int}$ is specific enthalpy of water vapor evaluated at the interface temperature, t_{int} . These terms are defined as,

$$c_{p,a} = c_{p,da} + Wc_{p,v} \quad (3.16)$$

$$h_{g,int} = h_g^0 + c_{p,v}t_{int} \quad (3.17)$$

If Lewis number is taken as unity, then after simplification, we get

$$dh = \frac{h_D}{\dot{m}_a} (h_{s,int} - h) dA \quad (3.18)$$

where $h_{s,int}$ is the enthalpy of saturated air at the air-water interface temperature. Equation (3.18) may be integrated between its entering and leaving states to give

$$\frac{h_D A}{\dot{m}_a} = \int_{h_{in}}^{h_{out}} \frac{dh}{(h_{s,int} - h)} = NTU \quad (3.19)$$

The numerical value of the above integral is typically defined as the “number of transfer units” (NTU). The NTU is a measure of the air-water interface area required to affect the required heat transfer duty. The required NTU is analogous to the value UA/\dot{C}_{min} typically used in heat exchanger design, where \dot{C}_{min} is the smaller value where \dot{C}_{min} is the smaller value of $\dot{m}c_p$ of the two fluids passing through the heat exchanger. In order to integrate equation (3.19), it is necessary to evaluate the local value of $(h_{s,int} - h)$ along the airflow path. Two additional equations are required for this purpose. The first is an energy balance that defines the local mixed air enthalpy as a function of the local fluid temperature (the media to be cooled). The second equation relates the local air enthalpy at the interface ($h_{s,int}$) to the bulk air enthalpy at the local fluid temperature. These equations are discussed in the following paragraphs.

In equation (3.11), the term $(\dot{m}_w c_{p,w} dt_w)$ accounts for the local enthalpy change of the water film as it passes over the tube bundle. In the upper region of the tube bundle, the water film is heated and then it is cooled in the lower part of the bundle. Equation (3.11) shows that some of the heat removed from the fluid goes to heating (or cooling) the water film. Equations (3.2) & (3.4) indicate that the mass flow rate does not remain constant as some of the water evaporates. Although these equations are usually discarded since only a few percent of water is evaporated, they are maintained here for higher accuracy. Such an assumption would have produced a slightly smaller water enthalpy and temperature along its path. Now, if the temperature of the interface film is considered the same as the bulk water temperature, then all the terms with the subscripts (s, int) will be replaced by (s, w). This approach was used in the current work. Webb [17], however, assumed that t_w is nearly equal to $(t_{\text{int}} + 0.5)$.

The heat and mass transfer coefficients must be known in order to solve the controlling equations. The coefficients of interest are h_D , $h_{c,w}$ and $h_{c,f}$. Mizushima et al. [6] developed a correlation for $h_D A'_V$ based on their tests of four tube bundles with $d_{t,os} = 12.7, 19.05$ and 40 mm where $d_{t,os}$ is the outside diameter of the tube. Their correlation may be written as [17]

$$\frac{h_D A'_V}{G_a} = 2.54 \times 10^{-2} \text{Re}_a^{-0.1} \text{Re}_w^{0.15} d_{os}^{-1.6} \quad (3.20)$$

where the data spanned $50 < \text{Re}_w < 240$ and $1.2 < \text{Re}_a \times 10^{-3} < 14$. It should be noted that h_D is the mass transfer coefficient based on $(h_{s,w} - h)$ where it is assumed that the air-water interface is at the bulk water temperature t_w and $h_{s,w}$ is the saturated air enthalpy at

bulk water temperature. For typical flow geometry and operating conditions, Webb [17] discussed that t_w should be not more than $0.5 \text{ } ^\circ\text{C}$ greater than t_{int} . The water film coefficient, $h_{c,w}$, required in solving equation (3.14) was measured by Mizushina et al. [6] for 12.7, 19.05 and 40 mm diameter tubes. It is given by

$$h_{c,w} = 2102.9(\Gamma/d_{t,os})^{1/3}, \quad 0.195 < (\Gamma/d_{t,os}) < 5.556 \quad (3.21)$$

where $\Gamma = (\dot{m}_{w,in} d_{t,os}) / (2n_{tr} \hat{P}_t L)$

where Γ is the water-film flow rate per unit tube length. The following typical values for the heat transfer coefficients may be considered [17]

1. $h_{c,p} = 7400 \text{ W/m}^2 \text{ } ^\circ\text{C}$ (for water)
2. $h_{c,p} = 4000 \text{ W/m}^2 \text{ } ^\circ\text{C}$ (for 50 % glycol)
3. $h_{c,r} = 3400 \text{ W/m}^2 \text{ } ^\circ\text{C}$ (for R-22)

However, the correlations given by [6, 10-14], for convective and condensation heat transfer coefficients inside the tubes as well as the mass transfer and the film heat transfer coefficients outside the tubes, were used.

The dimensionless temperature, for each, is defined as shown below. The effectiveness of the evaporative fluid cooler and condenser were defined as the ratio of actual energy to the maximum possible energy transfer from the fluid in the tubes and were given by the following equations:

$$\mathcal{E}_{efc} = \frac{t_{p,in} - t_{p,out}}{t_{p,in} - t_{wb,in}}; \quad R_{efc} = \frac{t_{p,in} - t_{p,out}}{t_{p,in} - t_w} \quad (3.22 \text{ a,b})$$

$$\mathcal{E}_{ec} = \frac{h_{r,in} - h_{r,out}}{h_{r,in} - h_{wb,in}}; \quad R_{ec} = \frac{t_r - t_w}{t_r - t_{wb,in}} \quad (3.23 \text{ a,b})$$

The effectiveness of the evaporative cooler and condenser are based on the logic that the lowest possible temperature achievable for the fluid is the wet bulb temperature. Regarding the evaporative condenser, Ettouney et al. [57] explained that the maximum amount of heat removed from the condenser occurs as the condensate temperature cools to the wet bulb temperature of the air.

The system of five differential equations describing the operation of the evaporative fluid cooler is given by equations (3.2), (3.4), (3.9), (3.11) and (3.18). The system of five differential equations describing the operation of the evaporative condenser is given by equations (3.2), (3.4), (3.12), (3.13) and (3.18). The above equations will be solved numerically under different operating conditions to address the problems related to design and performance evaluation of evaporative coolers and condensers.

3.2 COOLING TOWERS

As mentioned earlier, the cooling tower is one of the most important evaporative heat exchangers in use today. The main physical difference from the evaporative fluid cooler and condenser, mentioned in the previous section, is that heat is rejected by evaporation, from a gravity-drained water film into air flowing through a cooling tower “packing” instead of tube bundles. As before, water flows from top to bottom and air flows in the opposite direction. Though the cooling tower is basically divided into three parts i.e. spray zone, packing and rain zone, we discuss here only the modeling procedure for the packing. Details regarding the modeling of the other two zones will be discussed in chapter 4. It is assumed that the heat-mass transfer analogy applies and the representative value of the Lewis number is assumed to be 0.9. Since there is no third fluid involved,

subsystem III of Figure 3.1 is ignored in regards to the modeling of cooling towers as shown in Figure 3.5.

3.2.1 Mass balance equations

Now, the air-side water vapor mass balance at steady-state can be written as follows:

$$\dot{m}_a W + h_D A_V (W_{s,w} - W) dV = \dot{m}_a \left[W + \left(\frac{\partial W}{\partial V} \right) dV \right] \quad (3.24)$$

Simplifying, we get

$$\dot{m}_a dW = h_D A_V (W_{s,w} - W) dV \quad (3.25)$$

3.2.2 Energy balance equations

The overall energy balance of moist air can be expressed as:

$$\dot{m}_a h + h_c A_V (t_w - t_a) dV + h_D A_V \cdot h_{fg,w} (W_{s,w} - W) dV = \dot{m}_a \left[h + \left(\frac{\partial h}{\partial V} \right) dV \right] \quad (3.26)$$

Simplifying, we get

$$\dot{m}_a dh = h_c A_V (t_w - t_a) dV + h_D A_V \cdot h_{fg,w} (W_{s,w} - W) dV \quad (3.27)$$

The overall energy balance of water in terms of the heat and mass-transfer coefficients yields:

$$\left[\dot{m}_w + \left(\frac{\partial \dot{m}_w}{\partial V} \right) dV \right] \left[h_{f,w} + \left(\frac{\partial h_{f,w}}{\partial V} \right) dV \right] = \dot{m}_w h_{f,w} + h_c A_V (t_w - t_a) dV + h_D A_V \cdot h_{fg,w} (W_{s,w} - W) dV \quad (3.28)$$

Simplifying, we get

$$\dot{m}_w dh_{f,w} + \dot{m}_a dW \cdot h_{f,w} = h_c A_V (t_w - t_a) dV + h_D A_V \cdot h_{fg,w} (W_{s,w} - W) dV \quad (3.29)$$

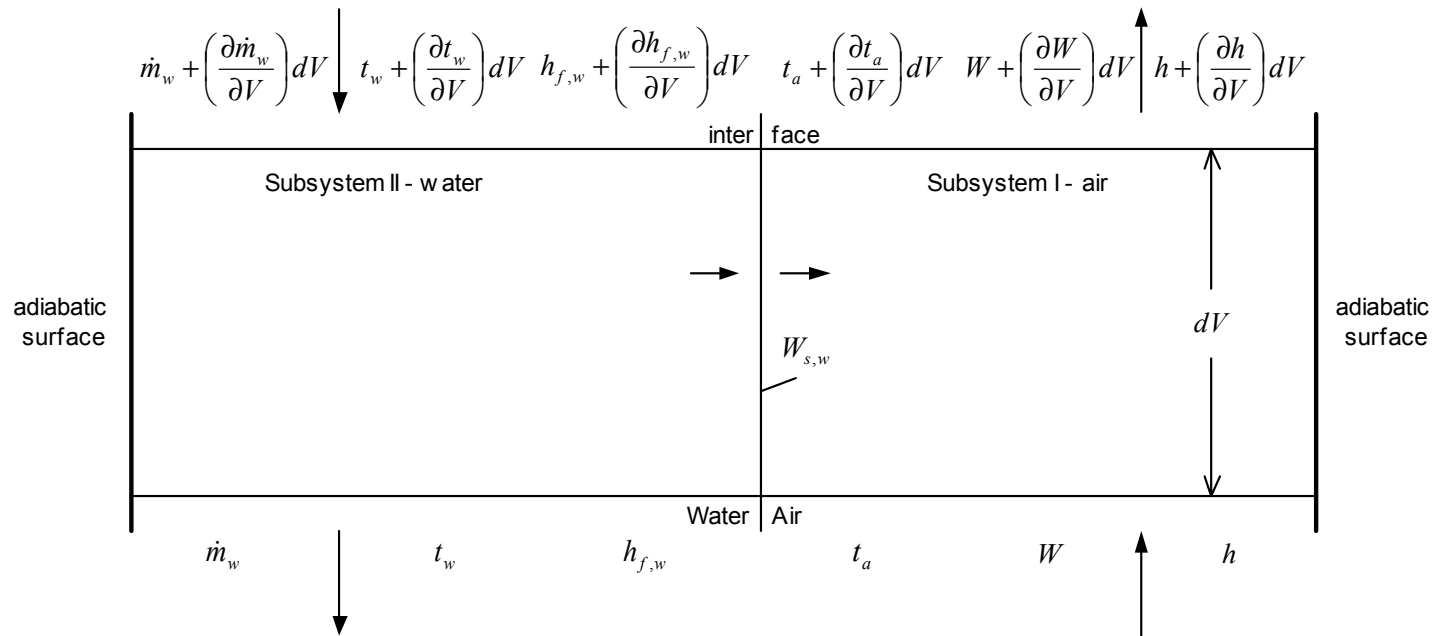


Figure 3.5: Infinitesimal control volume of the basic model for cooling tower

3.2.3 Final system of equations

Now, equating (3.27) and (3.29), we get the energy balance between the air and water,

$$\dot{m}_a dh = \dot{m}_w dh_{f,w} + \dot{m}_a dW h_{f,w} \quad (3.30)$$

It should be noted that the last term in the above equation represents the effect of water evaporation on the energy equation and \dot{m}_w is the water flow rate at any height of the tower. In most cases, the decrease in the water flow rate is not considered since only a few percent of water is evaporated [29] and $\dot{m}_w = \dot{m}_{w,in} = \dot{m}_{w,out}$ but it is included in the current analysis for greater accuracy. If this decrease is taken into account with respect to the water flow rate at the outlet, then

$$\dot{m}_a dh = [\dot{m}_{w,out} - \dot{m}_a (W_{in} - W)] dh_{f,w} + \dot{m}_a dW h_{f,w} \quad (3.31)$$

Now, by substitution of $Le = h_c / h_D c_{p,a}$ in equation (3.27), we obtain

$$\dot{m}_a dh = h_D A_V dV [Le c_{p,a} (t_w - t_a) + (W_{s,w} - W) h_{fg,w}] \quad (3.32)$$

Combining equations (3.25) and (3.32), we get

$$\frac{dh}{dW} = Le c_{p,a} \frac{(t_w - t_a)}{(W_{s,w} - W)} + h_{fg,w} \quad (3.33)$$

Using the approximation of constant $c_{p,a}$, we have

$$h_{s,w} - h = c_{p,a} (t_w - t_a) + h_g^0 (W_{s,w} - W) \quad (3.34)$$

Equation (3.33) may then be written as

$$\frac{dh}{dW} = Le \frac{(h_{s,w} - h)}{(W_{s,w} - W)} + (h_{fg,w} - h_g^0 Le) \quad (3.35)$$

Noting that $dh_{f,w} = c_{p,w} dt_w$ and substituting this into equation (3.31), then manipulating the result as well as equations (3.25) and (3.35) after dividing by dt_w , so that water temperature is the integration variable, we get

$$\frac{dW}{dt_w} = \frac{1}{h_{f,w}} \left[\frac{dh}{dt_w} - \frac{(\dot{m}_{w,out} - \dot{m}_a (W_{in} - W)) \cdot c_{p,w}}{\dot{m}_a} \right] \quad (3.36)$$

$$\frac{dV}{dt_w} = \frac{\dot{m}_a}{h_D A_V} \left[\frac{1}{(W_{s,w} - W)} \right] \frac{dW}{dt_w} \quad (3.37)$$

$$\frac{dh}{dt_w} = \left[Le \frac{(h_{s,w} - h)}{(W_{s,w} - W)} + (h_{fg,w} - h_g^0 Le) \right] \frac{dW}{dt_w} \quad (3.38)$$

The mass transfer coefficient is unknown but it is usually correlated in the form [29]

$$\frac{h_D A_V V}{\dot{m}_{w,in}} = c \left(\frac{\dot{m}_{w,in}}{\dot{m}_a} \right)^n \quad (3.39)$$

where c and n are empirical constants specific to a particular tower design. Multiplying both sides of the above equation by $(\dot{m}_{w,in} / \dot{m}_a)$ and considering the definition for NTU gives the empirical value of NTU as

$$NTU_{em} = \frac{h_D A_V V}{\dot{m}_a} \Big|_{em} = c \left(\frac{\dot{m}_{w,in}}{\dot{m}_a} \right)^{n+1} \quad (3.40)$$

The coefficients c and n in the above equation were fitted to the measurements of Simpson and Sherwood [43] for four different tower designs over a range of performance conditions by Braun et al. [48]. Also, the dimensionless temperature and effectiveness, for the cooling tower, were defined as given below [50], where the effectiveness of the cooling tower is the ratio of actual energy to maximum possible energy transfer.

$$\varepsilon_{ct} = \frac{h_{out} - h_{in}}{h_{s,w} - h_{in}}; \quad R_{ct} = \frac{t_{w,in} - t_{w,out}}{t_{w,in} - t_{wb,in}} \quad (3.41 \text{ a,b})$$

The system of three differential equations describing cooling tower operation is given by equations (3.36), (3.37) and (3.38) with equation (3.40) used to calculate the mass transfer coefficient. These will be solved numerically under different operating conditions to address the problems related to design and performance evaluation of cooling towers.

CHAPTER 4

SPRAY AND RAIN ZONE

In a counterflow cooling tower, the hot process water, which is to be cooled, is sprayed into an upward flowing air stream using a number of nozzles. Nozzles are arranged in such a manner that the distribution of water entering the fill is uniform. Since the spray produced in a cooling tower obviously depends on the type of nozzle employed, non-uniformity of flow, for instance, occurs where nozzles producing circular spray patterns with radial variation overlap patterns of the sprays from adjacent nozzles. Due to heat and mass transfer, the water temperature is reduced while the air enthalpy is increased because the air is heated and saturated by the water as it rises. Furthermore, the additional heating of air by the heat transferred from the droplets in the spray zone increases the velocity of convective airflow in the cooling tower and results in an increase in the intensity of evaporative cooling in the fill packing. Up to 15 percent of the cooling may actually occur in the spray zone. The spray may be directed downwards or upwards. In the latter case, the longer residence time improves the transfer process in the spray zone. The lightest drops (less than about 0.3mm in diameter) are carried upwards by the air to the droplet eliminators where most are collected and returned downwards to the fill in the form of larger drops. The typical height from the nozzle to the top of the fill is about 18". This is the height normally required for the spray pattern to develop. Using a

greater number of smaller nozzles could lessen the distance but the cost and tendency to plug up increase. It is noted that, generally, this height is regardless of a tower's capacity.

The rain zone is required on a conventional tower to permit airflow into the fill. Unfortunately, from a thermal perspective, this is a very inefficient portion of the cooling tower. Observations show that the droplets and jets in the rain zone are formed due to dripping of water from the sheets of the fill. Therefore, the radius of the droplets is quite large. Relatively small droplets will not enter the rain zone due to reasons explained above. The cooling achieved in one foot of fill can be more than the cooling in ten feet of free-fall water and, as a consequence, is a very ineffective use of pump energy. The rain zone is the least efficient area and is only as large as necessary to allow even airflow. For blow through towers, it tends to be bigger to make room for the fans. Though a significant part of the total heat and mass transfer in large counterflow cooling towers occurs in the rain zone below the packing, this is not the case for small-sized towers. Large counterflow wet-cooling towers usually have a rain zone beneath the fill in which ten to twenty percent of the total heat that is rejected by the tower may occur. In view of this considerable contribution to the overall performance, knowledge of the characteristics of the rain zone is important for reliable prediction of the total performance. For a typical 100 ton blow through tower, the rain zone may be 36", the fill 36" and the spray zone 18". As the overall size of a tower increases, the fill would increase to as much as 54" and the rain zone height would increase proportional to air flow.

4.1 SUMMARY OF WORK BY DREYER, KROGER & FISENKO

Below is a summary of some important works found in the literature for evaluating the spray and rain zones.

4.1.1 Work by Dreyer

A one-dimensional mathematical model and computer simulation program was developed for the modeling of counterflow cooling towers. It used basic aerodynamic, hydrodynamic and heat-mass transfer information to accurately predict the performance of cooling towers, especially the splash pack, without depending on cooling tower test data. Such a model would make it possible to study the effects of different types of water distribution systems on the performance of a given pack. A model that correctly predicts the drop size and velocity distributions through the fill packing, would also allow accurate prediction of the performance of the rain zone below the pack.

It is, generally, not possible to model the cooling of a poly-disperse spray with a single representative drop size. Dreyer used the concept of packets to allow drops of similar diameter, temperature and velocity to be lumped together with each packet having a unique combination of these parameters. All the droplets in the rain zone (below a film pack) will be the result of dripping. The droplets formed by dripping could be up to 8 mm or 9 mm in diameter. To specify the number of drops per packet, the mass flow rate represented by each packet was used. In a practical rain zone, there is a wide distribution of droplet sizes. This distribution of drop sizes can best be described by a log-normal or Rosin-Rammler distribution function. He noted that the mathematical modeling of cooling of a poly-disperse spray of drops should be performed by dividing the water mass into different size zones and integrating each zone independently along the direction of the drop motion.

The numerical procedure required dividing the spray zone into a number of elements, considering the outlet air to be saturated and assuming the outlet enthalpy at the

top of the spray zone. From this and the known ambient condition, the mean air properties were calculated by using the properties from each end. These were used to determine the mean air velocity as

$$v_{a,m} = \frac{\dot{m}_{da}(1 + W_{a,m})}{\rho_{a,m} A_{fr}} \quad (4.1)$$

The initial drop size distribution formed by the water distribution system was then determined and number of packets with drop size range assumed. The initial velocity of the drops leaving the water distribution system was considered as zero with all drops at the same temperature $t_{w,in}$.

As mentioned above, the zone is divided into a certain number of elements. The mean drop velocity $v_{d,m}$ in the element was then calculated by assuming the drop velocity at the end of the element. The drop Reynolds number based on the relative velocity between the drop and the air was found as

$$\text{Re}_d = \frac{\rho_{a,m}(v_{d,m} + v_{a,m})d_d}{\mu_{a,m}} \quad (4.2)$$

There are two forces acting on a drop as it falls; namely, the gravitational force acting down and a drag force acting upwards. The drag coefficient experienced by the falling drop was calculated by using the formula below:

$$C_D = \frac{24}{\text{Re}_d}(1 + 0.173 \text{Re}_d^{0.657}) + \left(\frac{0.413}{1 + 16300 \text{Re}_d^{-1.09}} \right) \quad (4.3)$$

The upward drag force was found from the equation below

$$F_{D,up} = 0.5 \rho_{a,m} (v_{a,m} + v_{d,m})^2 A_{fr,d} C_D \quad (4.4)$$

and the downward force experienced by the drop was found as

$$F_{D,down} = \left(\frac{\pi d_d^3}{6} \right) (\rho_w - \rho_{a,m}) g \quad (4.5)$$

From the force balance, the average drop acceleration in the element was determined as

$$a = \frac{(F_{D,down} - F_{D,up})}{m_d} \quad (4.6)$$

The velocity of the drop leaving an element was found using the equation below. If this velocity did not match the assumed value of the outlet velocity for an element, the above procedure was repeated (using the currently calculated value of the outlet velocity as the assumed value) until convergence was achieved.

$$v_{d,out} = \sqrt{v_{d,in}^2 + 2a.dz} \quad (4.7)$$

If the terminal velocity of drops in a packet was found to be less than the upward moist air velocity, the mass of those drops was redistributed among the remaining packets since those drops would travel upwards. It was noted that these packets usually represented a very small mass flow rate, which resulted in a change in the velocity and temperature in the remaining packets that was not noticeable.

The total number of drops along with pressure drop in each packet in an element was then determined and the heat transfer coefficient on the outside of the drops found from the Ranz and Marshall correlation [58], i.e.

$$Nu_d = 2 + 0.6 Re_d^{0.5} Pr^{1/3} \quad (4.8)$$

The mass transfer coefficient was then calculated from the analogy between heat and mass transfer as follows

$$h_{D,d} = \frac{Nu_d k_{a,m}}{Le c_{p,a,m} d_d} \quad (4.9)$$

Finally, after calculating the air saturation enthalpy at the water temperature, the temperature change in each packet in an element was found using the equation below:

$$\Delta t_w = \frac{h_{D,d}(N\pi d_d^2)(h_{s,w} - h)}{c_{p,w}\dot{m}_w} \quad (4.10)$$

By continuing this procedure with a step-by-step calculation, any depth of spray zone could be evaluated. The rain zone required the same procedure but with a different range for drop sizes and number of packets. At the bottom of the tower, if the calculated inlet air enthalpy was found to be the same as the specified inlet air enthalpy, this confirmed the correct choice of outlet air enthalpy; otherwise, the complete procedure had to be repeated with a new choice of outlet air enthalpy.

4.1.2 Work by Kroger

A series of equations were derived that were sufficiently accurate to describe the divergent data generated by a numerical analysis of the rain zones of various cooling tower geometries (circular, rectangular and counter flow). They were semi-empirical, incorporating both analytical and numerically derived expressions and intended for use in a one-dimensional performance evaluation. The pressure drop and mass transfer coefficients for the rain zone of different geometries was presented by simple expressions in terms of standard variables.

Considering the air flow patterns in the inlet section of a circular counter flow cooling tower, a two-dimensional cylindrical co-ordinate potential flow function, $\phi(r, z)$, was used to define the radial and axial components of the air velocity by

$$v_{a,r} = -\partial\phi/\partial r \quad (4.11)$$

$$v_{a,z} = -\partial\phi/\partial z \quad (4.12)$$

The continuity equation for steady, axi-symmetric, incompressible flow written in terms of the potential function was given by

$$\frac{\partial^2 \phi}{\partial r^2} + \frac{1}{r} \frac{\partial \phi}{\partial r} + \frac{\partial^2 \phi}{\partial z^2} = 0 \quad (4.13)$$

The boundary conditions were applied assuming uniform air velocity through the fill and the solution to this problem was obtained by using Bessel functions. Kroger noted that, except for a small discontinuity at the upper edge of the tower inlet, the flow could be approximately described by a simple linear model representing the velocity components as

$$v_{a,r} = -0.5v_{avg} r / H_{rz} \quad (4.14)$$

$$v_{a,z} = v_{avg} z / H_{rz} \quad (4.15)$$

where v_{avg} is the average velocity of the air leaving the rain zone. These are subsequently used to calculate the drop velocity relative to the airflow

$$|v_{a,d}| = \sqrt{(v_{a,z} - v_{d,z})^2 + (v_{a,r} - v_{d,r})^2} \quad (4.16)$$

The total drag force on a droplet was found from

$$F_D = C_D A_d \rho_a v_{a,d}^2 / 2 \quad (4.17)$$

Droplets are not spherical as most assume, but take on a flattened elliptical shape as they approach terminal velocity. This deformation was taken into account by Dreyer [51] by the ratio of the drag coefficient of a deformed drop to that of a solid sphere as

$$C_D / C_{D,sph} = 1 - 0.17185(1 - E') + 6.692(1 - E')^2 - 6.605(1 - E')^3 \quad (4.18)$$

Considering an accelerating drop and neglecting buoyancy force, the forces acting on the drop are gravity and drag. The resulting force was found from

$$|\overline{F}_d| = \sqrt{(\sin \theta_{a,d} |F_D| - m_d g)^2 + (\cos \theta_{a,d} |F_D|)^2} \quad (4.19)$$

with the relative angle $\theta_{a,d} = \arctan[(v_{a,z} - v_{d,z}) / (v_{a,r} - v_{d,r})]$.

Considering initial velocity to be zero, the droplet velocity and displacement were found by integrating the equations below.

$$dv_{d,z}/dt = F_{D,z} / m_d - g \quad (4.20)$$

$$dv_{d,r}/dt = F_{D,r} / m_d \quad (4.21)$$

The pressure drop correlation was determined considering an annular control volume in the rain zone. The rate of change in the mechanical energy of the air, caused by drag on a single droplet, for radial and axial directions, was given by

$$dE_{a,r}/dt = F_{D,r} v_{a,r} \quad (4.22)$$

$$dE_{a,z}/dt = F_{D,z} v_{a,z} \quad (4.23)$$

Finally, the total pressure drop was found by summing the work done in all the control volume and substituting it into the energy equation.

The mass transfer correlation proposed by Ranz and Marshall for a single drop was considered to be accurate for the entire rain zone where the mean Reynolds number seldom exceeds 1500. Since the mass transfer coefficient is typically to be used in a Merkel type analysis, it was unnecessary to calculate the heat transfer coefficient. The relation between mass transfer coefficient h_D and β derived by Poppe [59] for droplets larger than 1 mm was also employed.

$$h_{D,rz} = (\beta P_a / R_v T_a) \ln \left[\frac{W_s + 0.622}{W + 0.622} \right] / (W_s - W) \quad (4.24)$$

The Merkel number for an entire rain zone was found from

$$h_{D,rz} A_{V,rz} H_{rz} / G_w = 1 / (G_w \pi r_{d,in}^2) \int_0^{H_{rz}} \int_0^{r_{d,in}} n_{cv} h_D S_d \quad (4.25)$$

where S_d represented the mean surface area of the droplets. The final relation was simplified, rendered into a non-dimensional form and solved numerically.

Using a similar approach, equations for rain zones with different geometries were also derived. In particular for the case of a rectangular tower with a purely counter flow rain zone, the equation for mass transfer coefficient, after simplification, is;

$$\begin{aligned} \frac{h_{D,rz} A_{V,rz} H_{rz}}{G_w} &= 3.6 \left(\frac{P_a}{R_v T_a} / \rho_w \right) \left(\frac{D}{v_{a,in} d_{d,eff}} \right) \left(\frac{H_{rz}}{d_{d,eff}} \right) Sc^{0.33} \times \ln \left[\frac{W_s + 0.622}{W + 0.622} \right] / (W_s - W) \\ &\times \{ 5.01334 b_1 \rho_a - 192121.7 b_2 \mu_a - 2.57724 + 23.61842 \times [0.2539 (b_3 v_{a,in})^{1.67} + 0.18] \\ &\times [0.83666 (b_4 H_{rz})^{-0.5299} + 0.42] \times [43.0696 (b_4 d_{d,eff})^{0.7947} + 0.52] \} \end{aligned} \quad (4.26)$$

The authors explained that this equation was useful in determining the effective drop diameter for the rain zone.

Experimental results were found to compare favorably with the numerical results though it was noted that the expressions were curve fits of numerically generated data and that they would reflect any deficiency in the numerical analysis.

4.1.3 Work by Fisenko et al.

A mathematical model of the performance of a natural-draft cooling tower was developed consisting of two interdependent nonlinear boundary-value problems, under steady-state operational conditions, with a total of 9 ODEs and the algorithm of self-consistent solution. The first boundary-value problem describes evaporative cooling of water drops in the spray zone of a cooling tower; the second boundary-value problem describes film cooling in the pack. Fisenko et. al. [53] explained that the contribution of

heat and mass transfer in the rain zone could also be included into the mathematical model but with another radius. As a rule, the radius of the droplet is quite large here and an appreciable fraction of water falls down in the form of jets. As this takes place, the mean radius of the droplets in the rain zone may several times exceed the radius of the droplets in the spray zone. Therefore, the evaporative cooling of water in the rain zone was neglected. Also, the approximation of replacing complex jet-droplet flows in a cooling tower by an ensemble of equally sized droplets was employed.

The upward moist air velocity v_a was calculated by using dimensions of a large tower, the mean moist air density and the change in mean moist air density. This expression is obtained from the standard expression for the convective flow velocity in a cooling tower and from the continuity equation for the moist air flow through the pack and the cooling tower throat. It describes the internal aerodynamics of the cooling tower in one-dimensional approximation. The moist air velocity in the zone of heat and mass transfer was taken to be constant, because the size of this zone is much less than the cooling tower height.

It was noted that the contribution of the cooling of droplets to the heat balance of the tower depends mainly on their radius. The radius of the droplets in the spray zone of the cooling tower depends on the water flow rate: the higher the water flow rate, the smaller is the droplet size due to larger pressure drop on sprinklers. Their calculations showed that the dependence of the radius of the droplets in the spray zone on the hydraulic load (water mass flow rate per unit area) is attributable to the design of the sprinkler nozzle and is not associated with the phenomenon of breaking of the droplets. Furthermore, at maximum hydraulic load, the velocity of the droplets leaving the sprinkler

is not sufficient for breaking. The maximum radius of the droplet falling with the velocity v_d is determined from the equality of the contributions of the aerodynamic drag force and the surface tension and the air ascending flow velocity v_a determines the minimal size of the droplets participating in the process of evaporative cooling. If the force of aerodynamic resistance exceeds that of the gravity, which is true for rather small droplets, the droplets are carried away by the ascending airflow. The coordinate origin was taken at the point of the beginning of droplet fall with the z-axis directed downward.

The influence of the number of the droplets per unit volume n_v on the moist air parameters was taken into account. The Reynolds number and Nusselt number were defined using the relations below

$$\text{Re}_d = \frac{2\rho_a r_{d,\text{eff}} [(v_d - v_a)^2 + v_{d,\text{hor}}^2]^{0.5}}{\mu_a} \quad (4.27)$$

$$\text{Nu}_d = 2 + 0.5 \text{Re}_d^{0.5} \quad (4.28)$$

where $v_{d,\text{hor}}$ is the horizontal component of drop velocity.

Using the analogy between the heat and mass transfer processes, for a droplet falling in an ascending airflow, the mass transfer coefficient $h_{D,d}$ was determined as

$$h_{D,d} = \rho_a \frac{D \text{Nu}_d}{2r_{d,\text{eff}}(z)} \quad (4.29)$$

where D is the diffusion coefficient of water vapor. Here, the mass transfer coefficient was taken in terms of the common mass flux ($\text{kg}/(\text{m}^2 \cdot \text{s})$) units instead of the volume flux ($\text{m}^3/(\text{m}^2 \cdot \text{s})$) that was originally used by Fisenko.

The aerodynamic drag force of a droplet was calculated by using the formula below:

$$C_D = \frac{24}{\text{Re}_d} \left(1 + \frac{1}{6} \text{Re}_d^{2/3} \right) \quad (4.30)$$

Fisenko et. al. took into account the additional increase in the elevation of a droplet with growth of a hydraulic load as well as the horizontal velocity component of falling droplets along with the vertical component of the velocity. It was noted that the horizontal component of the droplet velocity influenced the heat and mass transfer coefficients via the Reynolds number.

The system of differential equations used to calculate the processes of heat and mass transfer between the falling droplet and the ascending moist air included the following equations:

The change in the effective droplet radius $r_{d,\text{eff}}(z)$ due to evaporation was described by the following equation

$$\frac{dr_{d,\text{eff}}(z)}{dz} = - \frac{h_{D,d} [W_{s,w}(t_d(z)) - W(z)]}{\rho_w v_d(z)} \quad (4.31)$$

The equation for calculating the change in the drop velocity $v_d(z)$ is given by

$$\frac{dv_d(z)}{dz} = \frac{g}{v_d(z)} - C_D \frac{\rho_a [v_d(z) - v_a]^2}{2v_d(z)} \frac{\pi r_{d,\text{eff}}^2}{m_d} \quad (4.32)$$

The equation determining the volume-averaged temperature $t_d(z)$ of the drops is

$$\frac{dt_d(z)}{dz} = \frac{3[h_{c,d}\{t_a(z) - t_d(z)\} - h_{D,d} \cdot h_{fg}\{W_{s,w}(t_d(z)) - W(z)\}]}{c_{p,w} \rho_w \cdot r_{d,\text{eff}}(z) \cdot v_d(z)} \quad (4.33)$$

The equation for calculating the averaged dry-bulb temperature $t_a(z)$ of the moist air is

$$\frac{dt_a(z)}{dz} = \frac{4\pi r_{d,\text{eff}}^2(z) n_V}{c_{p,a} \rho_a (v_d(z) - v_a)} [h_{c,d}\{t_a(z) - t_d(z)\}] \quad (4.34)$$

The equation for describing the change in the humidity of moist air $W(z)$ is

$$\frac{dW(z)}{dz} = -\frac{4\pi r_{d,eff}^2(z) \cdot n_V}{\rho_a (v_d(z) - v_a)} h_{D,d} [W_{s,w}(t_d(z)) - W(z)] \quad (4.35)$$

The five boundary conditions taken for this system consisted of the initial values of the droplet radius, temperature and velocity at the beginning of the droplet fall while the air temperature and density of water vapor were taken at the final point of the fall of the droplets (the point at which the air leaves the fill packing). The derivation of these equations can be found in the Appendix.

4.2 COMPARISON AND SELECTION

In any detailed analysis of the performance characteristics of a wet counter flow cooling tower, the transfer processes in the spray or rain zone may not be ignored. Earlier studies considered these transfer processes too complex or relatively unimportant to analyze. In large counter flow wet-cooling towers, these zones make a considerable contribution to the overall performance, therefore, knowledge of mathematical models for reliable prediction of the total performance are important and also to be able to exploit the contribution of these regions to the full.

Kroger analyses the heat, mass and momentum transfer in the rain zone of counter flow wet-cooling towers in terms of standard variables by a method that is essentially two-dimensional, though it was intended for use in a one-dimensional performance evaluation. This method describes the interaction between the air (continuous phase) and the drops (dispersed phase) but neglects the effect of the drops on the turbulence model. Dreyer and Fisenko et. al. use models that are one-dimensional, though Fisenko does suggest that the air temperature could be more accurately described by a two-dimensional equation. Dreyer developed a one-dimensional mathematical model and computer simulation program that used basic aerodynamic, hydrodynamic and heat-mass transfer

information to accurately predict the performance of cooling towers. Fisenko et. al., on the other hand, developed two interdependent nonlinear boundary-value problems with a total of 9 ODEs and an algorithm of self-consistent solution. The first of these is of more interest as it concerned the spray zone and consisted of five differential equations. And, even though, the rain zone was not evaluated in this particular study, it was simply stated that the first boundary-value problem could be employed using a larger effective drop diameter.

Dreyer stated that a model that correctly predicted the drop size and velocity distributions through the fill packing, would also allow accurate prediction of the performance of the rain zone below the pack. In a rain zone, there is a wide distribution of droplet sizes. This distribution of drop sizes was described by a Rosin-Rammler distribution function. Dreyer used the concept of packets to allow drops of similar diameter, temperature and velocity to be lumped together with each packet having a unique combination of these parameters. Both Kroger and Fisenko have used an effective drop diameter to simplify the problem, which makes the problem sensitive to the selection of this diameter. Fisenko et. al have shown a method to determine it by using experimental data as described before while Kroger et. al. supplied mass transfer correlations that could be used to calibrate the effective drop diameter.

Fisenko used the mean value of the moist air velocity by taking the mean value of moist air properties for the complete tower. Also, this velocity was taken to be constant in the zone of heat and mass transfer because the size of this zone is much less than the cooling tower height. Kroger's two-dimensional model for the rain zone predicts the potential flow field accurately at each point, though the flow could be approximately

described by a simple linear model representing the (radial and axial) velocity components.

The drop Reynolds number, used by Dreyer, was based on the relative mean velocity between the drop and the air. Fisenko et. al., on the other hand, used a combination of mean and local velocities as well as the horizontal drop velocity component to calculate this number. More importantly, unlike Fisenko, Dreyer considered the flattened elliptical shape drops assume while approaching terminal velocities. This deformation was taken into account in the computation of the drag coefficient using the droplet's deformation ratio. Kroger, knowing that this approach described the physical nature of the problem accurately, referenced Dreyer's work in his own paper. One important thing to note is that Dreyer indicated that there was uncertainty about the calculation of the drag of accelerating liquid drops due to difficulty in accounting for internal circulation, deformation and drop shape oscillations. He concluded that the internal circulation and drop oscillation effects were much less pronounced than the effect of drop deformation on the drag of liquid drops falling in gaseous surroundings.

The mass transfer coefficient is one of the most important factors to be determined. Fisenko et. al. and Dreyer applied the analogy between the heat and mass transfer. The analysis by Kroger, for the rain zone, perhaps makes the most accurate prediction of mass transfer coefficients considering the previous discussion, especially, as it is not restricted to a certain type of geometry. It was noted that Kroger and Fisenko et. al. used the diffusion coefficient of water vapor instead of thermal diffusivity, which was employed by Dreyer.

In light of the above discussion, the model of Fisenko et. al. was adopted regarding the spray and rain zones owing to the apparent accuracy of the model and relatively easy application in the software employed.

CHAPTER 5

FOULING OF HEAT EXCHANGERS

The problem of fouling is encountered in industrial operations and processes with natural water or aqueous solutions containing dissolved or undissolved inorganic salts. Some of these salts or their combinations have inverse solubility characteristics, so that they are less soluble in the hot fluid adjacent to the heat transfer surface. Examples of such salts are $CaCO_3$ and $CaSO_4$. Figure 5.1 shows the behavior of normal and inverse solubility salt solutions, given by Bott [60]. For normal solubility salt solution, at point A, solution is under saturated but on cooling to point B it is just saturated. On further cooling, the solution becomes supersaturated and crystal nucleation occurs at point C. As crystallization and cooling proceeds, solution concentration falls and moves in the direction of D. Now, for an inverse solubility salt solution it is under saturated at point A, as it is heated it reaches the solubility limit at point B at temperature T_1 and then under continued heating the solution becomes supersaturated reaching point C at temperature T_2 where precipitation starts.

The formation of scale on heat transfer surfaces is a common phenomenon where aqueous solutions are involved, e.g. the use of natural waters for cooling purposes or evaporative desalination. Unless suitable measures are taken, the problem of scale formation can give rise to serious consequences. In steam boilers, for instance, the

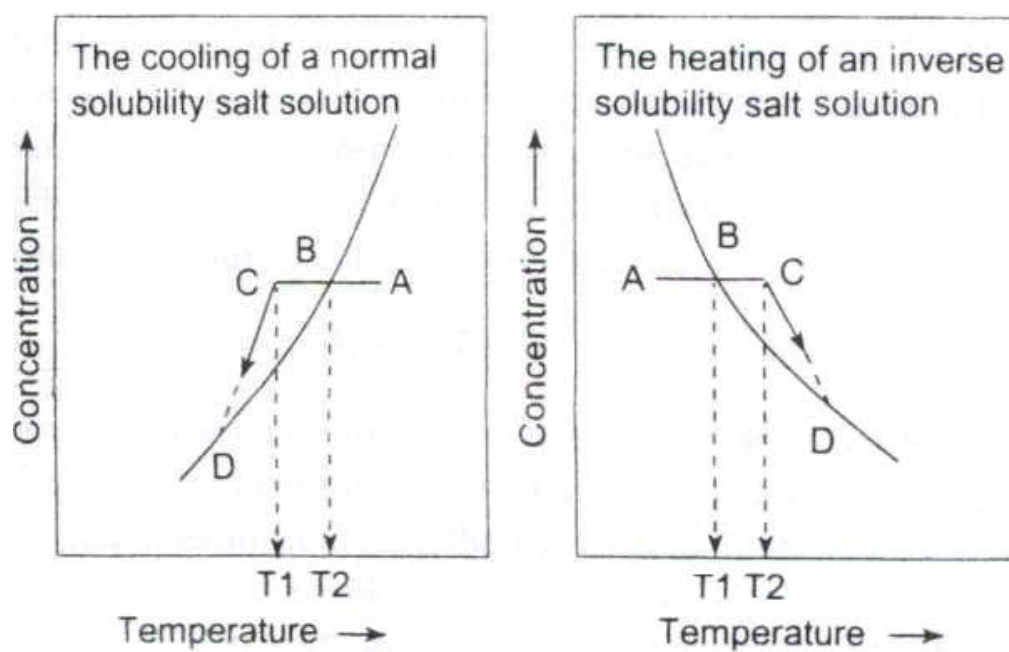


Figure 5.1: Behavior of normal and inverse solubility salt solutions [60]

presence of scale on water-side can give rise to high metal temperatures that may result in mechanical failure of heat-transfer equipment. Bott commented on the potential of scale formation in industrial equipment as very high. As an example, he observed that for 1-million gallon/day desalination plant in normal concentration conditions, a maximum of about 1400-kg of $CaCO_3$ could be precipitated each day. In terms of thickness, it would represent a build up of 0.1mm per day on the total heat exchanger surfaces within a typical plant. Although this may be regarded as an extreme example it does illustrate fouling problems in industrial plants.

Mizushina [7] considered a scaling heat transfer coefficient while describing characteristics and methods for the thermal design of evaporative coolers but did not pursue it in detail. Morse and Knudsen [61] conducted a systematic study of the fouling characteristics of conventional heat exchangers, in which fouling was formed from simulated cooling tower water. Story and Knudsen [62] discussed effect of surface temperature on the scaling behavior. Lee and Knudsen [63] designed an experimental apparatus to simulate the operating conditions of cooling tower. This is a somewhat extensive investigation to determine the effect of flow velocity, surface temperature and water quality on scaling of heat exchanger tubes. Coates and Knudsen [64] have discussed results of their experiments conducted for obtaining data regarding $CaCO_3$ scaling. Watkinson and Martinez [65] studied scaling due to $CaCO_3$ in copper tubes under conditions that promote rapid and severe scaling. In this regard, artificially hardened water of high dissolved and suspended solids circulated through a heated test section. Effect of flow velocity, tube diameter and bulk temperature on asymptotic fouling resistance has been determined. Haq [66] conducted fouling related experiments and

statistically analyzed $CaCO_3$ fouling data. The objective of Haq's study was to demonstrate that fouling resistance varies from point to point along a horizontal tube and also for the same point it varies from replicate to replicate. The operating parameters were temperature, pressure, solution concentration and velocity, which were kept constant during the experiments. Konings [67] on the basis of experimental work with cooling water, treated by different methods to eliminate scaling, presented a table of guide values for the fouling resistance. An experimental study of tube-side fouling resistance in water chilled evaporator was carried out by Haider et al. [68] in which 12.6 ft long evaporator tubes were used and fouling data were taken for four different geometry. The fouling characteristics of cooling water for precipitation and particulate fouling are also discussed by Knudsen [69] where he emphasized serious problems when heat exchangers are over designed due to the use of incorrect design fouling allowance.

Hasson [70] reviewed practical and fundamental aspects of precipitation fouling ($CaCO_3$ scaling). He considered the problem of defining precipitation-fouling tendency by reviewing principles of solution equilibria and precipitation kinetics for salt systems frequently encountered in heat exchanger applications. Branch and Muller-Steinhagen [71] developed a model for fouling in shell-and-tube heat exchangers by combining Hasson's ionic diffusion model for $CaCO_3$ scaling. Hesselgreaves [72] discussed the effect of system parameters on the fouling performance of heat exchangers. A model for $CaCO_3$ scale formation, which gives reliable prediction of the fouling rate with alteration of feed water chemistry, was developed by Tretyakov et al. [73]. Khan [74] presented the fouling resistance data of $CaCO_3$ scaling to study the influence of tube surface temperature, Reynolds number and tube diameter. It was reported that the influence of

Reynolds number in the range investigated ($Re = 900 - 1700$) is almost negligible, which was also noticed by Lee and Knudsen [63] who have presented the same conclusion for their experimental data on asymptotic fouling resistance. The data obtained from experiments are presented in the form of a dimensionless fouling resistance model for estimation and prediction purpose.

5.1 FACTORS OF IMPORTANCE IN FOULING PROCESS

Research into the various mechanisms involved in the fouling process has revealed that three variables that may be considered as being of greater significance than others. The levels of temperature, fluid velocity, and concentration of the foulant precursor in a particular system represent the determining factors in the extent of the fouling likely to be encountered. Some of these factors are discussed here. In addition to these variables, the direction of heat flux as it affects the temperature distribution across the heat exchanger interfaces may also be very important.

5.1.1 Temperature

There are certain general guidelines that should be considered in the design and operation of heat exchangers in order to minimize the incidence of fouling. It should be emphasized that in relative terms, low temperatures favor the following situations [60]:

1. Reducing the effects of chemical reaction and corrosion. Usually, higher temperatures accelerate these reactions;
2. Lowering the effects of microbial growth at temperatures below the optimum for growth of super-saturation conditions where inverse solubility salts are present in solution; and

3. Avoidance of super-saturation conditions where inverse solubility salts are present in solution.

On the other hand, relatively higher temperatures are more likely to favor the following situations [60]:

1. Reduction of biological fouling at temperatures above the optimum for growth of the particular species, present in the system.
2. Avoidance of freezing conditions so that partial solidification of the process stream at the transfer surface does not occur.
3. Avoidance of super-saturation conditions where normal solubility salts are present in the system.

There are other important (so-called) secondary effects of temperature. Over a long period of time under the conditions in a process heat exchanger, the deposit is subject to the continuing effects of temperature, which may affect the foulant aging process. The results may be beneficial or detrimental. The effects of temperature may render the deposit hard and difficult to remove through chemical or crystallogical changes in the deposit (e.g., polymerization of low-molecular weight compounds or chemical changes in the deposit such as the sulfation of oxide layers in high-temperature systems). Deposit fusion may occur under certain high-temperature conditions [75]. For example, as a deposit grows on a super heater in a boiler, the outer surface will be subject to increasing temperature due to the insulation effect of the deposit, and the surface temperature of the deposit may eventually reach the melting point of the ash. In food processing applications soft, easily removable deposits may become cooked onto the surface through the incidence of higher operating temperatures only present for short periods (e.g., deposits of milk solids in pasteurization operations). Conversely, the temperature condition, notably

changed temperature distribution as the foulant layer develops, may give rise to planes of weakness in the deposit and subsequent spilling. This is possible due to the inability of the adhesion forces to support the weight of deposit or the effects of differential expansion and contraction).

It should be emphasized that large temperature differences within a system, particularly gas systems, may give rise to the movement of particles along a temperature gradient, thereby enhancing the fouling process if the fluid is being cooled.

5.1.2 Effects of Fluid Velocity

A number of effects due to velocity may be appreciated involving the effect on fluid shear and changing temperature distribution.

Effects of Fluid Shear:

Usually increased velocity increases the shearing action at the deposit-fluid interface. High shear forces may result in removal of deposits. For instance, loose soot particles on the surface of a heat exchanger may be readily removed via increased velocities. Increased velocity in the vicinity of the deposit is the essence of the function of so-called soot blowers used in boiler plants. On the other hand, if the deposition involves mass transfer or diffusion, higher velocities will increase the diffusion toward the surface if a concentration gradient exists. In cooling water systems, where bio fouling is occurring, higher velocities may result in enhanced nutrient availability at the surface. In gas-side fouling, higher velocities will result in greater particle momentum depending on particle size, which, in turn, may accelerate the fouling process.

Effect on Heat Transfer:

The effects of velocity on heat transfer further complicate the situation. As the velocity increases, the rate of heat transfer increases, and to some extent this may offset the effects of the resistance to heat transfer brought about by the deposit layer. Improvements in the rate of heat transfer may also accompany the increased turbulence brought about by the rough character of the deposit-fluid interface

Reduction of Fouling:

In general, the higher the velocity, the less the effects of fouling are likely to be, but this must be balanced against increased pressure drop and higher pumping costs. For shell-and-tube heat exchangers, a rough guide is to design for liquid velocities of 2 m/s in tubes or higher if possible. However, if velocities are too high, problems of erosion can occur and, even at moderately high velocities, the protective oxide layer on surfaces could be removed, thereby accelerating the corrosion of the surface. In some instances a thin layer of deposit on the surface can act as a protective agent, reducing the effects of corrosion. In addition, because the cost of pumping rises as the square of velocity, pumping costs could rise out of all proportion to the benefits with respect to fouling.

One reason for maintaining high velocities is the reduction of the incidence of stagnant areas, which may encourage fouling either by sedimentation or temperature effects. Stagnant areas may distort the temperature profile and give rise to accelerated fouling reactions, corrosion, or the development of microorganisms. It is therefore, important that attention to fluid distribution is particularly important on the shell side of shell-and-tube heat exchangers because the many changes in direction of the fluid can give rise to 'dead spots' and consequent sedimentation.

5.1.3 Operation of Heat Exchangers

It should be emphasized that wherever possible, design velocities and temperatures should be maintained irrespective of changes in operating throughput. For instance, reduced velocity, even for short periods, can produce highly fouled surfaces. Often these enhanced deposition rates produce layers that are not capable of removal by increased velocities when the heat exchanger is back on normal operation. The time period between cleaning can be markedly reduced with attendant increased operating costs. Furthermore, the lower velocities may so alter the temperature distribution, even if only for a short time, that the nature of the deposit is changed. It may become more tenacious and difficult to remove. Provision for the maintenance of flow conditions in a heat exchanger that is likely to suffer as a result of velocity changes should be considered at the design stage. Recycling fluid circuits should be included where necessary, so that adequate velocities can be maintained even under reduced throughput operation.

5.1.4 Fouling in Counter Flow Wet Cooling Towers

Fouling, as defined for cooling towers, is the process of deposition of foreign matter, including bio-growth; on the fill air and water flow area. It inhibits the cooling process or allows excessive weight to build up in the cooling tower. In more severe circumstances, however, fouling can result in a reduction in the overall cooling efficiency of the unit, primarily due to foulant bulk and location interfering with air and water flow through the tower. Mortensen and Conley [76] investigated the fouling in low-clog fills considering several fouling mechanisms, the base condition chosen was 100% bio-growth sequence, with comparisons in 100% silt, and a very severe combined silt and bio mechanism. Fill packs of varying geometry, spacing, configuration, texture, water

loading, and various materials of manufacture were investigated under field conditions. Silt laden fill cells were tested separately either with clean water or with water seeded and fertilized to yield the increased bio/silt risk exposure. They reported growth rates and weight additions of up to 20 lbs/ft³ of test fill, in 40 to 120 days. Further testing showed pack fouling or plugging to be microbiological growth adherence, with or without silt, to the plastic film water flow area, with a biological slime binder being essential to the progress of the pack plug. They indicated that various laboratory analysis of fill foulant from power plants showed them to be from 9% to 35% organic, indicating biological/living matter. Some industrial tower plugs were 100% organic. Observation of a seasonal increase in fouling supports the existence of an essential biological element in this fouling mechanism. Laboratory testing carried out by Mortensen and Conley [76] indicated that silt alone was not capable of creating substantial plugging in film fills either of Cross-corrugated (CC) or Non-textured tubular (NTT) type.

Thomas et al. [77] analyzed one “mud” plug sample from their laboratory test unit, and it revealed that bacteria potentials are very high at 1.15×10^9 organisms/ml in the solid, with the largest groupings being the *Bacillus Brevis*, *Cytophaga*, *Flavobacterium Indologenes* or *Odoratum*, and *Pseudomonas*. Further analysis identified water borne organisms, which produce sticky bio-film material as Extra Cellular Polysaccharide Producers (ECPS) with “the microbial mass cementing or sticking together general debris”. These organisms are foulants in a number of industrial processes, including cooling towers and without diligent biocidal treatment tend to thrive in the aerobic (Oxygen saturated), temperature (80-120 °F), and nutrient rich environment provided in the fill.

It should be emphasized that cooling tower effectiveness is not independent of other plant efficiency factors. Major factors in fill fouling are the water chemistry of the system and the water treatment conditioning which modifies it. Mirsky et al. [78] reported that no fill can be totally immune to fouling, indicating that water conditions can be constructed that are too harsh for any cooling tower fill geometry no matter how well conceived. All sources reviewed agree that, ideally, fill should be kept clean from the start. McCarthy and Ritter [79] during their research of water treatment reported that it might be possible to reverse the fouling of cooling tower fills, however a preventive-maintenance approach is preferred. According to Mortensen and Conley [76], the following major chemicals should be avoided in circulating water with PVC Film-type fill, in order to avoid fill fouling,

1. Acetone
2. Benzene
3. Chloroform
4. Chlorinated Hydrocarbons (example: Ethyl Chloride)
5. Ketones
6. Methyl Ethyl Ketone (MEK)
7. Phenol
8. Tetrahydro Furan (THF)
9. Toulene
10. Xylene

Bio-growth control is the predominant water treatment issue in controlling fill fouling. Without high bacterial growth rates in the affected fill areas, plug formation would be halted or proceed at very slow rates according to documented field experience. Several factors seem basic to the bio-growth control mechanism [76].

1. Biocidal control system must be reliable and provide the ability to target biocide to a given portion of the cooling loop, specifically the cooling tower fill, as necessary.
2. Biological activity/bacteria counts must be controlled to specific target levels for a given cooling tower fill.
3. Some high nutrient waters may be, in effect, biologically uncontrollable during periods of Total Organic Carbon Elevation.

The effectiveness of a chlorination system using hypochlorite should serve as a benchmark for judging the operation and cost effectiveness of any alternate chemical system. Mortensen and Conley [76] indicated that a system with Aerobic Bacteria counts above 1.0×10^6 cfu/ml (i.e., colony forming units per ml) based on several water samples taken directly from the fill can be considered at great risk for substantial biological fouling. Suspended solid levels should be carefully noted. Control of bacteria in the cooling system is very important to avoid fouling. Reduction of available suspended solid material helps to minimize fouling risk.

Fill cleaning, in cooling towers similar to heat exchangers is either by physical or chemical means. Physical cleaning is accomplished by various techniques such as pressure washing, perforated sprayers (providing high volume water at low pressure),

flood washing, drying, air lancing and sonic horns. Such cleaning operation will restore thermal efficiency of the cooling towers. Chemical methods employed (on and off line), include application of high concentration biocides, use of dispersants (chosen for their particular suitability for the plug or solid composition), and altering of pH. Some researchers have reported significant recovery of thermal efficiency with the biocide technique, and limited plug removal with chemical dispersants.

5.1.5 Fouling in Counter Flow Coolers and Condensers

There are three things that cannot be tolerated in evaporative cooling equipment: excessive corrosion, scale and biological fouling. All three of these can damage the equipment and lead to premature failure. Since the principle of evaporative cooling is the same as that used by conventional cooling towers, it is understood that the nature of the fouling problems associated with these evaporative heat exchangers will be the same as well. Macleod-Smith [80] iterated that the use of water and the responsibility of manufacturers and service providers to avoid the risk of Legionella bacteria in the recirculated water was an important issue even though evaporative condensers have never been linked to any large outbreak of Legionnaire's Disease because noticeable levels of Legionella are certainly found in the water in evaporative condensers. It was further noted that owners and service providers often concentrate too much on the threat of these bacteria and overlook the equally important need for control against corrosion and scaling, which, thus, has reduced the life of the evaporative condenser especially the condensing coil. The authors stressed that a good water treatment programme will address the threat of corrosion, scaling, microbiological growth and fouling and ensure that is each is addressed without prejudicing the other.

Water treatment for evaporative condensers (and coolers) presents different challenges as compared to an open-circuit cooling tower since the volume of water to be treated is much smaller. This suggests that the treatment should be easier but this is not necessarily the case. The volume may be smaller but the turnover of the water is much quicker and the materials of construction of the condensing coil are of great importance and must be considered carefully. The main elements of a water treatment system for evaporative condensers are as follows (Macleod-Smith; 2002):

1. Pre-treatment
2. Bleed Control
3. Scale Control
4. Corrosion Control
5. Microbiological Control
6. Record Keeping

Evaporative coolers are also highly susceptible to the formation of crust and scale, and the growth of foul-smelling organisms. Left unchecked, these accumulations promote rapid corrosion of the media frames and the cooler box, and expensive maintenance or replacement.

They investigated calcium carbonate (CaCO_3) scaling (see Figure 5.2) with the percentage design capacity as a function of scale thickness, which is itself a function of time. The figure shows that the capacity of the condenser decreases by almost 60% and still has not reached an asymptotic value. This decrease is considerable but it must be bore in mind that this is calcium carbonate scaling, which is deposited in an accelerated manner. Still, one of the biggest threats to evaporative condenser effectiveness as well as to the life of the equipment is scaling. Even a moderate amount of scaling significantly

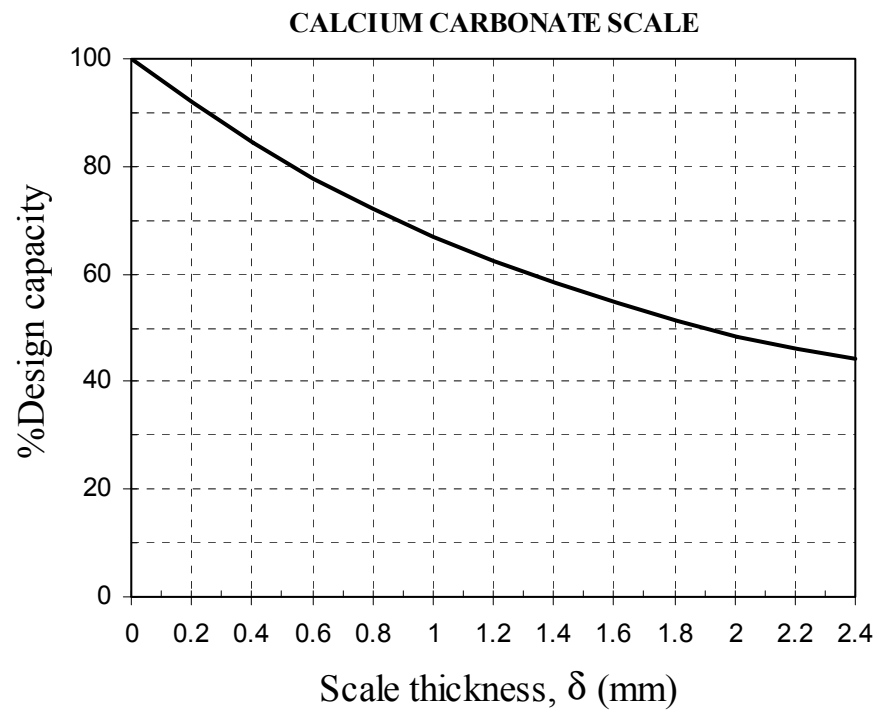


Figure 5.2: Decrease in percentage design capacity versus scaling thickness

reduces thermal efficiency and corrosion of the coil beneath a layer of scale can lead to a drastic shortening of life.

To protect the coil, it is necessary for it to be both continually wetted and any scaling tendency of the water to be controlled. Perversely, the more the coil surfaces are thoroughly wetted, the less the risk of scaling. It is also important that the spray system above the coil is regularly inspected to ensure there are no blocked nozzles or unwetted areas of the coil. Most condensers are done with a combination scale and corrosion inhibitor as a single blended chemical. The choice of inhibitor will depend on the make-up water quality and the materials of construction and the materials of construction of the condenser. Though, the use of acid to control scaling is not recommended with evaporative condensers as it poses an additional threat to the life of the condensing coil.

5.2 CHARACTERIZATION OF FOULING MECHANISM

The most widely accepted characterization of fouling mechanism is based on the general material balance equation first proposed by Kern and Seaton [81]:

$$\frac{dR_f}{dt} = \Phi_{dep} - \Phi_{rem} \quad (5.1)$$

Here, the term Φ_{dep} should depend on the type of fouling mechanism (sedimentation, crystallization, organic material growth etc.), while Φ_{rem} depends on both the hardness or adhesive force of the deposit and the shear stress due to the flow velocity as well as the system configuration. The rate of deposition (Φ_{dep}) and the rate of removal (Φ_{rem}) have been given many different forms by various investigators [82-83]. However, the most widely accepted combinations result in the following three fouling growth (or fouling resistance) models [84-85]:

$$R_f(t) = A + B t \quad \text{for } t > 0, \quad (5.2)$$

$$R_f(t) = A + B \ln(t), \quad \text{for } t \geq 1 \quad (5.3)$$

$$R_f(t) = R_f^*[1 - \exp(-t/\tau)] \quad \text{for } t \geq 0 \quad (5.4)$$

where $R_f(0) = A$ [for equation (5.2)], $R_f(0) = 0$ [for equation (5.4)], and $R_f(1) = A$ [for equation (5.3)]. It is important to note that if the time is measured in relatively smaller units (compared to the time required to reach a critical fouling level) such as minutes, hours, or days, then $R_f(1) = A \approx R_f(0)$, and the range of equation (5.3) could be treated as $t \geq 0$. In the following discussion, we will assume such measurements of time and will consider the range as $t \geq 0$ in the corresponding equations and figures.

5.2.1 Fouling Models with Induction Time

It is frequently observed that when the heat-transfer surface is exposed to the fluid stream, for some time, there is no measurable growth of fouling resistance. A delay time between the start of fouling growth process and the formation of fouling deposits is often observed. This period is defined as an induction or delay time (t_i). Thus, the fouling growth models discussed earlier can be generalized by introducing the delay time as

$$R_f(t) = A + B (t - t_i), \quad \text{for } t \geq t_i, \quad (5.5)$$

$$R_f(t) = A + B \ln(t - t_i), \quad \text{for } t \geq t_i \quad (5.6)$$

$$R_f(t) = R_f^*[1 - \exp\{-(t - t_i)/\tau\}] \quad \text{for } t \geq t_i \quad (5.7)$$

5.2.2 Stochastic Analysis of Fouling Models

Both replicate laboratory experiments [86-87] in the study of fouling growth models as well as field investigations suggest that there is a considerable scatter in the

values of R_f at any time t and similarly for any fixed value of R_f there will be a corresponding scatter in the values of t . The scatter in R_f can be expressed by its probability-distribution function $f[R_f(t)]$. The main indicators of this distribution are its mean value $\bar{\mu}[R_f(t)]$ and standard deviation $\sigma[R_f(t)]$. It is often desirable to discuss the scatter in terms of the non-dimensional parameter defined as coefficient of variation,

$$K[R_f(t)] = \sigma[R_f(t)] / \bar{\mu}[R_f(t)] \quad (5.8)$$

The evolution of the $R_f(t)$ distribution with respect to t is represented by the random sample functions of the fouling resistance growth. Each sample function represents a realization of the process. For understanding the concept, consider a heat exchanger that has many tubes. The fouling resistance response of the tubes will show a considerable scatter. This scatter or randomness is due to several reasons; some of these reasons are (Zubair et al., 1992 and 1997b):

- Mal-distribution of fluid-flow in heat exchanger tubes;
- Variations and fluctuations in velocity around the nominal value;
- Variations and fluctuations in pressure around the nominal value;
- Variations and fluctuations in surface temperature around the average value;
- Perturbations in the foulant chemistry;
- Plate or tube material variability of metallurgical features;
- Variability of surface finish; and
- Fluctuations in the initial quality characteristics of heat exchanger tubes attributed to manufacturing and assembling process.

It is, thus, apparent that each heat exchanger tube will have its own fouling resistance growth curve. These curves will follow some type of fouling kinetic models such as linear, asymptotic or falling rate of the growth process. The ensemble of "m" such realizations for each of these curves are shown in Figure 5.3. Mathematically, these functions are same as discussed earlier in equations (5.2) through (5.7). However, due to a number of sources of randomness described above, the parameters of the above equations should be treated as random. These random functions represent fouling resistance growth laws as;

$$\mathbf{R}_f(t) = \mathbf{A} + \mathbf{B}t, \quad \text{for } t \geq 0, \quad (5.9)$$

$$\mathbf{R}_f(t) = \mathbf{A} + \mathbf{B} \ln(t), \quad \text{for } t \geq 1 \quad (5.10)$$

$$\mathbf{R}_f(t) = \mathbf{R}_f^* [1 - \exp(-t/\tau)], \quad \text{for } t \geq 0 \quad (5.11)$$

$$\mathbf{R}_f(t) = \mathbf{A} + \mathbf{B} (t - \mathbf{t}_i), \quad \text{for } t \geq \mathbf{t}_i, \quad (5.12)$$

$$\mathbf{R}_f(t) = \mathbf{A} + \mathbf{B} \ln(t - \mathbf{t}_i), \quad \text{for } t \geq \mathbf{t}_i \quad (5.13)$$

$$\mathbf{R}_f(t) = \mathbf{R}_f^* [1 - \exp(-(t - \mathbf{t}_i)/\tau)], \quad \text{for } t \geq \mathbf{t}_i \quad (5.14)$$

where **bold** letters represent random parameters with their appropriate distribution; having mean and variance. It is important to emphasize that in most cases there is no significant initial fouling; that is, 'A' is negligible.

5.2.3 Asymptotic Fouling Model

An asymptotic fouling model (equation 5.11) is often observed in cooling water heat exchangers and this is also seen from the experimental data [76]. On the transformed y-axis, this can be written as

$$\ln[1 - R_f / R_f^*] = t / \tau \quad (5.15)$$

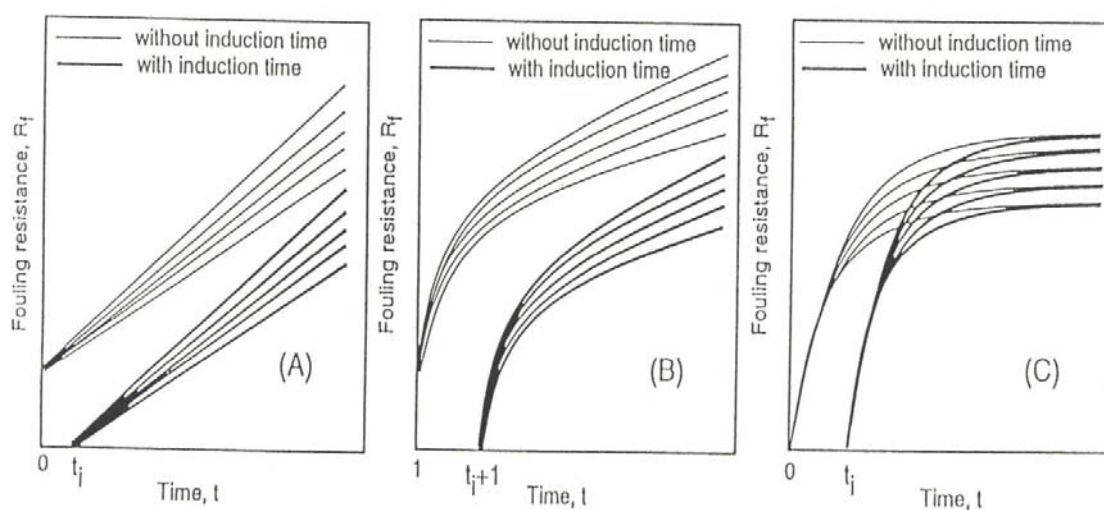


Figure 5.3: Typical sample functions of fouling-resistance models

The time constant can be expressed in terms of the critical acceptable value of fouling resistance $R_{f,cr}$ and the time to reach this critical value t_{cr} as follows:

$$\tau = t_{cr} / \ln[1/1 - R_{f,cr} / R_f^*] \quad (5.16)$$

$$t_{cr} = M / [1 - \sqrt{\alpha} \Phi^{-1}(p)] \quad (5.17)$$

where α is the scatter parameter and its value is taken as 0.3. The risk level, p , represents the probability of the fill surface being fouled up to a critical level after which cleaning is needed.

Substituting and rearranging, we get

$$R_f(t, p; \sqrt{\alpha}) = R_f^* [1 - \exp\{-\ln[1/1 - R_{f,cr} / R_f^*] [1 - \sqrt{\alpha} \Phi^{-1}(p)] t / M\}] \quad (5.18)$$

Khan and Zubair [88] developed a model showing a correlation between the normalized fill index due to fouling $\eta_{F,norm}$ and the weight gain, w . The model is of the form

$$\eta_{F,norm} = \frac{\left(\left(\frac{h_D A_V V}{m_w} \right)_{cl} - \left(\frac{h_D A_V V}{m_w} \right)_{fl} \right)}{\left(\frac{h_D A_V V}{m_w} \right)_{cl}} = C_1 (1 - \exp(-w / C_2)) \quad (5.19)$$

where the weight gain is a function of time. C_1 represents the increase in $\eta_{F,norm}$ when fouling reaches its asymptotic value and C_2 is the weight gain constant.

The linear version of above model was expressed as

$$\ln \left[\frac{1}{1 - (\eta_{F,norm} / C_1)} \right] = w / C_2 \quad (5.20)$$

The slope ($1/ C_2$) of the graph drawn using the above equation was found to be 0.1577. Equation (5.20) has of the same form as that of equation (5.15). Currently, following a similar approach as before, we get

$$C_2 = \frac{w_{cr}}{\ln[1/1 - (\eta_{F,norm} / C_1)]} \quad (5.21)$$

$$w_{cr} = M / [1 - \sqrt{\alpha} \Phi^{-1}(p)] \quad (5.22)$$

Again, substituting and rearranging by following the previous approach, we get

$$\eta_{F,norm}(w, p; \sqrt{\alpha}) = C_1 [1 - \exp\{-\ln[1/1 - \eta_{F,norm} / C_1] [1 - \sqrt{\alpha} \Phi^{-1}(p)] w / M\}] \quad (5.23)$$

where M , now, is the median weight to reach the critical level of fouling.

For evaporative coolers and condensers, the model represented in equation (5.18) will be used where t is replaced by scale thickness (δ) in this case, which is also a function of time and M , then, will be the median thickness to reach the critical level of fouling. Also, the equivalent of equation (5.19) is:

$$\eta_{C,norm} = \frac{(\dot{Q}_{cl} - \dot{Q}_{fl})}{\dot{Q}_{cl}} = C_1 (1 - \exp(-\delta / C_2)) \quad (5.24)$$

where $\eta_{C,norm}$ can be termed as the normalized condenser/cooler performance index.

In this regard, we will perform a parametric study to understand the effect of fouling on typical performance parameters such as effectiveness with respect to cooling towers, evaporative coolers and condensers.

CHAPTER 6

EXERGY ANALYSIS

It is essential to consider both the first and second laws in solving problems related to thermodynamic processes. We note that energy is the consequence of the first law, while entropy is due to the second law. Energy may be calculated on the basis of any assumed state of reference, whereas proper selection of reference state is very important in the case of exergy calculations. Another main feature of energy is that it increases with the increase of temperature and pressure. For an ideal gas, it is independent of pressure. However, in the case of exergy, it reaches minimum at the reference (environment) temperature during isobaric processes; at lower temperatures it increases as the temperature drops below the reference. Furthermore, exergy of an ideal gas is dependent on pressure. It is, therefore, understood that not all states with the same quantity of energy have the same potential to cause change. Thus, any efficiency defined on the basis of first law will be lacking in one manner or the other. It is exergy, not energy that represents the true potential of a system to perform an optimal work. Therefore, analyses based on exergy are important when different types of energy are to be compared. For example, heat and work, in air-conditioning processes.

Wepfer et al. [89], as well as many engineering thermodynamic textbooks (e.g. Bejan; 1997) [90], have used several examples to illustrate the application of second law to a variety of Heating Ventilating and Air-Conditioning processes. Wepfer et al. used a

ratio of exergy of the products to the exergy supplied to measure the second-law efficiency of the processes. This was found to be confusing; for example, certain quantities were not used in the calculations even though they were contributing to the overall effectiveness of the process. Also, in the steam-spray humidification process discussed by Wepfer et al., efficiency was seen to become negative under certain operating conditions. Bejan defined the second-law efficiency as a ratio of the total exergy leaving the system to the total exergy entering the system, which confines the efficiency between 0 and 1. He defined the total exergy as the sum of thermomechanical and chemical exergies, where the latter is the maximum work that could theoretically be harvested as the mixture (if it exists) comes in equilibrium with the environment. Qureshi and Zubair [91] presented a second-law based parametric study, using Bejan's definition of second-law efficiency, of some of the processes considered by Wepfer et al. as well as two additional processes.

6.1 ANALYTICAL FRAMEWORK

For a steady-state steady-flow system, we have [90]

$$\sum_{in} \dot{m} = \sum_{out} \dot{m} \quad (6.1)$$

$$\dot{W}_{cv} = \sum_{i=0}^n \dot{Q}_i + \sum_{in} \dot{m}h - \sum_{out} \dot{m}h \quad (6.2)$$

$$\dot{S}_{gen} = \sum_{out} \dot{m}s - \sum_{in} \dot{m}s - \sum_{i=0}^n \frac{\dot{Q}_i}{T_i} \quad (6.3)$$

$$\dot{X}_w = \sum_{i=1}^n (\dot{X}_Q)_i + \sum_{j=1}^q (\dot{N}\bar{x}_{tot})_j - \sum_{k=1}^r (\dot{N}\bar{x}_{tot})_k - T_o \dot{S}_{gen} \quad (6.4)$$

where

$$\dot{X}_Q = \dot{Q} (1 - T_o / T) \quad (6.5)$$

and the js and ks refer to inlet and outlet ports, respectively. \dot{X}_w is the exergy delivery rate or useful mechanical power output by the control volume as an open system and \dot{X}_Q is the exergy content of the heat transfer.

The steady flow exergy balance for an open system is simply written as

$$\sum_{in} \dot{X} = \dot{X}_D + \sum_{out} \dot{X} \quad (6.6)$$

The exergy flow of an open system is represented by the second and third terms on the right hand side of Eq. (6.4), where \bar{x}_{tot} is the total molal flow exergy of the mixture stream, given by

$$\bar{x}_{tot} = (\bar{h} - \bar{h}^*) - T_o (\bar{s} - \bar{s}^*) + \sum_{i=1}^n (\bar{g}_i^* - \bar{g}_{o,i}) y_i \quad (6.7)$$

where ()^{*} indicates properties evaluated at the restricted dead state (RDS). This dead state means that the stream is brought to thermal and mechanical equilibrium (only) with the environment.

As stated before, the total flow exergy is the sum of the thermomechanical and chemical flow exergies, i.e.

$$\bar{x}_{tot} = \bar{x}_x + \bar{x}_{ch} \quad (6.8)$$

However, with reference to the RDS (T_o , P_o), thermomechanical specific molal flow exergy is given by

$$\bar{x}_x = (\bar{h} - \bar{h}^*) - T_o (\bar{s} - \bar{s}^*) \quad (6.9)$$

$$\text{where} \quad \bar{h}^* = \sum_{i=1}^n \bar{h}_i^* y_i, \quad \bar{s}^* = \sum_{i=1}^n \bar{s}_i^* y_i \quad (6.10)$$

The molal chemical flow exergy released as the bulk state of the stream changes from the RDS to the dead state is given by

$$\bar{x}_{ch} = \sum_{i=1}^n (\bar{g}_i^* - \bar{g}_{o,i}) y_i \quad (6.11)$$

The total flow exergy per mole of humid air is deduced from eqn. (6.8) – (6.11):

$$\begin{aligned} \bar{x}_{tot} = & y_{da} [\bar{h}_{da} - \bar{h}_{da}^* - T_o (\bar{s}_{da} - \bar{s}_{da}^*) + (\bar{g}_{da}^* - \bar{g}_{o,da})] \\ & + y_v [\bar{h}_v - \bar{h}_v^* - T_o (\bar{s}_v - \bar{s}_v^*) + (\bar{g}_v^* - \bar{g}_{o,v})] \end{aligned} \quad (6.12)$$

The proportionality between specific humidity ratio W and specific humidity ratio on a molal basis \tilde{W} is given by

$$\tilde{W} = 1.608 W \quad (6.13)$$

where the specific humidity ratio is

$$W = \dot{m}_v / \dot{m}_{da} \quad (6.14)$$

It represents number of kilograms of water that correspond to one kilogram of dry air in the air-water vapor mixture.

The second-law efficiency, which is a measure of irreversible losses in a given process, is defined as

$$\eta_{II} = \frac{\text{total flow exergy leaving}}{\text{total flow exergy entering}} \quad (6.15)$$

On using Eq. (6.6), we get in general

$$\eta_{II} = 1 - \frac{\text{exergy destruction}}{\text{total flow exergy entering}} \quad (6.16)$$

Exergy analysis will be carried out using the above equations for cooling towers, evaporative condensers and evaporative coolers. In this regard, the effect of important

design variables that influence the second-law efficiency of these systems will be investigated.

CHAPTER 7

SENSITIVITY ANALYSIS

In general, any independent variable X can be represented as

$$X = \bar{X} \pm U_X \quad (7.1)$$

where \bar{X} denotes its nominal value and U_X its uncertainty about the nominal value. The $\pm U_X$ interval is defined as the band within which the true value of the variable X can be expected to lie with a certain level of confidence (typically 95%), as reported by Kim and Simon [92]. In general, if a function $Y(X)$ represents an output parameter, then the uncertainty in Y due to an uncertainty in X is expressed in a differential form as

$$U_Y = \frac{dY}{dX} U_X \quad (7.2)$$

For a multivariable function $Y = Y(X_1, X_2, X_3, \dots, X_N)$, the uncertainty in Y due to uncertainties in the independent variables is given by the root sum square product of the individual uncertainties computed to first order accuracy as [93]

$$U_Y = \left[\sum_{i=1}^N \left(\frac{\partial Y}{\partial X_i} U_{X_i} \right)^2 \right]^{1/2} \quad (7.3)$$

Physically, each partial derivative in the above equation represents the sensitivity of the parameter Y to small changes in the independent variable X_i . The partial derivatives are therefore referred to as *sensitivity coefficients*.

By normalizing the uncertainties in the response parameter Y and the various input variables by their respective nominal values, equation (7.3) can be written as

$$\left(\frac{U_Y}{\bar{Y}}\right) = \left\{ \sum_{i=1}^N \left[\left(\frac{\partial Y}{\partial X_i} \frac{\bar{X}_i}{\bar{Y}} \right) \left(\frac{U_{X_i}}{\bar{X}_i} \right) \right]^2 \right\}^{1/2} \quad (7.4)$$

The dimensionless terms in braces on the right hand side of the above equation represent the respective sensitivity coefficients and uncertainties in their normalized forms and are, therefore, referred to as *normalized sensitivity coefficients* and *normalized uncertainties* denoted by NSC and NU , respectively [94]. Equation (7.4) can therefore be written as

$$\left(\frac{U_Y}{\bar{Y}}\right) = \left\{ \sum_{i=1}^N [NSC_{X_i} NU_{X_i}] \right\}^{1/2} \quad (7.5)$$

A dimensionless factor ϵ_{X_i} is introduced to represent the positive and negative uncertainty in the variable X_i such that

$$U_{X_i} = \bar{X}_i \epsilon_{X_i} \quad (7.6)$$

With the help of this substitution and on replacing partial derivatives by ratios of discrete changes, the normalized sensitivity coefficients and uncertainties can be expressed as

$$NSC_{X_i} = \left(\frac{\Delta Y_i}{\bar{Y}} \frac{\bar{X}_i}{\Delta X_i} \right)^2 ; \quad NU_{X_i} = (\epsilon_{X_i})^2 \quad (7.7)$$

ΔX_i , in the above equation can be written as

$$\Delta X_i = \bar{X}_i (1 + \epsilon_{X_i}) - \bar{X}_i (1 - \epsilon_{X_i}) = \bar{X}_i (2 \epsilon_{X_i}) \quad (7.8)$$

Therefore, equation (7.5) now becomes

$$\epsilon_Y = \left\{ \sum_{i=1}^N \left[\left(\frac{\Delta Y_i}{\bar{Y}} \frac{1}{2 \epsilon_{X_i}} \right) (\epsilon_{X_i}) \right]^2 \right\}^{1/2} \quad (7.9)$$

Another parameter of interest is the relative contribution of each input variable uncertainty to the overall uncertainty in the dependent variable, defined by James et al. [94] as

$$\left(\frac{\frac{\partial Y}{\partial X_i} U_{X_i}}{U_Y} \right)^2 = \left(\frac{NSC_{X_i} NU_{X_i}}{\epsilon_Y} \right)^2 \quad (7.10)$$

An examination of above equations shows that the propagation of the uncertainty in a particular input parameter through the analysis equations into the result is dependent on the magnitude of the normalized sensitivity coefficients. If the NSC of a variable is of the order of unity, then its uncertainty, on being squared, is propagated essentially unchanged. If it is greater than unity its uncertainty is amplified whereas if it is less than unity, its effect is diminished. Moreover, since the sensitivity coefficients of the various input variables are normalized relative to the same nominal value \bar{Y} , a one on one comparison of the coefficients can be made thereby yielding a good estimate of the sensitivity of the result to each of the variables.

Relative contribution of a variable to the overall uncertainty involves the square of the product of its normalized sensitivity coefficient and uncertainty. Consequently, it is their product that is of significance and not the individual terms themselves. Relative contribution of any variable to the overall uncertainty can be controlled to a large extent by bringing down the uncertainty of that variable.

Thus, it is seen that the normalized sensitivity coefficients and relative contributions are obtained as significant characteristic parameters in the uncertainty analysis of any dependent variable. While the sensitivity coefficients identify the input parameters to which the performance parameters are most sensitive, irrespective of the uncertainty in the input variables themselves, the relative contributions identify the dominant uncertainty contributors.

Currently, only *NSC* is of interest and the method used to calculate the sensitivity coefficients is simple. The input variable is perturbed as necessary in both positive and negative directions and the response variables are calculated at both instances. The difference of the response values divided by the difference of the respective input values yields the required sensitivity coefficient. Then the nominal values for both are used, as shown in equation (7.7), to calculate the *NSC*.

Sensitivity analysis will be carried out using the above method for cooling towers, evaporative condensers and evaporative coolers. In this regard, the effect of contributing input variables that influence the sensitivity of the response variables of these systems will be investigated.

CHAPTER 8

VALIDATION

The current chapter contains the validation of all the models discussed in chapter 3 and the calculation approach for the solution of the problem. A mathematical model is considered to be correct if it accurately describes the physical process under consideration. The model invariably needs to be validated against experimental data, so that further work can be done.

8.1 VALIDATION OF COOLING TOWER MODEL

We know that a cooling tower consists of three parts i.e. spray zone, packing or fill material and the rain zone. As explained in chapter 4, the heat and mass transfer occurring in the spray zone is described by a set of five differential equations and the same model is also used for the rain zone. Three differential equations are used for the packing section of the tower. Now, these are numerically solved using Engineering Equation Solver (EES) software and along with the assumptions detailed in chapter 3, it is also assumed that there is a negligible pressure drop in the tower.

8.1.1 Validation of Packing Model

Calculations regarding the packing or fill material of the cooling tower have been validated from the data provided by Simpson and Sherwood [43] as this offers the most comprehensive data in terms of experimental measurement as well as physical description

of the tower used. Table 8.1 contains some experimental values that were compared. It can be seen that the experimental and predicted values are in excellent agreement and the error associated with these predictions was found to be less than 1%. Also, there is an improvement as compared to the work by Khan and Zubair [50] that used an improved model to predict these parameters (without incorporating the spray and rain zones) but did not take into account the decrease in water flow rate due to evaporation. In light of this, the model used is understood to be valid.

8.1.2 Validation of the Spray and Rain Zone Models

The spray and rain zone model, developed by Fisenko et. al. [53], was validated separately using the data provided by Dreyer [50]. Dreyer indicated that the only good work available in the literature regarding determination of drop velocity was by Laws [95] that he used to compare with his own model.

The results, shown in Figure 8.1 at different heights, clearly illustrate that the experimental and predicted values are in good agreement for the two drop-diameters tested. It is noted that Dreyer estimated the error in the experimental measurements of velocity to be less than 3% and we find that the current model predicts the drop velocities with an error of less than 2.5%. Furthermore, an example given by Dreyer [51] was also used to compare the results of the model with his work. In this case, by using an effective drop diameter of 1.75 mm for Fisenko's model, it was found that the results from both models agreed well with each other regarding the values of outlet air enthalpy at the top of the spray zone, the water temperature and droplet velocity at the end of the spray zone.

TABLE 8.1: Comparison of experimental and predicted values of outlet wet-bulb temperature

$t_{w,in}$	$t_{w,out}$	$t_{db,in}$	$t_{wb,in}$	\dot{m}_a	$\dot{m}_{w,in}$	$t_{wb,out}$ (Exp)	$t_{wb,out}$ (Calc)
(°C)	(°C)	(°C)	(°C)	(kg/s)	(kg/s)	(°C)	(°C)
31.22	23.88	37.05	21.11	1.158	0.754	26.05	26.31
41.44	26	34.11	21.11	1.158	0.754	30.72	30.97
28.72	24.22	29	21.11	1.187	1.259	26.17	26.30
34.5	26.22	30.5	21.11	1.187	1.259	29.94	29.93
38.78	29.33	35	26.67	1.265	1.008	32.89	32.98
38.78	29.33	35	26.67	1.250	1.008	32.89	33.04

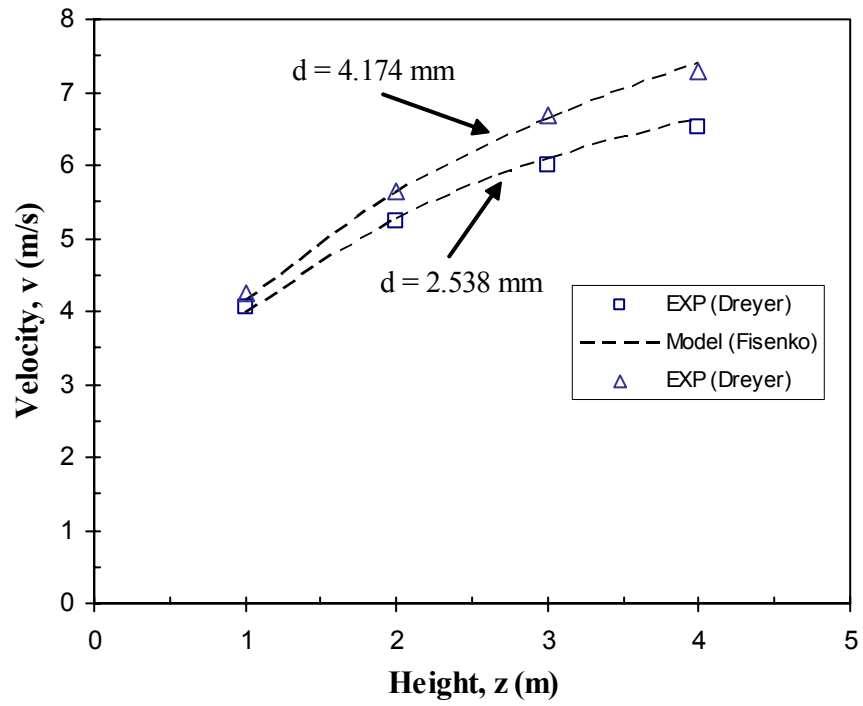


Figure 8.1: Verification of spray/rain zone model by comparing velocity prediction

8.1.3 Validation of the Complete Model

The complete model i.e. spray zone plus fill plus rain zone were coupled for this purpose as well. First, Fisenko et. al.'s model [53] was combined with the cooling tower model detailed in Threlkeld [32] involving a variable water mass flow rate to describe the spray zone and packing only. The assumption that there is a negligible pressure drop was still employed. This combined model was verified using the experimental data provided by Simpson and Sherwood [43] that used a small-sized tower. Table 8.2, shows the results of this comparison.

It is noted that these results show an improvement in the prediction of the outlet air wet-bulb temperature as compared to the values in the previous section. As the outlet air was considered to be saturated, the dry-bulb temperatures were also compared and it was found that these predictions agree well with the experimental values with a maximum error of 3.6%. For the purposes of validation, a comparison of volume prediction was also performed against the given volume of the tower used in the experiment. This was done in stages (for Run#3 in Table 8.1) by first using the packing model only, then the spray zone plus packing models and finally, all three parts i.e. spray zone plus packing plus rain zone, were coupled to see the improvement in the calculated volume. The calculation approach for the complete model is detailed in the next section. The error in volume prediction for each stage, as detailed above, was found to be 6.5%, 3.15% and 2.65% which show an improvement in volume prediction as each zone is added. The use of a model that incorporates these zones, commonly neglected in analyses, is, therefore, justified.

TABLE 8.2: Comparison of experimental and predicted values of the outlet wet- and dry-bulb temperatures modeled with spray zone and packing coupled

$t_{w,in}$	$t_{w,out}$	$t_{db,in}$	$t_{wb,in}$	\dot{m}_a	$\dot{m}_{w,in}$	$t_{wb,out}$ (Exp)	$t_{wb,out}$ (Calc)	$t_{db,out}$ (Exp)	$t_{db,out}$ (Calc)
(°C)	(°C)	(°C)	(°C)	(kg/s)	(kg/s)	(°C)	(°C)	(°C)	(°C)
31.22	23.88	37.05	21.11	1.158	0.754	26.05	26.19	27.16	26.19
41.44	26	34.11	21.11	1.158	0.754	30.72	30.76	30.94	30.76
28.72	24.22	29	21.11	1.187	1.259	26.17	26.22	26.67	26.22
34.5	26.22	30.5	21.11	1.187	1.259	29.94	29.80	30.27	29.80
38.78	29.33	35	26.67	1.265	1.008	32.89	32.86	33.27	32.86
38.78	29.33	35	26.67	1.250	1.008	32.89	32.92	33.27	32.92

8.2 VALIDATION OF EVAPORATIVE COOLER MODEL

The complete mathematical model of an evaporative fluid cooler comprising of equations (3.2), (3.4), (3.9), (3.11) and (3.18) is used with the assumption that the Lewis number is unity. Although the evaporative cooler, like the cooling tower, also has a spray and rain zone, it is not included in the current analysis. The set of five differential equations are solved using Engineering Equation Solver (EES) software and, as before, it is assumed that there is a negligible pressure drop.

Calculations regarding the evaporative fluid cooler have been validated from the experimental data provided by Jang and Wang [96] shown in Figure 8.2 and the results were found to be in good agreement. The work of Mizushina [6] and Finlay and Harris [97], giving point analyses, were also used in this regard. Furthermore, numerical examples given by Dreyer [19] and Erens [98] were also utilized that are contained in Table 8.3. It can be seen that these are in excellent agreement. In light of this, the model used is understood to be valid.

8.3 VALIDATION OF EVAPORATIVE CONDENSER MODEL

The mathematical model of an evaporative condenser comprising of equations (3.2), (3.4), (3.12), (3.13) and (3.18) is used. These are numerically solved using Engineering Equation Solver (EES) software and along with the assumptions detailed in chapter 3, it is also assumed here that there is a negligible pressure drop in the tower.

Calculations regarding the evaporative condenser have been validated from the experimental data provided by Leidenfrost and Korenic [5]. Figure 8.3 shows the comparison of the experimental and numerical values. It can be seen that the experimental and predicted values are in good agreement. The errors related with these predictions were

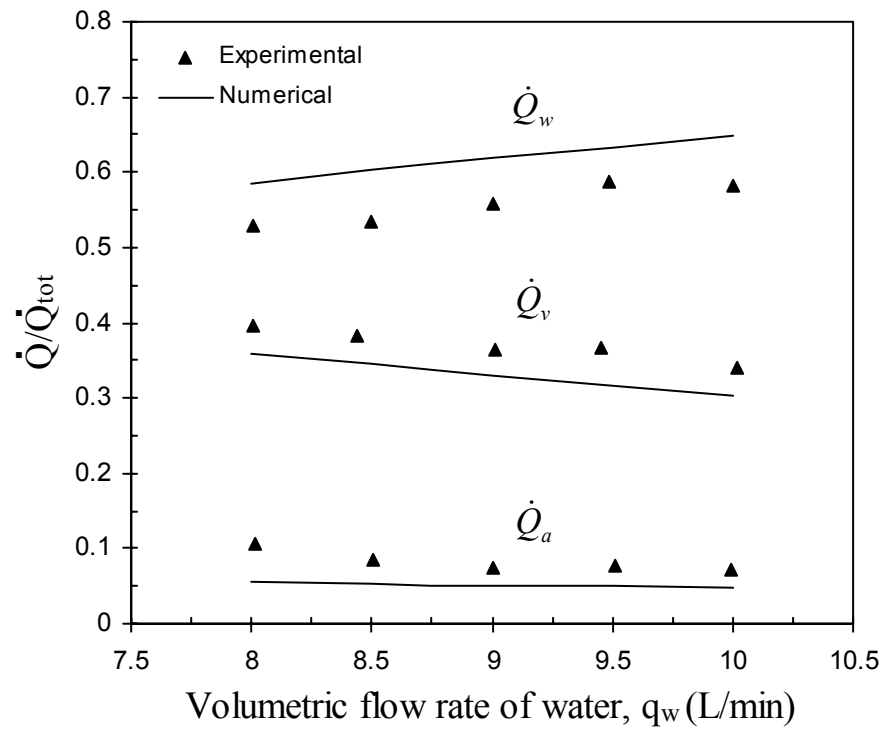


Figure 8.2: Verification of evaporative cooler model from the data of Jang and Wang

TABLE 8.3: Comparison of experimental and numerical values of process fluid outlet temperature with calculated values

\dot{m}_a	$\dot{m}_{w,in}$	\dot{m}_p	$t_{db,in}$	$t_{wb,in}$	$t_{p,in}$	$t_{p,out}$ (error)
(kg/s)	(kg/s)	(kg/s)	(°C)	(°C)	(°C)	(%)
1.88	2.667	15	25	19.5	50	-0.414
2.913	2.5	6	25	18	50	2.242
2.07	1.845	2.67	10	8.45	15.6	0
0.166	0.458	0.325	17.5	13.43	44.8	0.213

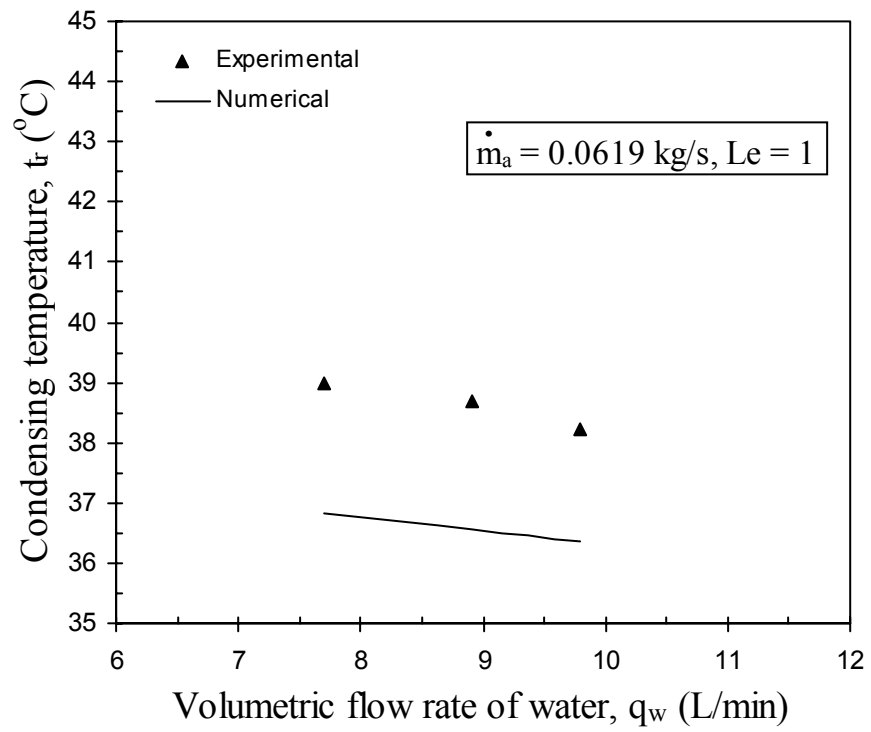


Figure 8.3: Verification of the evaporative condenser model

found to be less than 5.6%. Also, the results of two numerical examples given by Dreyer [19] were also compared and the errors associated with the heat transfer prediction were found to be less than 2.2%. In light of this, the model used is understood to be suitable.

The proposed fouling model, as presented by Khan and Zubair [88] for cooling towers, is also validated for the evaporative condenser. This is done using the data, for calcium carbonate (CaCO_3) scaling, provided by Macleod-Smith [80], shown in Figure (5.2). The model was fit to the linear version of their model given in Equation (5.20). The values of C_1 and $1/C_2$ were found to be 0.732 and 0.6, respectively. The experimental data and model values are shown in Figure 8.4, in which the normalized condenser performance index, $\eta_{C,norm}$, is presented as a function of scale thickness, δ . The two curves overlap, thus, validating the proposed fouling model.

8.4 CALCULATION APPROACH

The relevant equations for the above class of heat exchangers will be solved numerically by using EES software. It has built-in thermodynamic properties that are needed at each step of the numerical calculations. Generally, the only known quantities are the inlet and outlet water temperatures, water flow rate at the inlet (or top), air flow rate and the ambient air conditions. The dry- and wet-bulb temperature of air, temperature and enthalpy of water, humidity ratio and enthalpy of air will be obtained at each step of the numerical calculation starting from air-inlet to air-outlet values. It should be noted that since the calculations begin at the air inlet, the water flow rate is unknown and must be found iteratively by solving the relevant differential equations for the complete operating line a few times. For the complete model, the effective drop diameters must also be determined and, thus, the coupled problem must be solved in a different manner.

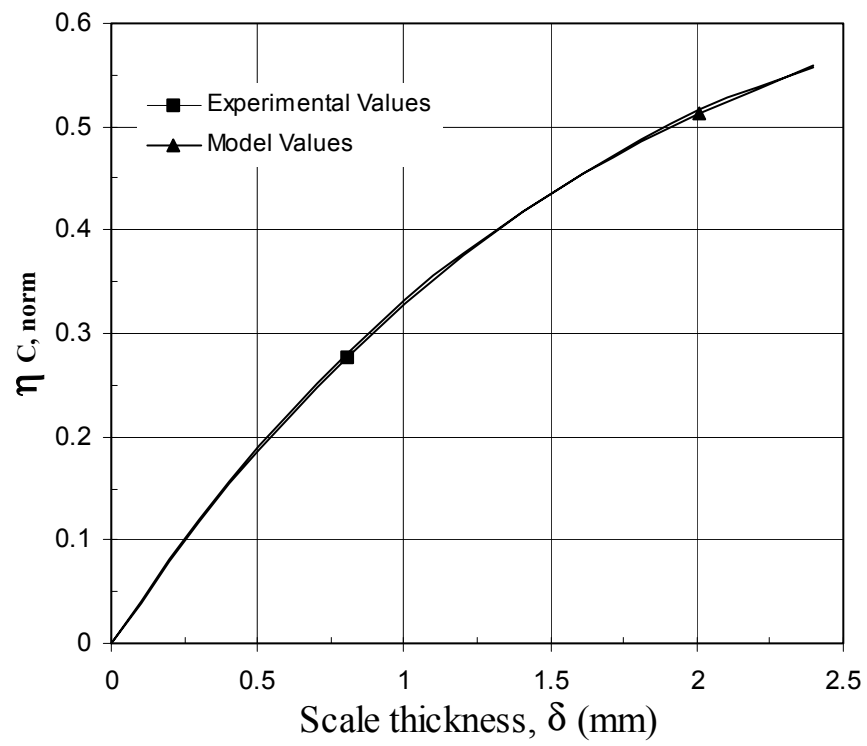


Figure 8.4: Comparison of the proposed fouling model with experimental data

The details regarding the determination of the effective drop radii are contained in the next section of this chapter. First, the rain zone is solved by assuming the water flow rate at the outlet to obtain the water and air temperatures to be used as the inlet condition for the packing model. Then the spray zone and packing model is coupled and solved simultaneously by assuming the outlet air enthalpy. Usually only 3 iterations are required to converge to the correct outlet air enthalpy by using the secant method. After this, the rain zone has to be evaluated using the new value of the water flow rate at the outlet and the whole procedure repeated until convergence is achieved. The error in the calculations is of the order of 10^{-6} . The software uses an automatic step size adjustment algorithm for the integration variable while numerically evaluating the integral between the specified limits.

Based on preliminary experience with regard to solving cooling tower and evaporative cooler equations, it is found that EES software provides faster and more accurate results because of reliable thermodynamic and thermo-physical properties of fluids, including air-water vapor mixtures.

8.4.1 Determination of Effective Drop Diameters

Fisenko et. al. [53] explained a method to determine the effective drop radius for the spray zone. This required an experimental value of the temperature drop occurring in the spray zone. Then, using the model, water temperature drop was calculated against various effective drop radii. The correct radius is found where the experimental and calculated water temperature drops are the same. In the current situation, Simpson and Sherwood did not provide such an experimental value and this was substituted with the temperature drop calculated from Dreyer's method of evaluating the spray zone as

detailed in chapter 4 where the experimental value of the outlet enthalpy was used instead of assuming it. Figure 8.5 shows the result of this method indicating that an effective drop radius of 0.9 mm was calculated.

Equation 4.26 was employed to determine the effective drop diameter for the rain zone, which is reproduced here again.

$$\begin{aligned} \frac{h_{D,rz} A_{V,rz} H_{rz}}{G_w} &= 3.6 \left(\frac{P_a}{R_v T_a} / \rho_w \right) \left(\frac{D}{v_{a,in} d_{d,eff}} \right) \left(\frac{H_{rz}}{d_{d,eff}} \right) Sc^{0.33} \times \ln \left[\frac{W_s + 0.622}{W + 0.622} \right] / (W_s - W) \\ &\times \{ 5.01334 b_1 \rho_a - 192121.7 b_2 \mu_a - 2.57724 + 23.61842 \times [0.2539 (b_3 v_{a,in})^{1.67} + 0.18] \\ &\times [0.83666 (b_4 H_{rz})^{-0.5299} + 0.42] \times [43.0696 (b_4 d_{d,eff})^{0.7947} + 0.52] \} \end{aligned} \quad (8.1)$$

where the term on the left-hand-side is called the Merkel number and the ‘a’ coefficients represent combinations of g, ρ_w, σ_w and constants as detailed below.

$$\begin{aligned} b_1 &= 998 / \rho_w & ; & & b_2 &= 3.06 \times 10^{-6} [\rho_w^4 g^9 / \sigma_w]^{0.25} \\ b_3 &= 73.298 [g^5 \sigma_w^3 / \rho_w^3]^{0.25} & ; & & b_4 &= 6.122 [g \sigma_w / \rho_w]^{0.25} \end{aligned} \quad (8.2)$$

with some restrictions as given below:

$$0.927 \leq \rho_a \leq 1.289, \text{ kg/m}^3 ; 1 \leq v_{a,in} \leq 5 \text{ m/s}$$

$$0.002 \leq d_d \leq 0.008, \text{ m} ; 1.717 \leq \mu_a \leq 1.92 \times 10^{-5}, \text{ kg/ms}$$

Equation (8.1) required the simultaneous solution of 18 equations and some constants like the diffusion coefficient of water vapor and mass flow rate of air. Besides calculating the effective drop diameter, the equation also calculates the mass transfer coefficient. The effective drop diameter was calculated to be 6.284 mm, which is approximately three times larger than that of the spray zone.

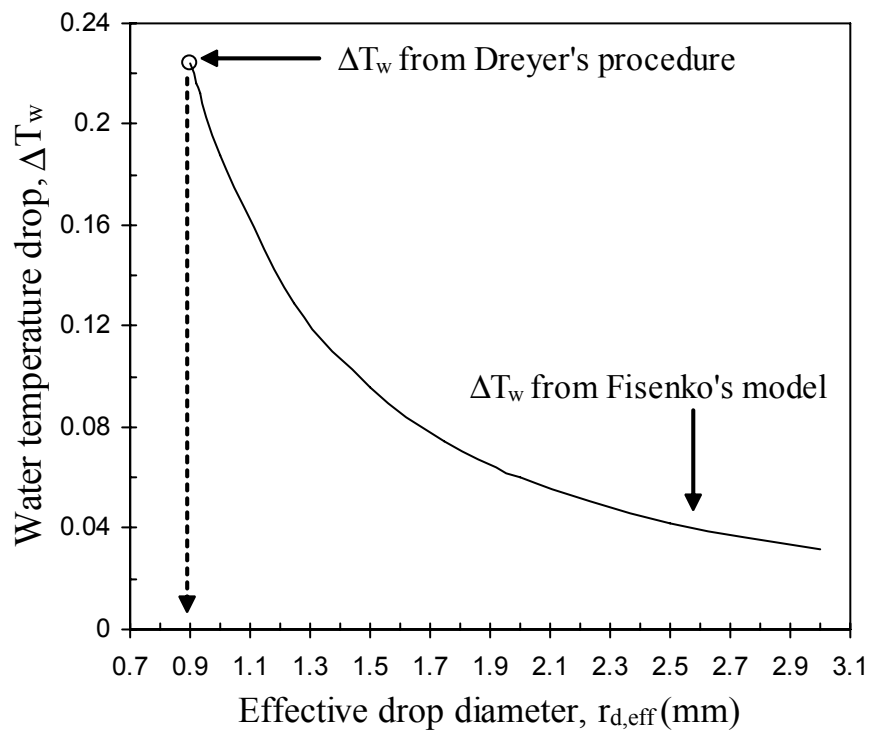


Figure 8.5: Determination of effective drop radius for the spray zone

CHAPTER 9

RESULTS AND DISCUSSION

This chapter discusses the effect of elevation and fouling on the design and rating of evaporative heat exchangers. Furthermore, the results of an exergy analysis on these heat exchangers are also presented.

9.1 RESULTS FOR COOLING TOWER

The specifications of the tower used in the analysis are the same as those of Simpson and Sherwood [43] unless otherwise indicated. It is to remind the reader that the NTU was not taken as constant and the Lewis number is taken as 0.9.

9.1.1 Effect of Pressure (Elevation)

The analysis is carried out for three different water to air flow ratios, $\dot{m}_{w,in} / \dot{m}_a = 1$, 0.75 and 0.5 with the air flow rate kept constant. Sutherland [30] mentioned that an increase in altitude of approximately 850 meters would result in a 10 kPa decrease of atmospheric pressure. This change in atmospheric pressure, due to elevation, would definitely effect the operation of a cooling tower because it directly influences the wet bulb temperature. It should be noted that Khan and Zubair [50] have demonstrated that variations in the wet bulb temperature of moist air have a significant effect on cooling tower performance. Figure 9.1 shows that the moist air wet bulb temperature decreases by 1.0 °C when the atmospheric pressure P_o decreases by 17 kPa. The dry-bulb temperature

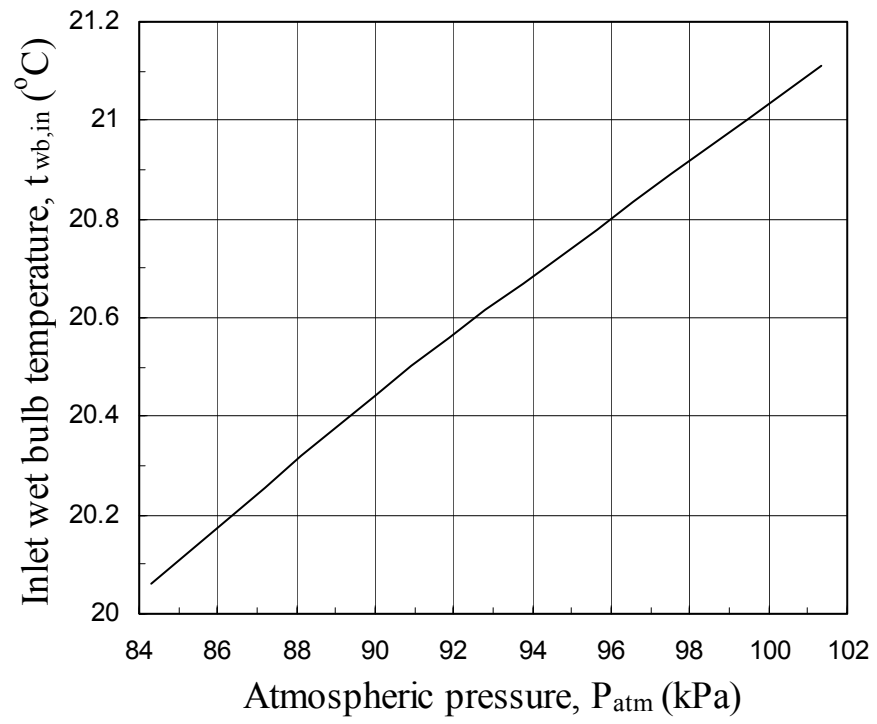


Figure 9.1: Variation in the inlet wet-bulb temperature versus pressure change

as well as the relative humidity of the air decreases with increasing altitude, lowering the wet-bulb temperature as well. Figures 9.2 and 9.3 are drawn for the following set of input data that is considered in Simpson and Sherwood [43]: $t_{db,in} = 29\text{ }^{\circ}\text{C}$, $t_{wb,in} = 21.11\text{ }^{\circ}\text{C}$, $t_{w,in} = 28.72\text{ }^{\circ}\text{C}$, $t_{w,out} = 24.22\text{ }^{\circ}\text{C}$. The plot of tower volume versus the decrease in atmospheric pressure is presented in Figure 9.2. The figure shows that for achieving the same water outlet temperature, the volume of the tower can be reduced by 0.15 m^3 approximately when $m_{ratio} = 1.0$. The reduction in required volume with the increasing altitude can be understood from the fact that both the dry and wet bulb temperatures decrease. The colder air cools the water comparatively better and, thus, requires less volume for the same range. Also, as the atmospheric pressure decreases, the value of $(W_{s,w} - W)$ increases and, thus, the volume decreases [30] (See eq. 3.37). However, the required volume is larger as the value of the mass flow rate ratio increases due to lesser time available for cooling the water and, therefore, requires a larger volume as compared to lower water flow rates. It is evident from Figure (9.3) that the percentage decrease in required volume is less as the value of the mass flow rate ratio decreases. In this regard, it is noted that a higher value of the mass flow rate ratio results in a higher rate of change of the humidity ratio and, consequently, a higher rate of change of the required volume (See eqs. (3.36) and (3.37)).

9.1.2 Effect of Fouling

The cooling tower model, discussed in the chapter 3, is used for design and rating calculations of a counter flow wet cooling tower. It is used in combination with the fouling model to study the thermal performance of the tower under fouled conditions.

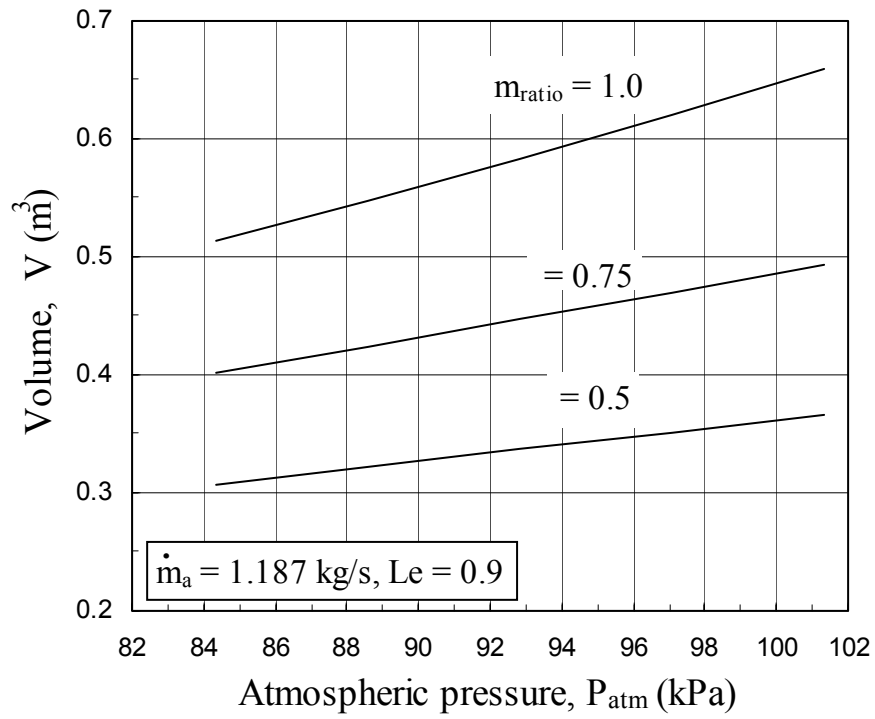


Figure 9.2: Variation in required volume versus pressure change

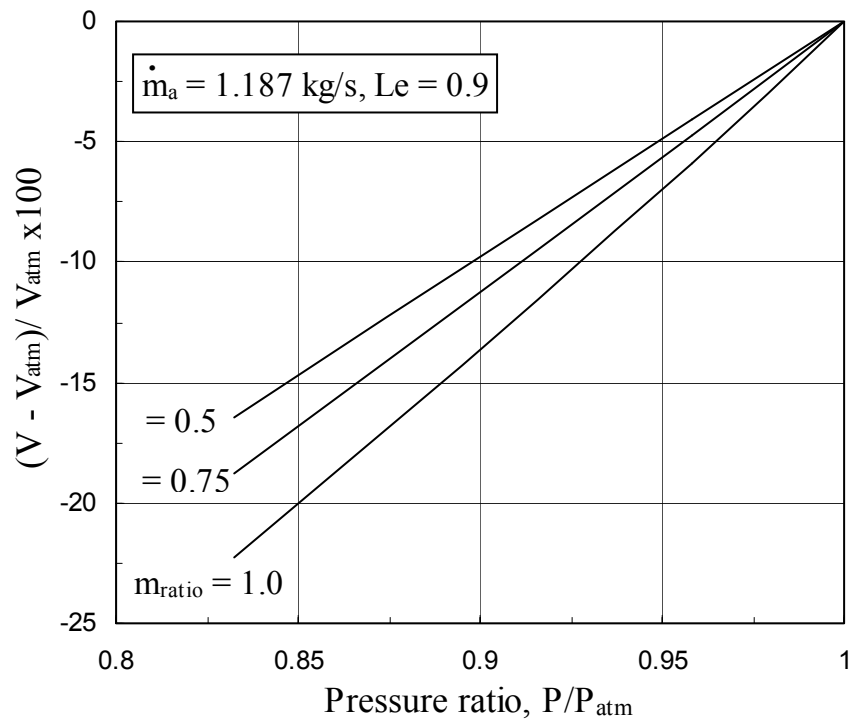


Figure 9.3: Percent decrease in required volume versus pressure ratio

9.1.2.1 Design

In design calculations, the volume of the cooling tower is calculated for the following set of input conditions: inlet air temperatures [dry bulb ($t_{db,in}$) and wet bulb ($t_{wb,in}$)], water inlet temperature ($t_{w,in}$), mass flow rates [air (\dot{m}_a) and water ($\dot{m}_{w,in}$)], normalized fill performance index ($\eta_{F,norm}$), and water outlet temperature ($t_{w,out}$).

We know that the fouling reduces the performance of a cooling tower, which is reflected in the decreased value of the tower effectiveness (shown in the next section). In order to achieve a constant value of the cooling tower effectiveness under fouled conditions, its volume has to be increased, which is shown in Figure (9.4). In this figure, a plot of the volume fraction (V_f / V_{cl}) of the cooling tower is shown as a function of constant C_f . It should be noted that the constant C_f represents the increase in value of $\eta_{F,norm}$ when the fouling reaches its asymptotic value.

9.1.2.2 Rating

In rating calculations, water outlet temperature ($t_{w,out}$) and tower effectiveness (ε_{ct}) are calculated for the following set of input conditions: inlet air temperatures [dry bulb ($t_{db,in}$) and wet bulb ($t_{wb,in}$)], water inlet temperature ($t_{w,in}$), mass flow rates [air (\dot{m}_a) and water ($\dot{m}_{w,in}$)], normalized fill performance index ($\eta_{F,norm}$) and tower volume (V).

The time and risk dependent effectiveness of the cooling tower is presented in Figure (9.5) in reduced coordinates. The reduced effectiveness $\varepsilon_{ct}(w, p; \sqrt{\alpha}) / \varepsilon_{ct}(0)$ versus reduced fouling weight w/M , for different risk level p and scatter parameter $\alpha^{1/2} = 0.3$, is plotted for the fouling-growth model discussed earlier. As expected, the effectiveness of the cooling tower degrades significantly with time

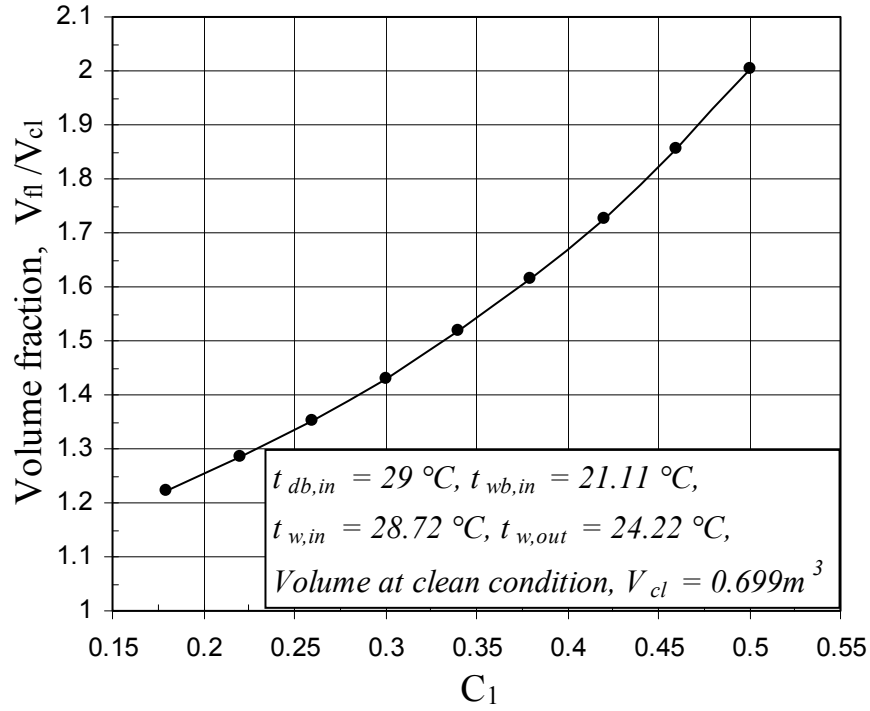


Figure 9.4: Volume fraction as a function of constant C_1

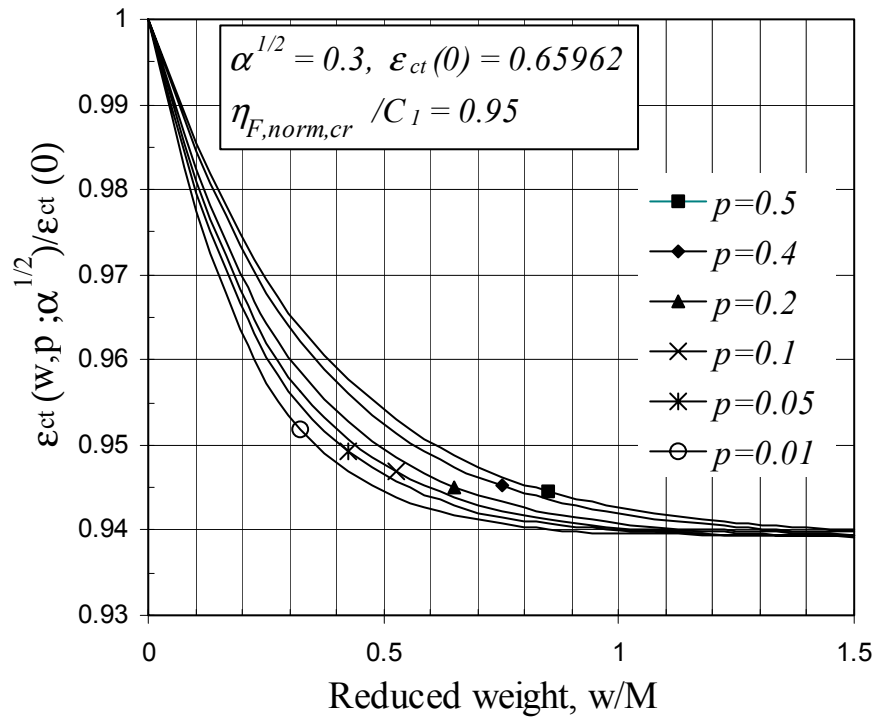


Figure 9.5: Normalized tower effectiveness versus reduced weight

indicating that for a low risk level ($p = 0.01$), there is about 6.0 % decrease in effectiveness for the given fouling model. The variations in the reduced water outlet temperature versus reduced fouling weight for different risk levels p and for scatter parameter $\alpha^{1/2} = 0.3$, is shown in Figure (9.6). The figure shows that for a low risk level (i.e., high reliability) when compared with the deterministic case ($p = 0.5$), the water outlet temperature is higher, indicating that there will be a lower rate of heat transfer due to fouling and, therefore, cleaning of the heat exchanger will be done earlier. It is noticed that there is about 1.2 % increase in water outlet temperature for the given fouling model.

9.1.3 Sensitivity Analysis Results

The computer model of the cooling tower discussed in chapter 3 was used for studying the sensitivity analysis of the cooling tower. It was noticed that the sensitivity coefficients could be misleading and, therefore, the normalized sensitivity coefficients were calculated. As before, the analysis is carried out for three different water to air flow ratios, $\dot{m}_{w,in} / \dot{m}_a = 1, 0.75$ and 0.5 with the air flow rate kept constant. It should be noted that, in plots regarding cooling tower design, $t_{wb,in}$ is varied from 12.11 to 23.11 °C and $t_{w,out}$ from 22.22 to 27.22 °C. On the other hand, in the figures regarding rating of cooling towers, $t_{wb,in}$ is varied from 12.11 to 26.11 °C and $t_{w,in}$ from 24.72 to 40.72 °C.

9.1.3.1 Design

The literature reports that for design calculations of the cooling tower, the air inlet wet bulb and water outlet temperatures are the two most important input parameters influencing the performance of cooling towers.

Figures (9.7), (9.8) and (9.9) are normalized forms of the plots between volume sensitivity coefficients $(\partial V / \partial t_{wb,in})$, $(\partial V / \partial t_{w,out})$, and $(\partial V / \partial t_{w,in})$ versus the inlet wet-

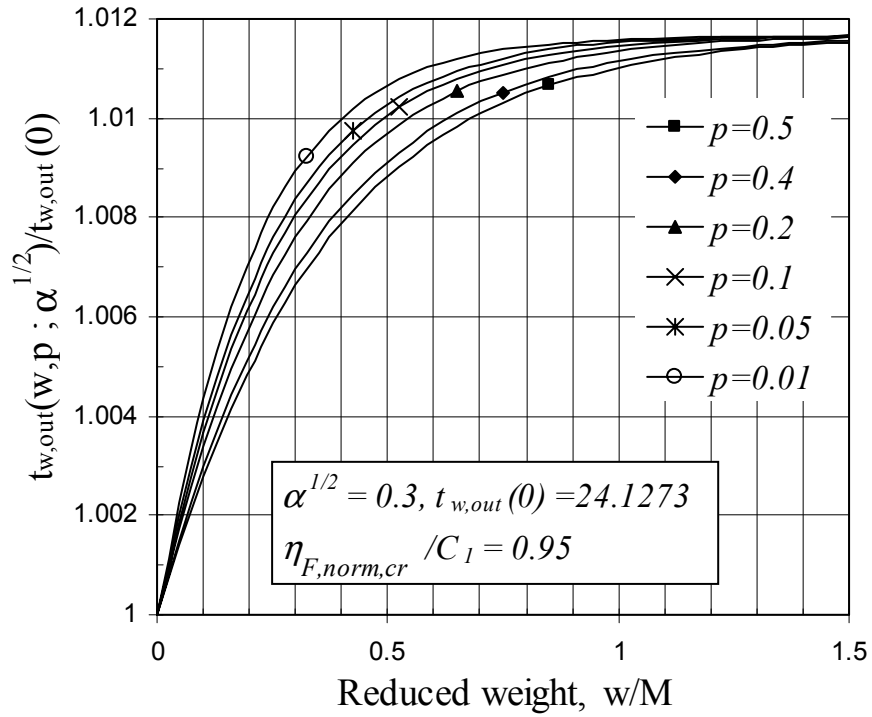


Figure 9.6: Reduced water outlet temperature versus reduced weight

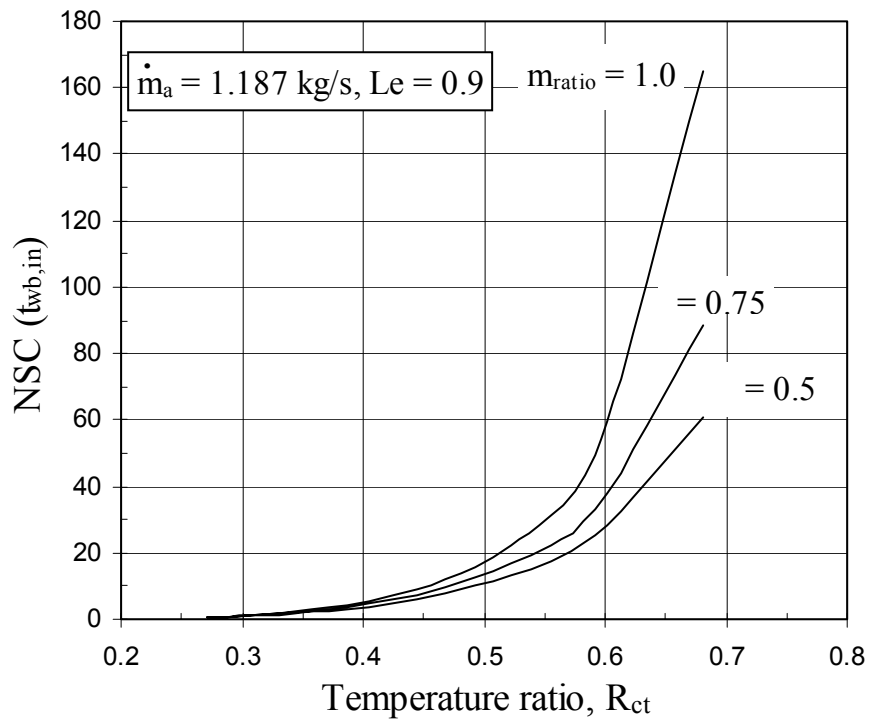


Figure 9.7: Variation of volume NSC w.r.t. air inlet wet-bulb temperature versus R_{ct}

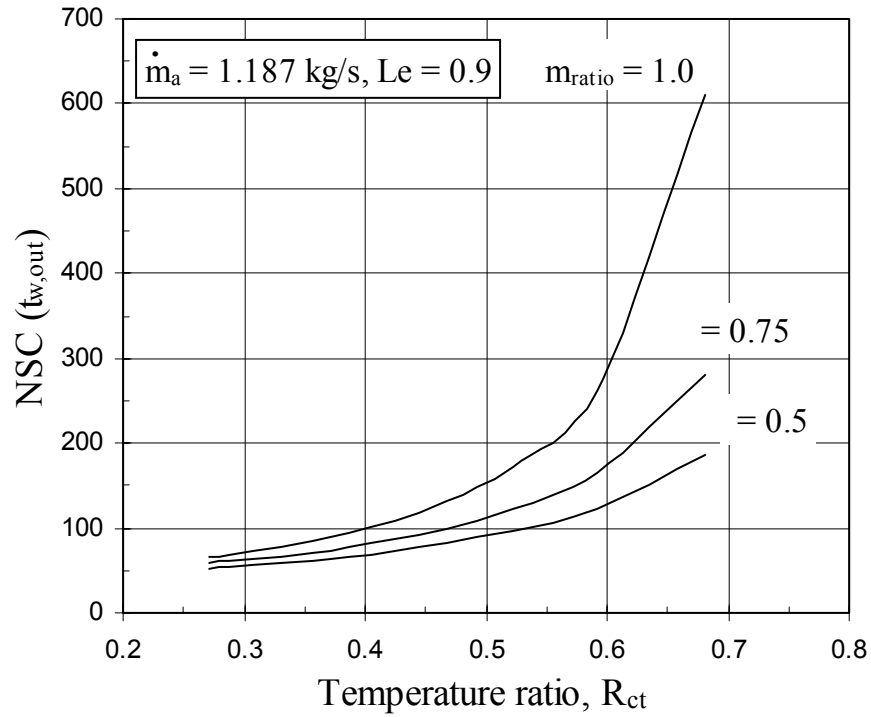


Figure 9.8: Variation of volume NSC w.r.t. water outlet temperature versus R_{ct}

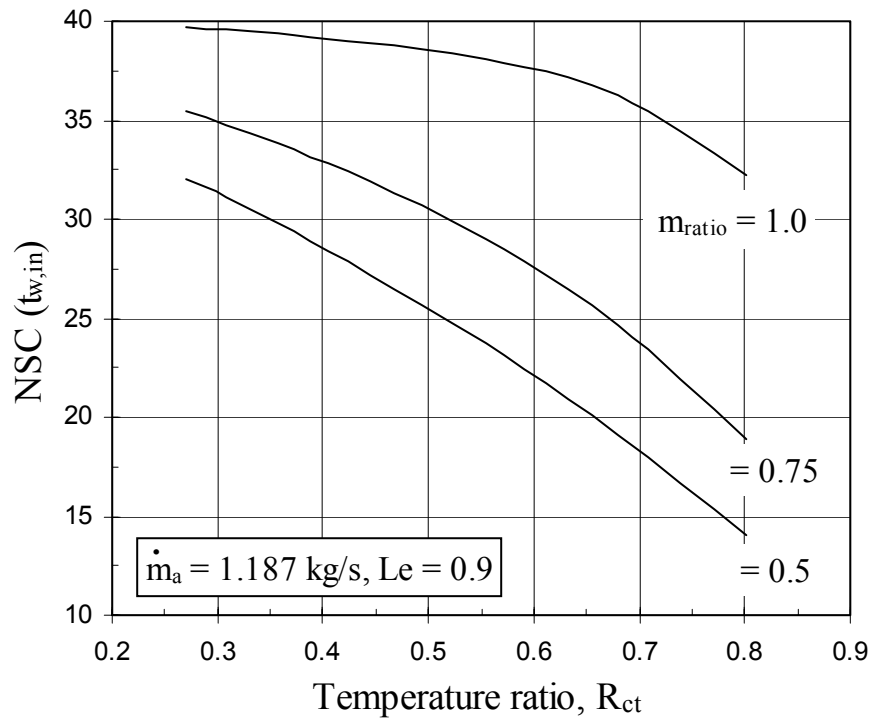


Figure 9.9: Variation of volume NSC w.r.t. water inlet temperature versus R_{ct}

bulb temperature, for different values of mass flow rate ratio. Figures (9.7) and (9.8) show that, as the value of the temperature ratio increases, the sensitivity of volume with respect to $t_{wb,in}$ and $t_{w,out}$ also increases. As $t_{wb,in}$ increases, the decreasing difference between $t_{wb,in}$ and $t_{w,in}$ gives rise to larger volume requirements as well as a higher rate of the change of volume. The increase in sensitivity with R is higher for large mass flow rate ratios (See eqs. (3.36) and (3.37)). On the other hand, in Figure (9.9), the sensitivity decreases with an increase in R but is still higher for large mass flow rate ratios. With $t_{w,in}$ constant, and being a comparatively less important factor, the volume change (ΔV) is less as $t_{wb,in}$ increases. Coupled with the fact that the nominal values of the volume are same for all three figures, the NSC decreases. As expected, the sensitivity coefficient with respect to $t_{w,out}$ is greater than $t_{wb,in}$. Figures (9.10) and (9.11) combine these three NSCs showing how they vary with respect to each other at different mass flow ratios and clearly indicating that the volume NSC with respect to water outlet temperature dominates.

Similarly, Figures (9.12), (9.13) and (9.14) are normalized forms of the plots between volume sensitivity coefficients $(\partial V / \partial t_{wb,in})$, $(\partial V / \partial t_{w,out})$, and $(\partial V / \partial t_{w,in})$ versus the outlet water temperature, for different values of mass flow rate ratio. Figure (9.12) shows that as the value of the temperature ratio increases (decreasing $t_{w,out}$), the sensitivity of volume with respect to $t_{wb,in}$ also increases and is higher for large mass flow rate ratios. At low R_{ct} , the low range accounts for the low sensitivity as volume required is small and the effect of change in $t_{wb,in}$ on the volume change is not much but, at high values of R_{ct} , as the range increases, the water outlet temperature approaches the inlet wet bulb temperature, increasing the sensitivity since the effect of change in $t_{wb,in}$ on the volume change increases. Figure (9.13) indicates that the NSC with respect to $t_{w,out}$

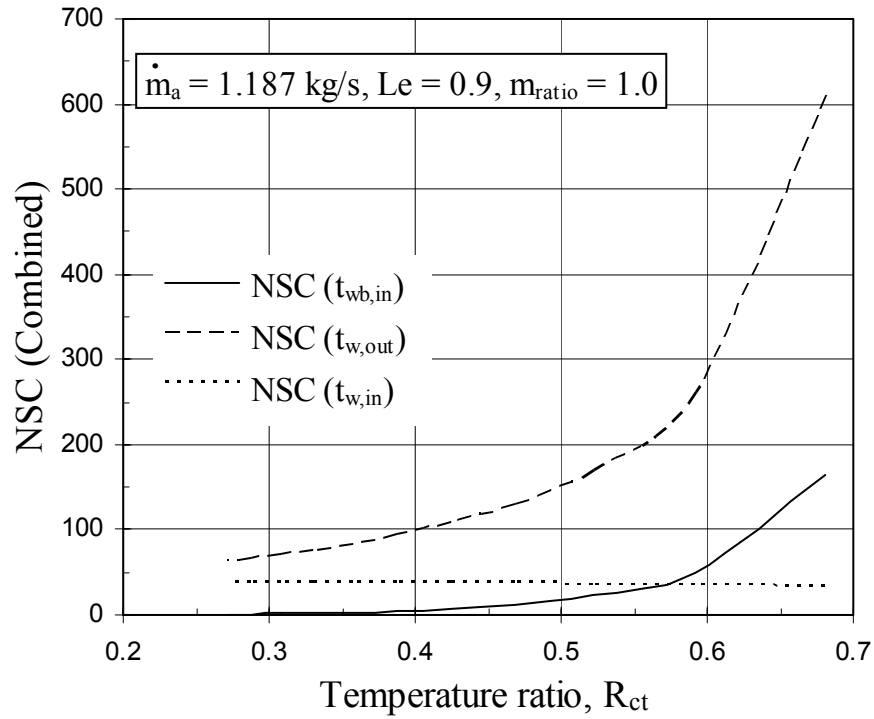


Figure 9.10: Variation of all NSCs versus R_{ct} with mass flow ratio of 1

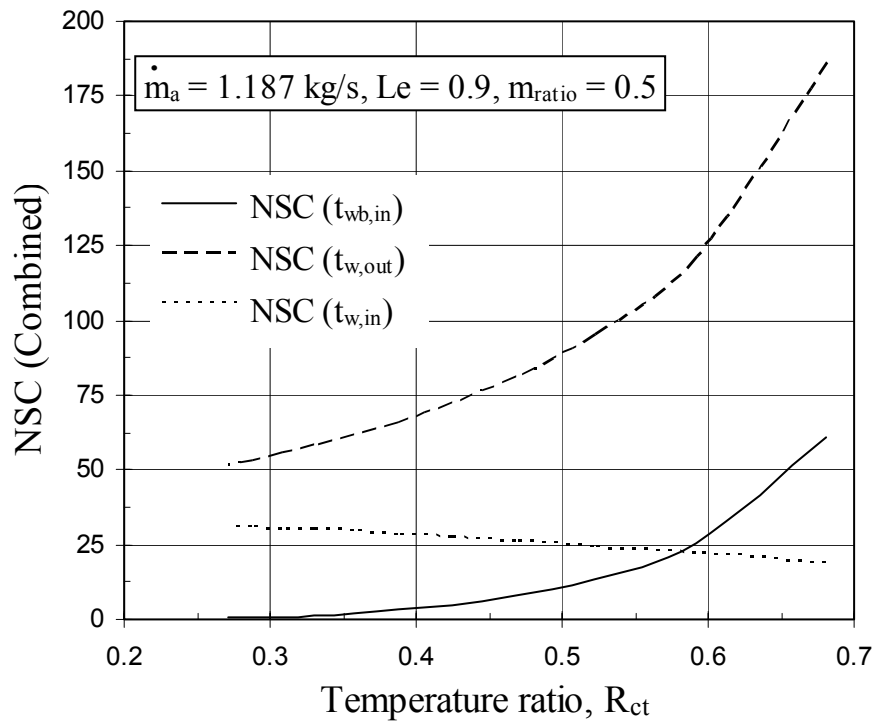


Figure 9.11: Variation of all NSCs versus R_{ct} with mass flow ratio of 0.5

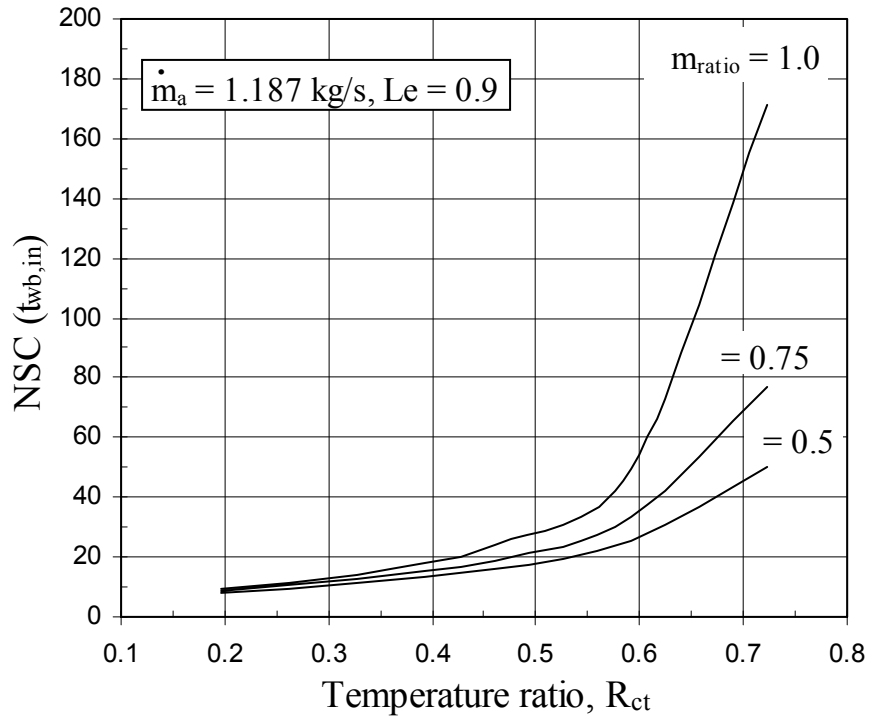


Figure 9.12: Variation of volume NSC w.r.t. air inlet wet-bulb temperature versus R_{ct}

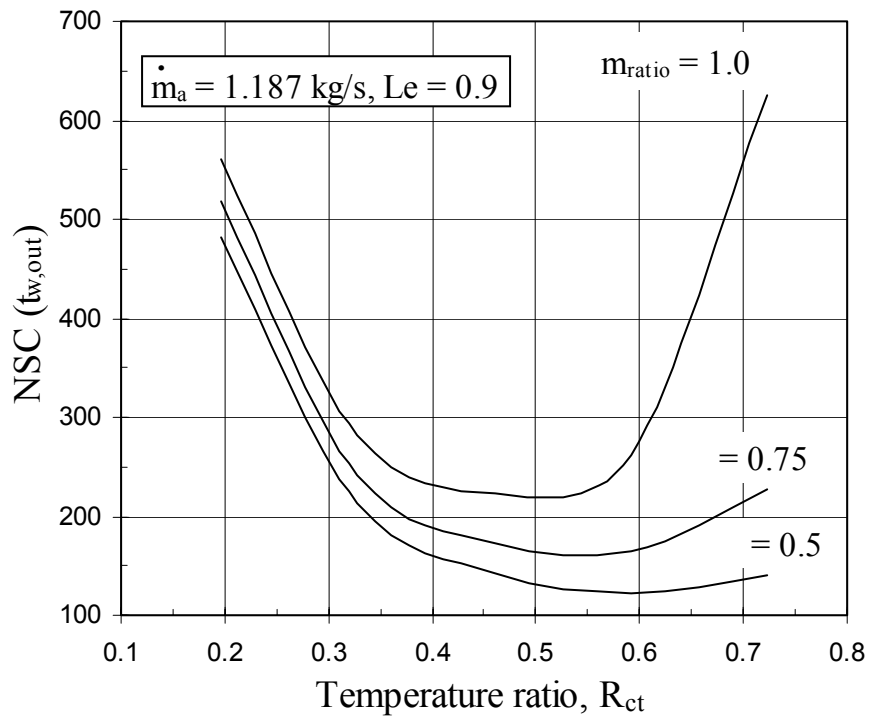


Figure 9.13: Variation of volume NSC w.r.t. water outlet temperature versus R_{ct}

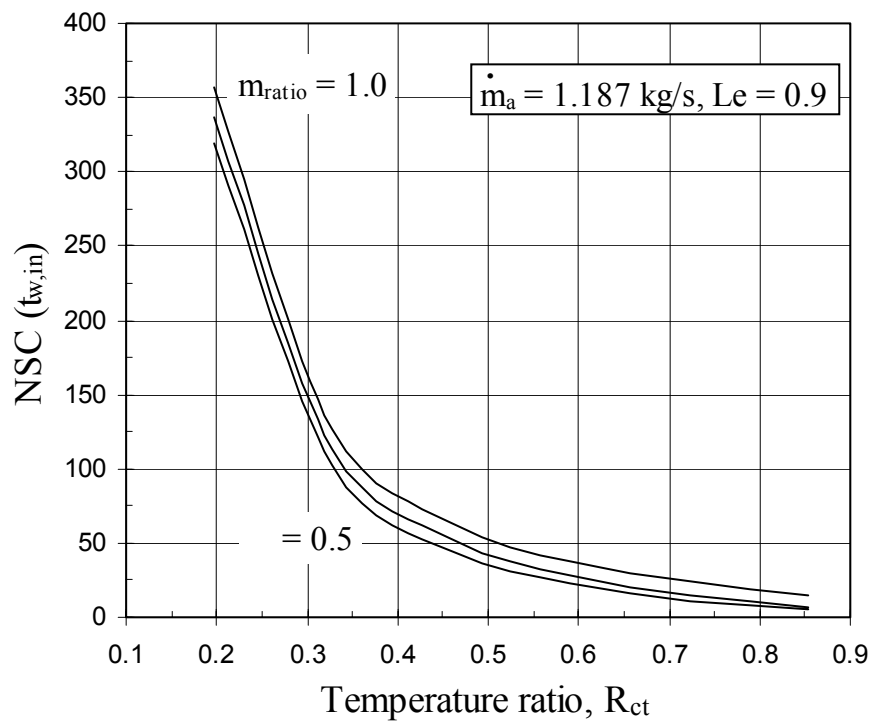


Figure 9.14: Variation of volume NSC w.r.t. water inlet temperature versus R_{ct}

minimizes at different values of the temperature ratio for different mass flow ratios. At low R_{ct} , the higher values of $t_{w,out}$ accounts for the high sensitivity. On the other hand, at high values of R_{ct} , the increasing sensitivity is caused by the decreasing difference between $t_{w,out}$ and $t_{wb,in}$. In Figure (9.14), the sensitivity decreases with an increase in R_{ct} but does not differ greatly for different mass flow rate ratios. At low R_{ct} (higher values of $t_{w,out}$), the effect of change in $t_{w,in}$ on the volume change is greater as compared to high values of R_{ct} when $t_{w,out}$ is far away from $t_{w,in}$. Again, we see that the sensitivity coefficient with respect to $t_{w,out}$ is greater than $t_{wb,in}$. Figure (9.15) and (9.16) combine these three NSCs showing how they vary with respect to each other at different mass flow ratios and, again, we see that the volume NSC with respect to water outlet temperature dominates throughout for the two extreme mass flow ratios investigated confirming previous studies in literature.

9.1.3.2 Rating

Figures (9.17) and (9.18) are normalized forms of the plots between effectiveness sensitivity coefficients $(\partial \varepsilon_{ct} / \partial t_{w,in})$ and $(\partial \varepsilon_{ct} / \partial \dot{m}_{w,in})$ versus the inlet wet-bulb temperature, for different values of mass flow rate ratio. These plots are drawn for rating calculations of the cooling tower data mentioned earlier at standard atmospheric pressure. Figures (9.17) and (9.18) show that as the value of the temperature ratio increases, the sensitivity of effectiveness with respect to $t_{w,in}$ and $\dot{m}_{w,in}$ also increases but is lower for large mass flow rate ratios. This trend was observed for \dot{m}_a also and the plot was identical to that of $\dot{m}_{w,in}$. It is understood that the effectiveness decreases with the increase in $t_{wb,in}$ [50]. In Figures (9.17), at low values of R_{ct} (or $t_{wb,in}$), the effect of change of $t_{w,in}$ on effectiveness change $(\Delta \varepsilon_{ct})$ is not significant due to the large difference between these

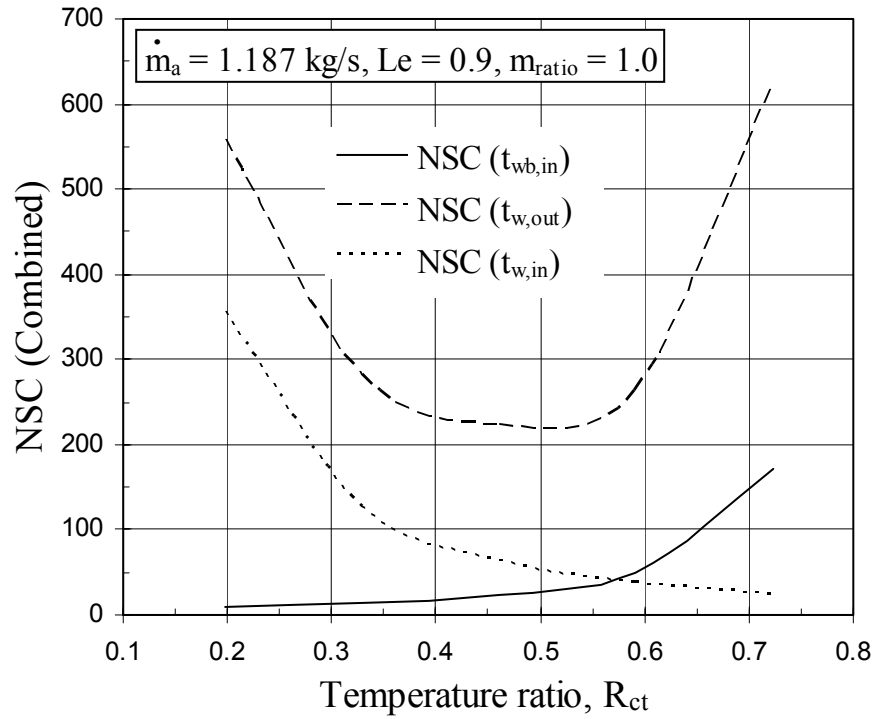


Figure 9.15: Variation of all NSCs versus R_{ct} with mass flow ratio of 1

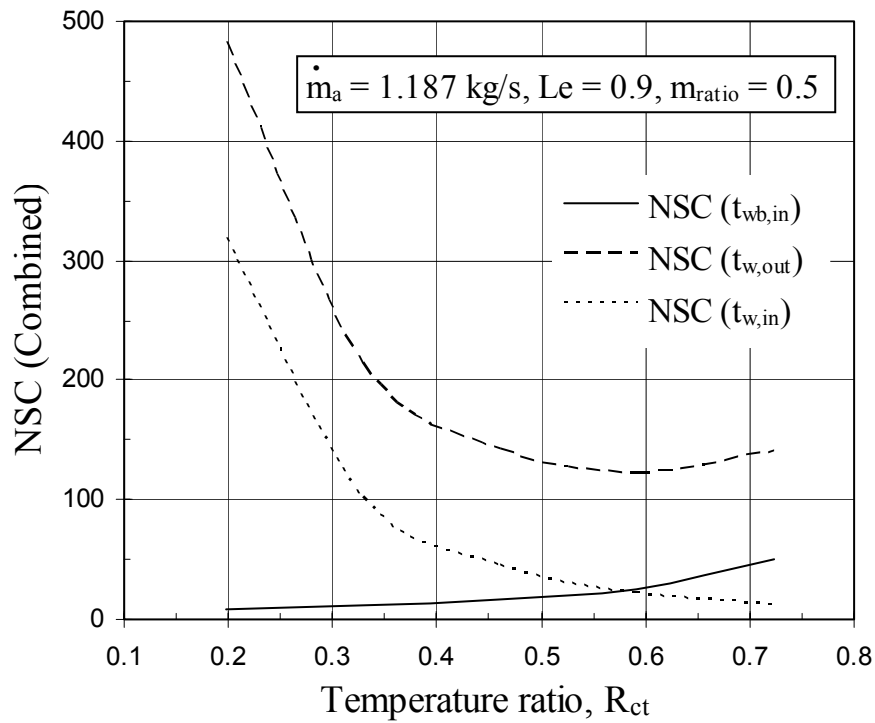


Figure 9.16: Variation of all NSCs versus R_{ct} with mass flow ratio of 0.5

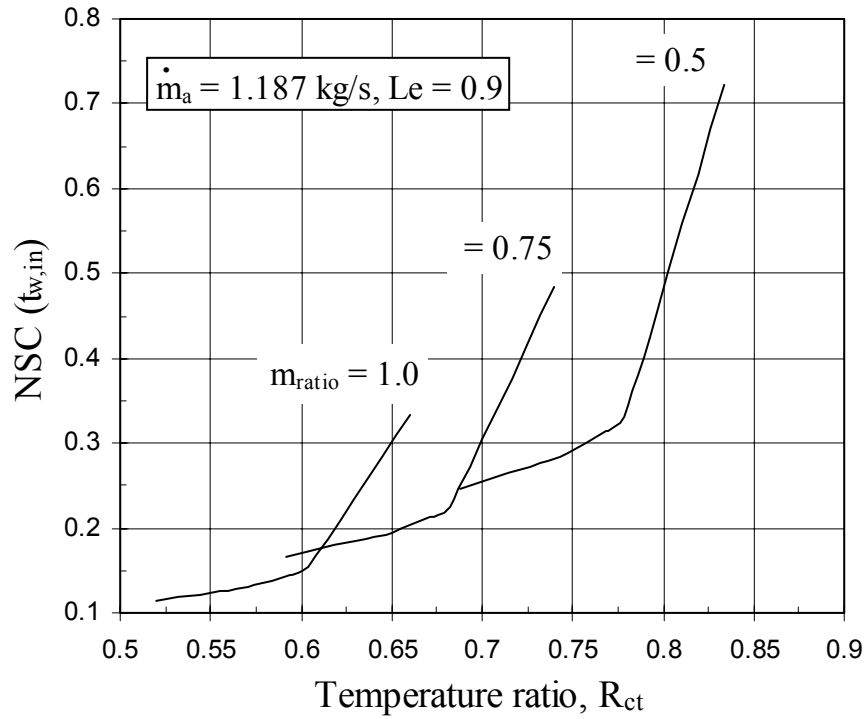


Figure 9.17: Variation of effectiveness NSC w.r.t. inlet water temperature versus R_{ct}

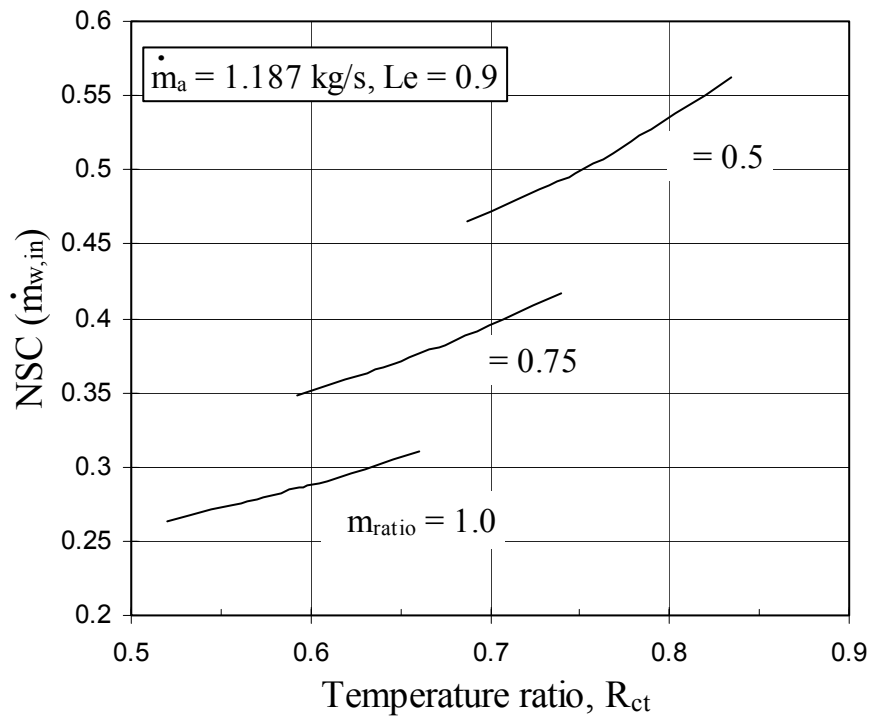


Figure 9.18: Variation of effectiveness NSC w.r.t. water flow rate versus R_{ct}

quantities as compared to when R_{ct} (or $t_{wb,in}$) has a high value and, subsequently, $(t_{w,in} - t_{wb,in})$ has a much smaller value. Thus, the NSC increases as the inlet wet bulb temperature rises. The behavior seen in Figures (9.18) can be understood from the fact that the value of $(t_{w,in} - t_{wb,in})$ decreases, as R_{ct} (or $t_{wb,in}$) increases. The effect of perturbing $\dot{m}_{w,in}$ is greater on effectiveness change ($\Delta\epsilon_{ct}$) at higher values of R_{ct} since moist air enthalpy is higher giving rise to a higher rate of change of the air enthalpy. Figures (9.19) and (9.20) combine these two NSCs showing how they vary with respect to each other at different mass flow ratios and it is seen that the effectiveness NSC with respect to water flow rate dominates mostly and only at a high value of the inlet wet-bulb temperature does the effectiveness NSC with respect to inlet water temperature become greater.

Similarly, Figures (9.21) and (9.22) are normalized forms of the plots between effectiveness sensitivity coefficients $(\partial\epsilon_{ct} / \partial t_{w,in})$ and $(\partial\epsilon_{ct} / \partial \dot{m}_{w,in})$ versus the inlet water temperature, for different values of mass flow rate ratio. It is understood that the effectiveness decreases with the increase in $t_{w,in}$ [50]. In Figure (9.21), we note that irrespective of the mass flow ratio, the sensitivity minimizes at an R -value of 0.775. The initial almost-vertical line is due to the very close values of $t_{w,in}$ and $t_{wb,in}$ (cooling range is small) but since the volume is fixed, the rate of effectiveness change resulting from perturbing $t_{w,in}$ is higher. No sharp slope is seen at higher values of $t_{w,in}$ as the inlet water temperature does not have a theoretical upper limit. Since the ability of a tower to cool water is limited (as volume is fixed), the sensitivity minimizes and then increases as $t_{w,in}$ increases. On the other hand, Figure (9.22) show that as the value of the temperature ratio increases, the sensitivity of effectiveness with respect to $\dot{m}_{w,in}$ also increases. This is because the higher water temperature constitutes a higher energy level making the tower

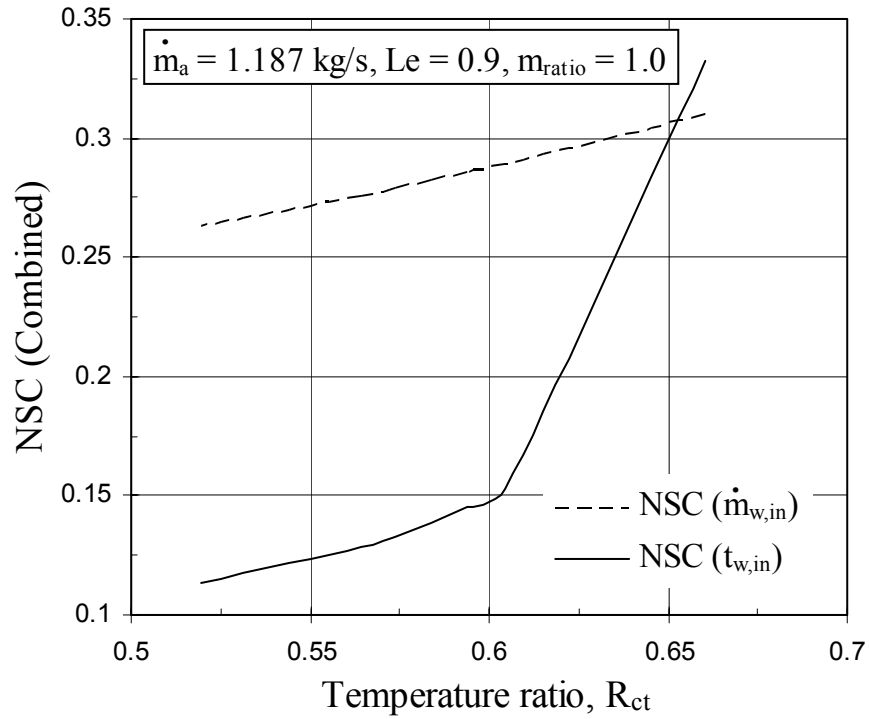


Figure 9.19: Variation of all NSCs versus R_{ct} with mass flow ratio of 1

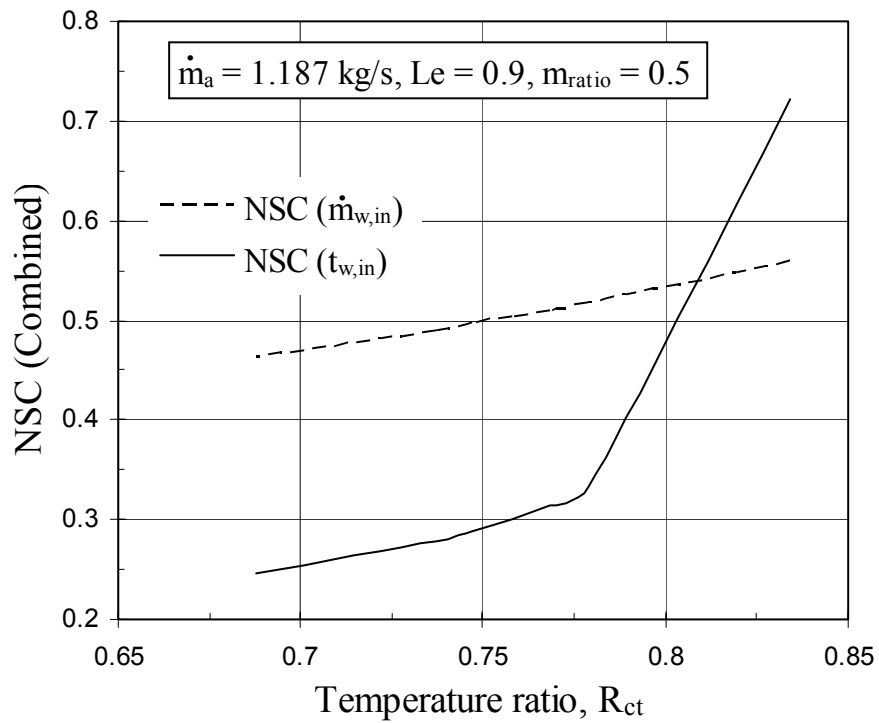


Figure 9.20: Variation of all NSCs versus R_{ct} with mass flow ratio of 0.5

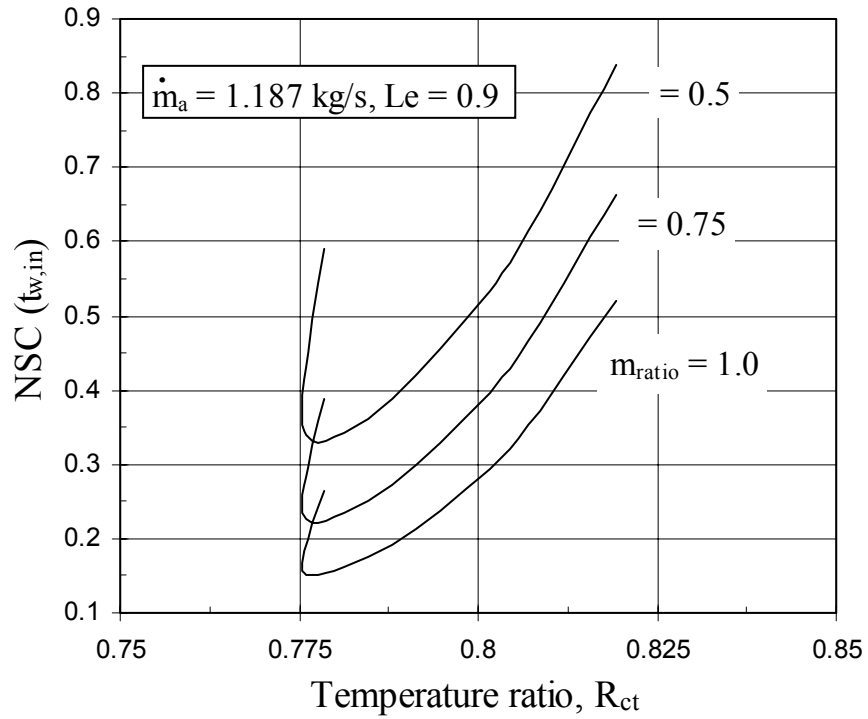


Figure 9.21: Variation of effectiveness NSC w.r.t. inlet water temperature versus R_{ct}

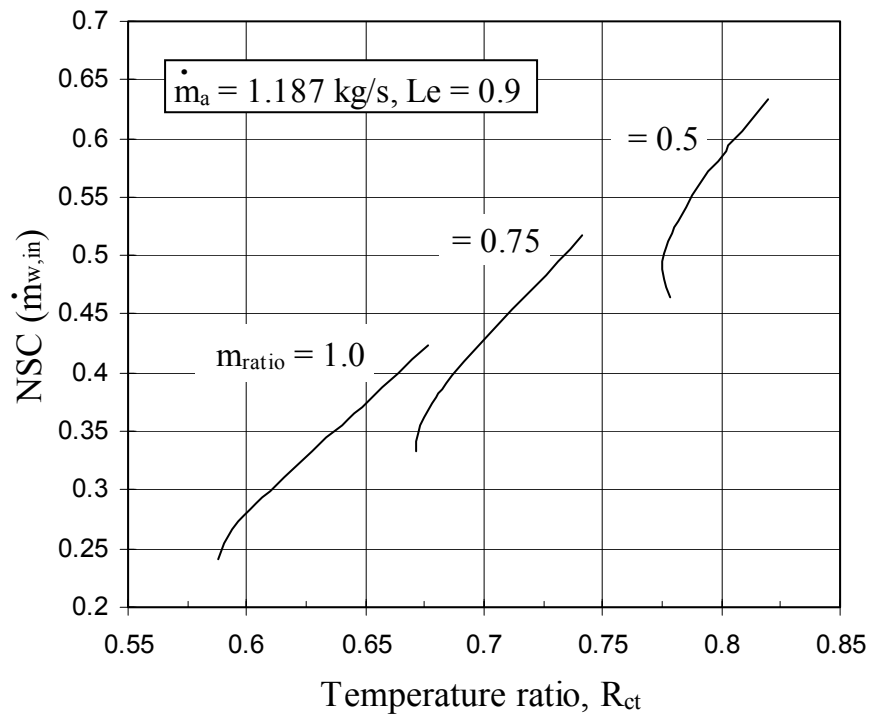


Figure 9.22: Variation of effectiveness NSC w.r.t. water flow rate versus R_{ct}

more susceptible to changes in its water flow rate and, thus, resulting in a greater effectiveness change for the same amount of perturbation of $\dot{m}_{w,in}$. For both figures, the sensitivity is lower for large mass flow rate ratios. It was seen again that the NSC plot for \dot{m}_a was the same as that for $\dot{m}_{w,in}$. In Figures (9.23) and (9.24), which combines these two NSCs, the sensitivities cross each other at two places showing the complexity of the cooling tower during its performance.

Figures (9.25) and (9.26) are normalized forms of the plots between water outlet temperature sensitivity coefficients $(\partial t_{w,out} / \partial t_{wb,in})$ and $(\partial t_{w,out} / \partial t_{w,in})$ versus the inlet wet-bulb temperature, for different values of mass flow rate ratio. It is noted that $t_{w,out}$ increases with the increase in $t_{wb,in}$ [50]. Figures (9.25) shows that as the value of the temperature ratio increases, the NSC also increases and is lower for large mass flow rate ratios. At low R-value, the possible cooling range is large and is probably near to the limit of the small-sized cooling tower used in the calculation and, thus, perturbing $t_{wb,in}$ has a smaller effect as compared to higher values of R_{ct} . Figure (9.26) illustrates that as the value of the temperature ratio increases, the NSC decreases and is higher for large mass flow rate ratios. For every 1°C rise in $t_{wb,in}$, the nominal value of the water outlet temperature would rise almost as much since $t_{wb,in}$ is the theoretical lower limit for the water temperature, yet it would change much less for every 1°C change in $t_{w,in}$. Thus, perturbing $t_{w,in}$ has a decreasing effect on water outlet temperature change as the increasing wet bulb temperature would increasingly limit the ability of the air to cool the water. Figures (9.27) and (9.28) combine these two NSCs and it is seen that, initially, the water outlet temperature NSC with respect to water inlet temperature dominates and then the other after a certain value of the temperature ratio.

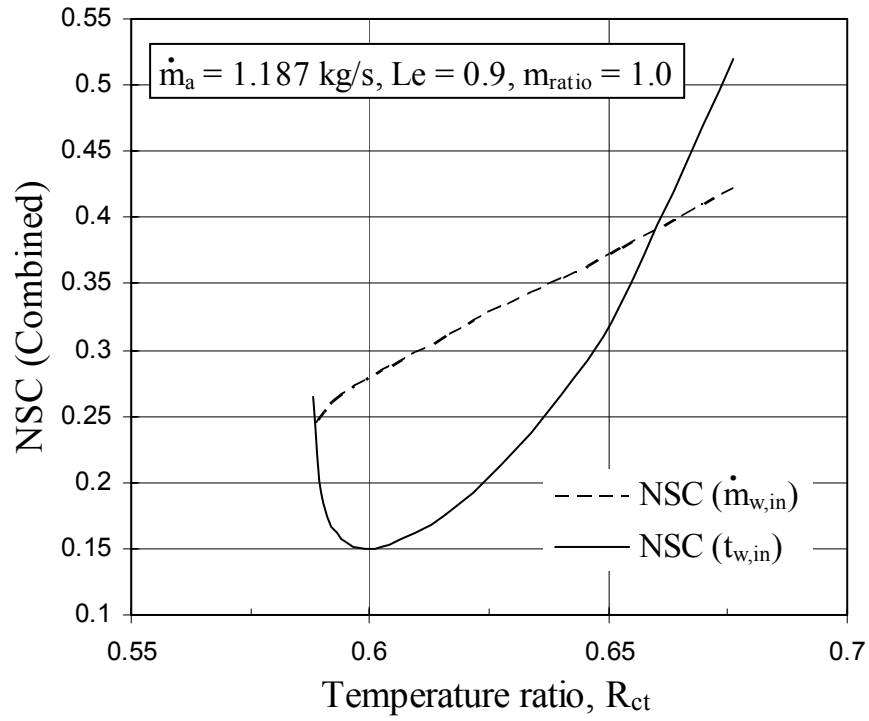


Figure 9.23: Variation of all NSCs Versus R_{ct} with mass flow ratio of 1

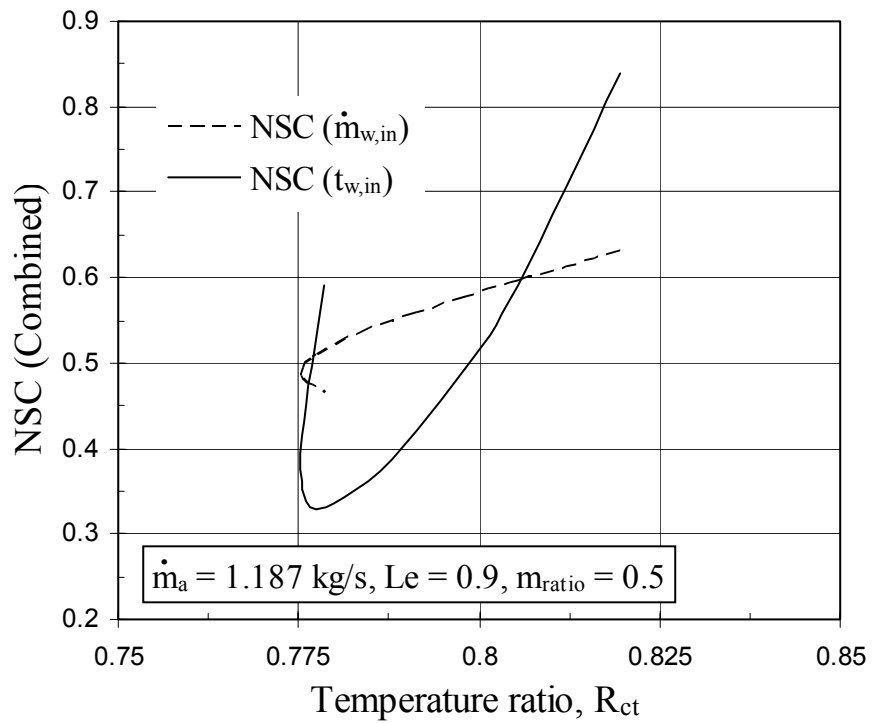


Figure 9.24: Variation of all NSCs versus R_{ct} with mass flow ratio of 0.5

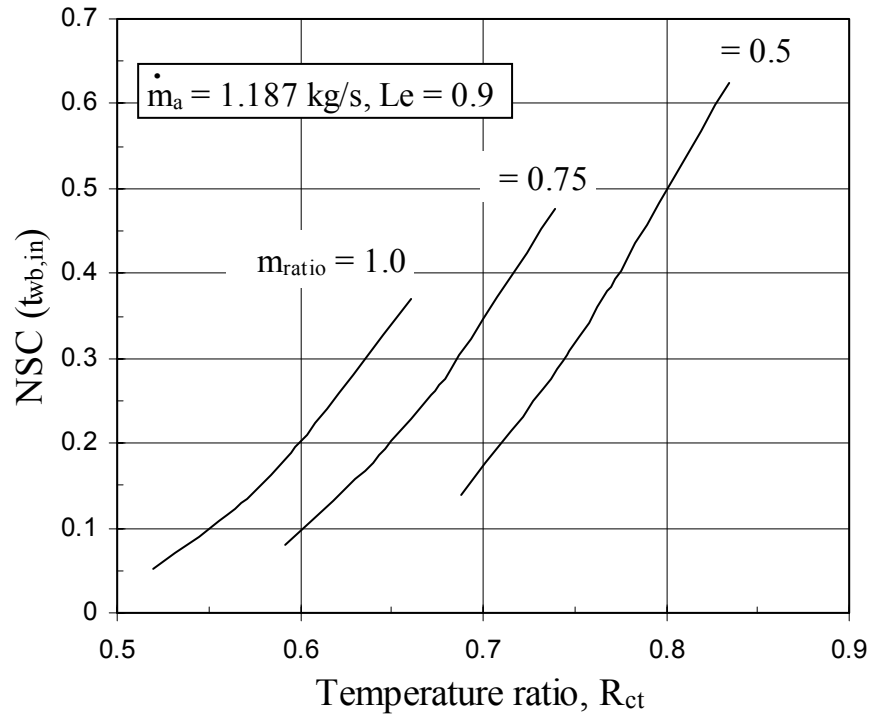


Figure 9.25: Variation of water outlet NSC w.r.t. inlet wet-bulb temperature versus R_{ct}

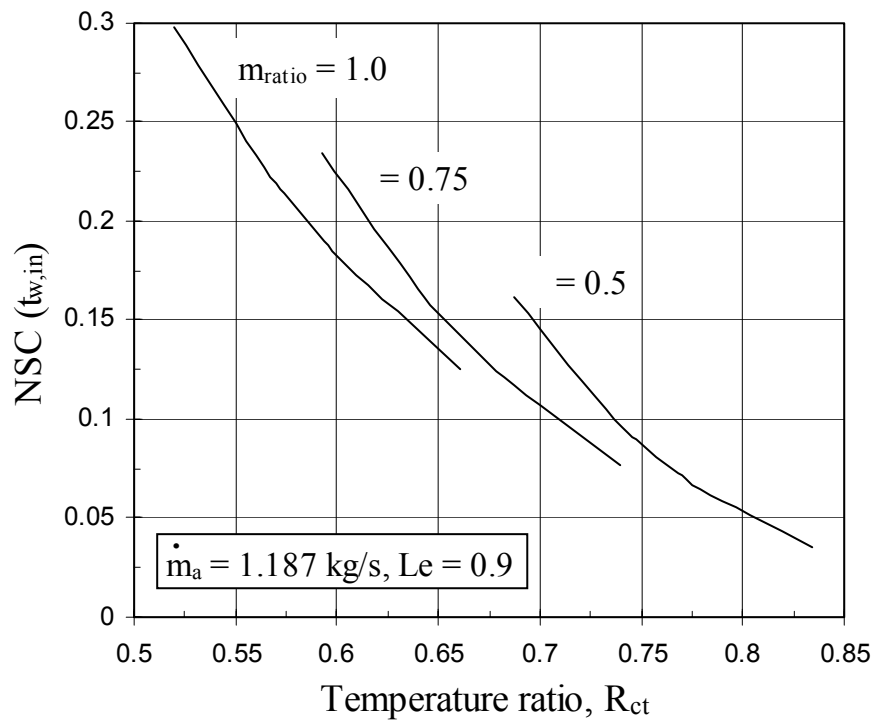


Figure 9.26: Variation of water outlet NSC w.r.t. water inlet temperature versus R_{ct}

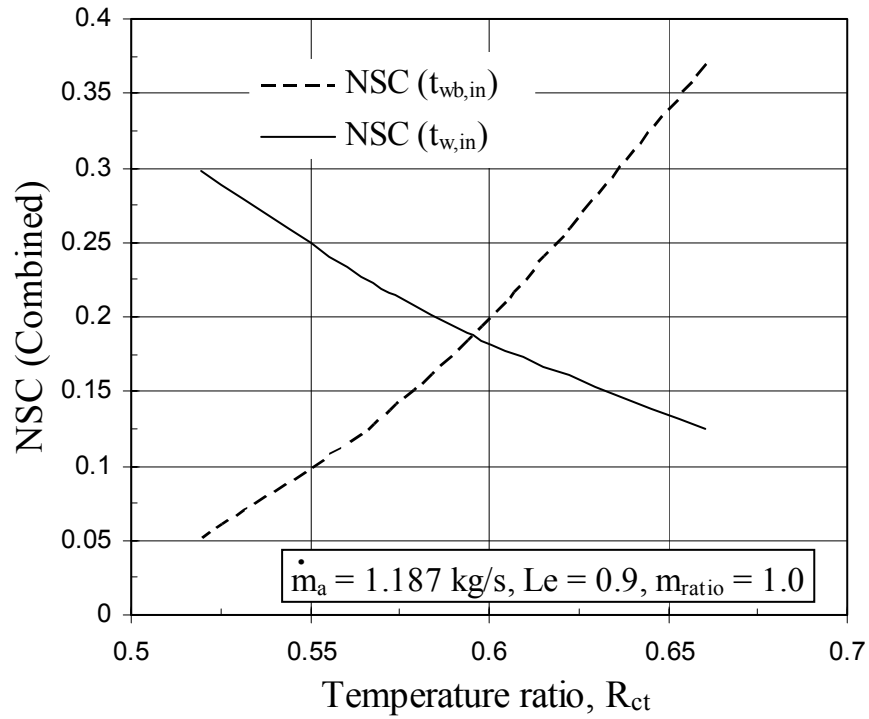


Figure 9.27: Variation of all NSCs versus R_{ct} with mass flow ratio of 1

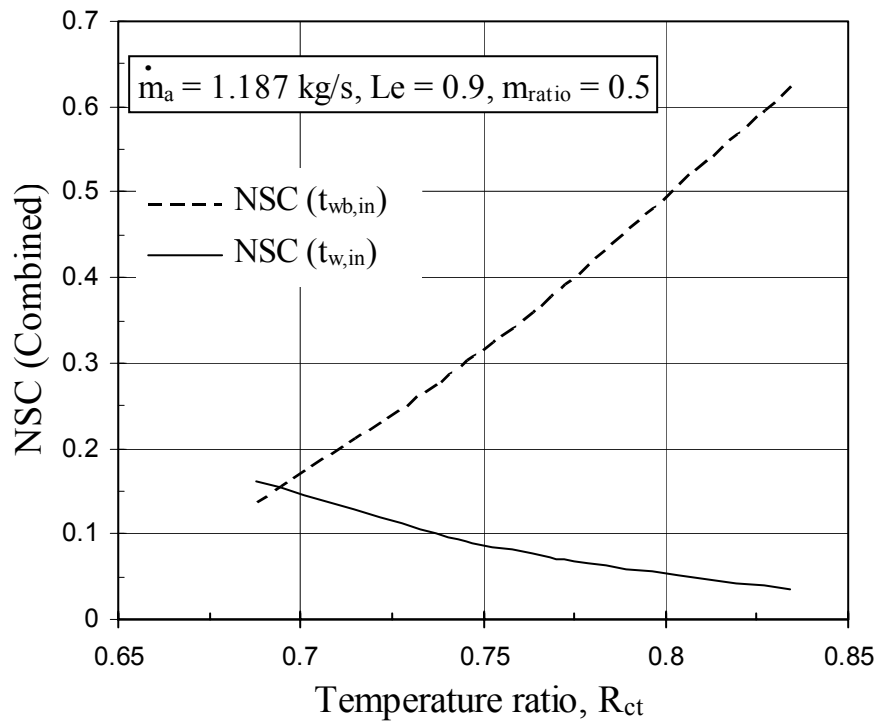


Figure 9.28: Variation of all NSCs versus R_{ct} with mass flow ratio of 0.5

Similarly, Figures (9.29) and (9.30) are normalized forms of the plots between water outlet temperature sensitivity coefficients ($\partial t_{w,out} / \partial t_{wb,in}$) and ($\partial t_{w,out} / \partial t_{w,in}$) versus the inlet water temperature, for different values of mass flow rate ratio. Also, it is noted that $t_{w,out}$ increases with the increase in $t_{w,in}$ [50]. Figure (9.29) shows that as the value of the temperature ratio increases, the NSC decreases and that the sensitivity is lower for large mass flow rate ratios. The explanation is similar to the one given for Figure (9.25) with the difference that the value of $(t_{w,in} - t_{wb,in})$ is increasing due to variation in $t_{w,in}$ instead of $t_{wb,in}$ that causes the water outlet temperature change to decrease with increasing R_{ct} (or $t_{w,in}$). Now, Figure (9.30) also shows the NSC decreasing with increasing temperature ratio but it is higher for large mass flow rate ratios. It was noted that rate of change of $t_{w,out}$ with respect to $t_{w,in}$ decreases with the increase in $t_{w,in}$ [50] which, coupled with the realization that the nominal value of $t_{w,out}$ is continuously increasing, explains the behavior seen. Figures (9.31) and (9.32) combine these two NSCs and it is seen that the water outlet temperature NSC with respect to water inlet temperature dominates continuously for the mass flow ratios investigated.

9.1.4 Exergy Analysis Results

The second-law efficiency is a measure of irreversible losses. Thus, if the efficiency is 1, it is understood that the entire process is reversible. It has been stated before that, for design calculations of the cooling tower, the inlet wet-bulb and water outlet temperatures are the two most important input parameters. A sensitivity analysis was carried out and it was seen again that these are the most notable input parameters influencing the second-law efficiency. The analysis was carried out for three different water to air flow ratios, $\dot{m}_{w,in} / \dot{m}_a = 1, 0.75$ and 0.5 with the air flow rate kept constant.

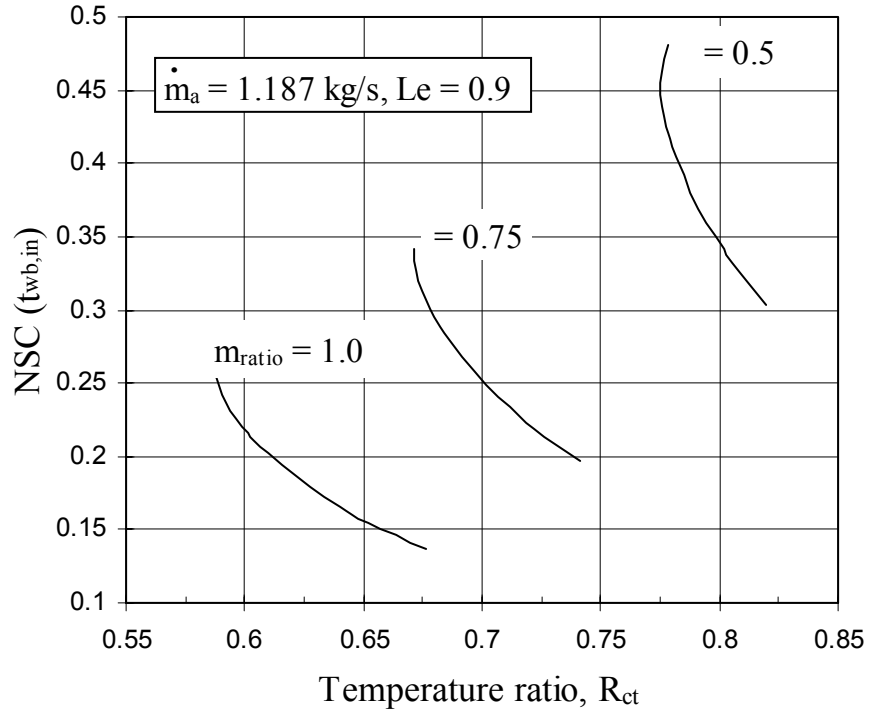


Figure 9.29: Variation of water outlet NSC w.r.t. inlet wet-bulb temperature versus R_{ct}

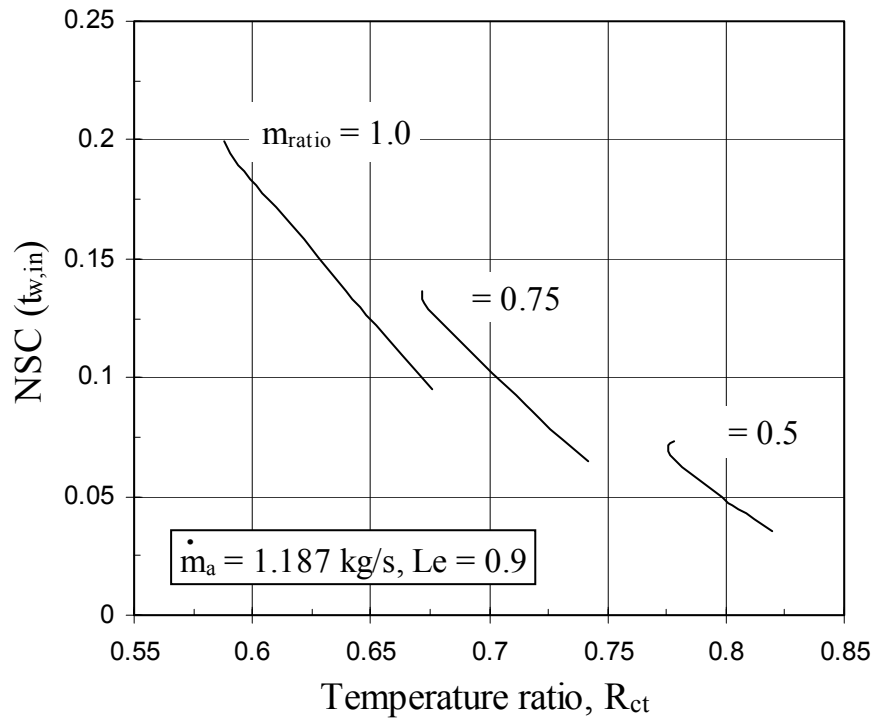


Figure 9.30: Variation of water outlet NSC w.r.t. water inlet temperature versus R_{ct}

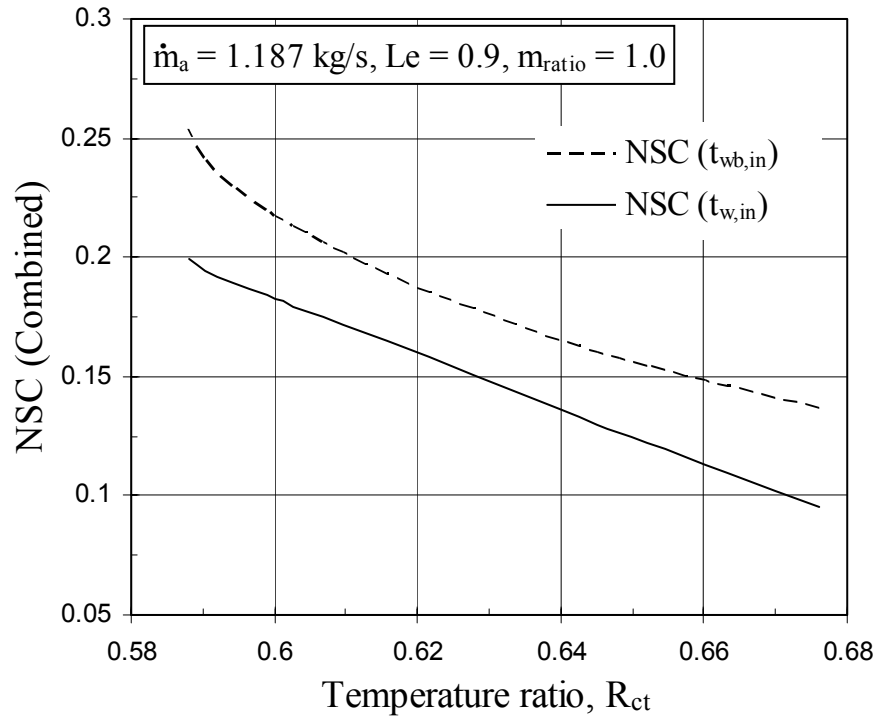


Figure 9.31: Variation of all NSCs versus R_{ct} with mass flow ratio of 1

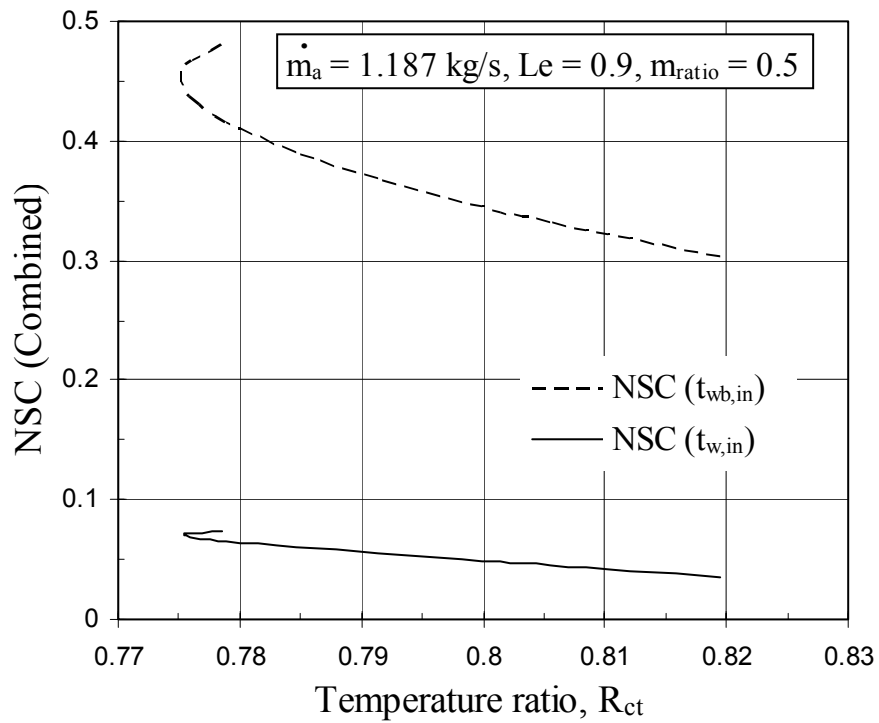


Figure 9.32: Variation of all NSCs versus R_{ct} with mass flow ratio of 0.5

Figure (9.33) illustrates the variation in the second-law efficiency, using equation (6.15), while Figure (9.34) the exergy destruction as the temperature ratio changes, for different mass flow ratios. The increase in the temperature ratio was caused by varying the inlet wet-bulb temperature from 12.11 to 26.11 °C. In Figures (9.33) and (9.34), it is noted that second-law efficiency increases as the exergy destruction decreases for the increasing temperature ratio. The exergy of the inlet moist air minimizes at a wet-bulb temperature of approximately 19.2 °C as it reaches the dead state humidity ratio and then continuously increases. The exergy of the outlet air stream constantly increases due to higher dry-bulb temperature as well as humidity ratios that are achieved. Also, since the water loss decreases with the increasing inlet wet bulb temperature (or temperature ratio), exergy of the makeup water also decreases. As $t_{wb,in}$ increases, the outlet water temperature also rises and, thus, the exergy of the outlet water stream increases. On the other hand, the exergy of the incoming water is constant. The exergy destroyed decreases due to the continuously decreasing value of $(t_{db,in} - t_{wb,in})$. These factors combine so that the second-law efficiency η_{II} increases and can be attributed to the decreasing value of $(t_{w,out} - t_{wb,in})$ as the volume of the tower is constant.

Similarly, Figure (9.35) shows the variation in the second-law efficiency and Figure (9.36) the exergy destruction as the temperature ratio changes, for different mass flow ratios. The increase in the temperature ratio was caused by varying the inlet water temperature from 24.72 to 40.72 °C. In Figure (9.35) and (9.36), it is noted that exergy efficiency decreases and exergy destruction increases for the increasing inlet water temperature (or increasing temperature ratio). The exergy of the exiting air stream continuously increases as it gets farther from the dead state humidity ratio. On the other

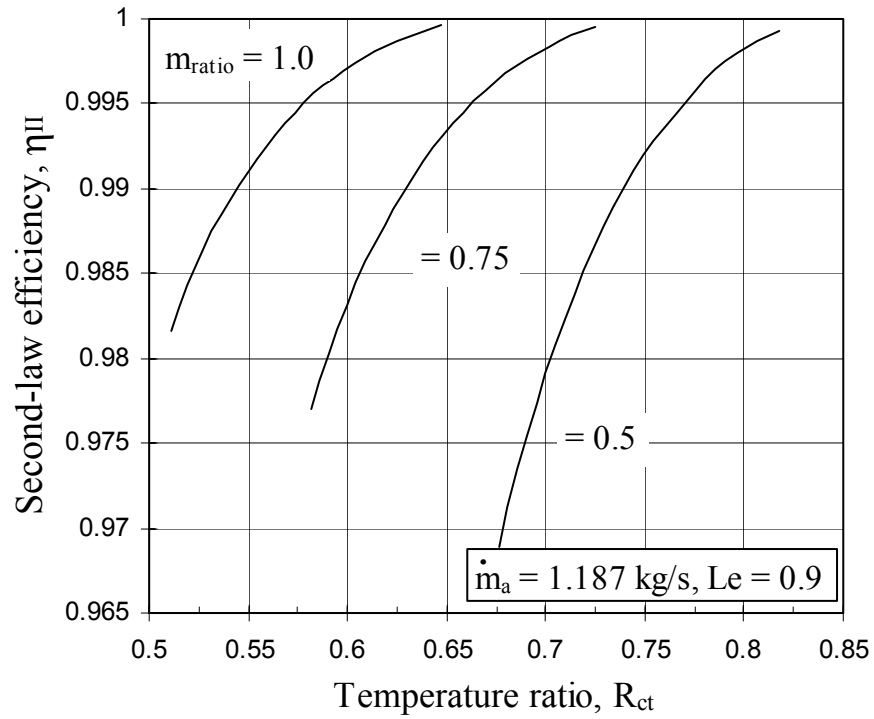


Figure 9.33: Variation of second-law efficiency versus R_{ct} (Eq. (6.15))

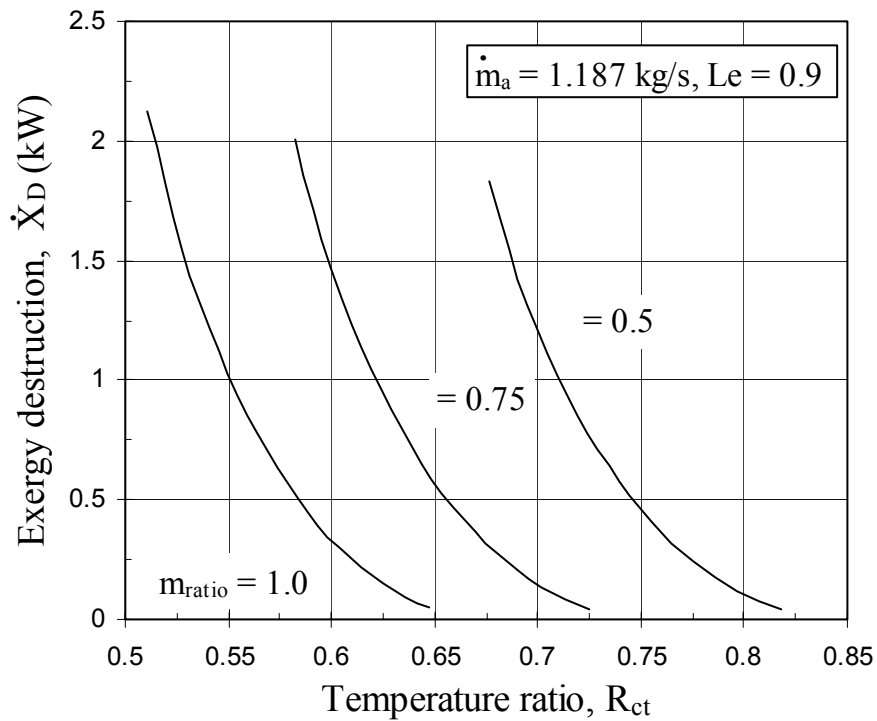


Figure 9.34: Variation of exergy destruction versus R_{ct}

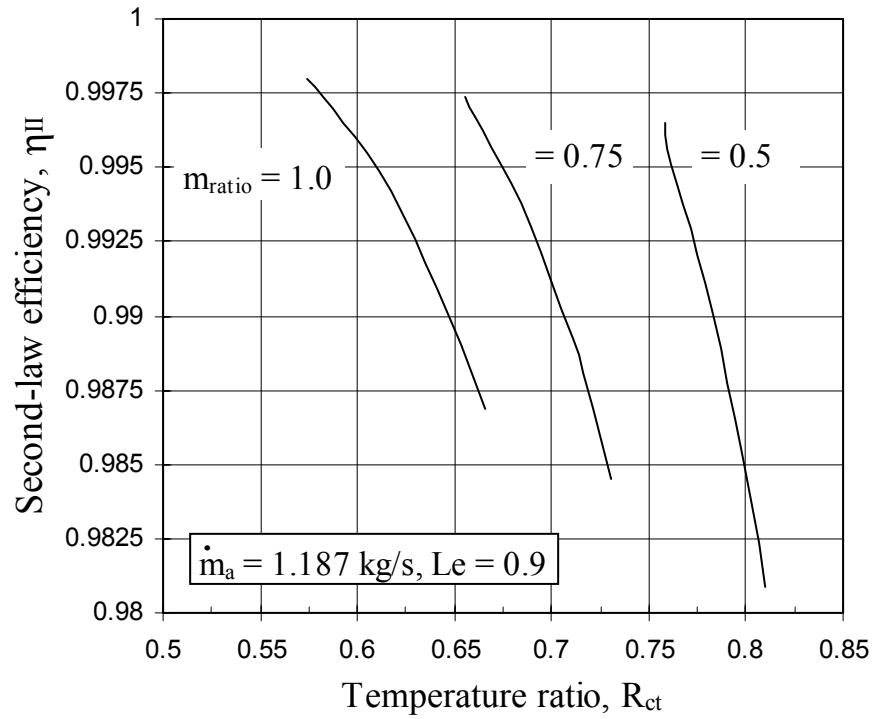


Figure 9.35: Variation of second-law efficiency versus R_{ct} (Eq. (6.15))

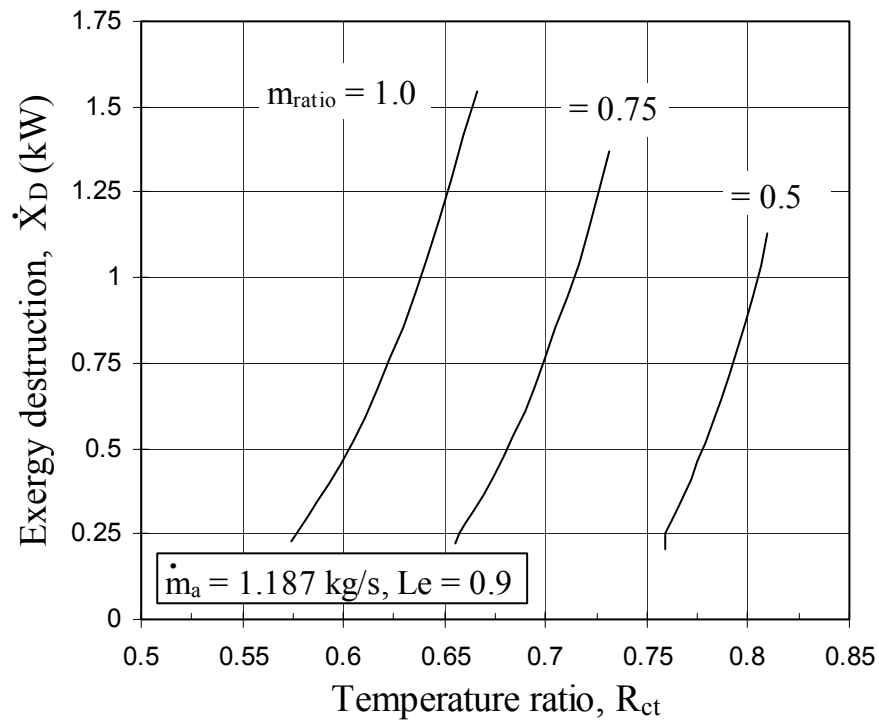


Figure 9.36: Variation of exergy destruction versus R_{ct}

hand, exergy of the entering air stream is constant. Also, since the water loss increases due to the increasing difference of the inlet water and wet-bulb temperatures, exergy of the makeup water also increases. The exergy of the outlet water stream decreases as its rising temperature approaches T_o . However, the exergy of the incoming water stream constantly increases due to higher water temperatures used. The increase in the exergy destruction is due to the continually increasing difference between the inlet and outlet water temperatures. These factors cause the second-law efficiency η_{II} to decrease and can also be understood from the fact that the effectiveness is also decreasing.

9.1.5 Evaporation and the Effect of Mass Flow Rate

The water to air mass flow ratio is an important factor and affects all aspects of the performance of the cooling tower as seen in the results already shown. Figures (9.37) and (9.38) show the variation of the effectiveness and temperature ratio in the typical range of the mass flow rate ratio; the former increasing and latter decreasing. The specifications of a medium-sized cooling tower were used to calculate the percentage of water evaporation as the humidity ratio varies from very dry to very wet condition. In this regard, the following data was used: $Le = 0.9$, $\dot{m}_a = 93.99 \text{ kg/s}$, $V = 203.2 \text{ m}^3$, $t_{w,in} = 50^\circ\text{C}$. The trends can be understood from the fact that the outlet enthalpy of the air increases with increasing mass flow rate ratio due to higher outlet water temperatures achieved that is the result of less residence time of the water in the tower (See eqs. (3.36) and (3.38)), therefore, the effectiveness increases.

Figure (9.39) shows that the percentage of water evaporated is lower at higher dry-bulb temperatures. It is important, in this regard, to understand that evaporation occurs as the water cools from the inlet water to the outlet water temperature. The lowest possible

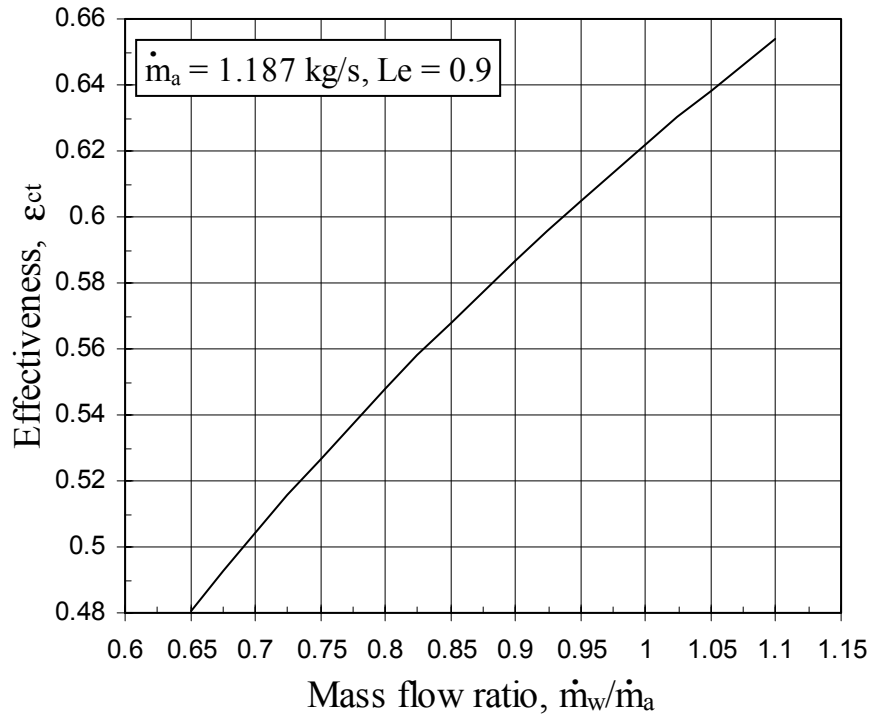


Figure 9.37: Variation of effectiveness with mass flow ratio

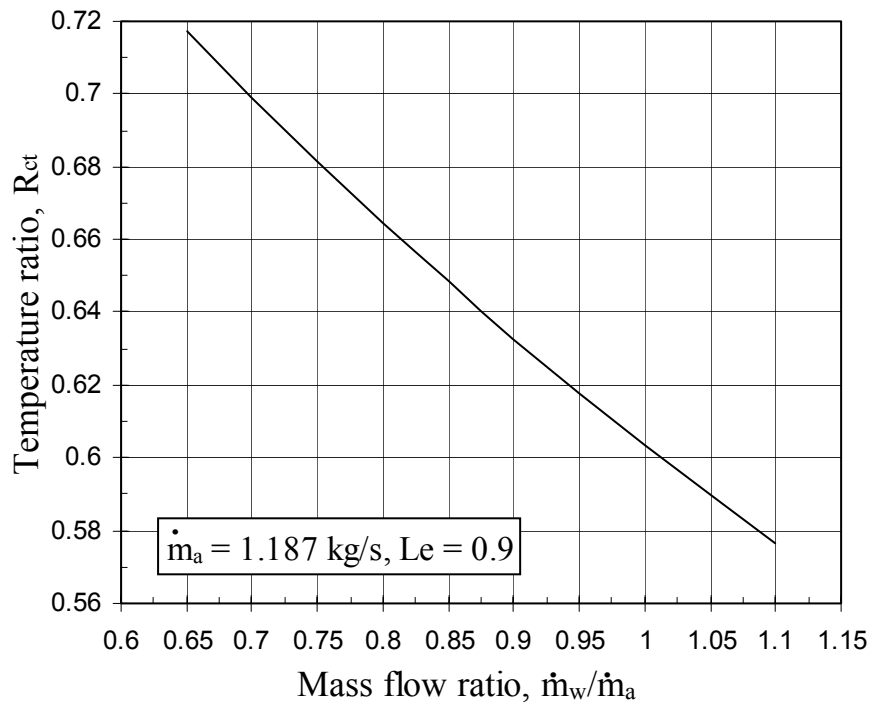


Figure 9.38: Variation of temperature ratio with mass flow ratio

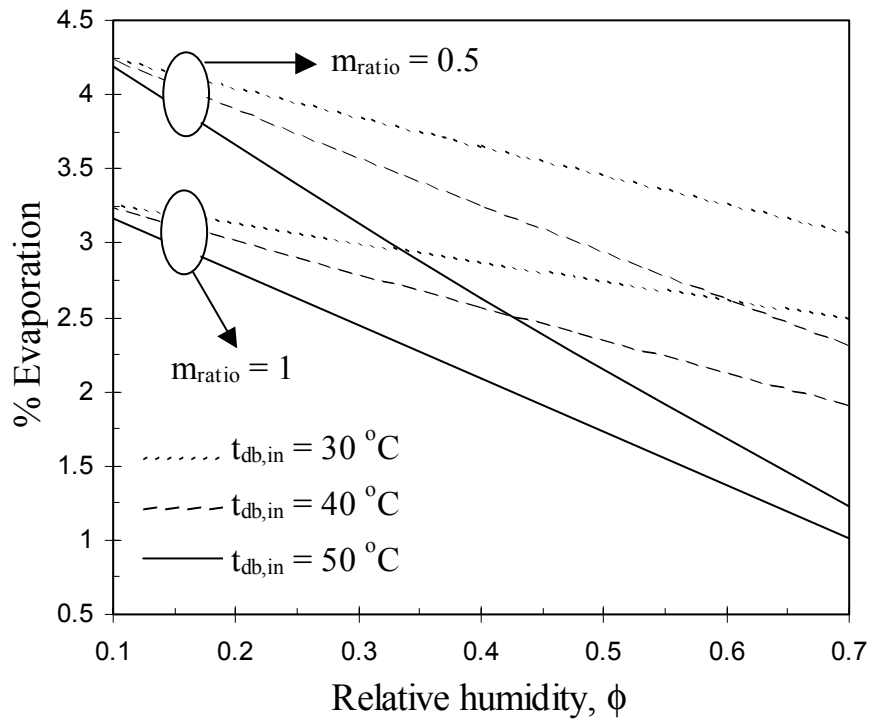


Figure 9.39: Percent evaporation for various air conditions and mass flow ratios

temperature that the water can achieve is the inlet wet-bulb temperature, which is currently governed by the initial dry-bulb temperature and relative humidity. Therefore, the potential for evaporation lies in the difference between the inlet water and inlet wet-bulb temperatures. For any value of the relative humidity, a higher dry-bulb temperature yields a higher wet-bulb temperature, which in turn, clearly indicates a smaller potential for evaporation. For very dry air, this is less evident irrespective of the mass flow ratio but becomes obvious for relatively wetter air.

9.2 RESULTS FOR EVAPORATIVE FLUID COOLER

The specifications of the evaporative cooler used in the analysis are the same as those of Mizushina and Miyashita [6]. It is to remind the reader that the water temperature is not considered as constant and the Lewis number is considered as unity.

9.2.1 Effect of Pressure (Elevation)

This analysis is carried out for three different water to air flow rate ratios i.e. 1, 0.75 and 0.5 for all the heat exchangers. It should be kept in mind that Sutherland [30] indicated a 10 kPa decrease in atmospheric pressure for an approximately 850 meters increase in altitude. Therefore, operation of the evaporative cooler will be affected due to elevation, as atmospheric conditions such as the wet bulb temperature will be directly influenced. The wet bulb temperature is, theoretically, the lowest temperature that the process fluid can achieve and, therefore, it is important to quantify the effect, in terms of design, on required surface area to achieve a prescribed amount of cooling.

Figures (9.40) and (9.41) are drawn for the following set of input data that is considered in Mizushina et al. [6] but with the same dry and wet bulb temperatures used in the cooling tower: $t_{db,in} = 29\text{ }^{\circ}\text{C}$, $t_{wb,in} = 21.1\text{ }^{\circ}\text{C}$, $t_{p,in} = 50\text{ }^{\circ}\text{C}$, $\dot{m}_p = 0.325\text{ kg/s}$. Figure

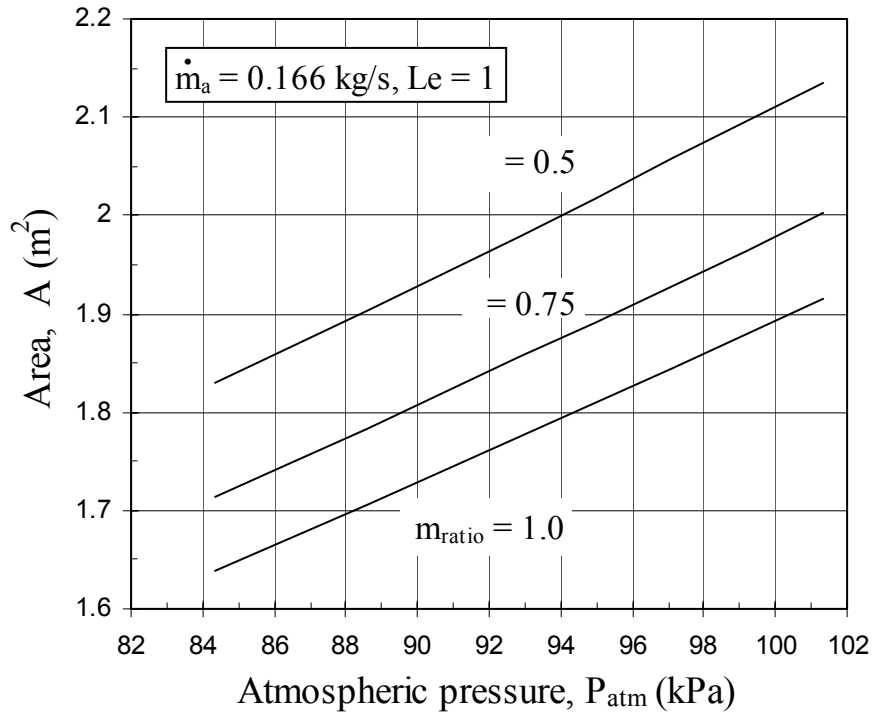


Figure 9.40: Variation in required surface area versus pressure change

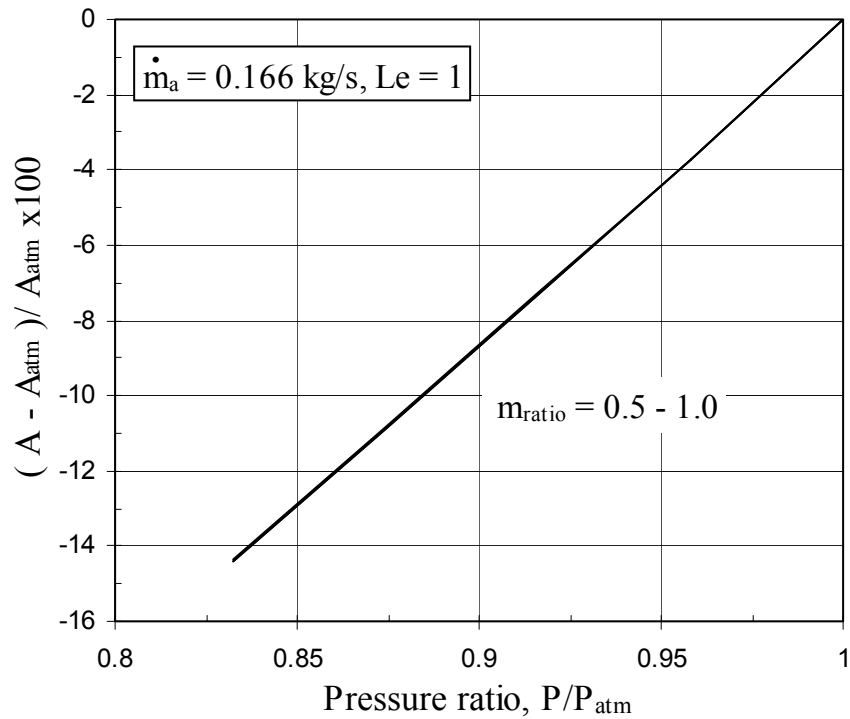


Figure 9.41: Percent decrease in required surface area versus pressure ratio

(9.40) shows the plot of the surface area required to achieve the necessary cooling of the fluid versus the decrease in atmospheric pressure. The figure shows that for achieving the same fluid outlet temperature, the surface area of the tubes can be reduced by 0.3 m^2 when $m_{ratio} = 0.5$. As in the cooling tower, the reduction in required surface area with the increasing altitude occurs because both the dry and wet bulb temperatures decrease. Less surface area is needed for the same amount of cooling because the colder air comparatively cools the water better. Also, equation (3.9) shows that, as the atmospheric pressure decreases, the value of $(t_p - t_w)$ increases due to the decreasing water temperature and, thus, the required surface area decreases. Now, the surface area is larger as the mass flow rate ratio decreases and is due to higher water temperatures achieved at lower mass flow rate ratios (See eqn. (3.9) and (3.11)). However, it is evident from Figure (9.41) that the percentage decrease in the required surface area, with respect to the surface area calculated at standard atmospheric pressure, is almost the same for each value of the mass flow rate ratio.

9.2.2 Effect of Fouling

The mathematical model for the evaporative fluid cooler, discussed in the chapter 3, is used for the design and rating calculations of a counter flow evaporative fluid cooler. It is used in combination with the fouling model to study the thermal performance of the tower under fouled conditions.

9.2.2.1 Design

In design calculations, the required surface area of the evaporative cooler is calculated using the following set of input conditions: inlet air temperatures [dry bulb

($t_{db,in}$) and wet bulb ($t_{wb,in}$)], fluid inlet temperature ($t_{p,in}$), fluid outlet temperature ($t_{p,out}$) and mass flow rates [air (\dot{m}_a), water ($\dot{m}_{w,in}$) and process fluid (\dot{m}_p)].

As with the cooling tower, fouling reduces the performance of an evaporative cooler as well. In order to attain a constant value of the evaporative cooler effectiveness under fouled conditions, the surface area has to be increased, which is illustrated in Figure (9.42). In this figure, a plot of the area fraction (A_{fl} / A_{cl}) of the evaporative cooler is shown as a function of the asymptotic fouling resistance R_f^* .

9.2.2.2 Rating

In rating calculations, outlet process fluid temperature ($t_{p,out}$) and effectiveness (ε_{efc}) are calculated for the following set of input conditions: inlet air temperatures [dry bulb ($t_{db,in}$) and wet bulb ($t_{wb,in}$)], inlet process fluid temperature ($t_{p,in}$), mass flow rates [air (\dot{m}_a) and water ($\dot{m}_{w,in}$)] and required surface area (A). The time and risk dependent effectiveness of the evaporative cooler is shown in a reduced system in Figure (9.43). The reduced effectiveness $\varepsilon_{efc}(\delta, p; \sqrt{\alpha}) / \varepsilon_{efc}(0)$ versus reduced fouling thickness t/M , for different risk level p and scatter parameter $\alpha^{1/2} = 0.3$, is plotted for the fouling-growth model discussed earlier. The effectiveness of the evaporative cooler degrades considerably with time indicating that, for a low risk level ($p = 0.01$), there is about 73% decrease for the given fouling model. The variations in the reduced process fluid outlet temperature versus reduced fouling thickness for different risk levels p and for scatter parameter $\alpha^{1/2} = 0.3$, is shown in Figure (9.44). The figure shows that for a low risk level (i.e., high reliability), when compared with the deterministic case (i.e. $p = 0.5$), the process fluid outlet temperature is higher, indicating that there will be a lower heat

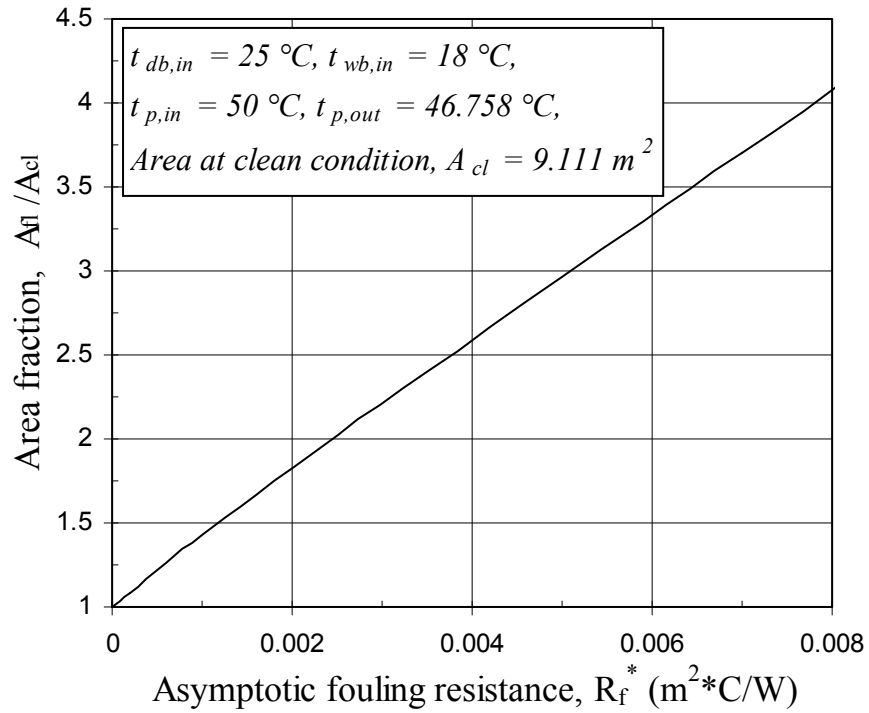


Figure 9.42: Area fraction as a function of fouling resistance

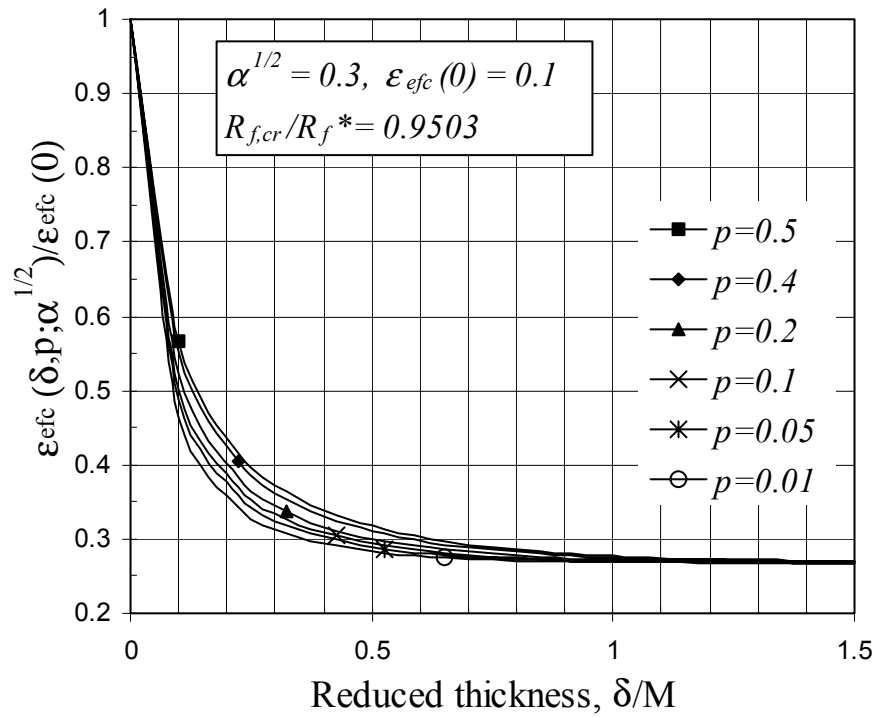


Figure 9.43: Normalized effectiveness versus reduced thickness

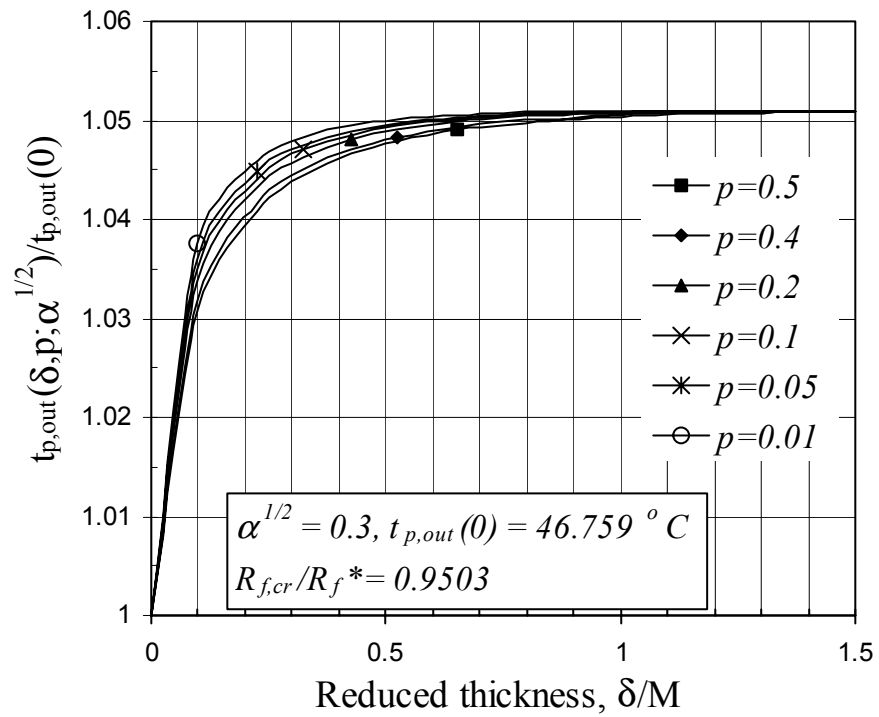


Figure 9.44: Reduced process fluid outlet temperature versus reduced thickness

transfer rate due to fouling. It is noticed that there is about 5.1 % increase in outlet temperature of the process fluid for the given fouling model. It should be noted that a risk level of 0.01 indicates that the operator is willing to take a 1 percent risk of a system shutdown. Thus, Figure (9.43) predicts a faster rate of effectiveness degradation and Figure (9.44) that of heat transfer rate, which will subsequently require a comparatively earlier cleaning of the evaporative cooler.

9.2.3 Sensitivity Analysis Results

The computer model of the evaporative cooler discussed in chapter 3 was used to perform a sensitivity analysis. Again, the normalized sensitivity coefficients were calculated and are shown for different mass flow rate ratios as well as in a combined form at the same mass flow ratios. As before, the analysis is carried out for the water to air flow ratios of 1, 0.75 and 0.5. It should be noted that, in plots regarding evaporative cooler design, $t_{wb,in}$ is varied from 12.11 to 23.11 °C and $t_{p,out}$ from 43 to 48 °C. On the other hand, in the figures regarding rating, $t_{wb,in}$ is varied from 12.11 to 26.11 °C and $t_{p,in}$ from 40 to 60 °C.

9.2.3.1 Design

Figures (9.45) and (9.46) are normalized forms of the plots between (surface) area sensitivity coefficients ($\partial A / \partial t_{p,out}$) and ($\partial A / \partial t_{p,in}$) versus the inlet wet-bulb temperature, for different values of mass flow rate ratio. Figures (9.45) and (9.46) show that as the value of the temperature ratio (or inlet wet bulb temperature) increases, the sensitivities in both cases increase in a very similar manner. The effect of mass flow rate ratio is negligible. In the former, as $t_{wb,in}$ increases, the decreasing difference between $t_{p,out}$ and $t_{wb,in}$ gives rise to larger surface area requirements as well as a higher rate of the change of

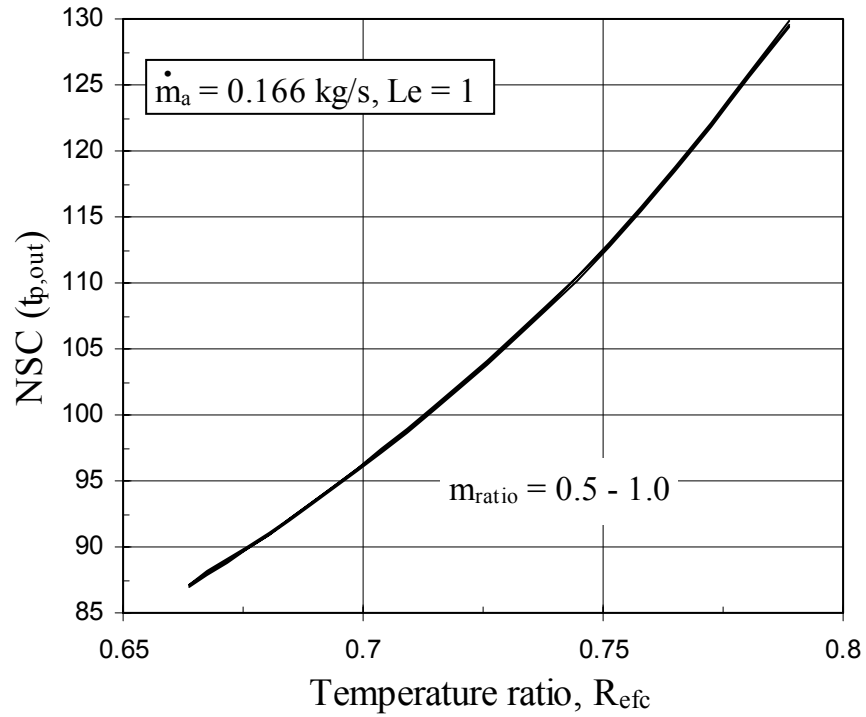


Figure 9.45: Variation of area NSC w.r.t. outlet process fluid temperature versus R_{effc}

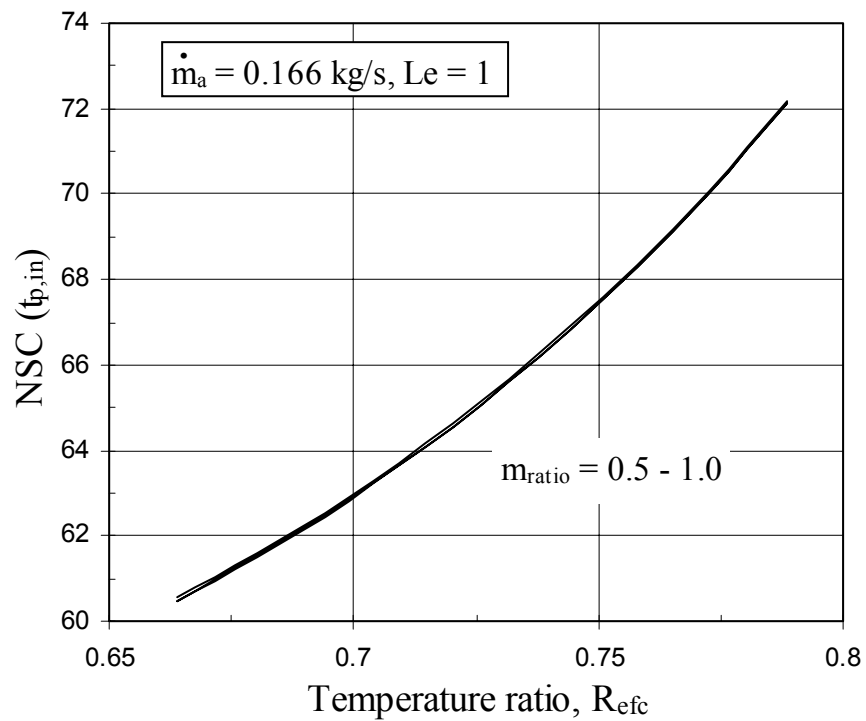


Figure 9.46: Variation of area NSC w.r.t. inlet process fluid temperature versus R_{effc}

the same as $t_{p,out}$ is constant. Mass flow rate ratio has a negligible effect as, with the inlet and outlet process fluid temperatures fixed, it mainly affects the steady-state water temperature, which subsequently changes the amount of water evaporated. Similarly, in Figure (9.46), the sensitivity increases with an increase in R_{efc} with mass flow rate ratios having a negligible effect. With $t_{p,in}$, its perturbation ($\Delta t_{p,in}$) as well as $t_{p,out}$ constant, the area as well as resulting changes in area (ΔA), due to the perturbation in $t_{p,in}$, increase that combine to increase the NSC. It should be kept in mind that the increase in area and negligible effect of mass flow rate ratio is due the same reasons as explained for the previous figure. Figure (9.47) combine these NSCs illustrating their variation with respect to each other and clearly indicating that the area NSC with respect to process fluid outlet temperature dominates at all mass flow ratios.

Figures (9.48) and (9.49) are normalized forms of the plots between (surface) area sensitivity coefficients ($\partial A / \partial t_{p,out}$) and ($\partial A / \partial t_{p,in}$) versus the process fluid outlet temperature, for different values of mass flow rate ratio. Figures (9.48) and (9.49) show that, as the value of the temperature ratio increases (or process fluid outlet temperature decreases), the sensitivities in both cases increase in a very similar manner with the effect of mass flow rate ratio being negligible. In Figures (9.48), as $t_{p,out}$ increases (or temperature ratio decreases), the decreasing difference between $t_{p,out}$ and $t_{p,in}$ gives rise to smaller surface area requirements as well as a lower rate of the change of the same. It was noted that the perturbation ($\Delta t_{p,in}$) is constant and all these factors combine to increase the NSC where its very high initial value is due to the very small value of $(t_{p,in} - t_{p,out})$. Mass flow rate ratio has a minor effect as it mainly changes the steady-state water temperature. Figure (9.49) is different from Figure (9.48) in this respect that, both, $t_{p,in}$ and

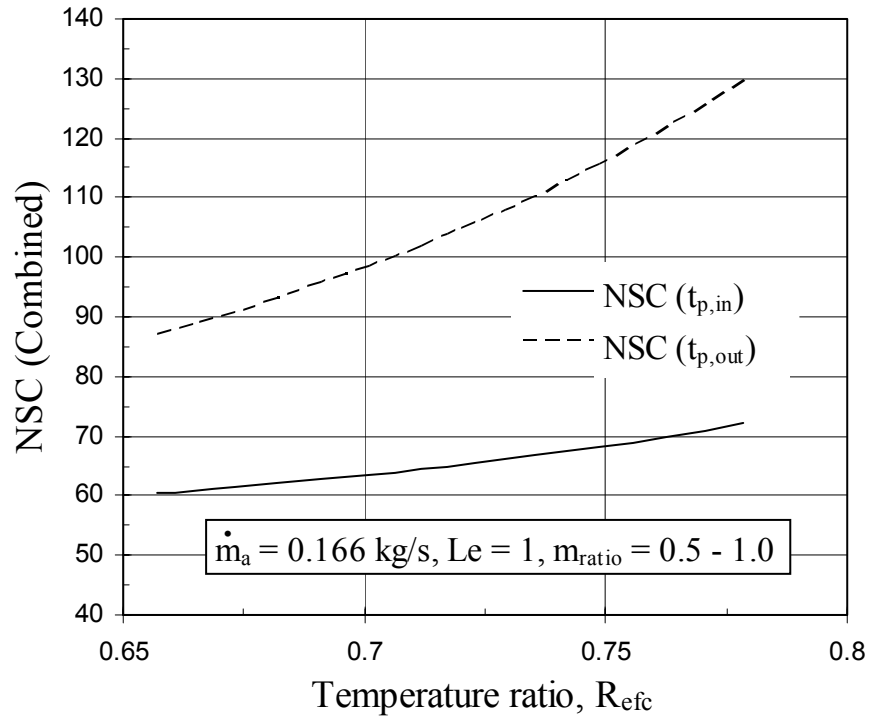


Figure 9.47: Variation of all NSCs versus R_{effc} for all mass flow ratios

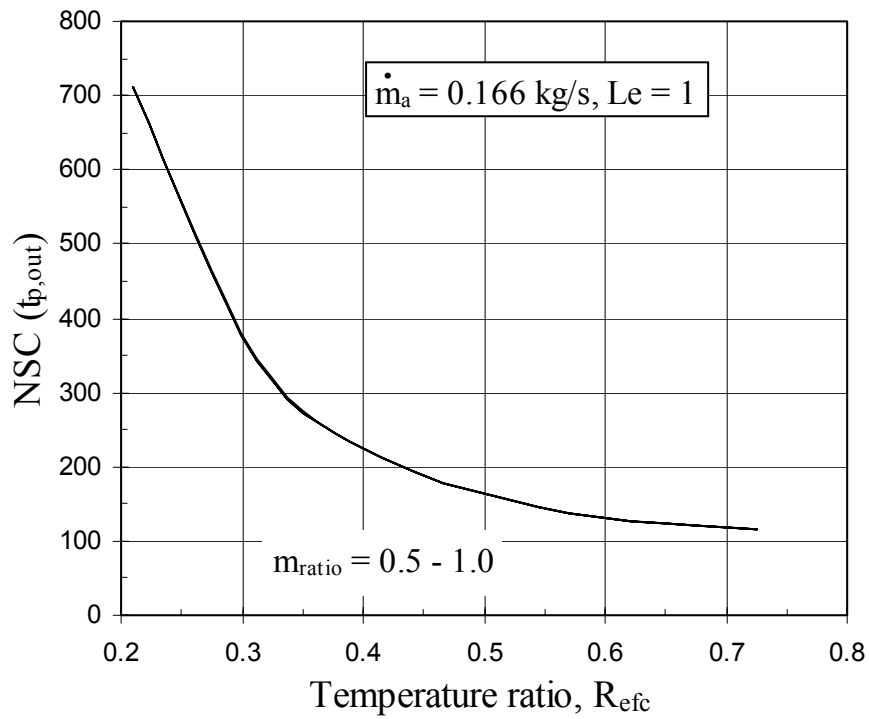


Figure 9.48: Variation of area NSC w.r.t. process fluid outlet temperature versus R_{effc}

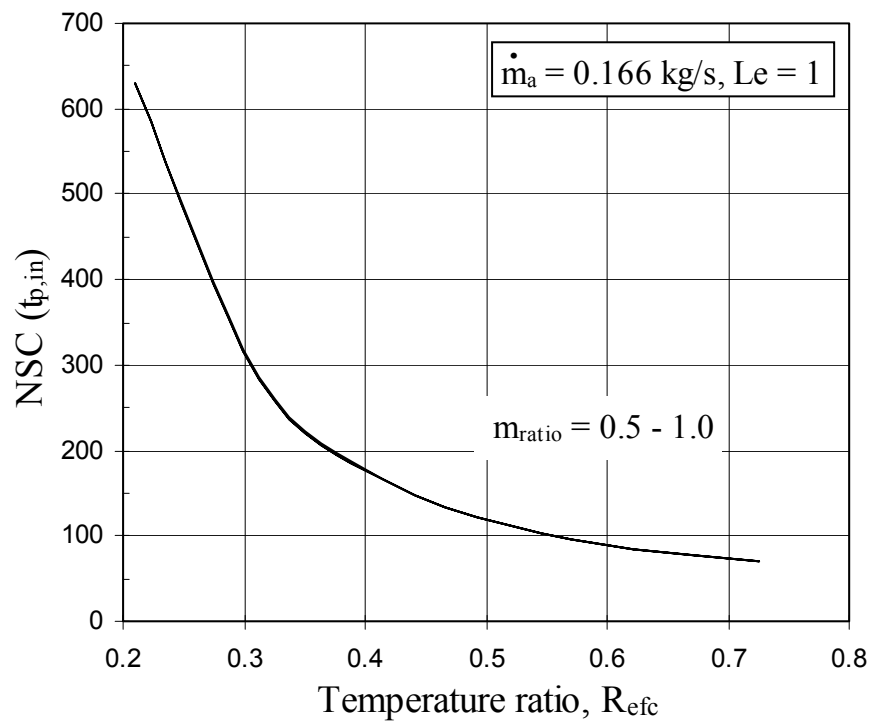


Figure 9.49: Variation of area NSC w.r.t. process fluid inlet temperature versus R_{etc}

its perturbation ($\Delta t_{p,in}$), are constant and these factors combine to decrease the NSC as the temperature ratio increases where, again, its very high initial value is due to the very small value of $(t_{p,in} - t_{p,out})$. Figure (9.50) shows that the NSCs decrease, in both cases, as the temperature ratio increases and reaches a minimum around 0.7 with the NSC with respect to $t_{p,out}$ always higher.

9.2.3.2 Rating

Figures (9.51) and (9.52) are normalized forms of the plots between effectiveness sensitivity coefficients ($\partial \varepsilon_{efc} / \partial t_{p,in}$) and ($\partial \varepsilon_{efc} / \partial \dot{m}_p$) versus the inlet wet-bulb temperature, for different mass flow rate ratios. These figures show that, as the inlet wet-bulb temperature increases (or temperature ratio decreases), the sensitivity of the effectiveness with respect to $t_{p,in}$ and \dot{m}_p also increases. In the latter case, the NSC is lower for large mass flow rate ratios but remains virtually unchanged in case of the former. In Figures (9.51), as $t_{wb,in}$ increases (or temperature ratio decreases), the effectiveness increases due to the decreasing difference between $t_{p,out}$ and $t_{wb,in}$ keeping in mind that the surface area is constant. With $t_{p,in}$ as well its perturbation ($\Delta t_{p,in}$) constant and the effectiveness increasing with the rising wet-bulb temperature, the combination of these quantities causes the NSC to decrease. Mass flow rate ratio has a small effect as most of the effect is compensated by a change in the steady-state water temperature, which subsequently changes the amount of water evaporated. In Figure (9.52) as well, the increasing wet-bulb temperature (or decreasing temperature ratio), increases the effectiveness due to the same reasons as explained before. With \dot{m}_p as well its perturbation ($\Delta \dot{m}_p$) constant and the effectiveness as well as the resulting changes in it ($\Delta \varepsilon_{efc}$)

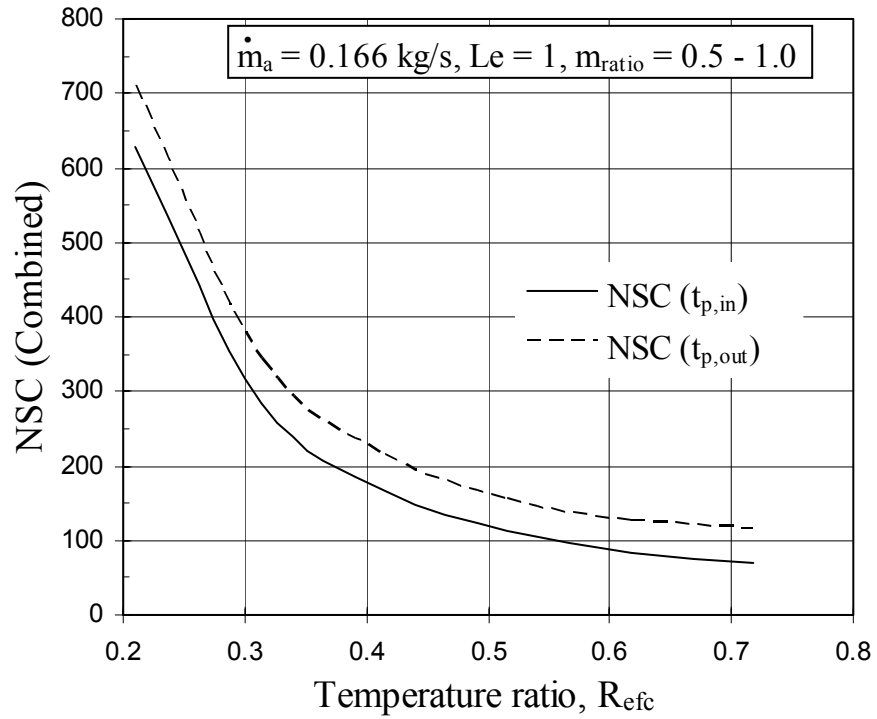


Figure 9.50: Variation of all NSCs versus R_{effc} for all mass flow ratios

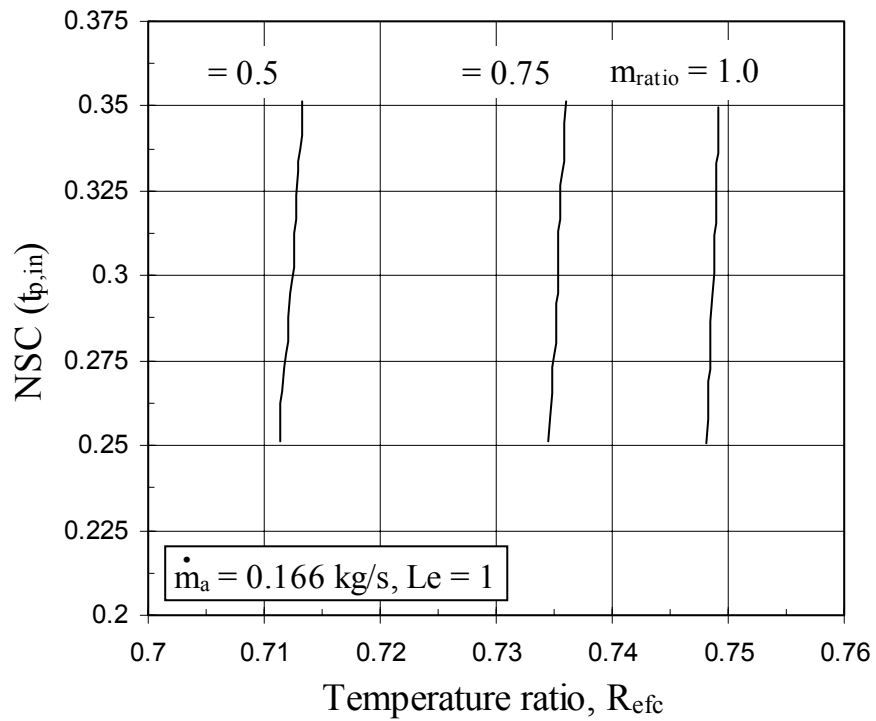


Figure 9.51: Variation of effectiveness NSC w.r.t. fluid inlet temperature versus R_{effc}

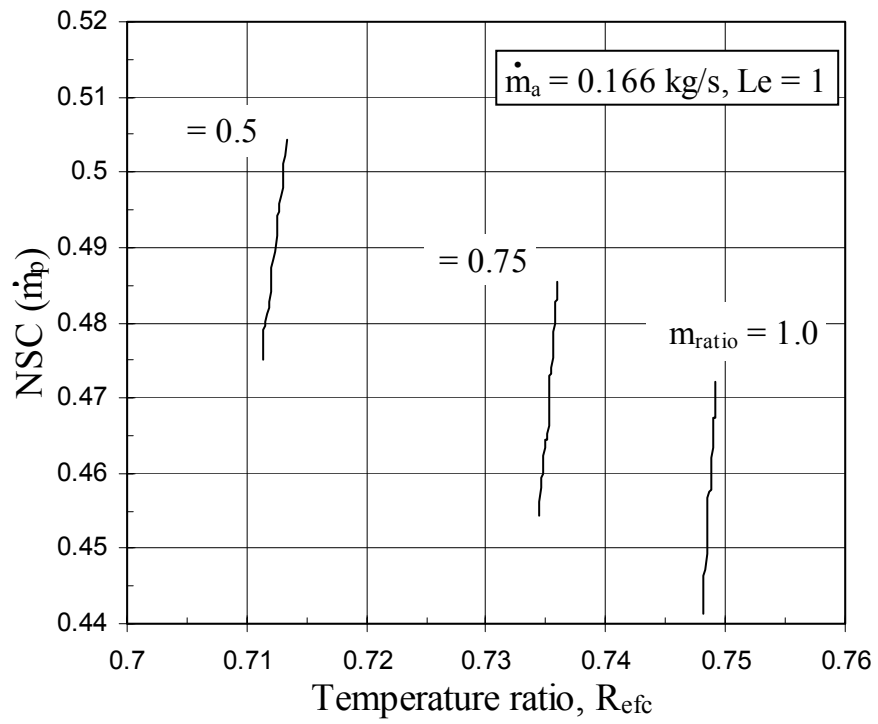


Figure 9.52: Variation of effectiveness NSC w.r.t. process fluid flow rate versus R_{effc}

increasing with the rising wet-bulb temperature, the combination of these quantities causes the NSC to decrease. At a comparatively lower mass flow ratio, effectiveness as well as changes in it ($\Delta \varepsilon_{efc}$) are smaller and, thus, NSC is higher. The lower effectiveness is due to the higher steady-state water temperature achieved that causes less heat transfer. Although this is also true for Figures (9.51) as well, the effect is more significant with respect to the process fluid flow rate as the system is more sensitive to this factor, which is evident from Figures (9.53) and (9.54) where these two NSCs are combined.

Similarly, Figures (9.55) and (9.56) are normalized forms of the plots between effectiveness sensitivity coefficients ($\partial \varepsilon_{efc} / \partial t_{p,in}$) and ($\partial \varepsilon_{efc} / \partial \dot{m}_p$) versus the inlet process fluid temperature, for different mass flow rate ratios. Figure (9.55) shows that as the temperature ratio (or $t_{p,in}$) increases, the NSC with respect to $t_{p,in}$ also increases and there is little effect of mass flow rate ratio. In Figures (9.55), as the temperature ratio increases, the effectiveness increases due to the increasing difference between $t_{p,in}$ and $t_{p,out}$ keeping in mind that the surface area is constant. Now, with ε_{efc} and $t_{p,in}$ increasing and the perturbation of the latter ($\Delta t_{p,in}$) constant, the combination of these quantities causes the NSC to increase as the process fluid inlet temperature increases at a much faster rate than the effectiveness. In Figures (9.56) as well, the increasing inlet process fluid temperature (or temperature ratio), increases the effectiveness due to the same reasons as explained before. The NSC with respect to the process fluid mass flow rate decreases due to the same reasons described for Figure (9.52). Also, differences seen in NSC values due to varying mass flow ratios, is due to a similar explanation as mentioned for Figure (9.52). The difference is due to the fact that, here, the temperature ratio increases due to the increasing process fluid inlet temperature but decreases for the

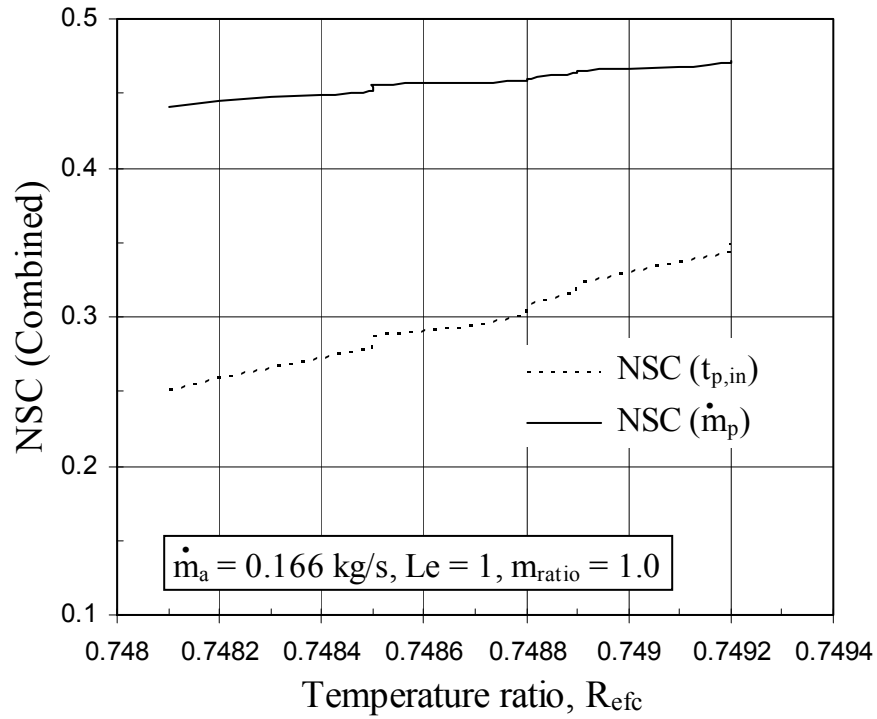


Figure 9.53: Variation of all NSCs versus R_{effc} with mass flow ratio of 1

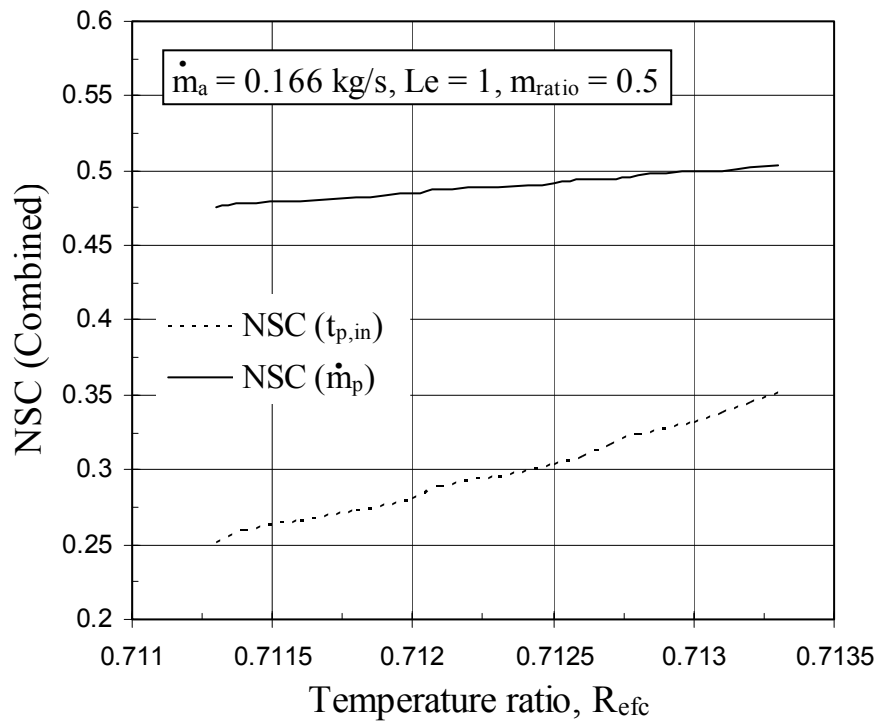


Figure 9.54: Variation of all NSCs versus R_{effc} with mass flow ratio of 0.5

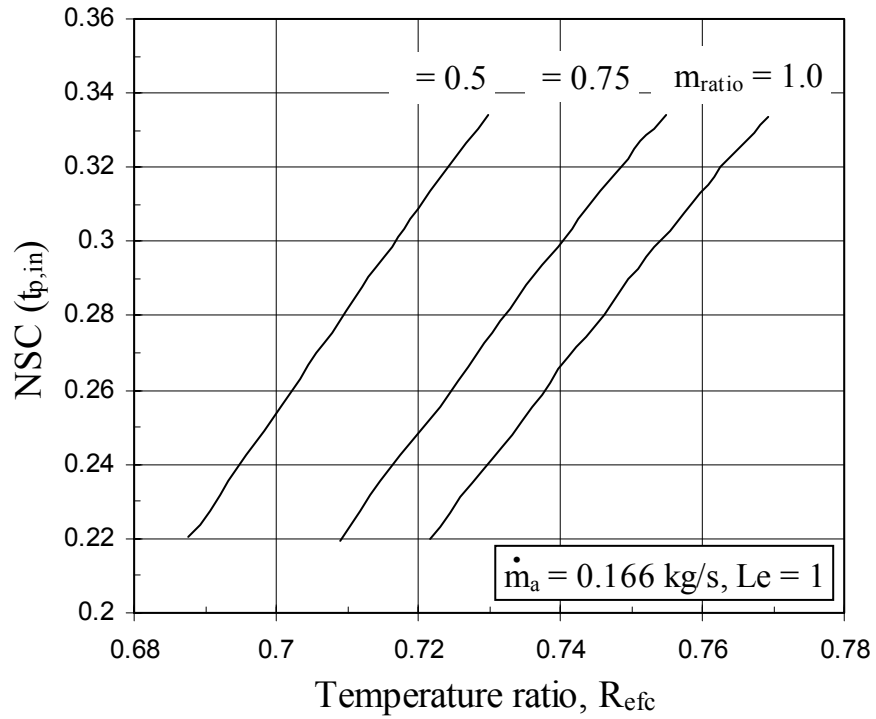


Figure 9.55: Variation of effectiveness NSC w.r.t. fluid inlet temperature versus R_{effc}

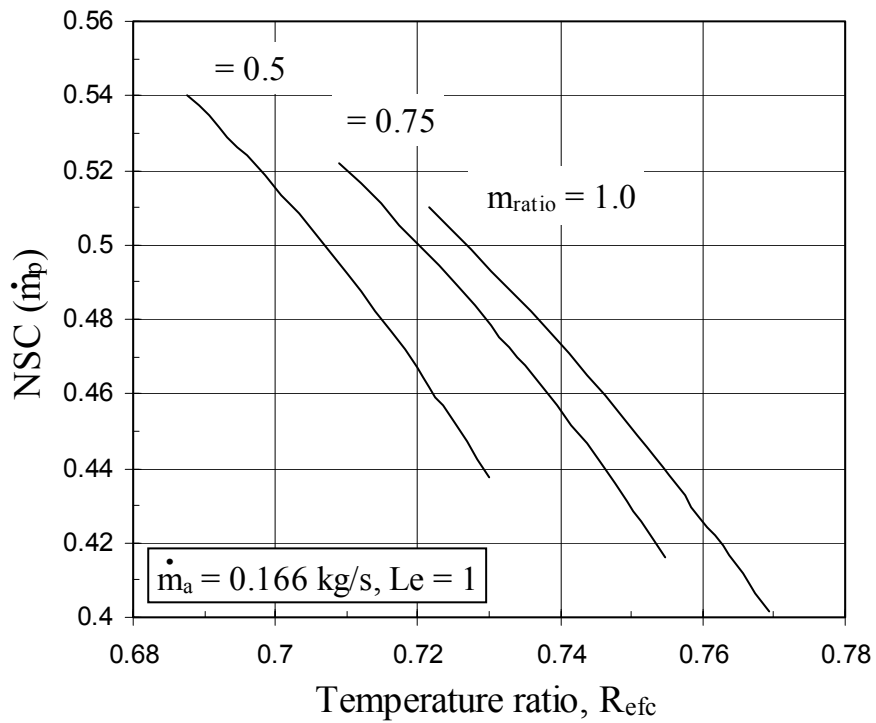


Figure 9.56: Variation of effectiveness NSC w.r.t. process fluid flow rate versus R_{effc}

increasing inlet wet-bulb temperature for Figure (9.52). Figures (9.57) and (9.58) combine these two NSCs to show that effectiveness is more sensitive to the process fluid flow rate.

Figure (9.59) is the normalized form of the plot between process fluid outlet temperature sensitivity coefficient ($\partial t_{p,out} / \partial t_{p,in}$) versus the inlet wet-bulb temperature, for different values of mass flow rate ratio. Now, as $t_{wb,in}$ increases (or temperature ratio decreases), $t_{p,out}$ increases due to the decreasing difference between $t_{p,in}$ and $t_{wb,in}$ keeping in mind that the surface area is constant. Thus, with $t_{p,in}$ as well as its perturbation ($\Delta t_{p,in}$) constant and changes in $t_{p,out}$ ($\Delta t_{p,out}$) decreasing with the rising wet-bulb temperature, the combination of these quantities causes the NSC to decrease. For lower mass flow ratios, the NSC is higher since the steady-state water temperature is higher in the closed circuit that causes $t_{p,out}$ as well as the changes in it ($\Delta t_{p,out}$) to rise.

Similarly, Figure (9.60) is the normalized form of the plot between process fluid outlet temperature sensitivity coefficient ($\partial t_{p,out} / \partial t_{p,in}$) versus the inlet process fluid temperature, for different values of mass flow rate ratio. Now, as $t_{p,in}$ (or temperature ratio) increases, $t_{p,out}$ also increases as the surface area is constant. In this regard, the changes in $t_{p,out}$ ($\Delta t_{p,out}$) decrease as the steady-state water temperature also rises reducing heat transfer from the process fluid. With the perturbation of $t_{p,in}$ ($\Delta t_{p,in}$) constant, the combination of these quantities causes the NSC to decrease as the process fluid inlet temperature increases. For lower mass flow ratios, the NSC is higher for the same reasons as described for Figure (9.59).

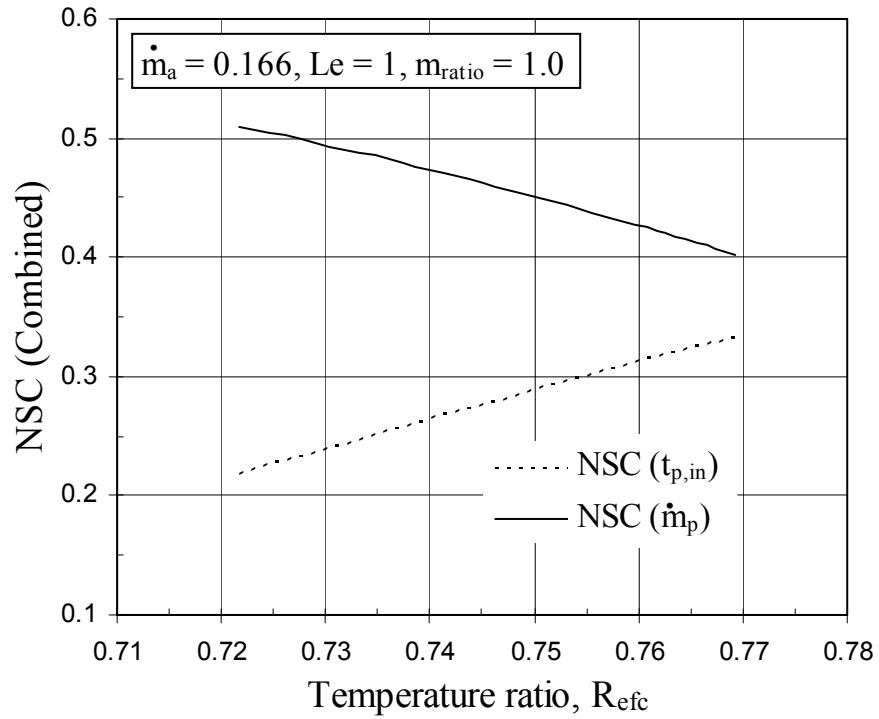


Figure 9.57: Variation of all NSCs versus R_{effc} with mass flow ratio of 1

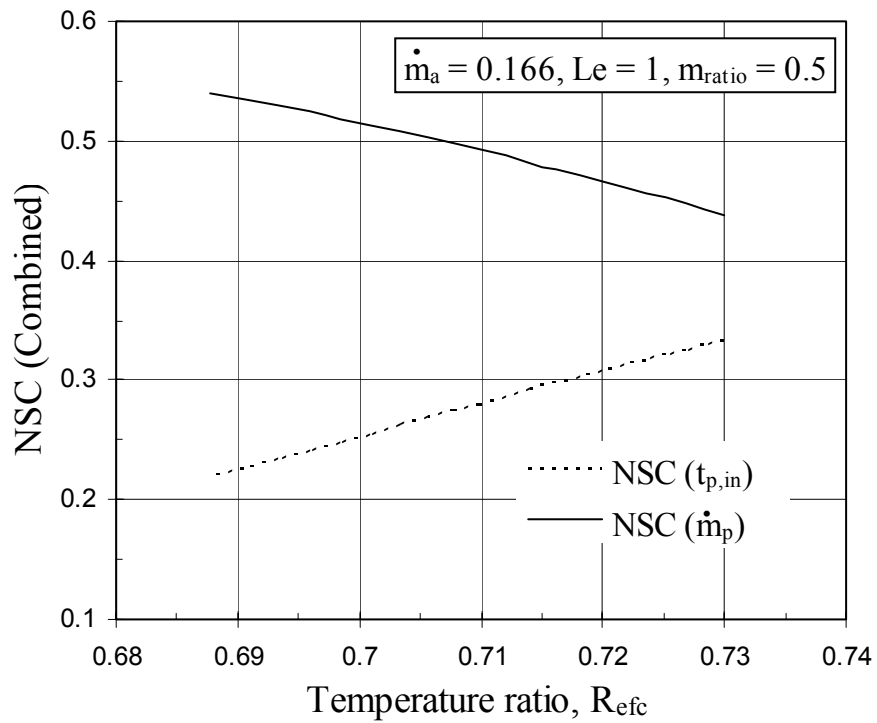


Figure 9.58: Variation of all NSCs versus R_{effc} with mass flow ratio of 0.5

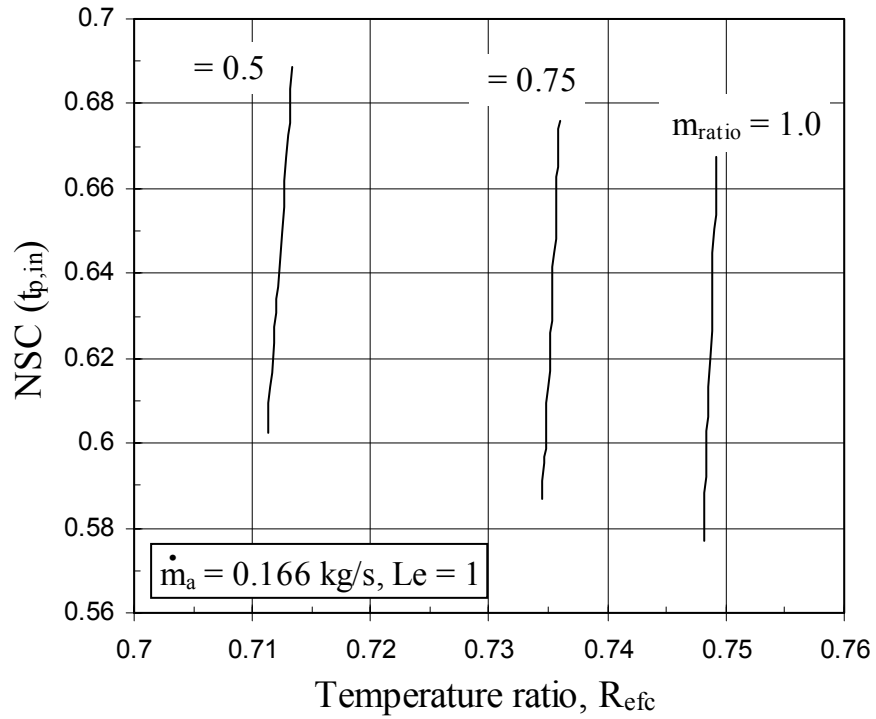


Figure 9.59: Variation of fluid outlet NSC w.r.t. fluid inlet temperature versus R_{effc}

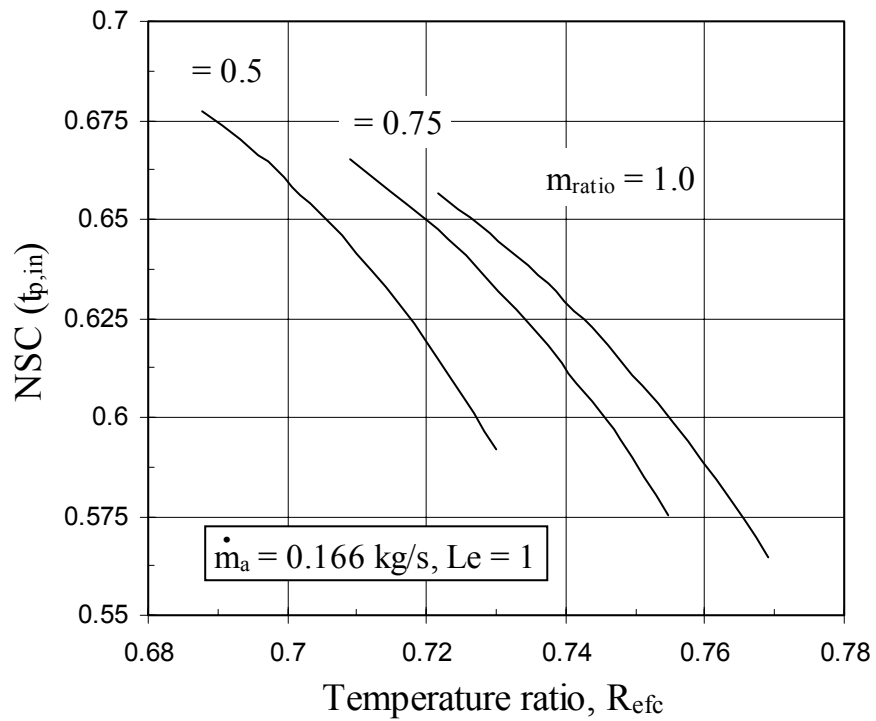


Figure 9.60: Variation of fluid outlet NSC w.r.t. fluid inlet temperature versus R_{effc}

9.2.4 Exergy Analysis Results

As before, a sensitivity analysis was carried out with respect to the second-law efficiency and it was seen that the most notable input parameters were the inlet wet-bulb and process fluid outlet temperatures that influenced it. Figure (9.61) shows the variation in the second-law efficiency, using equation (6.15), while Figure (9.62) the exergy destruction as the temperature ratio changes, for different mass flow ratios. It should be kept in mind that the increase in the temperature ratio was caused by varying the inlet wet-bulb temperature from 12.11 to 23.11 °C. From Figures (9.61), we see that second-law efficiency decreases and the exergy destruction increases as the temperature ratio increases (i.e. the inlet wet-bulb temperature decreases). As in the case of the cooling tower, the exergy of the inlet moist air minimizes at a wet-bulb temperature of approximately 19.2 °C as it reaches the dead state humidity ratio and then continuously increases with the increasing wet-bulb temperature. The exergy of the outlet air stream constantly increases due to higher dry-bulb temperature as well as humidity ratios that are achieved. Since the water loss decreases with the increasing inlet wet bulb temperature, exergy of the makeup water also decreases. Keeping in mind that the water temperature at the inlet and outlet are considered equal, we find that the rising wet-bulb temperature increases the water temperature due to the decreasing rate of evaporation and, consequently, the exergy of the water streams. With the process fluid exergy at the inlet is constant but increasing at the outlet due to higher temperatures achieved there, the exergy destroyed decreases due to the continuously decreasing value of $(t_{db,in} - t_{wb,in})$. These factors cause the second-law efficiency η_{II} to increase. With the surface area of the tubes constant, this can be attributed to the decreasing value of $(t_{p,in} - t_{wb,in})$.

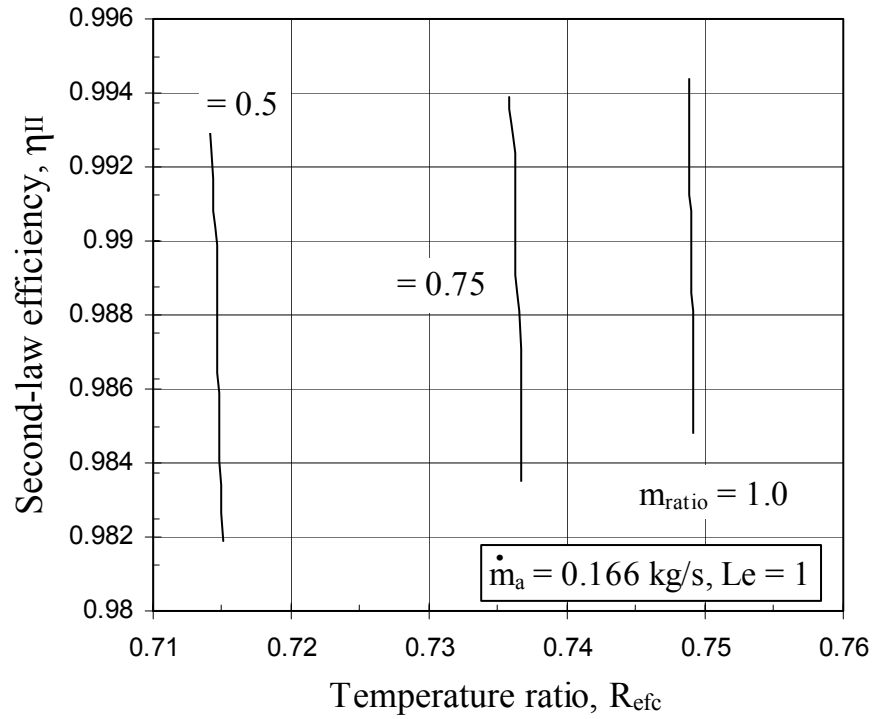


Figure 9.61: Variation of second-law efficiency versus R_{etc} (Eq. (6.15))

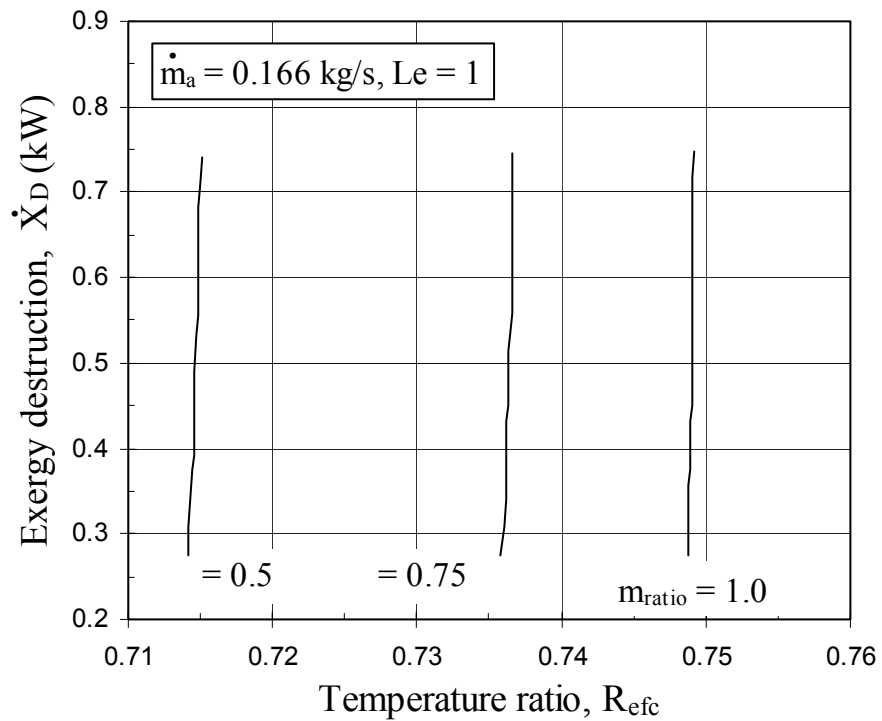


Figure 9.62: Variation of exergy destruction versus R_{etc}

Similarly, Figure (9.63) shows the variation in the second-law efficiency and Figure (9.64) the exergy destruction as the temperature ratio changes, for different mass flow ratios. Here, the temperature ratio was increased by varying the process fluid inlet temperature from 40 to 60 °C. It is noted that second-law efficiency decreases and the exergy destruction increases monotonically as the temperature ratio (or inlet process fluid temperature) increases. We see that the mass flow rate ratio has a small effect on the exergy destruction. The exergy of the outlet air stream constantly increases as it gets farther from the dead state humidity ratio. On the other hand, the exergy of the entering air stream is constant. As the inlet process fluid temperature increases, its exergy value rises as well. Furthermore, this causes higher water temperatures and an increase in the rate of evaporation due to the increased heat transfer, which increases the exergy of the makeup and recirculating water. It should be kept in mind that the temperature of the water is considered the same at the inlet and outlet. However, the exergy difference of the inlet and outlet process fluid streams constantly increases due to higher process fluid temperatures at the inlet. This causes the exergy destruction to increase and can be attributed to the continually increasing difference between the inlet and outlet process fluid temperatures. With the exergy destruction increasing, the second-law efficiency η_{II} decreases.

9.2.5 Evaporation and Effect of Mass Flow Rate

Figures (9.65) and (9.66) show the variation of the effectiveness and temperature ratio in the typical range of the mass flow rate ratio for the evaporative cooler; both increasing as the mass flow ratio increases. The data used was the same as that for all the previous evaporative cooler results. These trends can be understood from the fact that the

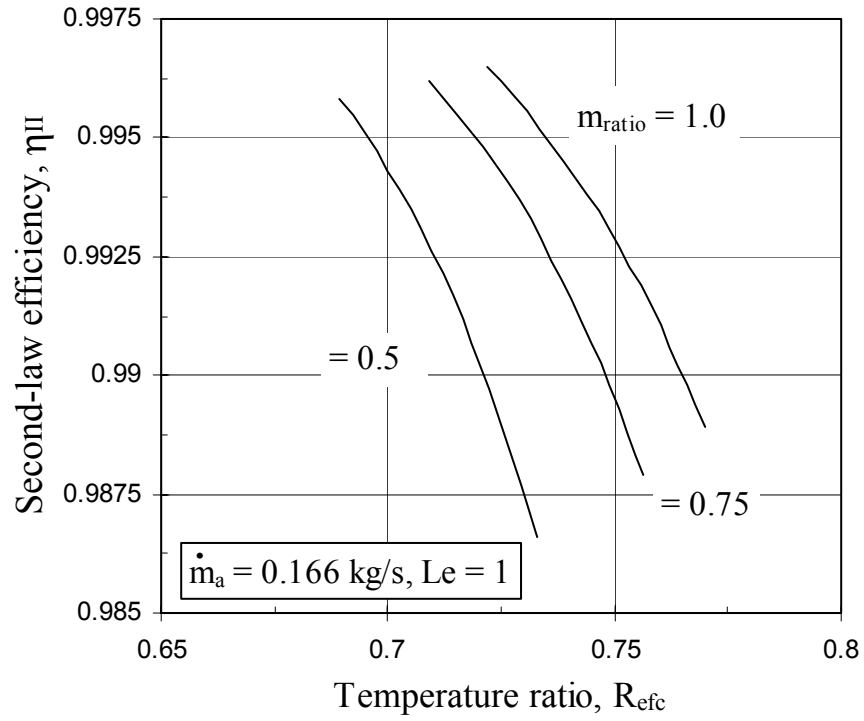


Figure 9.63: Variation of second-law efficiency versus R_{effc} (Eq. (6.15))

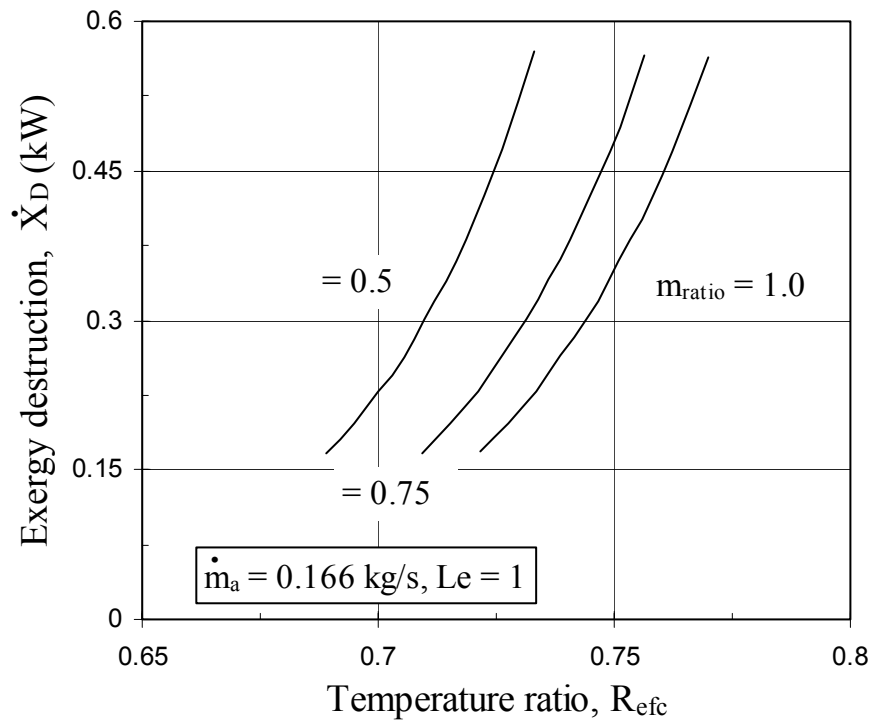


Figure 9.64: Variation of exergy destruction versus R_{effc}

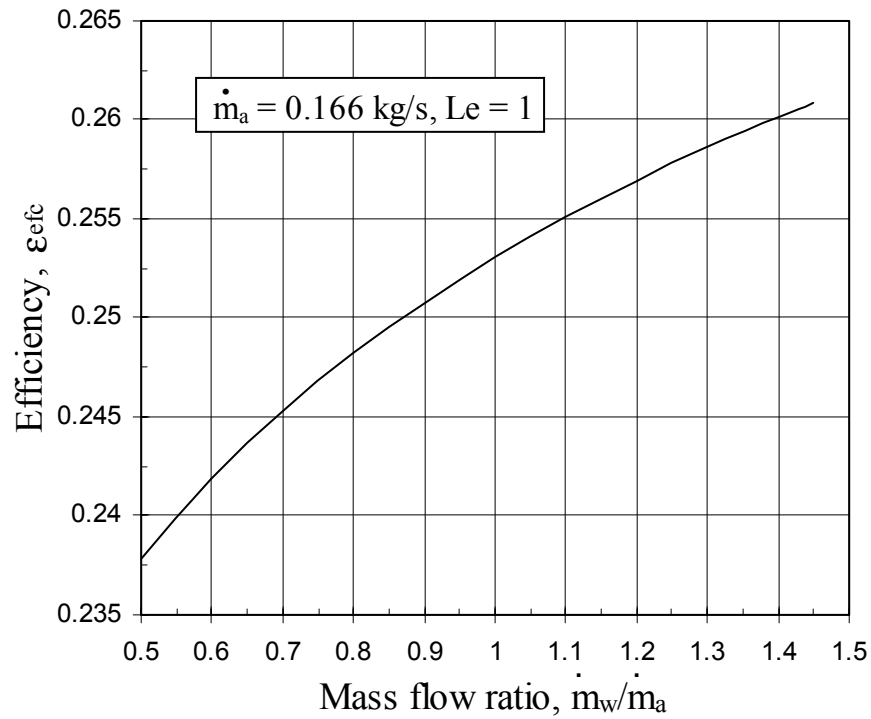


Figure 9.65: Variation of effectiveness with mass flow ratio

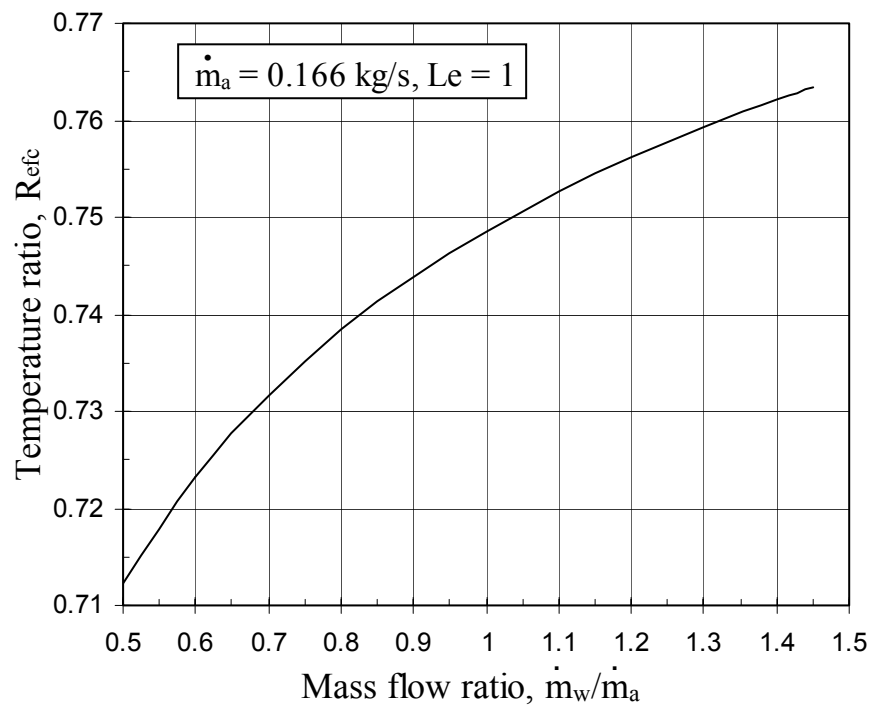


Figure 9.66: Variation of temperature ratio with mass flow ratio

outlet process fluid temperature decreases with increasing mass flow rate ratio due to lower water temperatures achieved (See eq. 3.11). Subsequently, higher values of U_{os} are obtained (See eqs. (3.14) and (3.21)) and, thus, the effectiveness increases (See eq. 3.22a). Again, the percentage of water evaporation is calculated as the relative humidity varies from very dry to very wet condition. Figure (9.67) shows a similar variation as was seen in the cooling tower because the same principles still apply even though an additional (process) fluid has been introduced.

9.3 RESULTS FOR EVAPORATIVE CONDENSER

The specifications of the evaporative condenser used in the analysis are the same as those of Leidenfrost and Korenic [5] and Dreyer [19] with R134a being the refrigerant used unless specified otherwise. It is to remind the reader that the water temperature is not considered as constant and the Lewis number is considered as unity.

9.3.1 Effect of Pressure (Elevation)

This analysis is carried out for three different water to air flow ratios i.e. 1, 0.75 and 0.5 for all the heat exchangers. It is to remind the reader that an increase in an altitude of approximately 850 meters would result in a 10 kPa decrease in atmospheric pressure. Since the evaporative cooler and condenser are very similar, it is not surprising that Figures (9.68) and (9.69) are very similar to its counterpart evaporative cooler plots. These are drawn for the following set of input data that is considered in Leidenfrost and Korenic [5] with the same dry and wet bulb temperatures used in the cooling tower: $t_{db,in} = 29\text{ }^{\circ}\text{C}$, $t_{wb,in} = 21.1\text{ }^{\circ}\text{C}$, $t_r = 44.6\text{ }^{\circ}\text{C}$, $\dot{m}_r = 0.013194\text{ kg/s}$, $\dot{m}_a = 0.06194\text{ kg/s}$. Figure (9.68) shows that, to meet the heat load of the condensing refrigerant, the surface area of the tubes can be reduced by 0.042 m^2 when $m_{ratio} = 0.5$. The reasons for the reduction in

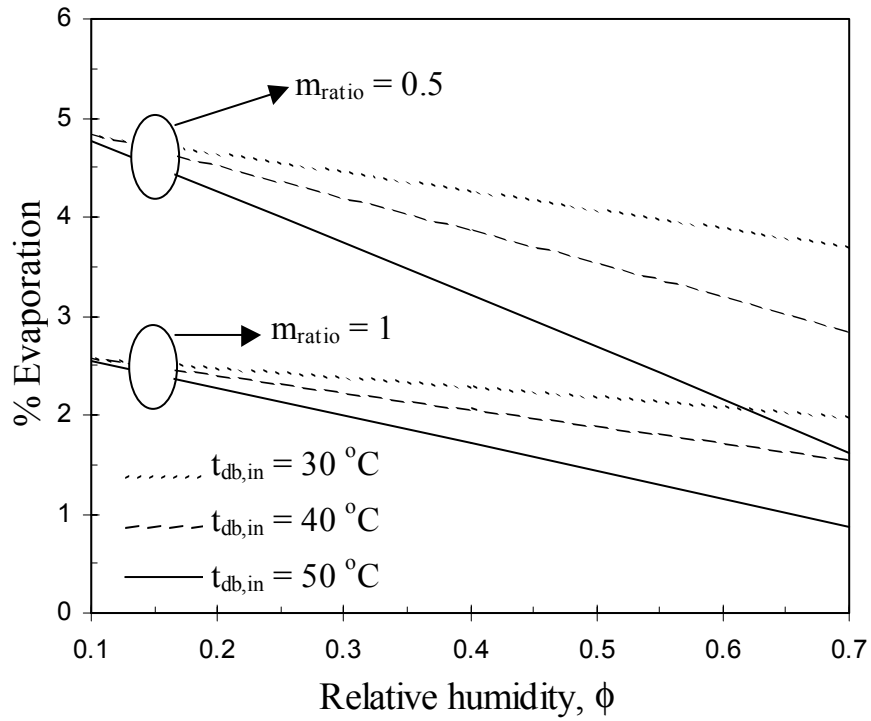


Figure 9.67: Percent evaporation for various air conditions and mass flow ratios

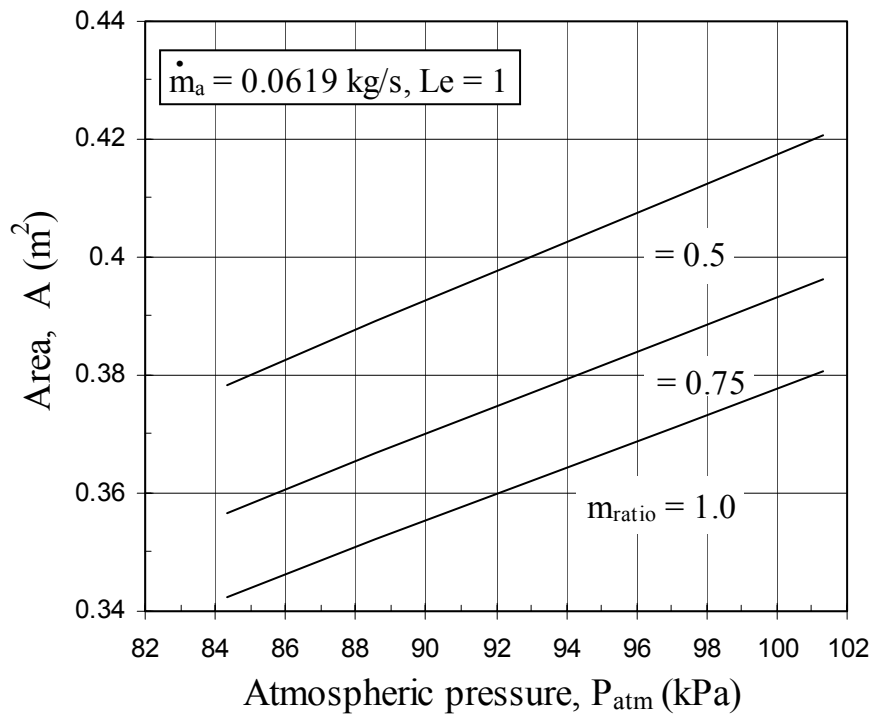


Figure 9.68: Variation in required surface area versus pressure change

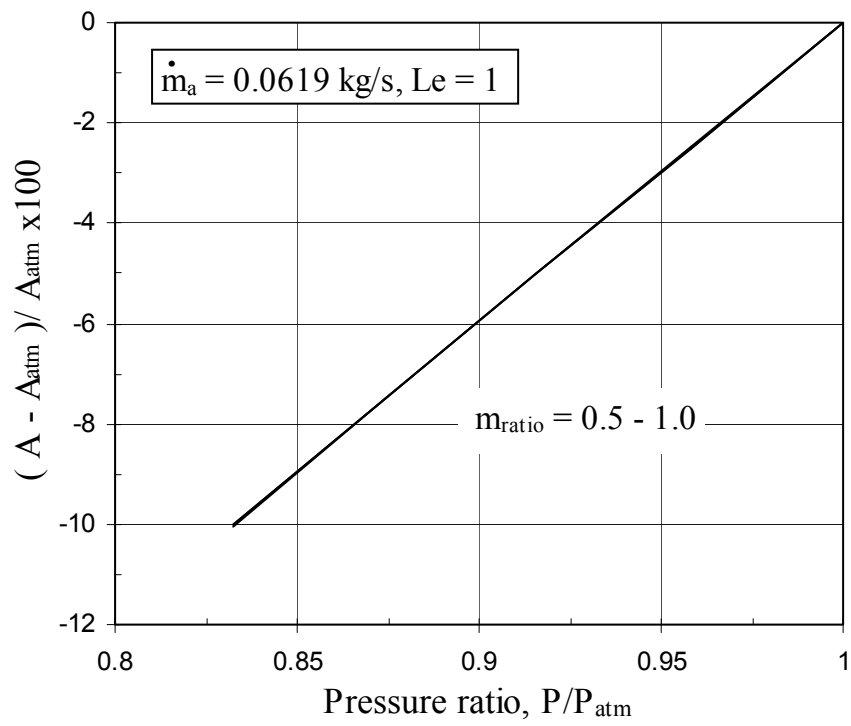


Figure 9.69: Percent decrease in required surface area versus pressure ratio

the required surface are the same as in the case of the cooling tower and evaporative cooler. Also, equation (3.13) shows that, as the atmospheric pressure decreases, the value of $(t_r - t_w)$ increases due to the decreasing steady-state water temperature and, thus, the required surface area decreases. Now, the surface area is larger as the mass flow rate ratio decreases and is due to higher water temperatures achieved at lower mass flow rate ratios (See eqn. (3.12) and (3.13)). However, it can be seen from Figure (9.69) that the percentage decrease in the required surface area, with respect to the surface area calculated at standard atmospheric pressure, is the same for each value of the mass flow rate ratio as was seen in the evaporative cooler.

9.3.2 Effect of Fouling

The mathematical model for the evaporative condenser, discussed in the chapter 3, is used for the design and rating calculations of a counter flow evaporative condenser. It is used in combination with the fouling model to study the thermal performance of the tower under fouled conditions.

9.3.2.1 Design

In design calculations, the required surface area of the evaporative condenser is calculated using the following set of input conditions: inlet air temperatures [dry bulb ($t_{db,in}$) and wet bulb ($t_{wb,in}$)], condensing temperature (t_r) and mass flow rates [air (\dot{m}_a), water ($\dot{m}_{w,in}$) and refrigerant (\dot{m}_r)]. The specifications of the evaporative condenser used in the analysis are the same as those used in an example by Dreyer [19] including the refrigerant.

As with the cooling tower and evaporative fluid cooler, fouling reduces the performance of the evaporative condenser as well. In order to attain a constant value of

the evaporative condenser effectiveness under fouled conditions, the surface area has to be increased since the overall heat transfer coefficient is reduced, which is illustrated in Figure (9.70). It represents a plot of the area fraction (A_f / A_{cl}) of the evaporative condenser as a function of asymptotic fouling resistance R_f^* .

9.3.2.2 Rating

In rating calculations, refrigerant outlet enthalpy ($h_{r,out}$) and effectiveness (ϵ_{ec}) are calculated for the following set of input conditions: inlet air temperatures [dry bulb ($t_{db,in}$) and wet bulb ($t_{wb,in}$)], condenser temperature (t_r), mass flow rates [air (\dot{m}_a) and water ($\dot{m}_{w,in}$) and refrigerant (\dot{m}_r)] and required surface area (A). The time and risk-based effectiveness of the evaporative condenser is shown in a reduced system in Figure (9.71). The reduced effectiveness $\epsilon_{ec}(\delta, p; \sqrt{\alpha}) / \epsilon_{ec}(0)$ versus reduced fouling thickness δ/M , for different risk level p and scatter parameter $\alpha^{1/2} = 0.3$, is plotted for the fouling-growth model discussed earlier. The effectiveness of the evaporative condenser degrades considerably with time indicating that, for a low risk level ($p = 0.01$), there is about 73% decrease for the given fouling model. The variation in the normalized load versus reduced fouling thickness, for different risk levels p and for scatter parameter $\alpha^{1/2} = 0.3$, is shown in Figure (9.72). It should be kept in mind that the fouling data used for the analysis was for calcium carbonate scale that is deposited due to accelerated growth [80]. The figure shows that for a low risk level (i.e., high reliability on performance), when compared with the deterministic case (i.e. $p = 0.5$), the ability to meet the load decreases, indicating that there will be a lower heat transfer rate due to fouling. It is noticed that there is about 73 % decrease in load capacity for the given fouling model. For a risk level of 0.01, which

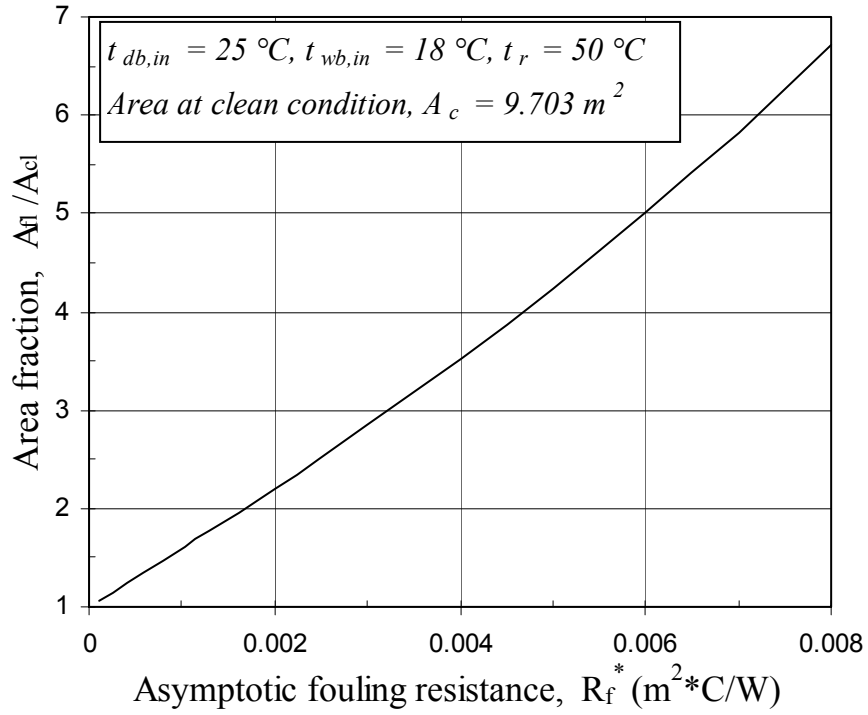


Figure 9.70: Area fraction as a function of fouling resistance

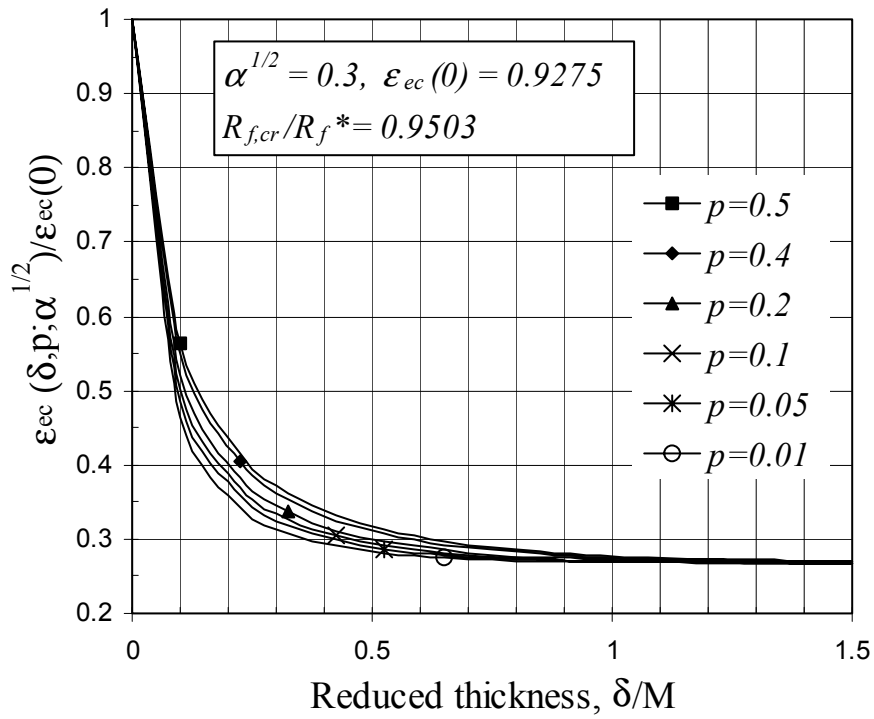


Figure 9.71: Normalized effectiveness versus reduced thickness

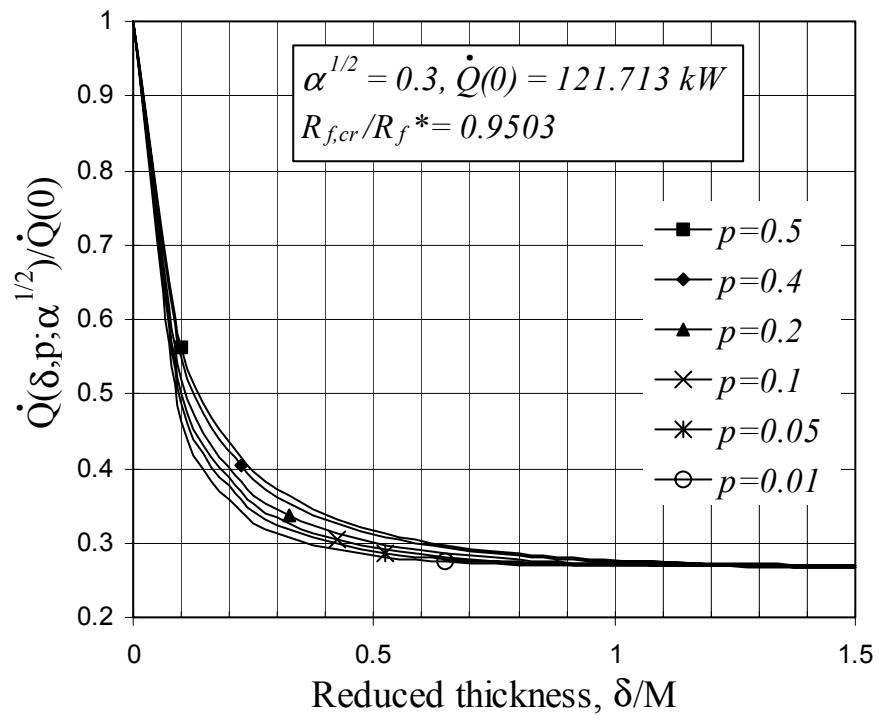


Figure 9.72: Normalized load versus reduced thickness

indicates that the operator is willing to take a 1 percent risk of a system shutdown, Figure (9.71) predicts a faster rate of effectiveness degradation and Figure (9.72) that of heat transfer rate compared to the deterministic case, which will subsequently require a comparatively earlier cleaning of the evaporative condenser.

9.3.3 Sensitivity Analysis Results

The computer model of the evaporative condenser discussed in chapter 3 was used to perform a sensitivity analysis. The normalized sensitivity coefficients were calculated and are shown for different mass flow rate ratios as well as in a combined form at the same mass flow ratios. As before, the analysis is carried out for the water to air flow ratios of 1, 0.75 and 0.5. The inlet wet bulb temperature is varied as in section 9.2.3 and t_r is varied from 35 to 50 °C.

9.3.3.1 Design

Figure (9.73) is normalized form of the plot between (surface) area sensitivity coefficient ($\partial A / \partial t_r$) versus the inlet wet-bulb temperature, for different values of mass flow rate ratio. Here, $t_{wb,in}$ is varied from 12.11 to 23.11 °C. Figure (9.73) shows that as the value of the temperature ratio increases, the NSC increases. The condensing temperature as well as its perturbation (Δt_r) is constant. As $t_{wb,in}$ increases, the decreasing difference between t_r and $t_{wb,in}$ gives rise to larger surface area requirements as well as a higher rate of changes in area (ΔA) (See eqn. (3.13)). The NSC is greater at lower mass flow rate ratios because of the lower value of the heat transfer coefficient there, which is the result of lower steady-state water temperature achieved.

Similarly, Figure (9.74) is the normalized form of the plot between (surface) area sensitivity coefficient ($\partial A / \partial t_r$) versus the condensing temperature, for different values of

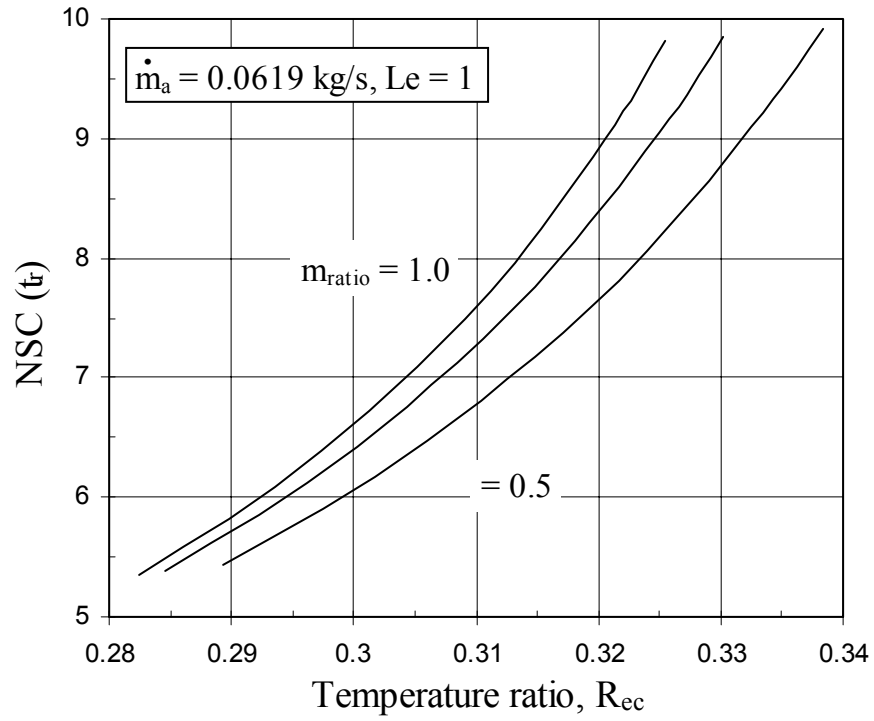


Figure 9.73: Variation of area NSC w.r.t. condensing temperature versus R_{ec}

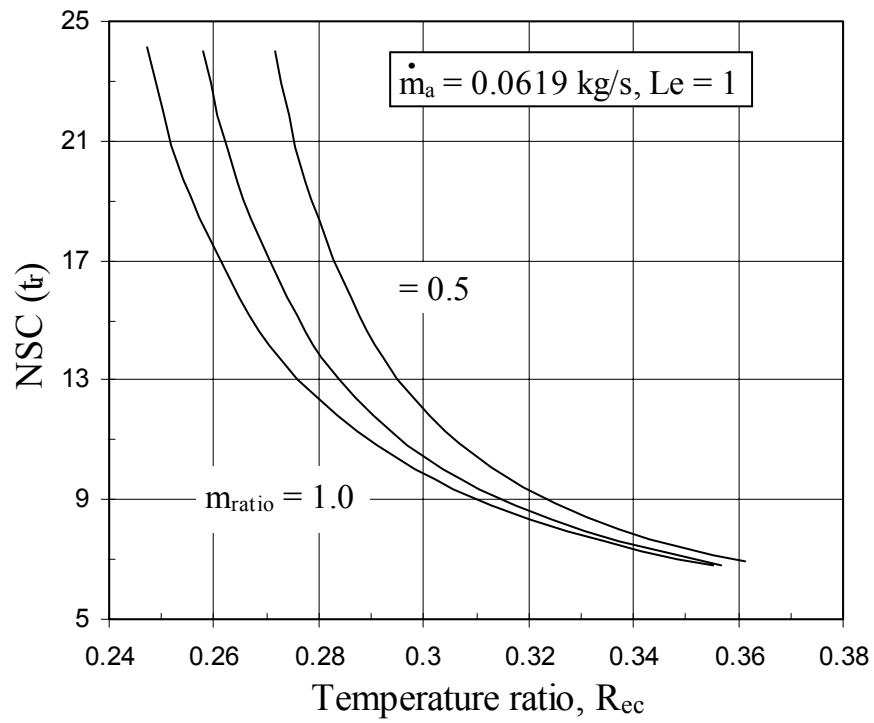


Figure 9.74: Variation of area NSC w.r.t. condensing temperature versus R_{ec}

mass flow rate ratio. Figure (9.74) shows that, as the value of the temperature ratio increases, the NSC decreases and is greater at lower mass flow rate ratios. As t_r increases, the heat load decreases, which subsequently requires less surface area and the increasing value of $(t_r - t_{wb,in})$ causes a smaller rate of change in area (ΔA) (See eqn. (3.13)) as well. With the perturbation of the condensing temperature (Δt_r) the same, these factors combine to decrease the NSC as the temperature ratio increases. The NSC is greater at lower mass flow rate ratios for the same reasons as explained for Figure (9.73).

9.3.3.2 Rating

Figure (9.75) is the normalized form of the plot between effectiveness sensitivity coefficient ($\partial \varepsilon_{ec} / \partial t_r$) versus the inlet wet-bulb temperature, for different values of mass flow rate ratio. Figure (9.75) demonstrates that, as $t_{wb,in}$ (and the temperature ratio) increases, the NSC also increases. The condensing temperature as well as its perturbation (Δt_r) is constant. As $t_{wb,in}$ increases, the decreasing difference between t_r and $t_{wb,in}$ decreases the effectiveness as the it becomes more difficult to condense the refrigerant but the rate of change in it ($\Delta \varepsilon_{ec}$) increases. The NSC is greater at lower mass flow rate ratios because of the lower value of the heat transfer coefficient there, which is the result of lower steady-state water temperature achieved.

Similarly, Figure (9.76) is the normalized form of the plot between effectiveness sensitivity coefficient ($\partial \varepsilon_{ec} / \partial t_r$) versus the condensing temperature, for different values of mass flow rate ratio. Figure (9.76) demonstrates that, as t_r (and the temperature ratio) increases, the NSC also decreases. The perturbation of the condensing temperature (Δt_r) is constant. As t_r increases, the increasing difference between t_r and $t_{wb,in}$ increases the effectiveness as well as the rate of change in it ($\Delta \varepsilon_{ec}$) as it becomes easier to condense

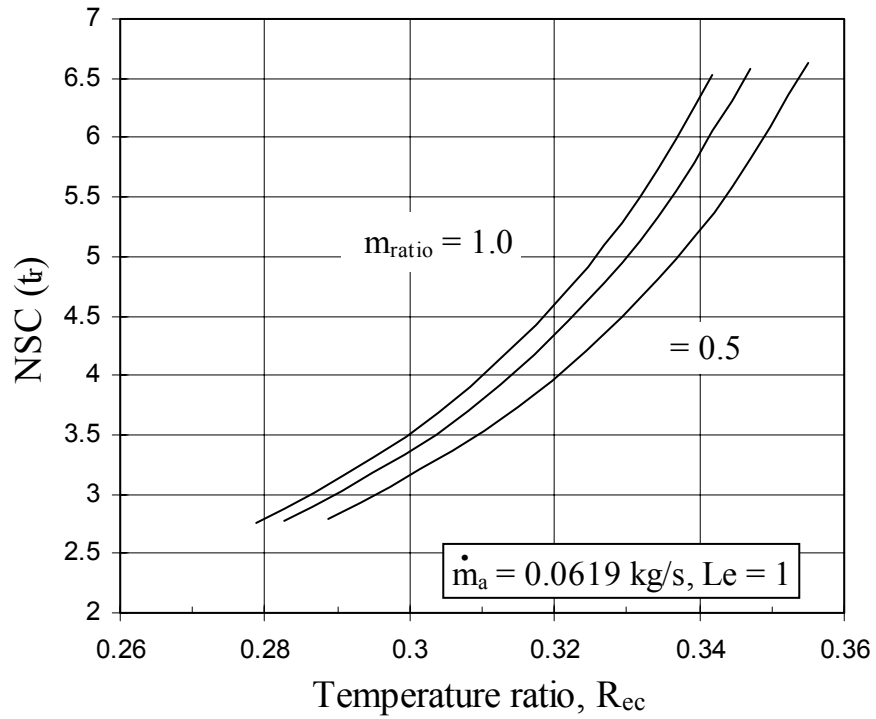


Figure 9.75: Variation of effectiveness NSC w.r.t. condensing temperature versus R_{ec}

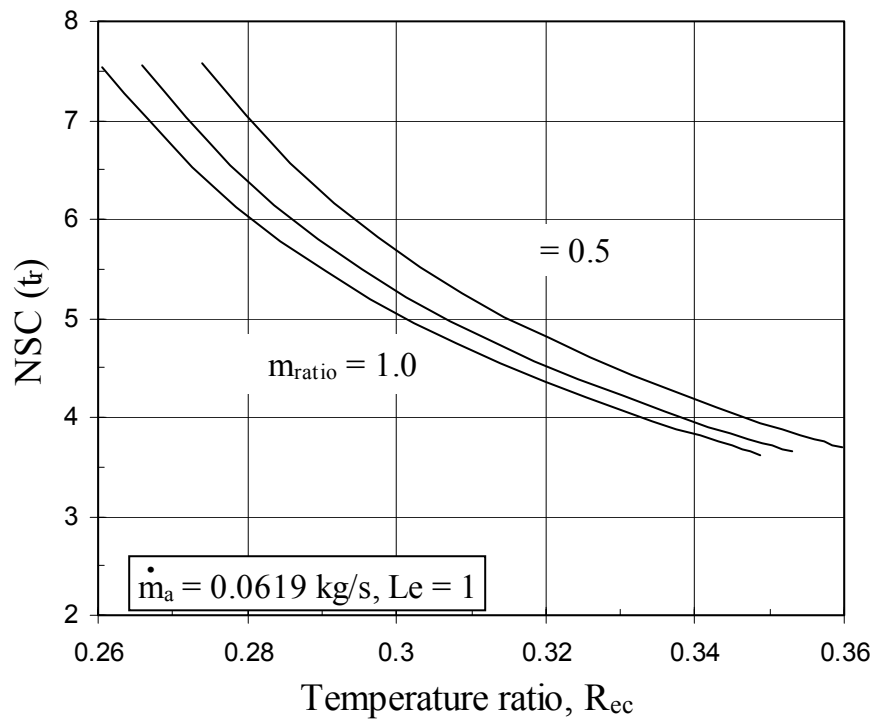


Figure 9.76: Variation of effectiveness NSC w.r.t. condensing temperature versus R_{ec}

the refrigerant. The NSC is greater at lower mass flow rate ratios due to the same reasons as described for Figure (9.75).

9.3.4 Exergy Analysis Results

As before, a sensitivity analysis was carried out with respect to the second-law efficiency and it was seen that the most notable input parameters were the inlet wet-bulb and condensing temperatures that influenced it. Figure (9.77) shows the variation in the second-law efficiency, using equation (6.15), and Figure (9.78) the exergy destruction as the temperature ratio changes, for different mass flow ratios. It should be kept in mind that the increase in the temperature ratio was caused by varying the inlet wet-bulb temperature from 12.11 to 23.11 °C. From these figures, we see that second-law efficiency increases and the exergy destruction decreases as the temperature ratio increases. As in the case of the cooling tower and evaporative cooler, the exergy of the inlet moist air minimizes at a wet-bulb temperature of approximately 19.2 °C as it reaches the dead state humidity ratio and then constantly increases. Again, the exergy of the outlet air stream constantly increases due to the higher dry-bulb temperature and humidity ratios attained. With the water loss decreasing, the exergy of the makeup water also decreases. The rising wet-bulb temperature increases the steady-state water temperature and, consequently, the water exergy values also rise. Also, lesser heat is transferred from the condensing fluid and, thus, the exergy of the refrigerant at the outlet also increases. These factors decrease the exergy destruction and can be attributed, in general, to the continuously decreasing value of $(t_{db,in} - t_{wb,in})$. At smaller mass flow ratios, exergy destruction is lower mainly due to smaller exergy values of the outlet air and water streams (See eqn. (3.2) and (3.11)). Subsequently, these factors cause the second-law

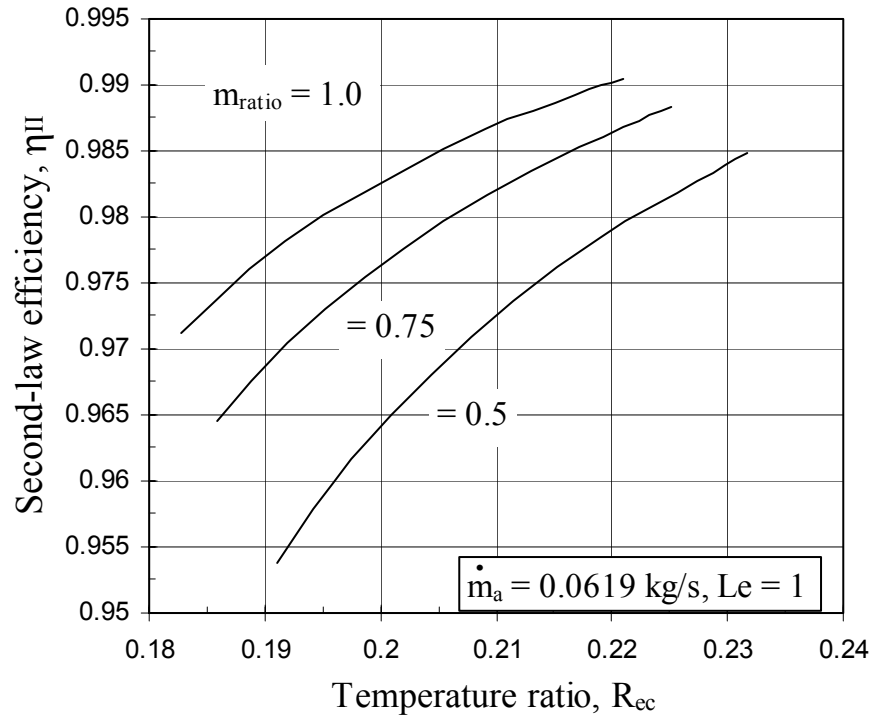


Figure 9.77: Variation of second-law efficiency versus R_{ec} (Eq. (6.15))

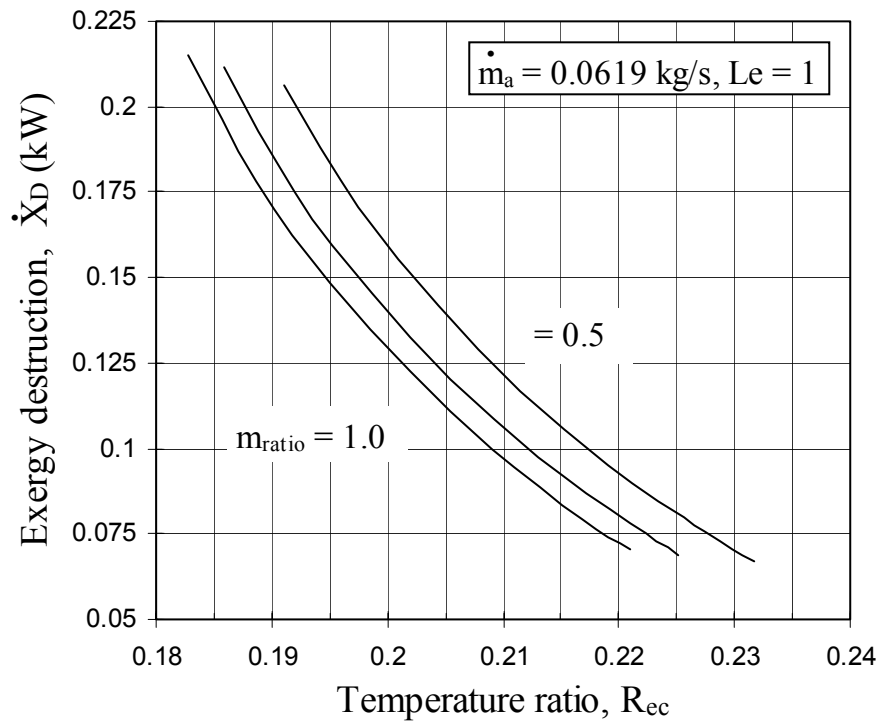


Figure 9.78: Variation of exergy destruction versus R_{ec}

efficiency η_{II} to increase and can be attributed to the decreasing value of $(t_r - t_{wb,in})$ as the surface area of the tubes is constant. As the mass flow rate ratio increases, the overall heat transfer coefficient also rises and, therefore, the second-law efficiency is higher as well.

Similarly, Figure (9.79) shows the variation in the second-law efficiency and Figure (9.80) the exergy destruction as the temperature ratio changes, for different mass flow ratios. The temperature ratio was increased by varying the condensing temperature from 35 to 50 °C. It is noted that second-law efficiency decreases and the exergy destruction increases as the temperature ratio increases. The exergy of the outlet air stream constantly increases as it moves away from the dead state humidity ratio due to the increasing value of $(t_r - t_{wb,in})$ that allows for the air to become more and more humid. On the other hand, the exergy of the entering air stream is constant, as the conditions there are not changing. As the water loss increases, due to the increasing value of $(t_r - t_{wb,in})$, exergy of the makeup water also increases. The exergy value of the refrigerant increases at the inlet with its rising temperature. A combination of these factors causes the exergy destruction to increase and can be attributed to the increasing value of $(t_r - t_{wb,in})$. The mass flow ratio does not have a significant effect on the exergy destruction mainly due to the fact that it largely affects the exergy of the water stream, which cancels out since they are equal (See eqn. (6.6)). Subsequently, the second-law efficiency η_{II} decreases since the surface area of the tubes is constant. As the mass flow rate ratio increases, the overall heat transfer coefficient also rises and, therefore, the second-law efficiency is higher as well.

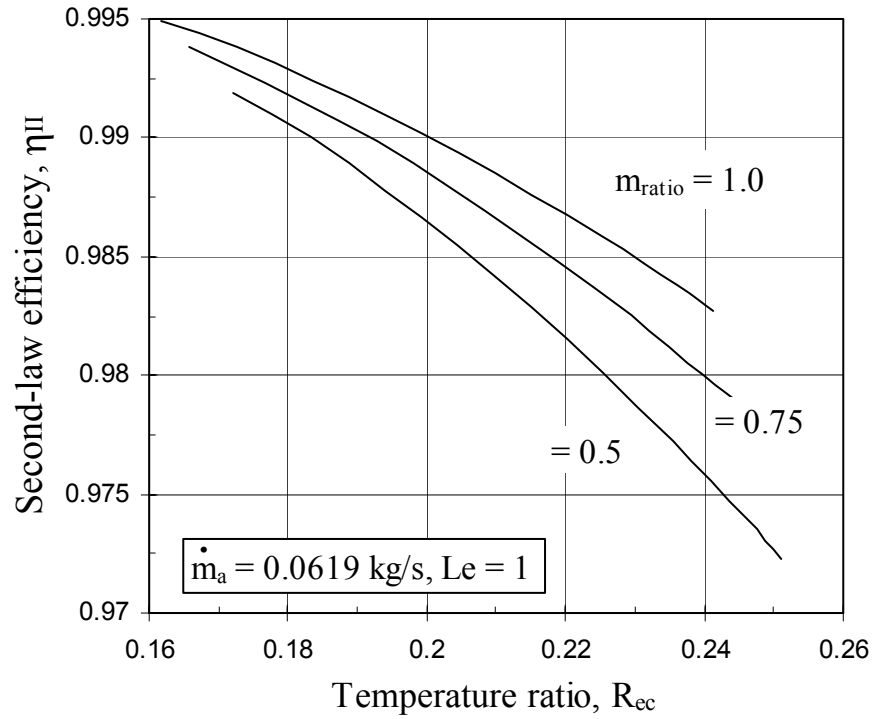


Figure 9.79: Variation of second-law efficiency versus R_{ec} (Eq. (6.15))

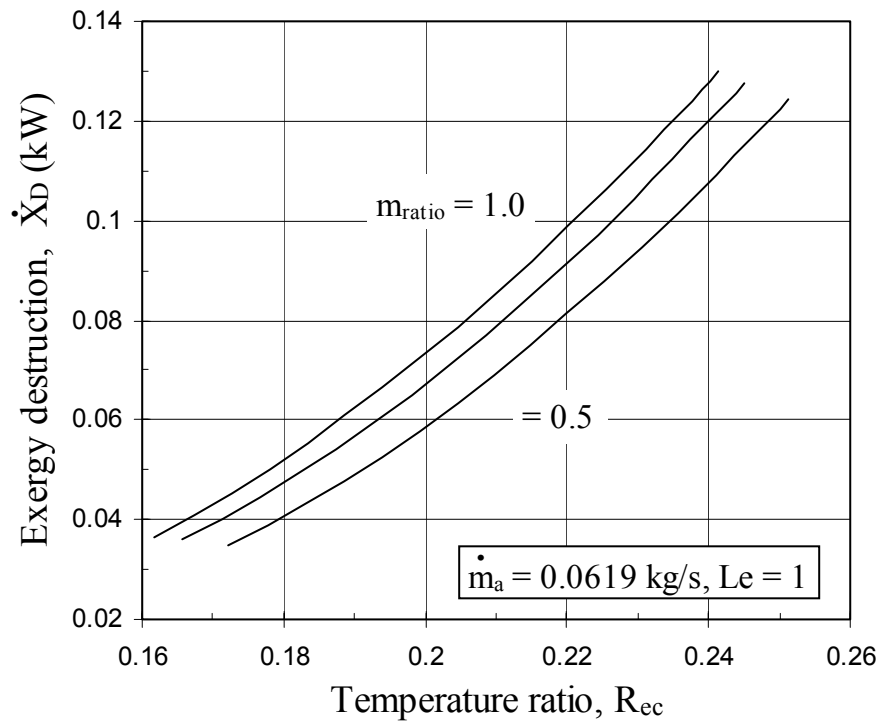


Figure 9.80: Variation of exergy destruction versus R_{ec}

9.3.5 Effect of Mass Flow Rate

Figures (9.81) and (9.82) show the variation of the effectiveness and temperature ratio R in the typical range of the mass flow rate ratio for the evaporative condenser. Both increasing and decreasing, respectively, monotonically as the mass flow rate ratio increases. For higher mass flow ratios, a higher steady-state water temperature is acquired by the system and, thus, temperature ratio decreases. Furthermore, a higher heat transfer coefficient is achieved (See eqn. (3.14 and 3.21)), which in turn increases the effectiveness of the evaporative condenser (See eqn. (3.23 a,b)). The input data used was that of Leidenfrost and Korenic [5] but with the same dry and wet-bulb temperatures used to calculate the amount of water evaporated in the cooling tower.

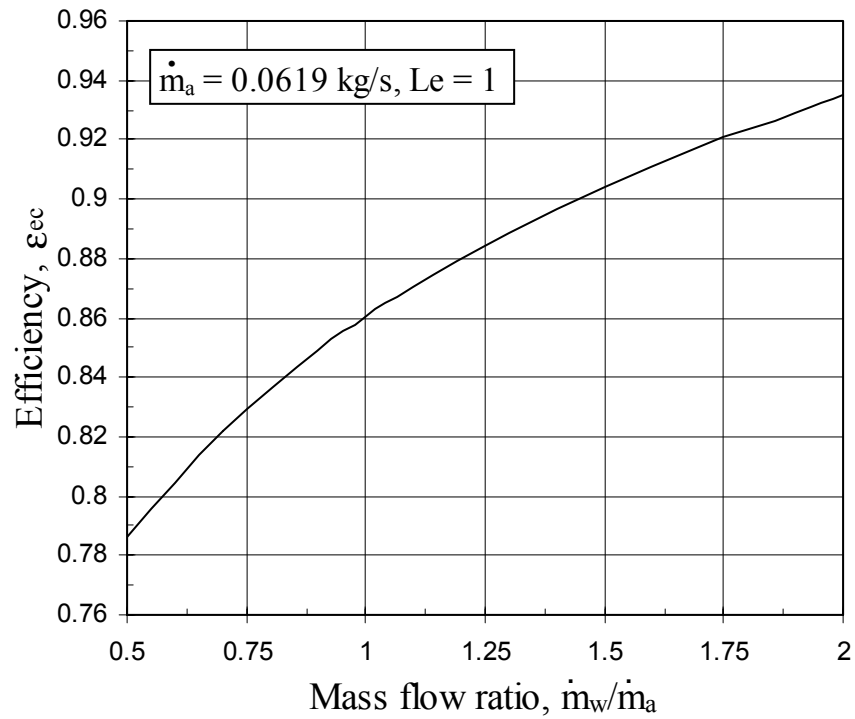


Figure 9.81: Variation of effectiveness with mass flow ratio

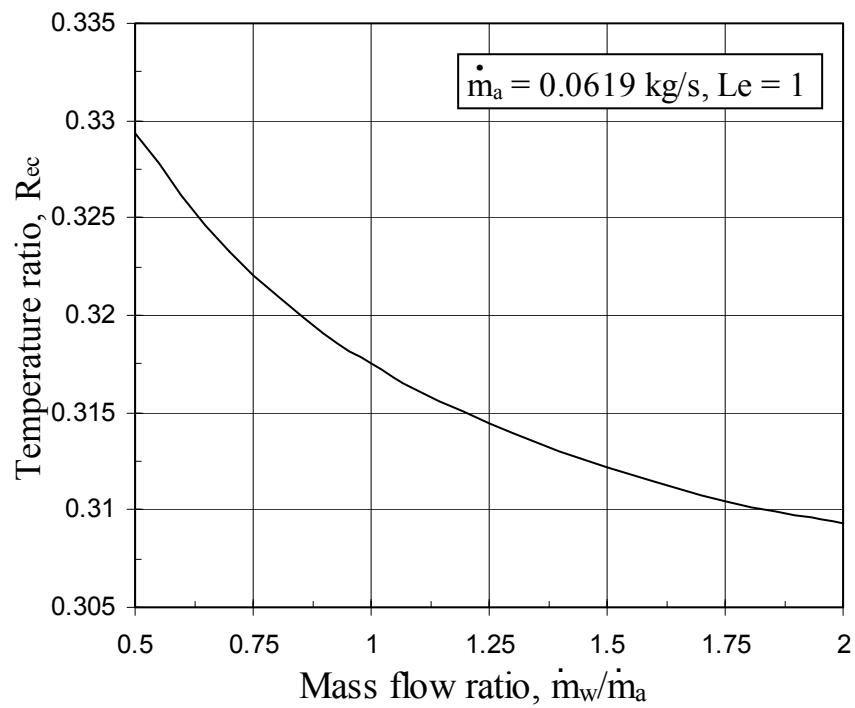


Figure 9.82: Variation of temperature ratio with mass flow ratio

CHAPTER 10

CONCLUSIONS AND RECOMMENDATIONS

The present work has aimed at the design, rating and exergy analysis of evaporative heat exchangers. The analytical models of cooling towers, evaporative condensers and evaporative coolers are developed and then systematically verified using experimental and numerical data available in the literature. Two important aspects of design and rating calculations are studied in more detail. In terms of design, the volume or surface area is not known and must be calculated for the required cooling load. In this regard, the effect of elevation and the impact of fouling on design are investigated. Furthermore, the concept of exergy analysis is applied to these evaporative heat exchangers to investigate the variation in second-law efficiency. In terms of rating, the volume or surface area is known and the performance of the heat exchanger, in terms of parameters such as effectiveness, is studied. In this regard, the effect of fouling and water to air flow ratio is explored. Also, a sensitivity analysis is carried out, in terms of both design and rating, to evaluate the response of various parameters to different input variables such as the inlet wet-bulb temperature.

10.1 CONCLUSIONS

From the results obtained, the following conclusions can be deduced:

- For design purposes, the inclusion of the spray and rain zones in the analysis of large towers is necessary.
- In cooling towers, a higher altitude results in (i) decrease in the wet bulb temperature; (ii) decrease in the required fill volume to achieve the same water outlet temperature; and (iii) larger percentage decrease in volume for a higher mass flow rate ratio.
- In a cooling tower, increasing the mass flow rate ratio (i) increases the effectiveness; (ii) decreases the temperature ratio along with the air approach; and (iii) helps towards a smaller make-up water requirement.
- For cooling towers, the sensitivity analysis shows that (i) all sensitivities, in design, are higher for larger mass flow ratios; (ii) outlet water temperature is the most important factor in design as the volume prediction is most sensitive to it; and (iii) in rating, all sensitivities, as far as effectiveness is concerned, are lower for larger mass flow ratios.
- Effectiveness is most sensitive to the water flow rate and inlet water temperature and is less sensitive to the inlet wet bulb temperature, though the inlet water temperature can become the dominant factor at higher values of the inlet wet bulb or water temperatures.
- Outlet water temperature is most sensitive to the inlet wet bulb and water temperatures and least sensitive to the water flow rate. Although, for lower mass flow ratios, the former dominates almost completely but for comparatively larger mass flow ratios, this dominance is attained at a much higher wet bulb temperature.
- In cooling towers, the impact of fouling shows that (i) volume fraction increases non-linearly with the increasing value of C_I ; and (ii) lower the risk level, lower the

effectiveness and higher the outlet water temperature with respect to the reduced weight.

- Effectiveness of the cooling tower degrades significantly with time indicating that, for a low risk level ($p = 0.01$), there is about 6.0 % decrease in effectiveness for the given fouling model.
- There is about 1.2 % increase in water outlet temperature for the given fouling model.
- In cooling towers, the exergetic analysis illustrates that (i) the second-law efficiency increases and the exergy destruction decreases as the inlet wet bulb temperature increases; and (ii) the second-law efficiency decreases and the exergy destruction increases as the outlet water temperature increases.
- In evaporative coolers and condensers, a higher altitude results in (i) decrease in the required surface area; and (ii) percentage decrease in required surface area is the same for all mass flow rate ratios.
- In evaporative coolers, increasing the mass flow rate ratio (i) increases the effectiveness and temperature ratio; and (ii) increases the make-up water requirement.
- For evaporative coolers, the sensitivity analysis shows that all sensitivities, in design, are not affected by the varying mass flow ratios investigated.
- Outlet process fluid temperature is the most important factor in design.
- Effectiveness is most sensitive to the process fluid flow rate and is comparatively less sensitive to the inlet process fluid temperature.
- Outlet process fluid temperature is most sensitive to the inlet process fluid temperature.

- In evaporative coolers, the impact of fouling shows that (i) area fraction increases linearly with the increasing value of the fouling resistance; and (ii) lower the risk level, lower the effectiveness and higher the outlet process fluid temperature with respect to the reduced thickness.
- Effectiveness of the evaporative cooler degrades significantly with time indicating that, for a low risk level ($p = 0.01$), there is about 73 % decrease for the given fouling model.
- There is approximately 5.1 % increase in outlet process fluid temperature for the given fouling model.
- In evaporative coolers, the exergetic analysis shows that (i) the second-law efficiency decreases and the exergy destruction increases as the temperature ratio increases due the changing inlet wet bulb temperature; and (ii) the second-law efficiency decreases and the exergy destruction increases as the temperature ratio increases due to the changing fluid outlet temperature.
- In evaporative condensers, increasing mass flow rate ratio (i) increases the effectiveness but decreases the temperature ratio; and (ii) increases the make-up water requirement.
- For evaporative condensers, the sensitivity analysis shows that condensing temperature is the most important factor in design as well as rating.
- In evaporative condensers, the impact of fouling shows that (i) area fraction increases linearly with the increasing value of the fouling resistance. However, we find that area fraction is always greater as compared to the evaporative cooler; and (ii) lower the risk level, lower the effectiveness with respect to the reduced thickness.

- Effectiveness of the evaporative condenser degrades significantly with time indicating that, for a low risk level ($p = 0.01$), there is about 73 % decrease for the given fouling model.
- In evaporative condensers, the exergetic analysis shows that (i) the second-law efficiency increases and the exergy destruction decreases as the temperature ratio increases due the changing inlet wet bulb temperature; and (ii) the second-law efficiency decreases and the exergy destruction increases as the temperature ratio increases due to the changing condensing temperature.

10.2 RECOMMENDATIONS

Due to the wide scope of the present research work, the following suggestions for future research may be considered.

- A long-term experimental work can be carried out to validate the proposed fouling models for the evaporative condenser and evaporative fluid coolers.
- Inclusion of the spray and rain zones can be studied for large-size evaporative heat exchangers to ascertain its effects on design and rating.
- Two-dimensional effects, including CFD analysis, in the design and rating calculations for these heat exchangers may be studied.
- The variation of Lewis number in a given cooling tower maybe be integrated in design and rating calculations using a one-dimensional model.

Appendix A

Derivation of Equation (3.15)

It was shown that, in the evaporative cooler and condenser, at the air-water interface, simultaneous heat and mass transfer takes place that can be expressed as

$$\dot{m}_a dh = h_c (t_{\text{int}} - t_a) dA + h_D (W_{s,\text{int}} - W) h_{fg,\text{int}} dA \quad (\text{A.1})$$

The following supplementary equations can now be used to simplify the equations above:

$$\text{i.} \quad c_{p,a} = c_{p,da} + Wc_{p,v} \quad (\text{A.2})$$

$$\text{ii.} \quad h_{g,\text{int}} = h_g^0 + c_{p,v} t_{\text{int}} \quad (\text{A.3})$$

$$\text{iii.} \quad h = (c_{p,da} + Wc_{p,v}) t_a + Wh_g^0 \quad (\text{A.4})$$

$$\text{iv.} \quad h_{s,\text{int}} = (c_{p,da} + W_{s,\text{int}} c_{p,v}) t_{\text{int}} + W_{s,\text{int}} h_g^0 \quad (\text{A.5})$$

Rewriting equation (A.1) and employing equation (A.2) gives

$$\begin{aligned} \dot{m}_a dh &= h_D dA \left[(W_{s,\text{int}} - W) h_{fg,\text{int}} + \left[\frac{h_c}{h_D c_{p,a}} \right] (c_{p,da} + Wc_{p,v}) (t_{\text{int}} - t_a) \right] \\ \dot{m}_a dh &= h_D dA \left[(W_{s,\text{int}} - W) h_{fg,\text{int}} + \left[\frac{h_c}{h_D c_{p,a}} \right] (c_{p,da} + Wc_{p,v}) t_{\text{int}} - (c_{p,da} + Wc_{p,v}) t_a \right] \end{aligned}$$

By rearranging equation (A.4) and substituting it into the relation above, it follows that

$$\begin{aligned} \dot{m}_a dh &= h_D dA \left[(W_{s,\text{int}} - W) h_{fg,\text{int}} + \left[\frac{h_c}{h_D c_{p,a}} \right] (c_{p,da} + Wc_{p,v} + W_{s,\text{int}} c_{p,v} - W_{s,\text{int}} c_{p,v}) t_{\text{int}} - h + Wh_g^0 \right] \\ &= h_D dA \left[(W_{s,\text{int}} - W) h_{fg,\text{int}} + \left[\frac{h_c}{h_D c_{p,a}} \right] [(c_{p,da} + W_{s,\text{int}} c_{p,v}) t_{\text{int}} - (W_{s,\text{int}} - W) c_{p,v} t_{\text{int}} - h + Wh_g^0] \right] \end{aligned}$$

Rearranging equation (A.5) and substituting it into the relation above, gives

$$\begin{aligned} \dot{m}_a dh &= h_D dA \left[(W_{s,\text{int}} - W) h_{fg,\text{int}} + \left[\frac{h_c}{h_D c_{p,a}} \right] [h_{s,\text{int}} + W_{s,\text{int}} h_g^0 - (W_{s,\text{int}} - W) c_{p,v} t_{\text{int}} - h + W h_g^0] \right] \\ &= h_D dA \left[(W_{s,\text{int}} - W) h_{fg,\text{int}} + \left[\frac{h_c}{h_D c_{p,a}} \right] [(h_{s,\text{int}} - h) - (W_{s,\text{int}} - W)(h_g^0 + c_{p,v} t_{\text{int}})] \right] \end{aligned}$$

By substituting equation (A.3), we get

$$\begin{aligned} &= h_D dA \left[(W_{s,\text{int}} - W) h_{fg,\text{int}} + \left[\frac{h_c}{h_D c_{p,a}} \right] [(h_{s,\text{int}} - h) - (W_{s,\text{int}} - W) h_{g,\text{int}}] \right] \\ &= h_D dA \left[(W_{s,\text{int}} - W) h_{fg,\text{int}} + \left[\frac{h_c}{h_D c_{p,a}} - 1 \right] [(h_{s,\text{int}} - h) - (W_{s,\text{int}} - W) h_{g,\text{int}}] \right. \\ &\quad \left. + [(h_{s,\text{int}} - h) - (W_{s,\text{int}} - W) h_{g,\text{int}}] \right] \end{aligned}$$

Assuming $h_{fg} \approx h_g$, we get

$$\begin{aligned} \dot{m}_a dh &= h_D dA \left[(h_{s,\text{int}} - h) + \left[\frac{h_c}{h_D c_{p,a}} - 1 \right] [(h_{s,\text{int}} - h) - (W_{s,\text{int}} - W) h_{g,\text{int}}] \right] \\ dh &= \frac{h_D dA}{\dot{m}_a} \left[(h_{s,\text{int}} - h) + \left[\frac{h_c}{h_D c_{p,a}} - 1 \right] [(h_{s,\text{int}} - h) - (W_{s,\text{int}} - W) h_{g,\text{int}}] \right] \quad (\text{A.6}) \end{aligned}$$

Equation (A.6) is the same as equation (3.15).

NOMENCLATURE

a	Average acceleration of drops, (m/s^2)
A	Outside surface area of cooling tubes, (m^2)
A_{fr}	Heat exchanger frontal area exposed to airflow, (m^2)
A_v	Surface area of water droplets per unit volume of cooling tower, (m^2/m^3)
A'_v	Surface area of cooling tubes per unit heat-exchanger volume, (m^2/m^3)
$b_{1..4}$	Dimensional coefficients
c_p	Specific heat at constant pressure, ($kJ/kg \cdot ^\circ C$)
C_1	Represents increase in performance index as fouling reaches its asymptotic value
C_2	Constant used in asymptotic fouling model
Calc	Calculated value
CFD	Computational Fluid Dynamics
\dot{C}	Capacity rate $\dot{m} c_p$, ($kJ/s \cdot ^\circ C$)
C_D	Drop drag coefficient
d	Diameter, (m)
D	Diffusion coefficient, (m^2/s)
E	Mechanical energy, (J)
E'	Deformation from spherical shape
EES	Engineering Equation Solver
Exp	Experimental value
F_D	Drag force, (N)

\bar{F}	Resultant force, (N)
G	Mass velocity = \dot{m} / A_{fr} , ($kg / s m^2$) .
g	Acceleration due to gravity, (m / s^2)
\bar{g}	Chemical potential, ($kJ/kmol$)
h	Enthalpy of moist air, (kJ / kg_{da})
\bar{h}	Molal enthalpy, ($kJ/kmol$)
h_c	Convective heat-transfer coefficient, ($W / m^2 \text{ } ^\circ C$).
h_D	Mass transfer coefficient based on $(h_{s,w} - h)$, ($kg / s m^2$)
$h_{f,w}$	Specific enthalpy of saturated liquid water evaluated at t_w , (kJ / kg_w)
$h_{fg,w}$	$h_{g,w} - h_{f,w}$, (kJ / kg_w)
h_g^0	Specific enthalpy of saturated water vapor at $0 \text{ } ^\circ C$, (kJ / kg_w)
$h_{g,w}$	Specific enthalpy of saturated water vapor at t_w , (kJ / kg_w)
H	Height, (m)
k	Thermal conductivity, ($W / m.K$)
K	Coefficient of variation of time to reach critical level of fouling
L	Length of the tube
Le	Lewis number = $h_c / h_D c_{p,a}$
m	Mass, (kg)
\dot{m}	Mass flow rate, (kg / s)
M	Median time, weight or thickness to reach the critical fouling resistance
n	Number of drops

n_{tr}	Number of tube rows
N	Number of moles, mol
\dot{N}	Molal flow rate, (mol/s)
NTU	Number of Transfer Units
NSC	Normalized Sensitivity Coefficient
NU	Normalized Uncertainty
Nu	Nusselt number = $h_c L / k$
$ODEs$	Ordinary Differential Equations
p	Risk level
P	Pressure, (kPa)
\hat{P}	Transverse tube pitch, (m)
q	Volumetric flow rate, (L/min)
\dot{Q}	Rate of heat transfer, (kW)
r	Radial direction, (m)
R	Temperature ratio
R_f	Fouling resistance, $(m^2 K / W)$
RDS	Restricted Dead State
Re	Reynolds number
s	Specific entropy, $(kJ/kg.K)$
\bar{s}	Molal entropy, $(kJ/kmol.K)$
S	Mean surface area
Sc	Schmidt number = $\mu_a / \rho_a D$

\dot{S}_{gen}	Rate of entropy generation, (kW)
t	Temperature, ($^{\circ}C$); time, (s)
T	Temperature, (K)
U_{os}	Overall heat transfer coefficient based on water-film surface area, ($W / m^2 C$)
U_Y	Uncertainty in parameter Y, units of Y
U_{X_i}	Uncertainty in parameter X_i units of X_i
v	Velocity, (m / s)
V	Volume of tower, (m^3)
w	Weight gain, (kg)
W	Humidity ratio of moist air, (kg_w / kg_{da})
\dot{W}	Rate of work done, (kW)
\tilde{W}	Humidity ratio on a molal basis, ($kmol_w / kmol_{da}$)
x	Specific flow exergy, (kJ/kg)
\bar{x}	Specific molal flow exergy, ($kJ/kmol$)
\dot{X}	Rate of exergy transport, (kW)
\bar{X}	Nominal value of X, units of X.
X_i	General input (random) variable.
y	Mole fraction
Y	Result parameter
\bar{Y}	Nominal value of Y, units of Y
Y_{j+}	Output parameter calculated with the j th variable set high

Y_{j-}	Output parameter calculated with the j th variable set low
z	Axial direction (m)
Ξ	Non-flow exergy, (kJ)

Greek Letters

α	Scatter parameter
β	Mass transfer coefficient, (m/s)
δ	Thickness, mm
ε	Effectiveness
\in	Represents the positive and negative uncertainty in a variable
Γ	Water flow rate per unit tube length, ($kg/s\ m$)
σ	Standard deviation, (h)
τ	Time constant, ($1/h$)
μ	Viscosity, ($kg/s\ m$)
$\bar{\mu}$	Mean value, (h)
ϕ	Relative humidity; also used for potential flow function (refer to Ch. 4)
Φ	Rate of deposition or removal, ($m^2 K / J$)
Φ^{-1}	Inverse of the normal distribution function
η_{II}	Second-law efficiency
$\eta_{F,norm}$	Normalized fill performance index
$\eta_{C,norm}$	Normalized condenser/cooler performance index
θ	Relative angle

Superscripts

* Asymptotic value; Properties evaluated at RDS (refer to Ch. 6)

Subscripts

a	(Moist) air
atm	Atmospheric pressure
avg	Average
c	Cold
cl	At clean condition
cr	Critical
ch	Chemical
ct	Cooling tower
cv	Control volume
d	Drop
da	Dry air
dep	Deposition
D	Destruction
ec	Evaporative condenser
efc	Evaporative fluid cooler
eff	Effective
em	Empirical
fl	In fouled condition
h	Hot
hor	Horizontal component (of velocity)

i	Induction for fouling
in	Inlet
int	Air-water interface
is	Inside
m	Mean
N	Number of input variables
o	Dead or reference state
os	Outside
out	Outlet
p	Process fluid
Q	Heat transfer
r	Refrigerant, or radial
rem	Removal
rz	Rain zone
s	Saturated state
sf	Surface
sph	Sphere
st	Steam
t	tube
tot	Total
v	Vapor
V	Per unit volume
w	(Cooling) water
wb	Wet bulb

w.r.t.	With respect to
W	Mechanical power
wb	Wet-bulb
x	Thermomechanical
z	Axial component

REFERENCES

1. Goodman, W., 1938, "The Evaporative Condenser," *Heating Piping and Air Conditioning*, Vol. 10, pp. 165-328.
2. Thomsen, E. G., 1946, "Heat Transfer in an Evaporative Condenser," *Refrigeration Engineering*, Vol. 51, No. 5, pp. 425-431.
3. Wile, D. D., 1950, "Evaporative Condenser Performance Factors," *Refrigeration Engineering*, Vol. 58, No. 1, pp. 55-63,88-89.
4. Parker, R.O., and Treybal, R.E., 1961, "The Heat, Mass Transfer Characteristics of Evaporative Coolers," *AIChE Chemical Engineering Progress Symposium Series*, Vol. 57, No. 32, pp. 138-149.
5. Leidenfrost, W., and Korenic, B., 1982, "Evaporative Cooling and Heat Transfer Augmentation Related to Reduced Condenser Temperatures," *Heat Transfer Engineering*, Vol. 3, No. 3-4, pp. 38-59.
6. Mizushina, T., Ito, R., and Miyashita, H., 1967, "Experimental Study of an Evaporative Cooler," *International Chemical Engineering*, Vol. 7, No. 4, pp. 727-732.
7. Mizushina, T., Ito, R., and Miyashita, H., 1968, "Characteristics and Methods of Thermal Design of Evaporative Coolers," *International Chemical Engineering*, Vol. 8, No. 3, pp. 532-538.
8. Finlay, I.C., and Grant, W.D., 1974, "The Accuracy of Some Simple Methods of Rating Evaporative Coolers," Report No. 584, National Engineering Laboratory, East Kilbride, Glasgow.

9. Tezuka, S., Takada, T., and Kasai, S., 1976, "Performance of an Evaporative Cooler," *Heat Transfer-Japanese Research*, Vol. 6, No. 1, pp. 1-18.
10. Kays, W.M., 1955, "Numerical Solution for Laminar Flow – Heat Transfer in Circular Tubes," *Transactions of ASME*, Vol. 77, pp. 1265-1274.
11. Gnielinski, G., 1975, *Forsch. Ing. Wesen*, Vol. 41, No. 1.
12. Filonenko, G.K., 1954, *Teploenergetika*, No. 4.
13. Chato, J.C., 1962, *Journal of ASHRAE*, pp. 52.
14. Shah, M.M., 1979, "A General Correlation for Heat Transfer during Film Condensation inside Pipes," *International J. Heat and Mass Transfer*, Vol. 22, pp. 547-556.
15. Finlay, I.C., and Grant, W.D., 1972, "Air Coolers, Cooling Towers and Evaporative Coolers," Report No. 534, National Engineering Laboratory, East Kilbride, Glasgow, pp. 165-328.
16. Peterson, D., Glasser, D., Williams, D., and Ramsden R., 1988, "Predicting the Performance of an Evaporative Condenser", *Trans. of the ASME*, Vol. 110, pp. 748-753.
17. Webb, R.L., 1984, "A Unified Theoretical Treatment for Thermal Analysis of Cooling Towers, Evaporative Condensers, and Fluid Coolers," *ASHRAE Transactions*, Vol. 90, Part1.
18. Webb, R.L., and Villacres, A., 1984, "Algorithms for Performance Simulation of Cooling Towers, Evaporative Condensers, and Fluid Coolers", *ASHRAE Transactions*, Vol. 90, Part2, No. 4, pp. 416-458.
19. Dreyer, A.A., 1988, "Analysis of Evaporative Coolers and Condenser," M.Sc Thesis, University of the Stellenbosch, Rep. of South Africa.

20. Poppe, M., and Rögner, H., 1984, “Evaporative Cooling Systems”, *VDI - Warmeatlas*, Section Mh.
21. Baker, D., 1984, *Cooling Tower Performance*, Chemical Publishing Co., Inc., New York, pp. 79-106.
22. Coffey, B.H., and Horne, G.A., 1914, “Theory of Cooling Towers Compared with Results,” *Am. Soc. of Refrig. Engrs.*
23. Merkel, F., 1925, “Verdunstungshuhlung,” *Zeitschrift des Vereines Deutscher Ingenieure* (V.D.I.), Vol. 70, pp. 123-128.
24. Nottage, H.B., 1941, “Merkel’s Cooling Diagram as a Performance Correlation for air-water evaporative cooling systems,” *ASHRAE Transactions*, Vol. 47, pp. 429-448.
25. Lichtenstein, J., 1943. “Performance and Selection of Mechanical-Draft Cooling Towers.” *ASME Transactions*, Vol. 65, No. 7, pp. 779-787.
26. Mickley, H.S., 1949, “Design of Forced Draft Air Conditioning Equipment,” *Chemical Engineering Progress*, Vol. 45, No. 12, pp. 739-745.
27. Carey, W.F., and Williamson, G.F., 1950. “Gas Cooling and Humidification: Design of Packed Towers from Small-Scale tests,” *Proceedings of the Institution of Mechanical Engineers*, Vol. 163, pp. 41-53.
28. ASHRAE, 1975, *ASHRAE Handbook and Product Directory-Equipment*, chap. 21, American Society of Heating, Refrigerating and Air Conditioning Engineers, Atlanta, GA, USA.
29. ASHRAE, 1983, *ASHRAE Equipment guide* chap. 3, Atlanta: American Society of Heating, Refrigerating and Air Conditioning Engineers, Atlanta, GA, USA.

30. Sutherland, J.W., 1983, "Analysis of Mechanical Draught Counterflow Air/Water Cooling Towers," *Journal of Heat Transfer*," Vol. 105, pp. 576-583.
31. Nahavandi, A.N., Kershaw, R.M., and Serico, B.J., 1975. "The Effect of Evaporation Losses in the Analysis of Counterflow Cooling Towers," *Journal of Nuclear Engineering and Design*, Vol.32, pp. 33-39.
32. Threlkeld, J.L., 1970, *Thermal Environmental Engineering*, Prentice-Hall, Englewood Cliffs, N.J., pp. 191-193.
33. Gosi, P., 1989, "Method and Chart for the Determination of Evaporation Loss of wet Cooling Towers," *Heat Transfer Engineering*, Vol.10, No. 4, pp. 44-49.
34. Whiller, A., 1976, "A Fresh Look at the Calculation of Performance of Cooling Towers," *ASHRAE Transactions*, Vol. 82, Part 1, pp. 269-282.
35. Jefferson, C.P., 1972, "Prediction of Breakthrough Curves in Packed Beds," *AIChE Journal*, Vol. 18, No. 2, pp. 409.
36. Stevens, D.I., Braun, J.E., and Klein, S.A., 1989, "An Effectiveness Model of Liquid-Desiccant System Heat/Mass Exchangers," *Solar Energy Journal*, Vol. 42, No. 6, pp. 449-455.
37. Raghavan, R., 1991, "Cooling Tower Analysis Consideration of Environmental Factors," *Practical Aspects and Performance of Heat Exchanger Components and Materials*, PWR-Vol. 14, ASME, pp. 33-39.
38. Sadasivan, M., and Balakrishnan, A.R., 1995, "On the Effective Driving Force for Transport in Cooling Towers," *ASME Journal of Heat Transfer*, Vol. 117, pp. 512-515.
39. Yadigaroglu, G., and Pastor, E.J., 1974, "An Investigation of the Accuracy of Merkel Equation for Evaporative Cooling Tower Calculations," *ASME Paper No. 74-HT-59*,

- Proceedings of the AIAA/ASME Thermophysics and Heat Transfer Conference*, Boston, MA, pp. 1-8.
40. Mohiuddin, A.K.M., and Kant, K., 1996, "Knowledge base for the systematic design of wet cooling towers. Part I: Selection and tower characteristics", *International Journal of Refrigeration*, Vol. 19, No. 1, pp. 43-51
41. Mohiuddin, A.K.M., and Kant, K., 1996, "Knowledge base for the systematic design of wet cooling towers. Part II: Fill and other design parameters", *International Journal of Refrigeration*, Vol. 19, No. 1, pp. 52-60.
42. Dreyer, A.A., and Erens, P.J., 1996, "Modelling of Cooling Tower Splash Pack," *International Journal of Heat and Mass Transfer*, Vol. 39, No. 1, pp. 109-123.
43. Simpson, W.M., and Sherwood, T.K., 1946, "Performance of Small Mechanical Draft Cooling Towers," *Refrigerating Engineering*, Vol. 52, No. 6, pp. 525-543, 574-576.
44. Berman, L.D., 1961. *Evaporative Cooling of Circulating Water*, 2nd edition, translated from Russian by R. Hardbottle and edited by Henryck Sawistowski. New York: Pergamon Press.
45. London, A.L., Mason, W.E., and Boelter, L.K., 1940, "Performance Characteristics of a Mechanically Induced Draft, Counterflow, Packed Cooling Tower," *Trans. of ASME*, 62, pp. 41-50.
46. Moffatt, R.J., 1966. "The Periodic Flow Cooling Tower: A Design Analysis," Technical report No. 62, Dept. of Mech. Eng., Stanford University, Ca.
47. Jaber, H., and Webb, R.L., 1989, "Design of Cooling Towers by the Effectiveness-NTU Method," *ASME Journal of Heat Transfer*, Vol. 111, pp.837-843.
48. Braun, J.E., Klein, S.A., and Mitchell, J.W., 1989, "Effectiveness Models for Cooling Towers and Cooling Coils," *ASHRAE Transactions*, Vol. 95. Part 2.

49. El-Dessouky, H.T.A., Al-Haddad, A., and Al-Juwayhel, F., 1997, "A Modified Analysis of Counter flow Wet Cooling Towers," *ASME Journal of Heat Transfer*, Vol. 119, pp. 617-626.
50. Khan, J.R., and Zubair, S.M., 2001, "An Improved Design and Rating Analyses of Counter Flow Wet Cooling Towers", *Journal of Heat Transfer*, Vol. 123, pp.770-778.
51. Dreyer, A.A., 1994, "Modelling of Cooling Tower Splash Pack," Ph.D. Dissertation, University of the Stellenbosch, Rep. of South Africa.
52. De Villiers, E., and Kroger, D.G., 1999, "Analysis of Heat, Mass and Momentum Transfer in the Rain Zone of Couterflow Cooling Towers," *Journal of Engineering for Gas Turbines and Power*, Vol. 121, No. 4, pp. 751-755.
53. Fisenko S.P., Petrushik, A.I., and Solodukhin, A.D., 2002, "Evaporative Cooling of Water in a Natural Draft Cooling Tower," *International Journal of Heat and Mass Transfer*, Vol. 45, pp. 4683-4694.
54. Lowe, H.J., and Christie, D.G., 1961, "Heat Transfer and Pressure Drop Data on Cooling Tower Packings and Model Studies of the Resistance of Natural Draft Towers to Airflow," *Proc. of the 2nd Int. Heat Transfer Conf.*, Boulder, Colorado, pp. 933-950.
55. Cale, S.A., 1982, "Development of Evaporative Cooling Packing, Commission of European Communities," Report EUR 7709 EN, Luxembourg.
56. Johnson, B.M. (ed.), 1989, "Cooling Tower Performance Prediction and Improvement," Vol. 1, Applications Guide, EPRI Report GS-6370, Vol. 2, Knowledge Base, EPRI Report GS-6370, EPRI, Palo Alto.
57. Ettouney, H.M., El-Dessouky, H.T., Bouhamra, W., and Al-Azmi B., 2001, "Performance of Evaporative Condensers", *Heat Transfer Engineering*, Vol. 22, pp. 41-55.

58. Ranz, W.E., and Marshall, W.R., 1952, "Evaporation from Drops", *Chemical Engineering Progress*, Vol. 48, No. 3, pp. 141-146.
59. Poppe, M., and Rögner, H., 1984, "Berechnung von Rückkühlwerken", *VDI - Warmeatlas*, pp. Mh 1 - Mh 15.
60. Bott, T.R., *Fouling of Heat Exchanger*, Elsevier Science Publishers Ltd., Amsterdam, 1995.
61. Morse, R.W., Knudsen, J.G., 1977, "Effect of Alkalinity on the Scaling of Simulated cooling tower water," *Canadian Journal Chem. Engg.*, Vol. 55, pp. 272-278.
62. Story, M., and Knudsen, J.G., 1978, "The Effect of Heat Transfer Surface Temperature on the Scaling Behavior of Simulated Cooling Tower Water," *AIChE Symp. Ser.*, Vol. 74, pp. 25-30.
63. Lee, S.H., and Knudsen, J.G., 1979, "Scaling Characteristics of Cooling Tower Water," *ASHRAE Trans.*, Vol. 85, pp. 281-302.
64. Coates, K.E., and Knudsen, J.G., 1980, "Calcium Carbonate Scaling Characteristics of Cooling Tower Water," *ASHRAE Trans*, vol. 86, pp. 68-91.
65. Watkinson, A.P., and Martinez, O., 1975, "Scaling of Heat Exchanger Tubes by Calcium Carbonate," *Journal of Heat Transfer*, Vol. 97, pp. 504-508.
66. Haq, M., 1995, "Reliability-Based Maintenance Strategies for Heat Exchangers Subject to Fouling," *Master of Science Thesis*, King Fahd University of Petroleum and Minerals, Saudi Arabia.
67. Konings, A.M, 1989, "Guide Value for the Fouling Resistances of Cooling Water with Different Types of Treatment for Design of Shell-and-Tube Heat Exchangers," *Heat Transfer Engineering*, Vol. 10, pp. 54-61.

68. Haider, S.J., Meitz, A.K., and Webb, R.L, 1992. "An Experimental Study of Tube-Side Fouling Resistance in Water-Chiller-Flooded Evaporators," *ASHRAE Trans*, Vol. 98, pp. 86-103.
69. Knudsen, J.G., 1989, "Coping with Cooling Water Fouling in Tubular Heat Exchangers," *AIChE Symp. Ser*, Vol. 85, pp. 1-12.
70. Hasson, D., 1981, "Precipitation Fouling. In: E.F.C. Somerscales ad J.G. Knudsen, Eds, *Fouling of Heat Transfer Equipment*. Hemisphere, Washington, D.C .
71. Branch, C.A., and Steinhagen, H.M.M., 1991, "Influence of Scaling on the Performance of Shell-and-Tube Heat Exchangers," *Heat Transfer Engineering*, Vol. 12, pp. 37-85.
72. Hesselgreaves, J.E., 1992, "The Effect of System Parameters on the Fouling Performance of Heat Exchangers," *Heat Transfer Engineering*," *ICHEME Symp. Ser*, Vol. 129, pp. 995-1006.
73. Tretyakov, O.V., Kristskiy, V.G., and Styazhkin, P.S., 1991, "Improved Prediction of the Formation of Calcium Carbonate Scale in the Heat Exchangers of Secondary Loops of Conventional Thermal and Nuclear Power Plants," *Heat Transfer-Sov. Res*, Vol. 23, pp. 532-538.
74. Khan, M.S., 1996, "Effect of Thermal-Hydraulic Parameters on the Induction Time of Calcium Carbonate Scaling," Master of Science Thesis, King Fahd University of Petroleum and Minerals, Saudi Arabia.
75. Hewitt, G.F., Shires, G.L., and Bott, T.R., 1994, *Process Heat Transfer*, CRC Press, Inc., Ann Arbor, pp. 762-772.
76. Mortensen, K.P., and Conley, S.N., 1998, "Film Fill Fouling in Counter flow Cooling Towers: Experimental & Fixed Results and "Generation II" Low-Clog Pack Design,"

- Marley Cooling Tower Company*, 5800 Foxridge Drive, PO Box # 2912, Mission, KS 66201-9875 USA.
77. Thomas, W.M., Steel, G., and Whitehouse, J.W., 1991, "Studies of Biofilm Ultrastructure and Composition on Plastic Packing Using Experimental Cooling Towers," *International Association of Hydraulics Research*, Cooling Tower Workshop, Pisa, Italy.
78. Mirsky, G.R., Monjoie, M., and Noble, R., 1993, "Research of Fouling Film Fill," *Paper presented at the Cooling Tower Institute Annual Meeting*, New Orleans, Louisiana, February 17-19.
79. McCarthy, R.E., and Ritter, J.G., 1993. "Case Histories of Cooling Tower Fill Fouling in the Electric Utility Industry," *Presented at the 55th Annual American Power Conference*, Nalco Chemical Company, Chicago, Illinois, April 13-15.
80. Macleod-Smith, R.I., 2002, "How to Control Legionella without Damaging your Evaporative Condenser," *Presented at the 11th Annual Institute of Refrigeration Conference, London, 26th November*; Baltimore Aircoil Ltd.
81. Kern, D.Q., and Seaton, R.E., 1959, "A Theoretical Analysis of Thermal Surface Fouling," *British Chemical Engineering*, Vol. 4, No. 5, pp. 258-262.
82. Epstein, N., 1978, "Fouling in Heat Exchangers," in *Heat Transfer 1978, Proceedings of the 6th International Heat Transfer Conference*, Vol. 6, pp. 235-253.
83. Epstein, N., 1981a, "Economic Evaporator Cycles With Scale Formation," in *Fouling of Heat Transfer Equipment*, eds. E.F.C. Somerscales and J.G. Knudsen, pp. 653-659, Hemisphere, Washington, D.C.

84. Zubair, S.M., Sheikh, A.K., and Shaik, M.N., 1992, "A Probabilistic Approach to the Maintenance of Heat-Transfer Equipment Subject to Fouling," *ENERGY*, Vol. 17(8), pp. 769-776.
85. Zubair, S.M., Sheikh, A.K., Budair, M.O., and Badar, M.A., 1997b, "A Maintenance Strategy for Heat-Transfer Equipment Subject to Fouling: A Probabilistic Approach," *Transactions of ASME, Journal of Heat Transfer*, Vol. 119(3), pp. 575-580.
86. Somerscales, E. F. C., and Kassemi, M., 1987, "Fouling Due to Corrosion Products Formed on a Heat-Transfer Surface," *ASME J. Heat Transfer*, Vol. 109, pp. 267-271.
87. Zubair, S.M., Sheikh, A.K., Budair, M.O., Haq, M.U., Quddus, A., and Ashiru, O.A., 1997a, "Statistical Aspects of CaCO_3 Fouling in AISI 316 Stainless Steel Tubes," *Transactions of ASME, Journal of Heat Transfer*, Vol. 119(3), pp. 581-588.
88. Khan J.R., Zubair S.M., 2004, "A study of fouling and its effects on the performance of counter flow wet cooling towers," *Proceedings of IMechE J. of Process Mechanical Engineering*; 218(E1), pp. 43-51.
89. Wepfer, W. J., Gaggioli, R. A., and Obert, E. F., 1979, "Proper Evaluation Of Available Energy for HVAC," *ASHRAE Trans.*, Vol. 85, Part I, pp. 214-230.
90. Bejan, A., *Advanced Engineering Thermodynamics*, 2nd ed., John Wiley & Sons, NY, 1997.
91. Qureshi, B.A., and Zubair, S.M., 2003, "Exergy Analysis of Various Psychrometric Processes," *Int. J. Energy Research*, Vol. 27, No. 12, pp. 1079-1094.
92. Kim, J.H., and Simon, T.W., 1993, "Journal of Heat Transfer Policy on Reporting Uncertainties in Experimental Measurements and Results," *Journal of Heat Transfer*, Vol. 115, Nos. 5-6.

93. Taylor B.N. and Kuyatt, C.E., Guidelines for Evaluating and Expressing the Uncertainty of NIST Measurement Results, National Institute of Standards and Technology Technical Note 1297, 1994).
94. James, C.A., Taylor, R.P., and Hodge, B.K., 1995, "The Applications of Uncertainty Analysis to Cross Flow Heat Exchanger Performance Predictions," In *ASME/JSME Thermal Engineering Conference*, pp. 337-345.
95. Laws, J.O., 1941, "Measurement of the Fall Velocity of Water Drops and Rain Drops," *Trans. Of the American Geophysical Union*, Part III, 22nd Annual Meeting, pp. 709-721.
96. Jang, J.Y. and Wang, Z. J., 2001, "Heat and Mass Transfer Performances of Closed-Type Cooling Towers," *Proceedings of the International Conference on Advanced in Computational Heat Transfer*, Palm Cove, Queensland, Australia, May 20-25, pp. 269-276.
97. Finlay, I.C., and Harris, D., 1984, "Evaporative Cooling of Tube Banks," *Int. Journal of Refrigeration*, Vol. 7, No. 4, pp. 214-224.
98. Erens, P.J., 1988, "Comparison of some Design choices for Evaporative Cooler Cores," *Heat Transfer Engineering*, Vol. 9, No. 2, pp. 29-35.

VITA

NAME: Bilal Ahmed Qureshi

PLACE OF BIRTH: Dhahran, Saudi Arabia.

ADDRESS: H. # 4, St # 7,
Safari Villas,
Rawalpindi,
PAKISTAN.

E-MAIL: baqureshi78@yahoo.com

EDUCATIONAL QUALIFICATION:

M.S (*Mechanical Engineering*)

April 2004

King Fahd University of Petroleum and Minerals
Dhahran, Saudi Arabia.

B.S (*Mechanical Engineering*)

November 2000

National University of Sciences and Technology
Rawalpindi, Pakistan.